University of Reading

Department of Physics

MORPHOLOGY AND ELECTRICAL PROPERTIES OF POLYETHYLENE BLENDS

A Thesis submitted for the
degree of Doctor of Philosophy

Ian L. Hosier B.Sc (Hons.)

February 1996

Contents

Acknowledgements

I wish to thank the following people for their help during my research;

I wish to express my sincere gratitude to Professor Alan Lettington for enabling me to carry out this research in the J.J Thompson Physical Laboratory. Professor David Bassett is acknowledged as head of the Polymer Physics group for the use of laboratory facilities.

I would like to thank my research supervisor Dr Alun Vaughan for his patience, guidance, and support during the period of my research, and for spending many hours proof reading this manuscript, and adding very helpful suggestions.

I would also like to express my gratitude to Dr Steve Swingler for giving an industrial perspective to the research, for access to equipment at the National Grid Company PLC, and for Wiebull fitting software. Also Dr Dax Patel for her assistance during my time spent at the National Grid Company.

I would like to thank past and present members of the polymer physics group for helping to maintain a friendly working atmosphere. In particular I would like to thank Mr C.J. Balagué for his technical assistance and services rendered during the tenure of this research. Mr R.H Olley is thanked in particular for guiding me through various computer packages and for helpful suggestions.

I would like to thank Dr James Janimak for many helpful discussions during the course of this work, particularly relating to mechanical deformation of polymers.

My parents for continued support, and finally to the Engineering and Physical Sciences Research Council and the National Grid Company PLC, for a CASE studentship, without which this research would have not been possible.

First submitted February 1996, revised and accepted May 1996. This electronic version created from the original scanned documents March 2002, PDF version generated May 2008. To preserve the integrity of this document, only minor typographical and formatting corrections have been made to the original manuscript.

Abstract

Structure-property relationships in binary polyethylene blends, and how they relate to electrical strength, have been investigated by various analytical steps.

Scanning and transmission electron microscopy have been used to characterise in detail the microstructure of blends composed of linear (LPE) and branched (BPE) polyethylene, these have shown a general increase in the size of isothermally crystallised spherulites with increasing LPE content. On increasing the crystallisation temperature, spherulites became more compact and better separated, whereas on quenching, a morphology essentially independent of LPE content was obtained. Differential scanning calorimetry revealed a two phase system whose composition did not depend on LPE content.

Electrical testing using an AC ramped voltage, between parallel ball bearing electrodes, was employed to characterise the electrical insulation strength of the materials.

Morphological, rather than molecular factors, were found to be key at influencing the electrical strength. Electrical strength was also found to be highly sensitive to the testing procedure and sample geometry employed.

From computer simulations it was found that the general patterns of tree growth depended on sample geometry, test conditions, and morphology, in a similar way to that found by experiment. The idea of dielectric failure due to a propagating damage structure is not inconsistent with the simulated or experimental data.

A variety of blend systems were also subjected to mechanical tensile deformation and it was found that the morphology was affected significantly, even for small deformations within the elastic limit. Consequently, the electrical strength was reduced by mechanical tensile strain.

A 16% increase in electrical strength over BPE alone, could be achieved by the use of a carefully formulated blend, which has potential for commercial exploitation.

CHAPTER 1-INTRODUCTION

1.1 The History of Polymer Science

Polymers have existed in natural form since life began, and those such as DNA, RNA and proteins have played a critical role in the life of all living things. Man has exploited naturally occurring fibres for a long time in the manufacture of clothing and tools, specifically by exploiting natural fibres such as animal skins for clothing, and wood to make weapons and tools. The origins of the polymer industry are generally accepted to be in the early nineteenth century when the first natural polymers were modified by man to suit specific applications. Much of the early work concerned the modification of natural rubber which when mixed with sulphur, made it more elastic and eliminated it's tackiness. (Charles Goodyear 1839).

Gun cotton (cellulose nitrate) was quickly recognised for its potential as an explosive (Christian Schonbein 1846), but was perhaps more useful as it could be moulded into specific shapes by the application of heat and pressure. In 1870 John and Isaiah Hyatt patented a similar material using 'plasticised' cellulose, the plasticiser being camphor, and leading to the well known 'celluloid'. The developments based on cellulose continued when Charles Cross and co-workers, in 1892 patented the regeneration process whereby cellulose fibres could be dissolved and regenerated in the form of textile fibres. Viscose rayon fibres were a great success in the clothing industry.

'Bakelite' resins (Leo Baekeland 1910) were the first truly synthetic polymers to be exploited commercially, followed by the German discovery of methyl rubber in World War 1 as a substitute for natural rubber. By 1920 the polymer industry was firmly established and scientists worldwide have been reporting their unusual properties ever since. Studies into polystyrene and polyoxymethylene confirmed the hypothesis that polymers were composed of long chains of simple molecules, and in 1920 Hermann Staudinger coined the phrase 'Macromolecule'. During the following 30 years many studies into the crystallisation and structure of polymers led to the first journals and publications devoted solely to the synthesis and characterisation of polymers, and most of the principles of polymer science were established. Whilst polymer science is now considered mature, many studies

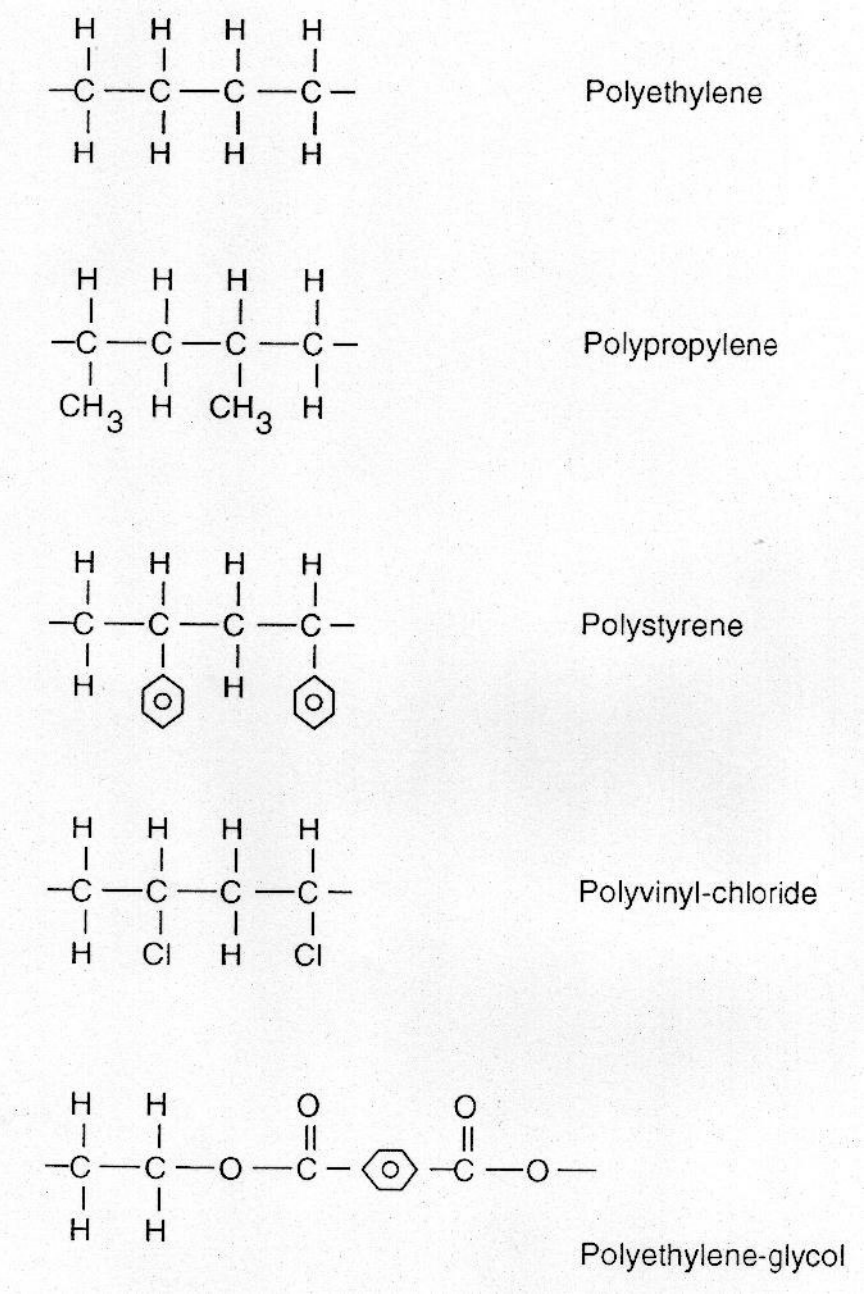

Figure 1.1: Schematic structure of some polymers.

into both the synthesis and applications of polymers continue and this is likely to be the trend, as better materials are produced to meet an increasing demand.

1.2 Molecular structure

A polymer is defined as a long molecule in which a sequence of atoms is repeated many times throughout the length of that chain. The group of atoms, which constitutes the repeating unit of the chain, determines many of the physical and mechanical properties of the final polymer. For example, in polypropylene the repeat unit is (CH_2=$CH(CH_3)$) whereas in polyethylene the repeat unit is (CH_2=CH_2). In many respects polypropylene is similar to polyethylene, but in polypropylene the presence of the bulky CH_3 side group makes the material somewhat less dense than polyethylene, which has only single H side groups. Nylon 6,10 forms strong fibres ($NH(CH_2)_6$-NH-CO-$(CH_2)_4$-$CO)_x$ due to strong hydrogen bonding which connects adjacent chains, in polyethylene only weak Van der Waals forces contribute. Figure 1.1 shows the structure of some polymers in diagrammatic form.

The factor 'x' which appears in the above nomenclature is known as the *degree of polymerisation* and is the number of repeat units used to form a polymer chain. In practice a polymer may be a material which has x=10,000 which is quite typical, but a material with x=5 for instance, would instead be classified as a low molecular weight substance, although there is some ambiguity in defining exactly the point at which a material becomes known as a polymer.

In the ideal case we could classify a polymer by specifying its chemical repeat unit and degree of polymerisation, in practice things are not quite so ideal. If we were to take a batch of polymer straight from the manufacturing process we would find that x is not the same for all the resulting molecules, not all chains have the same length. So then how do we define such materials?. To answer this we need to define a few terms.

Imagine selecting all chains out of such a distribution, all with the same length, to get N_i such chains of the same length. We can define a molecular (or molar) mass M_i as the weight of all such chains with molecular mass M_i. Going back to the full distribution of chains we can plot W_i against M_i to get the full molar mass distribution (see figure 1.2)

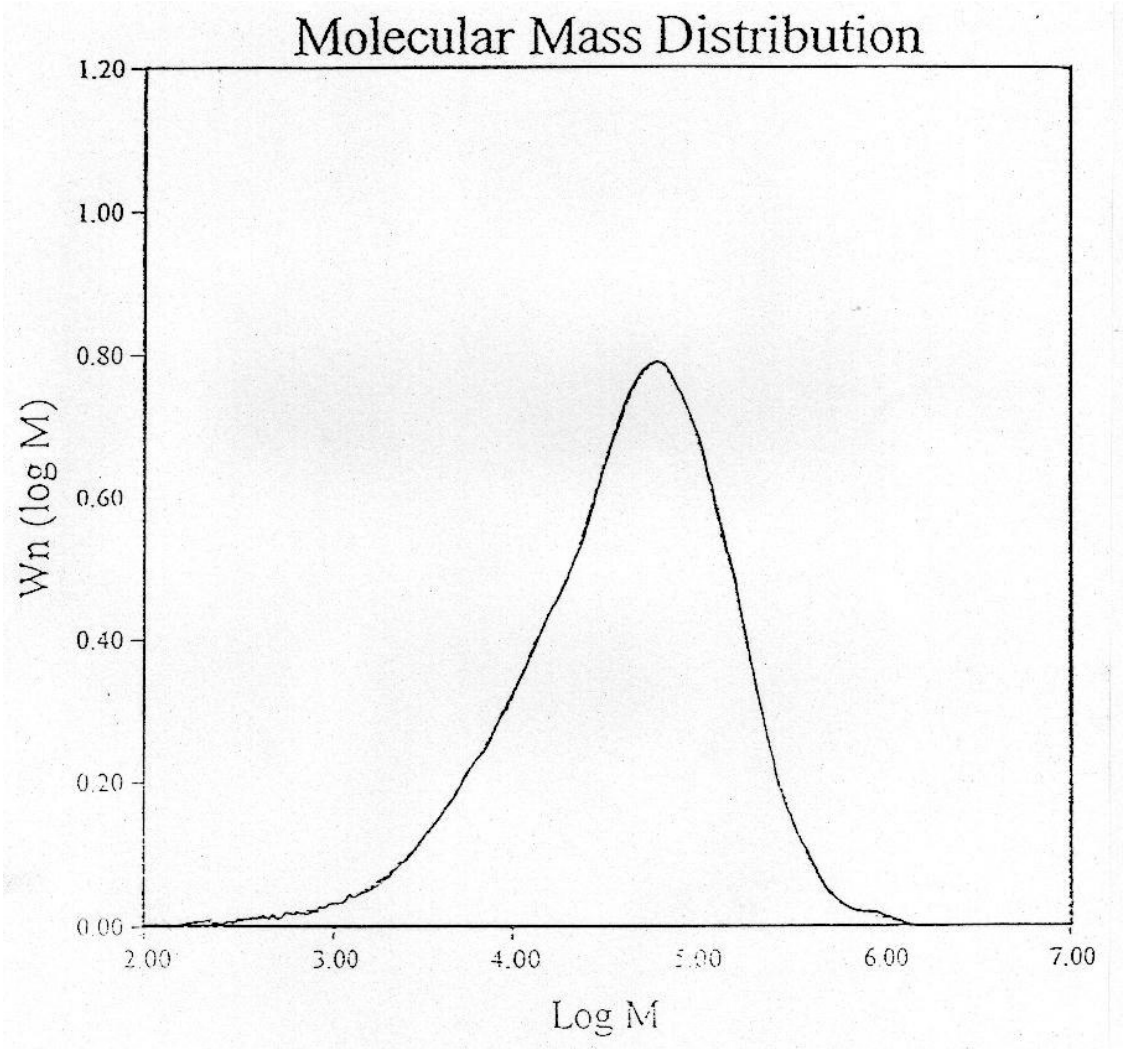

Figure 1.2: Molecular weight distribution of Borealis 4901 branched polyethylene.

mass of one mole (6.022×10^{23}) of such chains (units Kg/mole), and a term W_i as the total which shows the distribution of chain lengths present in a typical batch of polymer.

Two parameters are generally used to simplify this resulting distribution (but are no substitute for knowing the distribution itself) these are the weight average molecular weight which corresponds to the maximum of the distribution in figure 1.2 and the number average molecular weight which would correspond to a peak in the distribution if N_i had instead been plotted against M_i and are defined as follows;

$$M_w = \frac{\Sigma W_i M_i}{\Sigma W_i}$$

$$M_n = \frac{\Sigma N_i M_i}{\Sigma N_i}$$

with the sums being over all polymer chains. Another parameter P called the polydispersity is defined as

$$P = \frac{M_w}{M_n}$$

and gives a measure of the width of the distribution. In ideal situations we would hope to have P=1 (ie: all the chains are the same length), in practice P > 1 as there are a range of different chain lengths.

Here we have dealt with only the simplest of linear structures, in practice mechanisms of the manufacturing (polymerisation) process lead to the introduction of side groups, or branches, which can have a profound effect on properties.

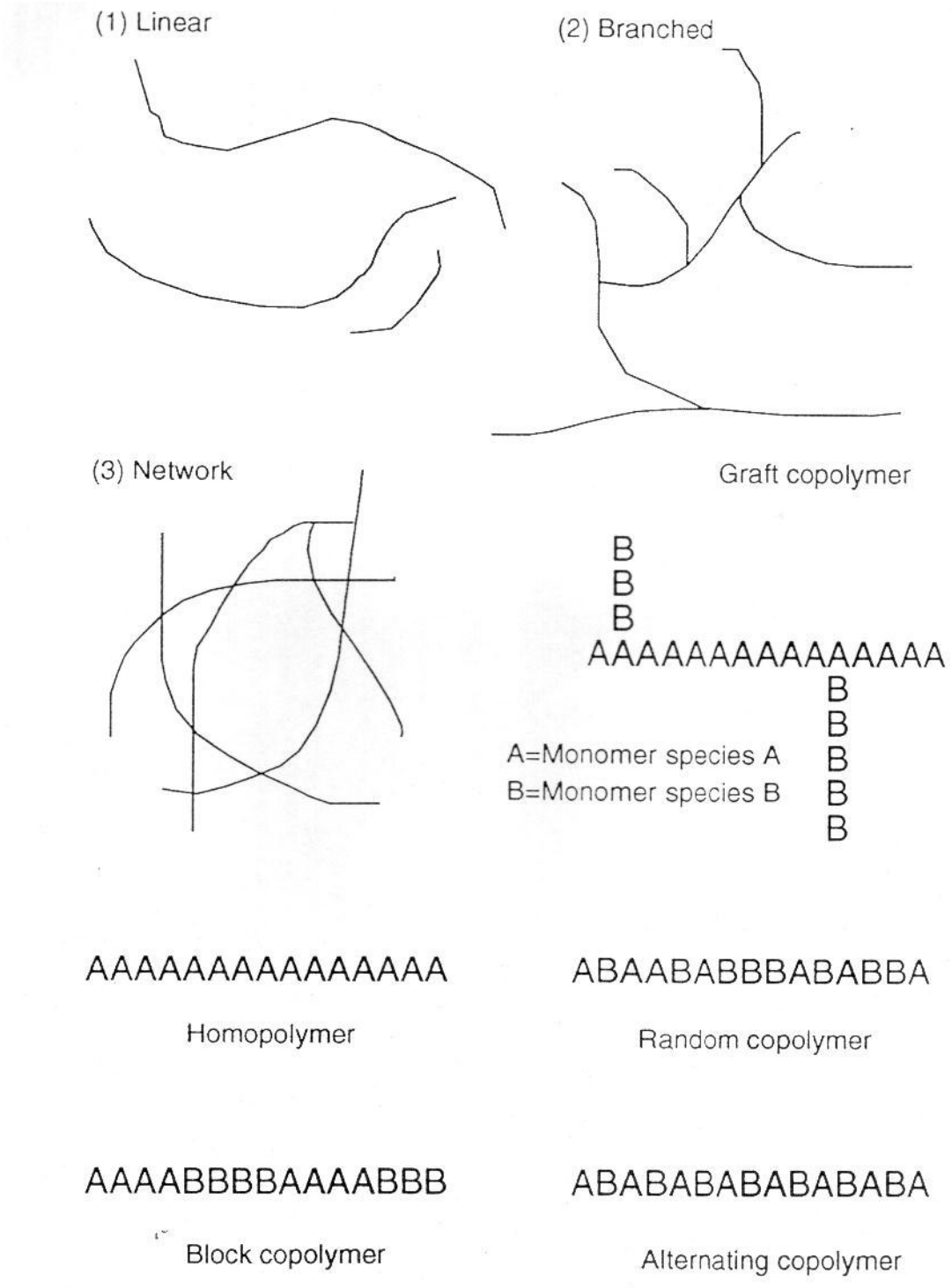

Figure 1.3: Structures of polymers and repeat unit configurations.

1.3 Types of polyethylene-molecular architecture

Polyethylene is one of the most common, and the simplest from a molecular viewpoint, of synthetic polymers. It was first produced by polymerising ethylene gas ($CH_2=CH_2$) at high pressure (1000-3000 atmospheres) and temperatures (80-300°C), a process which started in the 1930's (1) and still continues today. The process does not favour growth on any particular site and temperature control was poor, so that C-C bonds did not form sequentially giving a simple linear chain, but 'branches' of varying length were found to be randomly introduced. The polymer as a result was very difficult to characterise, having a mixture of long and short branches[1]. This type of polyethylene is called low density polyethylene. In a typical low density polyethylene (ie: Borealis Chem. 4901) there may be around 15 long branches per 1000 carbon atoms along the main chain, with a density of 910 Kg/m^3.

In the 1950's Ziegler and Natta discovered that polyolefins could be produced at atmospheric pressure and room temperature by using organometallic catalysts (2) and that the resulting material did not possess so many branches as the conventionally produced materials detailed above. Such polymers (produced by catalytic polymerisation) are referred to as high density polyethylene (HDPE) and contain just a few short branches.

In the 1970's it was discovered that polyethylene could be produced without long branches but with short ones by co-polymerising (using more than one monomer) ethylene with small organic molecules like 1-butene and 1-hexane. In such processes (3) it was possible, for the first time, to control the distribution and size of the branches along the main chain. The branching was dependent on the co-monomer used. A special class of these materials, co-polymerised with small molecules (such as Butene), and attracting a great deal of interest at present are known as linear low density polyethylenes (LLDPE).

Block co-polymers can combine the useful properties of both monomer species and the co-monomer can be incorporated in the main chain or in side branches. Figure 1.3 shows some types.

[1] Short branches are generally defined as those having less than 6 carbon atoms.

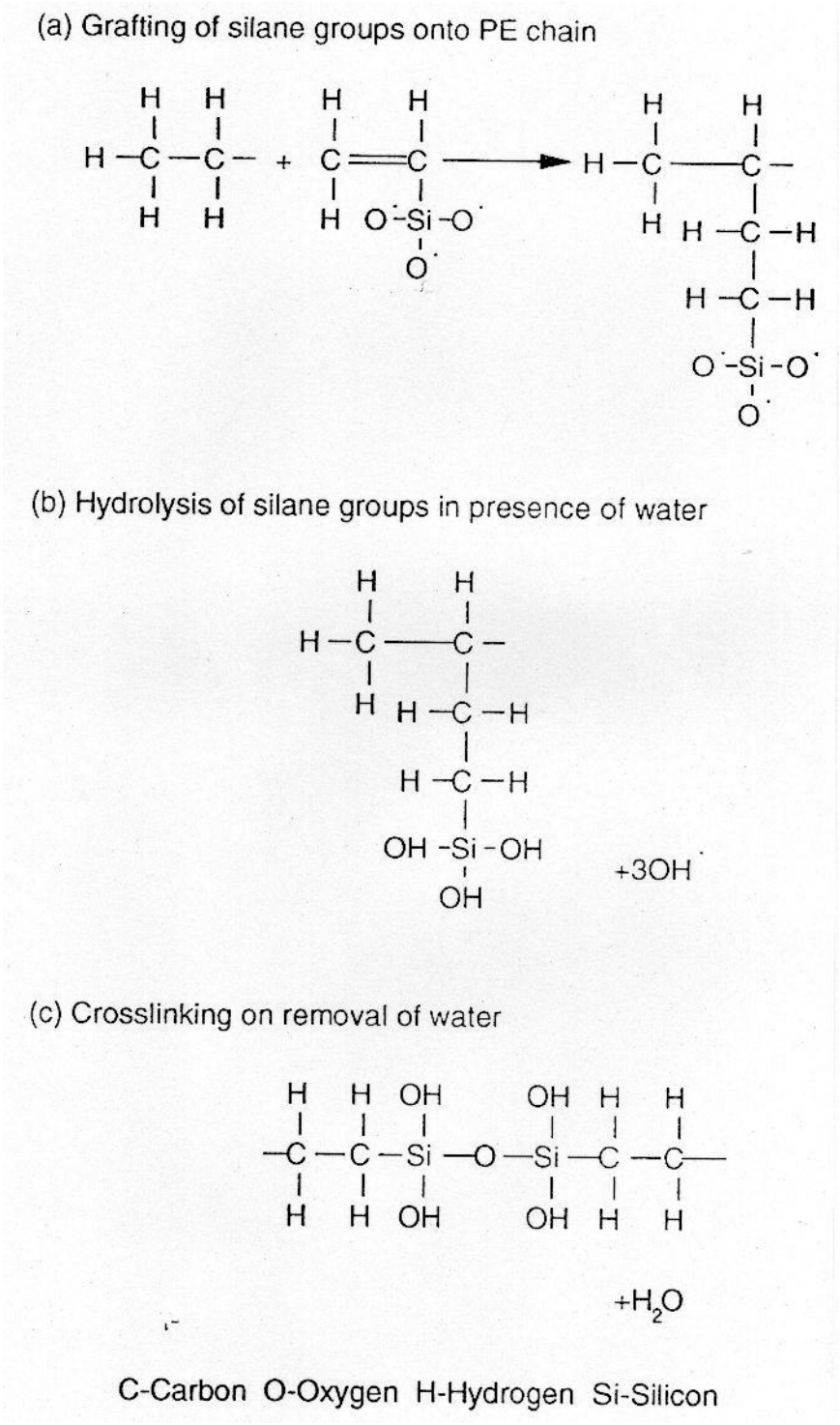

Figure 1.4: Chemistry of silane crosslinking in polyethylene.

1.4 Crosslinking

Crosslinking is the process where individual polymer chains can be joined together at a molecular level so as to give a network, of practically infinite molecular mass. Crosslinked polyethylene (XLPE) used as cable insulation has a greater resistance to elevated temperature and cracking than uncrosslinked materials. The polyethylene can be crosslinked by three methods (4,5,6); (a) the incorporation of peroxides, such as di-t-butyl peroxide, which decompose to produce radicals, which can then transfer to adjacent chains giving the chemical crosslinking, when subjected to high temperatures, (b) the reaction of grafted silane groups in the presence of water, (c) high energy electron radiation which generates radicals which then recombine with adjacent chains on removal of the radiation to generate crosslinks. Silane crosslinking has twin advantages for a laboratory study; (a) silane grafted materials are readily available commercially and (b) the crosslinking process takes place in water at relatively low temperatures. Figure 1.4 shows the chemistry of the silane crosslinking process and the grafting process (a). Crosslinking occurs in two stages; (b) hydrolysis of silane groups in the presence of water, (c) on removal of the water, silanol groups condense to give crosslinks between chains. Commercial vinyl-silane copolymers are readily available, so in practice the grafting process does not need to be performed in the laboratory, such materials can then be readily crosslinked.

1.5 Crystal structure

General. Crystalline solids consist of a regularly packed array of atoms, which may or may not be chemically bonded, in polyethylene the atoms are generally joined by C-C covalent bonds along the chains. It is possible to specify the structure of any crystalline solid by defining the spatial arrangement of a repeating set of atoms, known as the unit cell. In atomic solids, such as metals, the atoms pack billiard ball fashion, it is relatively easy to specify a unit cell and the structure can be defined in terms of, for example, simple cubic or hexagonal unit cells containing a few atoms.

The packing structures in a polymer are clearly far more complex than this and structures such as chain branches can make it even more so. In this case the unit cells are made up of

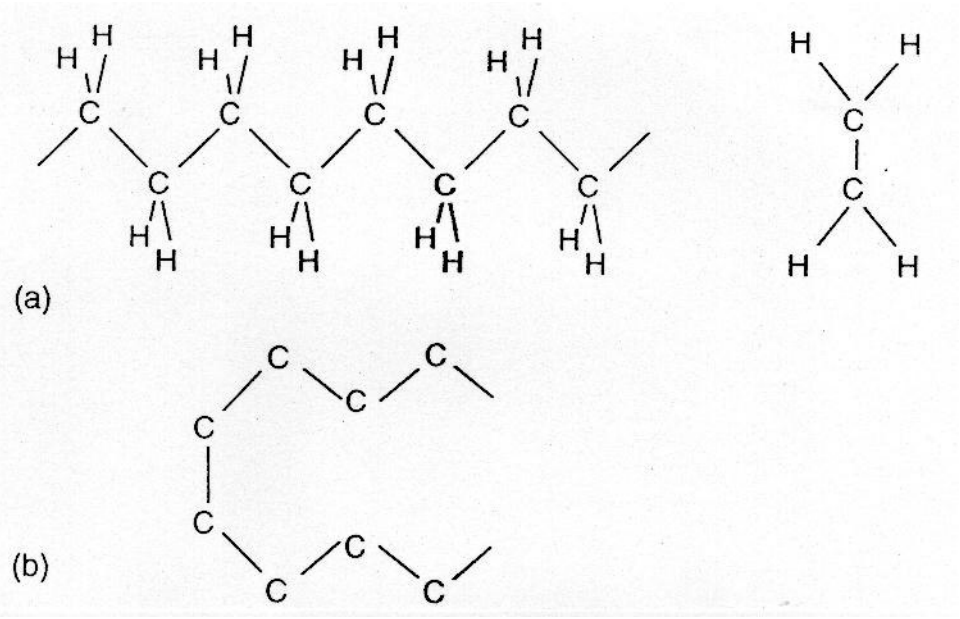

Figure 1.5: (a) Schematics of polyethylene chain, bond lengths not to scale. (b) High energy 'cis' configuration with H groups omitted for clarity.

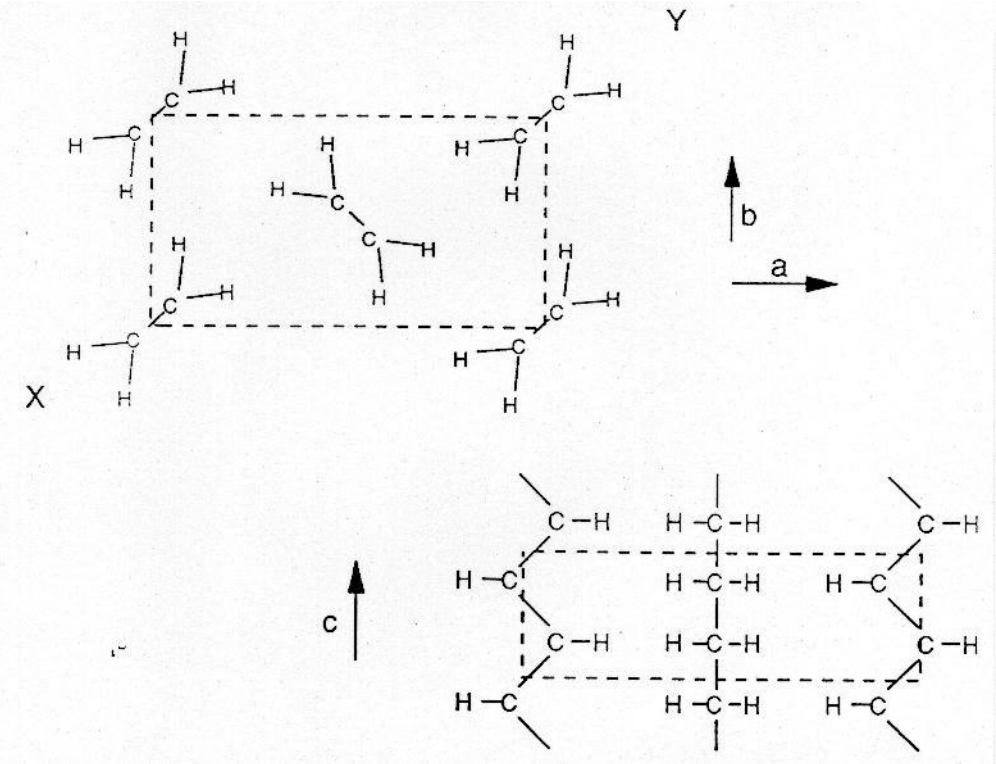

Figure 1.6: The unit cell of polyethylene with crystallographic directions indicated and section along X-Y looking perpendicular to the chain axis.

sections of polymer chains rather than individual atoms, the spatial arrangement of atoms on the polymer chain are determined by covalent bonding whereas adjacent chains are held together by secondary Van der Waals or hydrogen bonding. The crystals, due to these different forms of bonding in different directions, are very anisotropic.

Polyethylene. The structure of the polyethylene unit cell now deserves some examination. A single chain of linear polyethylene is shown in diagrammatic form in figure 1.5(a).

The H-C-H bond angle in PE is 112°, C-C angle is 107°, the C-C bond length is 0.15 nm and the C-H bond length is 0.11 nm (29). In the solid state the molecules adopt a planar zig-zag conformation in which the carbon atoms are described as being in a 'trans' conformation, this being the state with the lowest free energy. However other conformations are possible, particularly where a chain must fold back on itself, for instance at the surface of a crystal (figure 1.5(b)). This represents a simple chain folding method but such folds may be more complex and be made up of trans-gauche sequences.

The unit cell for polyethylene, at normal pressure, is orthorhombic, (figure 1.6), the crystallographic axes are also labelled. The 'c' axis is conventionally aligned along the chain axis, which in the case of a crystal lies perpendicular to the basal plane. The dimensions of the unit cell are (a=7.418Å, b=4,946Å, c=2.546Å) (7) but do depend somewhat on temperature. Polyethylene also has a hexagonal phase which can form under conditions of high pressure.

1.6 Polymer lamellae

Studies into the morphology of polymer crystals precipitated from solution concluded that polyethylene crystals are thin platelets or 'lamellae' (8), typically of order 100Å thick and with lateral dimensions of microns. The crystals could be observed independently suggesting that a crystal must be composed of a large number of chains and that the molecules must be folded many times within the crystal (9). Electron diffraction revealed that the chains were orientated more or less perpendicular to the plane of the crystal representing a very high degree of order (Fig 1.7(a)). In practice simple chain folding such as that shown here is energetically unfavourable as chain folding involves chain

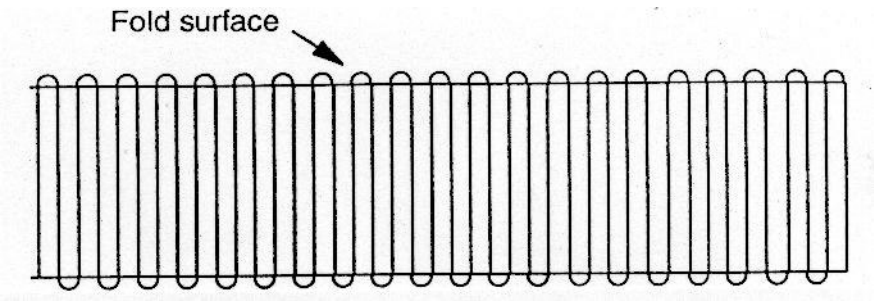

Figure 1.7(a): Idealised polymer crystal showing chain folding.

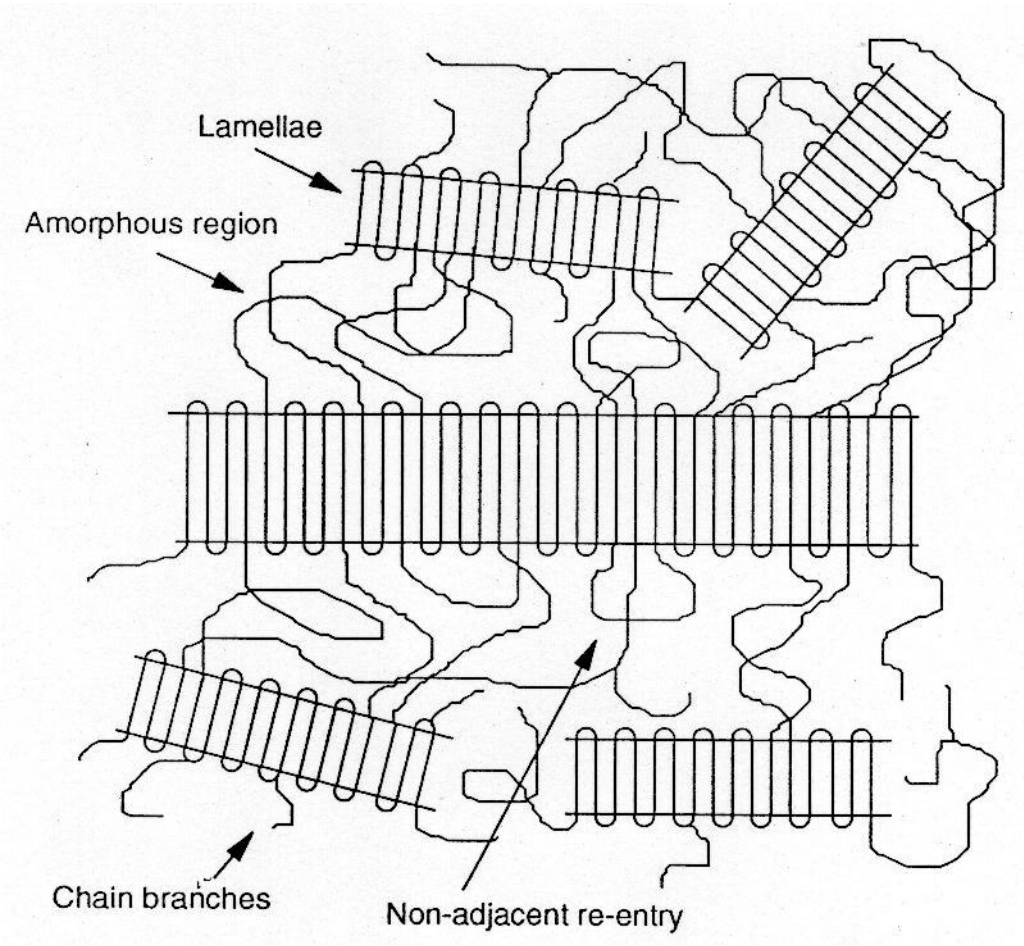

Figure 1.7(b): Some features of real semi-crystalline polymers.

conformations other than the lowest energy state (see fig 1.5(b)). Switchboard models (10,11) have been proposed, neutron scattering has shown that the probability of adjacent re-entry to be around _. Such ideas are represented diagrammatically in figure 1.7(b), which shows several chains, which may be part of many different crystals and the amorphous regions between lamellae.

The fold surfaces of the crystals are non-crystalline and as a result lamellae are only 80-90% crystalline overall. Because of this they differ from single crystals of other materials. They do however contain dislocations and other defects associated with crystal forms (12).

Assuming that the molecular conformation allows crystals to form, crystal thickness in part is controlled by chain branching, certainly bulky side groups would be very difficult to incorporate within the regular chain folding sequence inside the body of the crystal, resulting in thinner lamellae. The maximum lamellar thickness would be similar to the branch-branch distance if this were the case. Furthermore the defective branches, which are excluded from the crystal surfaces, result in thicker amorphous interlamellar regions, hence the term semi crystalline as applied to polymers. Such a process whereby less linear molecules are effectively rejected from crystalline regions during crystallisation is termed segregation (13).

The structure and amount of fold surface material is of relevance to electrical properties since often the material found on fold surfaces and in inter-lamellar regions is composed of defective species, impurities and rejected chain segments, these parts may serve as electrically weak sections.

Crystal thickness. When chain branching effects are insignificant, the size of the secondary nucleus is determined by the supercooling, δT. The experimental form of the relationship between crystal thickness and supercooling was known experimentally before it was predicted theoretically (14) by Hoffmann and Lauritzen. For a detailed account of the theory the reader is referred to the literature, however the relevant equation is:

$$l = \frac{2\sigma_e T_m^{\,o}}{\delta H \delta T} + \delta l$$

where T_m^{o} is the melting temperature of a crystal of infinite thickness, σ_e is the surface free

energy per unit area and δH is the enthalpy of crystallisation per unit volume. Thicker nuclei form at low levels of supercooling (or high crystallisation temperatures). Melting a lamellar crystal is thermodynamically the reverse of crystallisation and is summed up in the 'Thomson Gibbs equation';

$$T_m = T_m^o(1 - \frac{2\sigma_e}{\delta Hl})$$

Thicker nuclei melt at higher temperatures.

Annealing This is a term which is usually used to describe the processing of metals and the annealing of polymers resembles that of metals. Annealing a polymer lamellae causes it to thicken, the driving force being the decrease in Gibbs free energy caused by an increase in the volume to surface area ratio of the crystal. This increases T_m above the value expected if no thickening to occur, such a process is termed isothermal lamellar thickening and has been widely reported (15,16). Were lamellar thickening not to occur, the melting point for a given lamellae would be the same as the temperature at which it was formed. Although suppressed in some systems (ie: Polyethylene blends) (17) it is nevertheless present.

1.7 Spherulites

When crystals grow from concentrated solutions or from the melt they do not attain the form of individual lamellar crystals as described above. They tend to occur not in isolation but instead in ordered spherical arrays known as spherulites (18). They first form as a single lamellae which then acts as a site for further local order, nucleating further adjacent lamellae. It is thought that pressure from incorporated rejected material between lamellae, or even infilling *subsidiary lamellae* cause them to splay apart (12), leading to the development of a sheaf and finally to a spherulite (19). Growth continues until one of two things happens; (a) the available crystallisable material runs out, leaving amorphous regions between spherulites, or (b) the spherulites impinge, leaving amorphous material concentrated between lamellae. Figure 1.8 shows schematically these growth stages of a

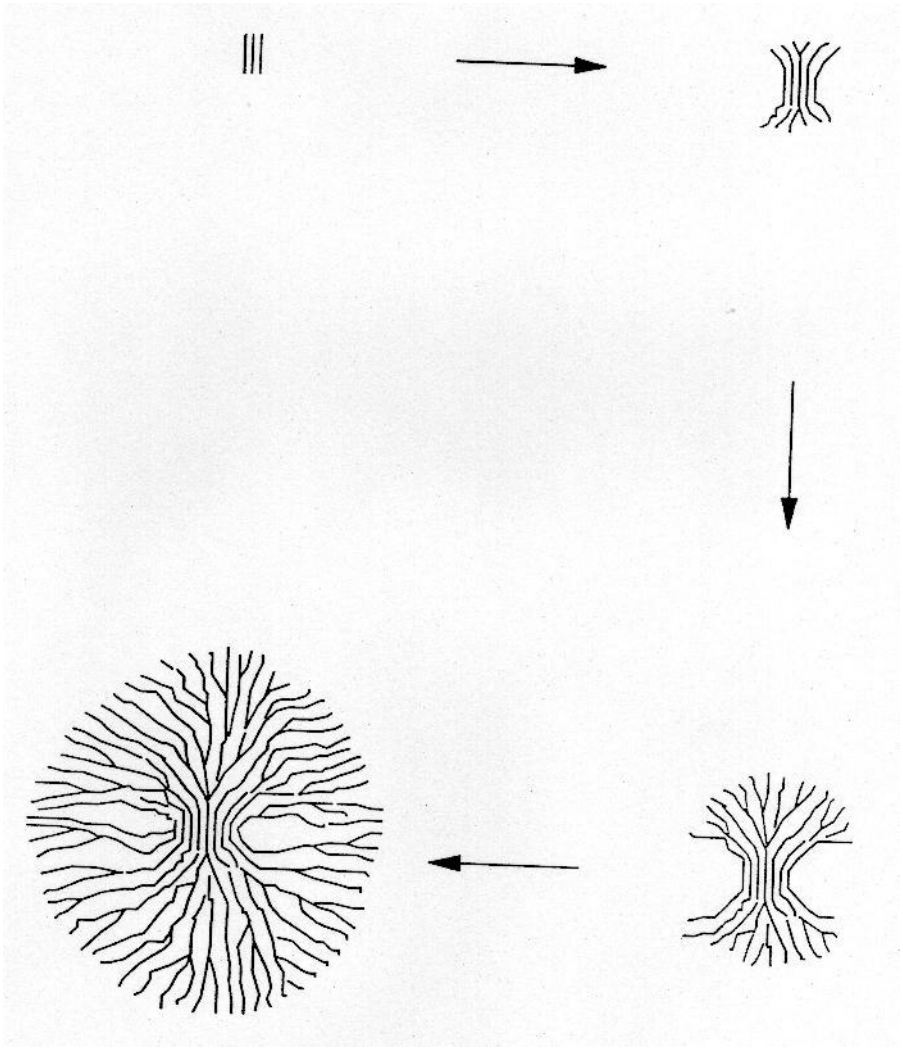

Figure 1.8: Growth stages of a spherulite.

spherulite.

Spherulites are not peculiar to polyethylene but appear in other systems also (20), individual lamellae as well as spherulites can be also grown under melt crystallisation (21), spherulites also appear in blends (22).

Some spherulites are seen to be ringed, or banded, which is attributed to a radial rotation of lamellar orientation (23). Electron microscopy has shown that the lamellae in a spherulite are very similar to those formed in isolation (21).

Melt crystallised polymers can never be totally crystalline, as far as is seen in solution crystals, due to restrictions placed on molecular mobility (chain entanglements in the melt) so it is never possible for all the chains to adopt the conformations required for crystallisation into lamellae.

1.8 Crystallisation kinetics

When the temperature of a polymer is reduced from the molten state to a temperature below its melting point there is a possibility for the randomly entangled melt to become aligned and form small ordered regions, this process is known as nucleation. Thermodynamically, formation of a new nuclei involves the creation of a new surface which increases the Gibbs free energy of the system, however new volume is also created which decreases the Gibbs energy. Therefore there will be a minimum size of nucleus where addition of further material causes the Gibbs free energy to begin to fall. Thermodynamically then, nuclei are only stable above a critical size and below the melting point of the polymer, since they would otherwise be destroyed by random thermal motion. The second step in crystal formation is growth, where crystal nuclei grow by the addition of further polymer chains. Crystallisation therefore consists of two distinct steps, each of which may be considered separately.

Nucleation can be of two forms heterogeneous or homogeneous. Heterogeneous nucleation is the formation of nuclei around foreign bodies or specially developed *nucleating agents* ie: Di-benzyl-sorbitol (24). Homogenous nucleation occurs intrinsically within the polymer itself, such as the process described above. The argument continues about which of these processes is dominant in particular polymers.

Homogeneous nucleation is controlled by, amongst other factors, by the temperature of crystallisation and may be described by primary nucleation theory (25-27) by an equation of the form;

$$N = N_o \exp \frac{-(\delta H + \delta \phi)}{k \delta T}$$

where N is the rate of nucleation, N_o is a constant, δH is the energy per unit volume to activate the diffusion of PE chains to the growth front (18,25) and $\delta \Phi$ is the free energy of formation of a critical size nucleus. In polyethylene rapid cooling generally results therefore, in a large number of nucleation sites, and slow cooling (or isothermal crystallisation at higher temperatures) would tend to decrease the number of nuclei formed in a given time interval. At lower temperatures smaller nuclei may exist without the possibility of disruption by random thermal vibrations and reptation (28) of polyethylene chains in the melt, at higher temperatures much larger nuclei would need to be formed for stability.

Growth is envisaged to take place one, two or three dimensionally giving rise to rods, discs or spheres respectively. Crystal growth will be evidenced by a change in lateral dimensions of lamellae (8) or spherulitic radius during crystallisation from the melt. A useful simplification here is that the change in linear dimensions of an object are usually linear with time (29) ie;

$$r = gt$$

where g is called the growth rate. If a polymer melt of mass W_o is cooled to its crystallisation temperature T_m, then spherulites will nucleate at rate N and grow. The total number of nuclei formed in time δt will be;

$$\frac{NW_o \delta t}{\rho_l}$$

After time t these nuclei would have grown into spherulites of radius r. The volume of each spherulite will be $4\pi g^3 t^3/3$. The total mass of spherulitic material δW at time t will be;

$$\delta W_s = \frac{4}{3}\pi g^3 t^3 \rho_s N W_o \frac{\delta t}{\rho_l}$$

where subscripts l and s refer to the liquid and solid respectively. The equation can then be integrated and by writing in terms of W_l we get;

$$\frac{W_l}{W_o} = 1 - \frac{\pi N g^3 t^4 \rho_s}{3 \rho_l}$$

this analysis is highly simplified and neglects the effects when spherulites impinge, which would serve to halt growth after a specified time, and also diffusion effects (18), however it describes most of the features of growth quite well. An analysis by Hoffman et al (14), which treats growth rate g of a single crystal as a function of crystallisation temperature T and other parameters yields;

$$g = g_o \exp\frac{-U}{R(T - T_m^o)} \exp\frac{-K_g}{T \delta T}$$

where δT is the supercooling. Growth rate therefore decreases with the crystallisation temperature. This is not inconsistent with spherulitic growth as observed experimentally. Crystallisation of spherulites is more complicated since the size of the resulting spherulites would also depend upon the amount of crystallisable material available. However in the

same system, crystallisation at low temperatures has been reported to yield large numbers of smaller spherulites, whereas higher temperatures lead to fewer, larger spherulites formed over a longer time scale (30).

1.9 Polymer blends

The production of blends of two or more polymers constitutes an attractive means of controlling macroscopic physical properties and, as a result, this topic has attracted a great deal of interest (31-33). These systems may contain one or more distinct phases and, although the concept of miscibility is often useful in describing how two polymers interact, in the case of blends of linear (LPE) and branched polyethylene (BPE), this aspect of behaviour is unclear (34,35). On the basis of indirect surface morphological studies of quenched samples, Barham and co-workers at Bristol have proposed that liquid-liquid phase separation (LLPS) (35-38) often occurs in polyethylene blends, so leading to a morphology containing distinct domains which are rich in LPE, which then nucleate spherulites in a controlled and reproducible way (38). Arguments based upon diffusion rates were employed (35) to support the assertion that only liquid-liquid phase segregation in the melt; rather than normal homogeneous nucleation, followed by diffusion of LPE rich material to growing spherulites; could be responsible for the domain structure seen in these systems.

Where crystallization occurs less rapidly, additional phase separation processes can influence the morphology (39). Isothermal crystallization at temperatures above those where extensive crystallization of the branched component takes place, leads to the formation of linear-rich spherulites (36,40); effectively, the linear component crystallizes within linear rich domains within a solution of branched polymer, although a degree of co-crystallization inevitably occurs between phases. Since this process of fractionation is a direct consequence of molecular segregation, on the basis of molecular perfection, during crystallization itself, it has been termed liquid-solid phase segregation (LSPS) (36). As a result of the various processes outlined above, a great variety of interesting morphologies (41,42) can be obtained, with thermal treatment and blend composition being the variables used to control the nature of the final microstructure. Thus, blending constitutes a powerful device, by which structural parameters and morphology can be varied in a systematic

manner.

1.10 Dielectric breakdown

Different modifications of polyethylene are widely used as cable insulation, mainly for power distribution, overhead, and particularly underground cables. Early designs used paper and oil for insulation, however with the advent of cheap high quality polyethylene, cable manufacturers quickly adopted these materials with little understanding of their properties, particularly those relating to electrical failure. The hydrophobic nature of polyethylene together with it's good mechanical properties (particularity when crosslinked) and low dielectric constant (2.2-2.3) (48) facilitated it's widespread use as an insulant which was little affected by water penetration. Therefore dielectric breakdown in polymers is a subject which is of great academic and technological interest. However the factors which affect a breakdown event, and the likelihood of an insulator failing, are many and varied, and may include space charge injection (43), impurities and additives (44), defect structures (45) and material parameters (46).

Although it is generally understood that, in the absence of polar solvents, failure occurs when a conducting pathway, which is known as an electrical tree, bridges the dielectric, the mechanisms that lead to this are complex (47,48). A detailed investigation of treeing, although important in the context of dielectric failure, is not the main purpose of the current investigation so brief details are given in line with the context of this study.

Current understanding of electrical tree growth stipulates a three stage process, firstly a critical field is exceeded which is accompanied by charge injection of high energy 'hot electrons', which depends on the work function of the electrodes (49), electroluminescence (50) has been reported to accompany this process. Subsequent photodegradation of polyethylene is believed to occur which results in a degraded voided region adjacent to the electrode (51). The final stage is understood to be due to partial discharges within the resulting voids (52) causing direct damage to the polymer, melting, and chain scission (53). Development of an electrical tree follows by a stepwise propagation of repeated partial discharges leading to eventual failure of the dielectric. In the presence of water or other polar solvents, the situation is further complicated since the water being of high dielectric

constant has been reported to migrate to regions of high electrical stress and cause further electromechanical damage (54) and form what is known as a water tree (55).

Although it is appreciated that structural factors can influence such dielectric failure processes in polymeric materials (48), few attempts have been made to study this area in detail, particularly in relating microstructure and other material properties to electrical breakdown phenomena. Most investigations have adopted crude approaches to the topic of morphology (56-62). Despite this reservation, a number of papers published in the late 70s and early 80s are of particular interest within the context of the work described subsequently. In these, a correlation between spherulitic development and dielectric strength was reported (58-62) and it was argued that the regions between spherulites dominate the breakdown behaviour. Hence, spherulitic development led to reduced electrical strength. Although a number of possible explanations were proposed to account for this behaviour (62), the true reason is still unclear. Wagner (63) showed that the discharge channels in thin polypropylene films were confined to spherulitic boundaries. Leda (64) showed that contradictory to the above data, that the inception voltage of electrical trees increased with spherulitic radius and that the tree channels go round the spherulites, a claim that was substantiated by direct observation of tree channels (65).

Fava (66) and Fischer (67) showed that the dielectric strength increases with increasing molar mass, it was suggested that regions containing low molecular mass material facilitated local breakdown events and partial discharges, possibly due to local voiding intrinsic to these regions.

Therefore much work has been attempted in the field of electrical breakdown, however in many cases results are contradictory and a confusing state of affairs exists. Further to this confusion is the apparent lack of a standard testing technique to assess the insulating properties.

1.11 Measuring and analysis of electrical strength data

There exists a wide variety of different geometries and testing methods to assess dielectric performance in polymers. Most tests involve applying a constant or alternating voltage stress to the insulation and finding out how long it takes to fail under those

conditions.

An electrode geometry that remains popular, due to its ease of implementation, is the needle-plate. However with this geometry problems may occur due to voiding, such as is caused when the needle is inserted, and electric field enhancement at the needle tip, both of which could lead to premature failure. In many cases this geometry is used in detailed studies of tree growth since the field enhancement ensures tree initiation times are low. An alternative geometry to use, which better approximates the geometry found in a cable is plate-plate geometry, however electric field enhancements at the edges of the electrodes may lead to flashovers (68) at the edges of the sample. A similar geometry, which attempts to avoid such problems, is that of opposing ball bearing electrodes. Provided that the radius of curvature of the ball bearings is much greater than the thickness of the sample, then this geometry approximates to a parallel plate system. Flashover at the edges of the electrodes is of course reduced since the electrodes at the edges are at a greater distance away from the sample compared to the equivalent parallel plate geometry. However it has long been recognised that electrode and sample geometries do affect breakdown data (69, 70).

An insulator in service experiences a constant level of electrical stress for many years and usually times to failure of such systems are measured. For comparing properties of different materials, such long term tests are impractical and as a result a variety of short term tests have been devised, two of which are worth mentioning here.

A constant voltage is applied to the sample and the time to failure is measured, with a large number of tests is needed to get an average value for the lifetime of the material. Over the years many distributions and statistical methods have been used to generate some sort of average lifetime data (71), the simplest method being simply to take an arithmetic mean and variance from a normal distribution. However tests, particularly at constant voltage stress, are often analysed using a two parameter Weibull distribution (72) which relates some quantity (Eg: Electrical stress) to the 'failure probability';

$$P_f = 1 - \mathrm{EXP}\left[-\left(\frac{E}{a} \right)^b \right]$$

Where a is the scale parameter and b the shape parameter (equivalent to mean and variance in the normal distribution. Data are plotted on 'Weibull paper' and the failure probability is estimated from the order in which a collection of many samples fail (73). The mean value of time to failure is taken to be that after which 63.7% of the batch of samples fails.

Voltage ramp tests are also widely used, these having the advantage of speed, sometimes many hours may elapse before failure occurs at constant voltage, although the argument could go the other way round, especially if the voltage ramp rate is low. Voltage ramp tests yield different data to constant voltage tests. In a ramp test the voltage applied to the sample is raised at a constant rate and the voltage at which failure occurs is measured. This data is then processed to give a measure of the performance of the material, usually with a modified form of Weibull or with a normal distribution. Laghari et al (74) proposed this type of test with thin film polypropylene specimens. As well as warning of the dangers of extrapolating such data too far, their main conclusion was that for comparative testing such a method compared well with results from constant stress tests.

Usually the chosen electrical test methods and geometry are limited by the equipment and budget available. Meaningful comparisons can still be made, provided one testing method and geometry are adhered to throughout, since even the test method used can affect the data obtained, particularly A.C test frequency (75) and ramp rate (76).

1.12 Thesis background

The purpose of this investigation is to increase understanding of electrical insulation strength, particularly with relation to morphological and molecular variations in well defined systems. Polymer blends have significant advantages over conventional single polymer systems, for instance the amount of crystallisable material can be controlled and well characterised systems of morphology can be obtained reproducibly. The secondary purpose of this investigation is to investigate ways of improving electrical strength in such systems with the aim of producing a better material for medium voltage cable applications, and to this aim the mechanical and thermal properties of such systems shall be investigated from the point of view of a viable industrial process. The rest of the thesis is broadly summed up as follows;

Chapter 2 contains an outline of the experimental techniques, used to carry out this work.

Chapter 3 contains a report on investigations into the effects of thermal treatment and LPE/BPE ratio, in a typical binary PE blend, looking at the effects of morphology on electrical breakdown.

Chapter 4 contains results relating molecular architecture to electrical properties, and contains an examination based upon changing the polymers in a binary blend of fixed LPE/BPE ratio.

Chapter 5 contains an examination of the effects of our testing procedure and also the sample dimensions on electrical strength data. Also in this section an alternative method of formulating blends is considered which is more applicable to industrial processing.

In chapter 6 three different systems, all with very different morphologies are examined and subjected to varying degrees of mechanical tensile stress, to probe the effects of this sort of treatment on morphology and electrical breakdown.

Chapter 7 discusses certain aspects concerned with commercialisation of cables incorporating polyethylene blends as insulants and addresses some practical problems.

In Chapter 8 we report on a simple computer simulation of electrical failure in solid dielectrics in order to quantify certain aspects of our results.

Chapter 9 contains a summary and suggestions for future work.

1.13 References

1) J.W Nicholson, in 'The chemistry of Polymers', Royal society of chemistry, Cambridge, 1991.

2) A.D Horton, Trends Polym. Sci. 1994, **2**, 158.

3) U.W Gedde in 'Polymer physics', Royal institute of Technology, 1992.

4) H.U Voigt, Kautschuk Gummi Kunstst 1981, **34**, 197.

5) S. Venkatraman and L. Kleiner, Adv. Polym. Tech. 1989, **9**, 265.

6) A. Gustafsson, PhD Thesis, Royal Institute of Technology, 1993, p11.

7) R.J Young and P.J Lovell, in 'Introduction to polymers', Chapman and Hill, London, 1991, p249.

8) D.C Bassett, R.H Olley and I.A.M. Al-Raheil, Polymer 1988, **29**, 1539.

9) A Keller, Phil. Mag. 1957, **2**, 1171.

10) P.J Flory, J. Amer. Chem. Soc. 1962, **84**, 2857.

11) F Kloos, S Go, and L. Mandelkern, J. Polym sci. Part B: Polym. Phys. 1975, **12**, 1145.

12) J.R White, J. mater. Sci. 1974, **9**, 1860.

13) A. Nesarikar, B. Crist and A.Davidovich, Jour. Polym. Sci. Part B 1994, **32**, 641.

14) J.D Hoffmann, G.T Davis and J.I Lauritzen in 'Treatise on solid state chemistry', **3**-'Crystalline and non crystalline solids', ed. N.B Hannay, Plenum, New York, 1976, p497.

15) Y.S Yadav and P.C Jain, Polym. comm. 1989, **30**, 229.

16) D.C Bassett and D. Patel, Polymer 1994, **35**, 1855.

17) C.C Puig, M.J Hill and J.A Odell, Polymer 1993, **34**, 3402.

18) H.D Kieth and F.J Padden, Jour. Polym. Sci. Part B 1987, **25**, 2371.

19) B.C Edwards and P J Phillips, Polymer 1974, **15**, 351.

20) D. Patel and D.C Bassett, Proc. R. Soc. Lond. A 1994, **445**, 577.

21) D.C Bassett, Makromol. Chem., Macromol. Symp. 1993, **69**, 155.

22) A.S Vaughan, Polymer 1992, **33**, 2513.

23) A.Keller, J. Polym. Sci. 1959, **39**, 151.

24) A. Thierry, C. Straupe, B. Lotz and J.C Wittmann, Polym. Comm. 1990, **31**, 299.

25) J.I Lauritzen and J.D Hoffman, J. Res. Nat. Bur. Stand. 1960, **64a**, 73.

26) J.I Lauritzen and J.D Hoffman, J. Res. Nat. Bur. Stand. 1961, **65a**, 297.

27) J.D Hoffman and J.J Weeks, J. Chem. Phys 1962, **37**, 1723.

28) J.D Hoffman and R.L Miller, Macromolecules 1988, **21**, 3038.

29) R.J Young and P.J Lovell, in 'Introduction to Polymers', Chapman and Hill, London, 1991, p278.

30) J M Rego-Lopez and U.W Gedde, Polymer 1989, **30**, 22.

31) D.R Paul and S. Newman, 'Polymer blends', **1**, Academic Press, New York, 1978.

32) D.R Paul and S. Newman, 'Polymer blends', **2**, Academic Press, New York, 1978.

33) D.J Walsh in, `Comprehensive Polymer Science', **2**, Polymer Properties, eds. C.Booth and C. Price, Pergamon Press, Oxford, 1989, p135.

34) R.D Alamo, J.D Londono, L. Mandelkern, F.C Seehling and G.D Wignall Macromolecules 1994, **27**, 411.

35) P.J Barham, M.J Hill and C.C.A Rosney, J. Mater. Sci. Letts. 1988, **7**, 1271.

36) M.J Hill, P.J Barham, A Keller and C.C.A Rosney, Polymer 1991, **32**, 1394.

37) M.J Hill and P.J Barham, Polymer, 1992, **33**, 4891.

38) M.J Hill, P.J Barham and A Keller, Polymer 1992, **33**, 2530.

39) S.R Hu, T Kyu and R.S Stein, J. Polym. Sci. Part B: Polym. Phys. 1987, **25**, 71.

40) J.M Rego-Lopez, M.T Conde-Braha, B Tenselius and U.W Gedde, Polymer 1988, **29**, 1045.

41) D.R Norton and A Keller, J. Mater. Sci. 1984, **19**, 447.

42) A.S Vaughan, Polymer, 1992, **33**, 2513.

43) G Krause, D Meurer and D Klee, IEEE. Trans. Electr. Insul. 1989, **24**, 419.

44) M Nagao, I Konba, T Tsurimoto, Y Mizuno and M Kosaki, Ann. Report of Conf. on Electrical Insulation and Dielectric Phenomena, Victoria B.C. 1992, 148.

45) E.A Franke, J.R Stauffer and E Czekaj, IEEE Trans. Electr. Insul. 1977, **12**, 218.

46) P.J Phillips, IEEE Trans. Electr. Insul. 1978, **13**, 69.

47) P Fischer in `Electrical Properties of Polymers', ed. D.A Seanor, Academic Press, New York, 1982, p319.

48) C.C Ku and R Leipins in `Electrical Properties of Polymers', Hanser, Munich, 1987.

49) A. K. Vijh and J. P Crine, J. Appl. Phys. 1989, **65**, 398.

50) S. S Bamji, A.T Bulinski and R.J. Densley, J. Appl. Phys 1988, **63**, 5841.

51) R. Patsch, IEEE Trans. Electr. Insul. 1992, **27**, 532.

52) G.C Crichton, P.W Karlsson and A. Pedersen, IEEE Trans. Electr. Insul. 1989, **24**, 335.

53) K. Uchida and N. Shimizu, IEEE Trans. Electr. Insul. 1991, **26**, 271.

54) Y. Poggi, V. Raharimalala and J. C Filippini, IEEE Trans. Electr. Insul. 1990, **25**, 1056

55) E. F Steennis and F. H Kreuger, IEEE Trans. Electr. Insul. 1990, **25**, 989.

56) R Cooper, B.R Varlow, D.R Edwards, P.B MacAllister and T.J Carter, Ann. Report of Conf. on Electrical Insulation and Dielectric Phenomena, Boston, 1980, p220.

57) P.H.H Fischer and K.W Nissen, IEEE Trans. Electr. Insul. 1976, **11**, 37.

58) S.N Kolesov, Elektrichestvo 1970, **9**, 84.

59) S.N Kolesov, Polym. Sci. USSR. 1980, **21**, 1993.

60) S.N Kolesov, IEEE Trans. Electr. Insul. 1980, **15**, 382.

61) H Wagner, 1974 Ann. Report of Conf. on Electrical Insulation and Dielectric

Phenomena ,IEEE, Washington D.C. 1975, 62.

62) B.V Ceres and J.M Schultz, J. Appl. Phys. 1984, **29**, 4183.

63) H. Wagner, Ann. Rep. CEIDP, National Academy of Sciences-NRC Washington DC, 1975, 62.

64) M. Leda, M. Navata and H. Kawamura, Proc. 4th ISH, paper 22.03, Athens, 1983.

65) N. Hozami, T. Okamoto and H. Fukagawa, Jap. Jour. Appl. Phys. 1988, **27**, 1230.

66) R.A Fava, Proc. IEE 1965, **112**, 819.

67) P. Fischer, Ann. Rep. CEIDP, National Academy of Sciences-NRC Washington DC, 1975, 661.

68) H. C Miller, IEEE Trans. Electr. Insul. 1993, **28**, 512.

69) J. H Mason, IEEE Trans. Electr. Insul. 1991, **26**, 318.

70) R. Lovell, IEEE Trans. Elec. Ins. 1976 ,**11**, 110.

71) M. Cacciari and G.C Montanari, IEEE Trans. Electr. Insul. 1991, **26**, 1112.

72) M. Cacciari, G. Mazzanti and G.C Montanari, IEEE Trans. Diel. Elec. Ins. 1994, **1**, 153.

73) J.C Fothergill, IEEE Trans. Electr. Insul. 1991, **26**, 1224.

74) J.R Laghari, P. Cygan and W. Khechen, IEEE Trans. Electr. Insul. 1990, **25**, 1180.

75) J.H Mason, IEEE Trans. Electr. Insul. 1992, **27**, 1213.

76) D.M Tu, W.B Liu, G.P Zhuang and Z.Y Liu, IEEE Trans. Electr. Insul. 1989 ,**24** , 589.

CHAPTER 2- EXPERIMENTAL PROCEDURES

2.1 Introduction

This chapter outlines the key experimental procedures involved in this work, many of these procedures are routinely used (ie: transmission electron microscopy) so will only be covered briefly for completeness. Other techniques are refinements of existing methods, or are completely new, and as such require detailed explanation.

2.2 Polyethylene blend preparation

Mixing together two polymers to form a blend and obtain a homogeneous mixture is not a new procedure (1-8). Many commercial plastics are in fact blends, where this term is used to describe a mixture of two or more materials, for example linear polyethylene with low density polyethylene. Blending offers materials which can combine the properties of two or more different materials to meet increasing demands for high performance materials, or as a tool for investigating microstructure (1). To achieve this, two main techniques are widely used to form blends, both of which are routinely used and are described here. Solution blending (1-6, 8), which gives high quality blends but with low output, and melt mixing which gives large amounts of blends of somewhat less quality (7).

2.2.1 Solvent blending procedure

There are two prerequisites for solvent blending, firstly the polymer must be soluble in the solvent selected and secondly the resulting blend must be able to be precipitated easily out of solution. Xylene was chosen here as it widely used to dissolve and mix many polymers (1-6), although other solvents (8) are sometimes used. Methanol was chosen as a non-solvent, in which to recover the blend. A concentration of 1% w/v (polymer/xylene) was used, with appropriate amounts of the polymers weighed out on a Griffin digital 4 balance. For example a 10% blend of LPE in BPE was composed of 0.2g of LPE and 1.8g of BPE, in 200ml of xylene. A refluxing apparatus was used to prepare the blends, this is to comply

with COSHH regulations, and so that none of the solvent or polymer is lost through evaporation. All operations are carried out in a fume cupboard as particular care must be taken not to inhale solvent vapours. The polymer and xylene were placed inside a round bottomed flask which was heated by a stirrer mantle (Electrothermal Model MA 250ml).

The mixture was heated to boiling point (140°C for p-xylene) within the stirrer mantle, and simultaneously stirred by use of a magnetic stirrer bar. The heat was turned down once the xylene was boiling gently and the mixture was left for ten minutes, at which point none of the pellets were visible. Next twice the volume of methanol, as xylene, was placed in a pyrex beaker and cooled to around -10°C by standing on a pellet of dry ice for 10 minutes, which was stirred occasionally to prevent local freezing. Once the methanol had cooled, the hot xylene/polymer mixture was poured onto the methanol quickly, whilst simultaneously stirring the methanol vigorously, the polymer then precipitated out as a white mass. This material was then filtered to remove most of the solvent, and the resulting polymer was left in the fume cupboard to dry overnight. The remaining glassware was then cleaned in hot xylene to remove all traces of polymer.

The polymer was next placed under vacuum (Harvard/LTE Qualivac oven with Edwards rotary pump) at 40°C for 36 hours to remove the remaining solvent. At this point the odourless blend was in the form of a porous solid. This was then melted for about 1/2 hour under vacuum at 180°C, to remove any included air, and to turn it into a more compact form, which was easier to use.

2.2.2 Melt blending procedure

This procedure mixes directly the melts of the two polymers and has the advantages of producing greater quantities of material, 400g or so, at once, but with more impurities than a solution blended equivalent. A Winkworth twin z blade mixer, model 1Z, was used here with a heated jacket enclosing the mixing chamber, the procedure was as follows;

The chamber was first cleaned to minimise contamination in two stages; firstly with Scotchbrite pads at ambient temperature to remove all visible signs of polymers. Then when the chamber had been heated to around 160°C, 300g of LDPE (but usually the majority component in the blend to be prepared) was introduced into the chamber. This was mixed

continuously at approx 40rpm under a nitrogen blanket, until it had completely melted (about ten minutes) and had became a dirty brown colour. This polymer was removed completely and put to waste and this process was repeated until the polymer came out clean.

Then for the blend proper; the polymers were weighed in the required proportions[2] and added to the preheated chamber, the motor was then switched at 40 rpm for about 20 minutes, or until all the polymer had visibly melted. The motor was then switched to a higher speed, 80rpm, to mix the polymers for a further 5 minutes, the motor was then switched off and the molten polymer, which had a tendency to collect on the chamber walls above the blades, and therefore not get mixed, was scraped down. This latter process was repeated about 8 times in total. The molten polymer was then removed from the chamber as much as possible and placed into a water bath to cool, after which it resembled very hard shiny silvery blocks.

The air was removed from these samples by heating to 160°C under vacuum, in aluminium foil trays. Over 24 hours the polymer melted and the air was drawn out by the vacuum. The sample was checked visually for air, and if no air bubbles remained, was then removed from the oven and cooled, at which point the foil was peeled away and the blend was ready for use. In situations where the foil was difficult to remove, it was dissolved away in a 50:50 mixture of distilled water and concentrated hydrochloric acid, which dissolved the foil but left the polymer intact.

2.3 Sample preparation-introduction

Samples of polymer blend now needed to be made into the required form, this depended upon its final use. Before using any blends their homogeneity was quickly checked by melting, in turn, typically 4-5 small pieces per blend taken from random pieces of the final product, in the DSC (sect. 2.4.1), no inhomogeneity was detected in any of the blends that were prepared, as detailed in the following chapters.

For electrical tests thin (below about 150 μm in thickness) disks are required, for examining microstructure surfaces of thin disks are undesirable, as normally internal

[2] Again the proportions of the components used were measured by mass, as in the previous procedure.

sections are required, because external surfaces can be unrepresentative of internal structure. Some care had to be exercised though, that the (thick-1mm) samples used for microstructural examination were representative of their thin counterparts used for electrical examination otherwise a comparative study would be meaningless. In reality the electrical disks were also examined and compared to the samples made for morphological examination. This was randomly carried out throughout, with no observed discrepancy between the two sample sets.

2.3.1 Specimens for morphological examination

Samples for the main morphological studies were prepared by manually pressing around 20mg of sample between a clean microscope slide and a 22mm square cover slip. Initially the polymer was heated to 180°C by a Koffler hotbench (type WME) turning the sample over regularly. When the sample had melted it was pressed to a disk of about 15mm in diameter with thickness 1mm. The means of subsequent crystallisation at a specific temperature here was provided by a Mettler FP 5 hotstage, which was attached to the stage of a polarising microscope.

One of the problems that was found with pressing the polymer samples was that a high degree of stress is imposed upon the polymer and this if left by itself would affect the final morphology, usually what was seen was a non-uniform distribution of spherulites. To remove such effects of stress, the sample was allowed to relax with no pressure for about 5 minutes after pressing to the required shape, which cured this problem. In addition it was possible to observe samples during the crystallisation in the FP5 hotstage, as detailed in section 2.6.2. Imaged in this way polymer melt appeared black whereas crystallised material appeared white, so a first estimation of crystallisation time was possible by this method, as well as a second check for any inhomogeneity introduced by the blending procedure, which might again be evidenced by a non-uniform distribution of spherulites (Figure 2.1).

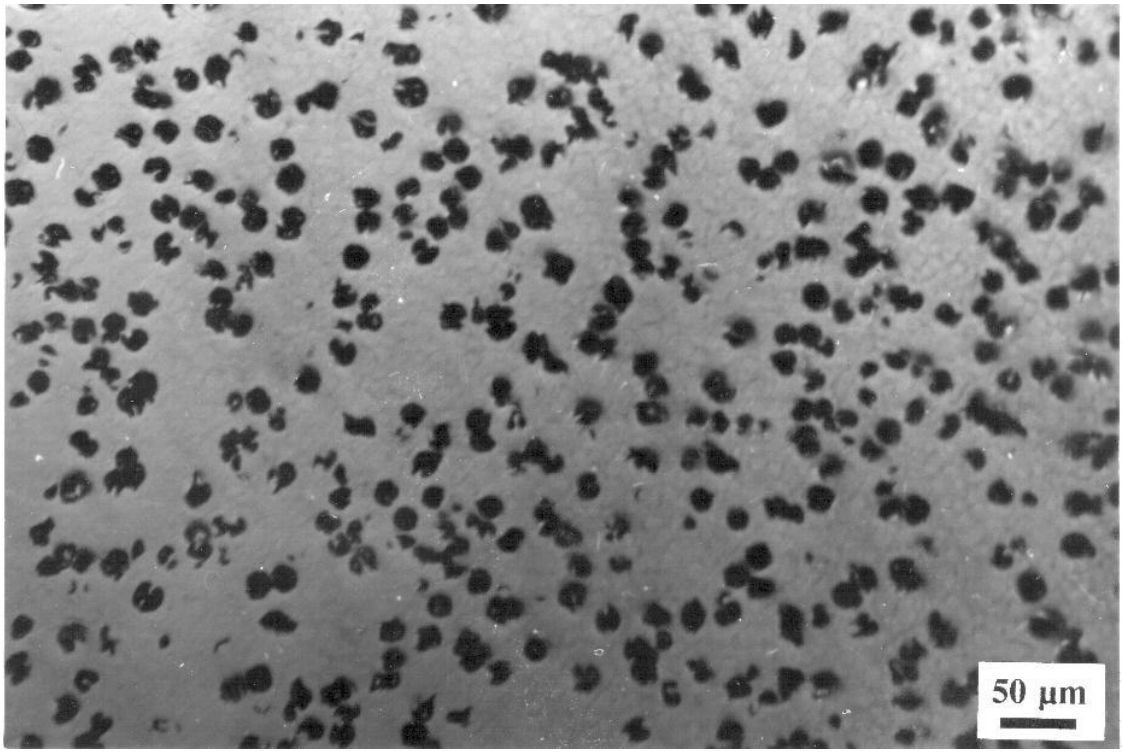

Figure 2.1(a): Homogeneous distribution of spherulites in a blend of 7% linear polyethylene (Rigidex 4901) in 4901 branched polyethylene crystallised at 124°C.

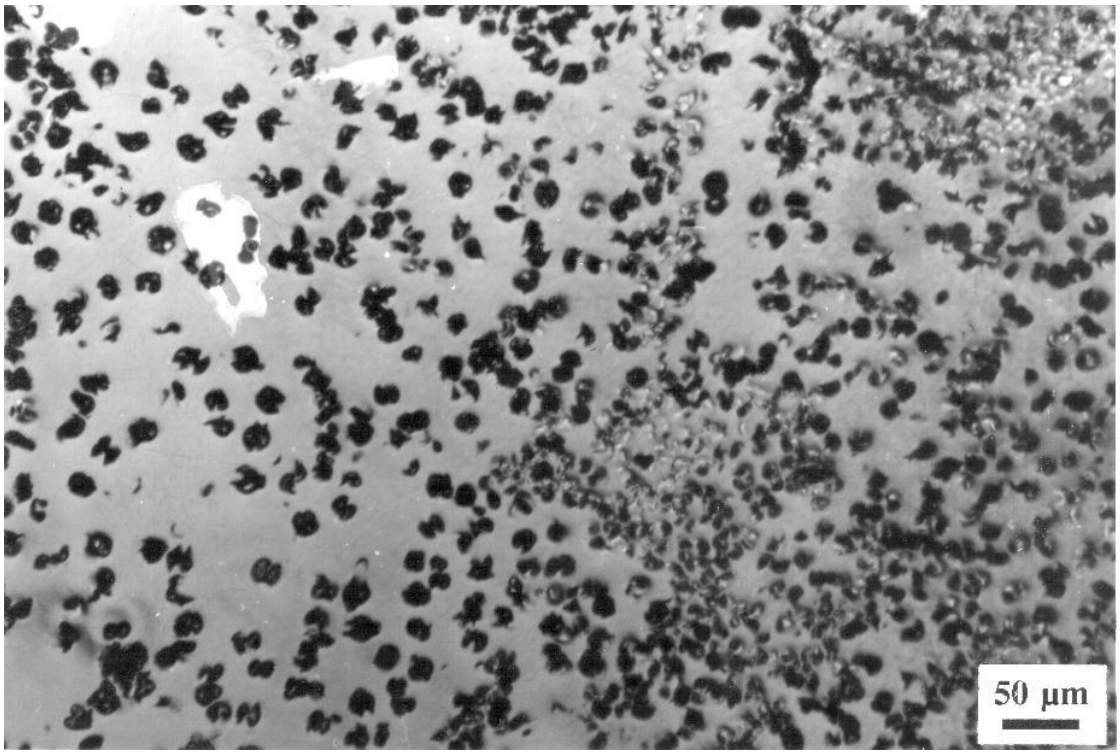

Figure 2.1(b): The same blend but showing an inhomogeneous spherulitic distribution.

For more quantitative estimates of crystallisation times, the DSC (section 2.4.1) was used to measure crystallisation times accurately. However the former method enabled time to be saved, since samples did not then have to be left for longer than necessary in the DSC.

After crystallisation was complete, samples were quenched into an ice/water mixture. Samples were removed from the slides by soaking in water then carefully prising them apart.

2.3.2 Samples for electrical testing

Limitations on the test voltages available for electrical testing, places an upper limit on the thickness of samples of about 150 microns. Clearly, samples this thin could never be produced by manual pressing, to this thickness or uniformity required for sensible electrical testing to be carried out. Previous studies (9,10) also indicated that for reproducible results to be obtained, samples with known and accurate geometries were required, as sample thickness is known to affect electrical strength measurements.

The press used was a Grasby Specac model 25.011 with heated platens and constant thickness film maker, specifically designed to meet these two requirements. The film maker kit has spacer rings for various thickness samples to be made up and the disks produced were about 2.5cm in diameter allowing about 5 electrical tests to be made on each without risk of electrical flashover (11) which would cause premature failure and invalidate the results. The film maker die, being detachable from the press and having a high mass, enabled samples to be transferred to a Grant model W28 oil bath, for crystallisation, quickly with negligible cooling.

All samples were pressed in turn between two clean aluminium sheets having thickness of 10 microns each. This was done to keep the polymer free from contaminants from the press, and to make the sample easier to remove from the die once pressed.

For an example of usage; to make a 75 micron thick disk, the 100 micron spacer ring was chosen, and about 80mg of polymer was placed centrally between the aluminium sheets, and then the die was positioned between the heated platens held at 180°C. The polymer was then allowed 5 minutes to melt before the pressure was brought to 2.5 tons, and the system was left in this state to relax for a further 5 minutes after which the load and die were removed. The disk was then removed whilst still hot for immediate placement into the

Grant temperature controlled oil bath for subsequent isothermal crystallisation followed by quenching, or straight into ice/water, depending on the required processing.

After crystallisation the resulting disks were removed from the foils, then washed in distilled water and then vacuum dried at ambient temperature, before use for about 12 hours. This vacuum drying was necessary to remove any absorbed water which could have affected the electrical data (12).

Since the polymer is contained between aluminium sheets whilst it is being used the specac film maker itself requires little cleaning, an occasional wipe with a drop of acetone and a soft cloth, when cold being sufficient. For film thicknesses not available with the spacer ring set supplied, small sheets of 'Kapton' were placed over the lower die plate to reduce the film thickness accordingly.

Some films prepared in this way were etched (see section 2.5), and the spherulitic distribution was examined, spherulites were uniformly distributed throughout the disks examined, provided that the disks had been allowed more than 2 minutes to relax after pressing.

2.3.3 Samples for mechanical testing

Samples for testing of mechanical properties needed to be of a regular and reproducible shape, since when measuring stress in a sample the dimensions are important. The shape used most commonly for tensile testing is the dumbbell because at high strains strip like samples tend to neck prematurely due to uneven deformation at their clamping points (13).

The samples were initially prepared in the form of flat sheets between clean copper sheets, one of which had a thin spacer rim around it's edge, about 1mm in thickness. 10cm x 20cm sheets were prepared with 20g of polyethylene, which was placed centrally in between the sheets. The complete mould was placed into a large area flat plate hydraulic press with heated platens maintained at 180°C. The heated plates were moved together so they just touched the two copper plates, for about 5 minutes, which allowed the material to melt. When the material had visibly melted and no pellets were noticeable, 2 tons of pressure was then applied to the system and then it was allowed to relax for around 10 minutes. The pressure was then removed, and the entire mould was taken for quenching or isothermal

crystallisation, as required, in the Grant oil bath (see above). The sample was then removed from the mould by soaking in water and prising apart gently with a screwdriver blade.

Dumbbells were cut from the sheet by a manual dumbbell cutter in a small mechanical hand press, the dumbbells used throughout had gauge length 20mm and width 4mm. Etching selected areas of sheets confirmed that the distribution of spherulites was uniform, if the relaxation time was at least 5 minutes.

Experimentally it was found that the thin film samples prepared for electrical tests, could be used for mechanical testing, if they were cut into strips about 20mm wide with parallel sides, and if all traces of their rims were removed. With films cut in this way electrical tests could be performed on previously strained samples. The mechanical properties of the films were verified against the dumbbell samples, the two correlated up to 120% strain, after which the films tended to tear.

2.3.4 Microtomy

The morphology of the surface of a sample will not in general be representative of its internal microstructure, since the boundaries impair the growth of spherulites, so a means of generating an internal surface is essential. The process of microtomy as routinely used at Reading, involves the use of a freshly broken glass knife (glass is far sharper than any metal edge) to remove layers from the surface of the polymeric sample. A Bright rotary retracting microtome was used to carry out this work, which is manually operated.

The sample was embedded onto the sample holder, in a pool of Cryo-m-bed (Taab Laboratory Equipment Ltd). The sample holder was then cooled using dry ice and when the embedding compound had solidified was mounted onto the microtome head. This cooling process, as well as solidifying the embedding compound, which fixes the sample onto the holder, often assists the cutting process, since at low temperatures many materials became brittle and easier to cut. Glass knives were cut using an ultramicrotome glass knife maker, glass knives were used at ambient temperature and were not cooled.

In this work with polyethylene the cutting speed was found to be critically important, it was found that a lower speed generated less knife damage, just as important is the thickness cut per step which to avoid extensive sample damage needed to be minimised as well. For

polyethylene a speed of 20-30 passes per minute at 2-5 microns thickness was found to be the optimum cutting conditions with minimum sample damage and was used throughout. Knives generally needed replacing at least once during the cutting process, especially towards the final stages of cutting, failure to do this resulted in a very 'rugged' microtomed surface, since the blade became blunt and scored the surface. Typically a layer of thickness 0.1 - 0.5 mm was removed by microtomy prior to etching.

2.4 Material characterisation

2.4.1 Differential scanning calorimetry

Since differential scanning calorimetry is a standard technique, we shall only detail our procedures for using the instrument and collecting data here.

The system at Reading, a Perkin Elmer DSC 2C, is semi-automatic with an IBM compatible computer logging the data, but with the experimental conditions having to be set manually. For all DSC runs, about 3-4mg of sample was placed inside an aluminium can which together with an empty reference pan, occupy two temperature controlled enclosures. Heat flow is measured as a function of temperature or time, in the normal way, via an analogue to digital card (MC^2 Thermal Systems). MC^2 Thermal Systems v9.11 thermal analysis software was used to collect and analyse the data.

Calibration of the instrument occurred in several steps, firstly the instrument was calibrated roughly at monthly intervals for heat flow, using a sapphire of known heat capacity. Before each experiment, the instrument was calibrated with high purity indium (T_m= 156.60°C) for the temperature axis. This was also done at each heating rate used, normally for melting runs, one heating rate was used throughout, this was 10 K/min.

The heat capacity of the metal cans was taken into account and removed from the data using the following procedure; a can for the sample was selected having a similar mass to the reference pan and both empty pans are run and data collected as if an experiment was in progress. Next the sample was added and the run repeated, data from both runs was subtracted and the resultant output was the heat flow and thermal characteristics of the sample. All DSC data was then further normalised for heat flow per unit mass, to enable

meaningful comparisons between samples.

For isothermal runs, the temperature was controlled manually and the instrument instead collected data as a function of time. First an isothermal run was performed using empty cans as detailed above, at the required crystallisation temperature for the required time period. The sample of interest was then added to the can and then melted at 180°C for 5 minutes. The temperature was then decreased as fast as possible down to the crystallisation temperature, data was then collected, starting at the point where the temperatures of the pans reached a steady state after cooling, this avoided instrumental transients appearing in the data. The two data sets were then subtracted and crystallisation times were estimated from the resulting exotherms.

2.4.2 X-ray diffraction

In looking at mechanical deformation of our polymeric blend systems it was useful to have an indication of the extent of orientation of the crystals brought on by the applied strain. X-ray scattering is a diffraction process, whereby crystals act somewhat similar to diffraction gratings as used for optical scattering; here X-rays are scattered due to differences in electron density. A set of parallel crystal planes scatter X-rays at a characteristic Bragg angle, ß, dependent on the spacing between adjacent crystals d [3], and the wavelength l, of the X-rays used (14).

$$l = 2d\sin\beta$$

Crystal spacings are relatively large (10-40nm) so they scatter X-rays through small angles. In the case of polymer lamellar crystals, additional scattering processes occur from planes of polymer chains within lamellae, these planes having much smaller separation, scatter X-rays through wider angles. Hence the terms *wide angle* and *small angle* x-ray scattering. Since in practice the magnitudes of scattering due to these two processes are different, X-rays from each are collected and processed separately.

[3] This is referred to as the *long spacing* since the gap between crystals also includes amorphous spaces between.

Consider the case of an undeformed sample, here crystalline lamellae are randomly oriented in space so the scattering is similar in all angular directions. On a parallel plate film, at a constant distance from the sample, a set of rings is produced corresponding to the solid angle of scattered X-rays at the characteristic Bragg angle. When samples are deformed, lamellae which become oriented by the applied strain, result in scattering that is not the same in magnitude across the whole of the solid angle, so instead a set of arcs is observed, the extent of which can tell us about the average degree of crystalline orientation (13).

Wide angle scattering was performed on a Philips PW1730/10 X-ray generator. The Cu Kα radiation was monochromatised by a graphite crystal to 0.15418nm. The X-ray patterns were recorded on photographic plate film using a pinhole collimator and a sample-film distance of 37mm. The beamstop was a small lead pellet (diameter 2mm) mounted at the centre of the film carrier. The equipment was calibrated using 350 mesh silicon powder which gives a characteristic scattering angle of 28.46°. With 4mm thick dumbbells, the exposure time was found to be 45 minutes to give a visible scattering pattern. For calibration the exposure time was 2 hours with a thin PE film (70 microns) lightly dusted with silicon powder, such an arrangement enabled the Si ring which is much fainter than the PE rings to be distinguishable.

Small angle scattering was performed on a Philips PW1120/90 X-ray generator again with Cu Kα radiation at 0.15418nm with pinhole collimation. X-rays were recorded on plate film loaded into a Rigaku-Denki small angle vacuum camera pumped by an Edwards rotary pump, the sample-film distance being 240mm. A sharp edged lead beam stop (diam. 1.4mm) was located in front of the film holder, held in place by a fine wire. Exposure times of 4 hours were used to generate a visible pattern.

2.4.3 Mechanical testing

A distinctive feature of the behaviour of polymers is that their response to a mechanical loading depends upon the rate of loading and the time period involved. This behaviour is in contrast to that of elastic solids such as metals, which at least at low strains, obey Hooke's law and that of viscous liquids where the mechanical behaviour is time dependent and obeys

Newton's laws. The observed mechanical behaviour of polymers lies somewhere in between that of elastic solids and viscous liquids and has been termed viscoelasticity (15). The phenomenon of creep is well known, a constant load is applied to a polymeric material and a gradual increase in the strain is observed, this thought to be due to the time taken for polymer chains to disentangle and take up new conformations. Similarly chain entanglements serve to slow the decrease in strain upon removal of the load (15). Such mechanical properties are important in terms of processing and usage, for instance in electrical cables, where the polymeric insulation can be subjected to mechanical strain during extruding and installation, or in engineering applications where a sustained loading may be applied. Understanding the deformation (strain) in a material brought about by a certain applied force (stress) is important, so simple stress-strain relationships are the first stage in understanding mechanical properties.

A Monsanto T 2000 tensile tester was used to apply mechanical loading to polymeric samples, the bottom end of the sample was clamped, whilst the top was attached to a motor driven crosshead, the sample was held in pneumatic clamps. The strain in the sample was measured by the crosshead position, whilst the stress was measured by a piezo-electric force transducer. Supplied T 2000 software, running under OS/2 provides output as a stress-strain graph, which was produced from the measurements and sample dimensions. Prior to use the crosshead was moved so the two clamps were 20 mm apart, the stress and strain were set to zero and the sample was then inserted. A thermocouple was placed on the sample which enabled it's temperature to be measured. Two types of test were performed;

In the mechanical tests performed here the samples were subjected to a degree of deformation (strain) and the stress required to do this was measured, at a crosshead speed of 10 mm/min. All samples were left in the tester for 5 minutes once the final strain was attained before being released. If stress needed to be measured during relaxation the speed was set to 10 mm/min and the head was allowed to return to it's original position at this speed whilst recording the stress, the sample was then released immediately.

Some runs involved heating samples in situ, to do a test of this nature the required strain was applied to the sample as above, it was then allowed to relax for 5 minutes at constant strain, then heat from a hairdryer was applied whilst the stress was measured. The sample was then released after cooling to room temperature for 10 minutes.

It became clear that the sample would relax in the hours following deformation so it was vital to perform subsequent tests on the sample certainly within a few hours of straining the sample. Film samples for electrical testing were normally tested the same day, immediately following deformation. For morphological examination, the dumbbells were sandwiched between two sheets of a block copolymer elastomer (trade name Cesskapol) using a small drop of toluene, which effectively halted the relaxation process and enabled examination at leisure.

2.4.4 Dynamic mechanical thermal analysis

In a viscoelastic material, if a stress is applied some time will elapse before the strain reaches it's full value for that applied stress, therefore the resultant strain will lag behind the applied stress. The same thing would occur if the stress were removed, the strain in the material would take some time to reduce back to zero. If a sinusoidally alternating stress was applied to the sample of the form:

$$\sigma = \sigma_o \sin(\omega t)$$

The time lag between the applied stress and the resulting strain can be written in terms of a 'phase lag' δ;

$$\varepsilon = \varepsilon_o \sin(\omega t + \delta)$$

For a perfectly elastic material δ would be zero, but for a viscoelastic material δ would depend on molecular properties of the material, which are closely linked with mechanical properties such as hardness.

Here we are particularly interested in determining the glass transition temperature T_g, which corresponds to the onset of chain motion, an essentially mechanical phenomenon. Below T_g mechanical deformation tends to deform chemical bonds within polymer chains, similar to deforming a metal, whilst above T_g mechanical deformation can cause chains to slide over one another, therefore viscoelastic behaviour is more pronounced. This

mechanical transition is exhibited as a change in δ, although tan δ is usually measured. In the context of deformed samples, an accurate determination of glass transition temperature is important as the presence of microvoids or cavities, in giving extra space in which molecules can move, may be detectable by a drop in the glass transition temperature. A technique called dynamic mechanical thermal analysis (DMTA) enables tan δ to be determined as a function of temperature.

The system used for the DMTA work was the Rheometrics RSA II Materials tester running in dual cantilever mode, located at the National Grid Science and Technology Laboratories, Leatherhead, with supplied Rhios software running under DOS. Samples, of dimensions 50 mm long by 6 mm wide were located in a pair of clamps located in a temperature controlled enclosure. One clamp which connects to the centre of the sample, carries the driving strain of amplitude 2-3 mm, whereas the other clamp which fits to the two ends of the sample, measures the stress, via a piezo electric transducer.

Two standard routines supplied with the software package were used, constant frequency with temperature sweep to find T_g, and constant temperature with frequency sweep, which was used to find a suitable operating frequency for the geometry used. Prior to use the system was calibrated with test masses and a steel strip as detailed in the calibration instructions supplied with the equipment. The Rhios software was used to control the runs and determine tan-delta. For temperatures beyond 60°C samples tended to slip inside the tester, and the minimum temperature available was -150°C.

To find the best vibrational frequency suitable for the geometry used, the value for T_g was estimated by a temperature sweep at an arbitrarily chosen frequency of 50 rad/s. The temperature was then fixed at -115°C and the frequency of testing was varied within the range possible with the equipment, from 1-200 rad/s, 100 rad/s was found to give a peak in the T_g transition, so was used throughout to look for changes in T_g, however the frequency used was not too critical.

2.4.5 Methods for estimating spherulitic size

Estimating the sizes of spherulites within a sample has difficulties, for instance in a surface, a variety of different cross sections through spherulites are available and these can

easily lead to an erroneous determination of spherulitic size. Furthermore a method of manually measuring the size of each spherulite, from a distribution in a micrograph for instance, to get an average would be very time consuming.

The problem of counting the number of spherulites in a certain area is less difficult, and providing the number of spherulites counted was high and was over a large sample area then a fairly accurate statistical average could be made.

In the blends considered here the spherulite sizes have been estimated by evaluation of SEM micrographs by the Cambridge Instruments Quantimet 570 system at Leatherhead. Spherulites from SEM micrographs which had been corrected for sample tilt were outlined by hand with each picture containing typically 20-30 spherulites. For each sample three such pictures were analysed by scanning the images into the system using a small video camera. The system could then analyse the perimeters of the spherulitic shapes and work out an equivalent circle diameter. In this way spherulitic sizes could be estimated relatively quickly in a way that was consistent, to an uncertainty of about 10%.

Estimating spherulitic number density was done initially by manually counting spherulites in a given area from optical photographs containing about 100 spherulites each, marking each spherulite with a dot of ink as it was counted. These results were then confirmed by the results from the Quantimet system.

2.5 Permanganic etching procedure

An understanding of materials has always required a knowledge of their physical structure as well as their chemical composition. In semi crystalline polymers, a knowledge of the spatial distribution of crystalline structures and amorphous regions is important in characterising such systems fully. Etching by chemical reagents, has attempted over the years to separate the crystal structure from the surrounding amorphous material thus rendering both phases amenable to examination. A standard technique, which has been routinely used on polyethylene and many other polymers, is permanganic chemical etching (16-18). Such etchants are well tried and give consistent and reliable results (19,20), the chemical etchant preferentially attacks amorphous regions leaving crystals standing proud of the surface and amenable to examination (16,20).

Two types of etchant were used consistently in this study;

The first gives superb lamellar detail, which was used with all the samples examined by transmission electron microscopy, was composed of 1% (w/v) potassium permanganate) mixed into 1:2 phosphoric:sulphuric acid. The second etchant, developed as a variant on the first, was ideally suited for SEM and optical work and gives crisp lamellar detail, but is less suitable for replication due to the somewhat rougher surfaces it produces. It is made from 1% (w/v) potassium permanganate in 1:4:10 parts water:phosphoric:sulphuric acid (16). The acid mixtures are made up and stored separately from the permanganate, which must be mixed with the relevant acid mixture immediately prior to use using the following procedure;

A relevant quantity of the acid mixture, as described above, (about 12ml per sample) was poured into a flask in the fume cupboard and was stirred vigorously whilst slowly adding the potassium permanganate. The mixture was left to mix at room temperature, for 10 minutes after all the permanganate had been added. The samples were then placed into suitable glass vials, with PTFE lined lids, and the etchant mixture added. After replacing the lids (not tightly), the vials were shaken vigorously in a Edmund Buhler KL2 sample shaker. The etching time was 4 hours, after which the etchant was mixed with hydrogen peroxide solution to neutralise the etch (produce manganese dioxide) and the samples removed, washed in distilled water and vacuum dried for 1 hour in accordance with published procedures (17).

2.6 Microscopy-overview

The science of microscopy is concerned with the mechanisms of imaging microscopic detail which can range from scales of several hundred microns (spherulites) to the nanometre (lamellar) level. In polymer physics many methods of imaging are used, but we shall concern ourselves here with the three methods routinely used at Reading; Optical microscopy, Scanning electron microscopy (SEM) and Transmission electron microscopy (TEM).

2.6.1 Optical microscopy

Optical microscopy was used routinely throughout this work for checking for sample damage after microtomy (sect.2.3.4), verifying spherulitic distributions in situ (for instance on the FP5 hotstage whilst crystallisation was occurring) and for assessing the extent of permanganic etching. Optical microscopy was not used for quantitative work, since electron microscopy gave better detail of morphological structures. Two types of microscope were used routinely, a polarising microscope which was used with the Mettler FP 5 hotstage, and a Zeiss reflection microscope. Both of these instruments have two eyepieces, which reduce the eyestrain associated with conventional single eyepiece microscopes. In both cases the magnification is the product of the eyepiece and objective magnifications.

2.6.2 FP 5 Polarising Microscope

The microscope which the Mettler FP 5 hotstage is mounted on, is a Vickers universal polarising microscope. The sample in the FP 5 hotstage is illuminated by a tungsten lamp from below, which is plane polarised by a small piece of polaroid filter, through a small window. Light is collected after passing through the sample by a conventional microscope assembly, mounted above the hotstage. The analyser is set so that its polarisation direction was set to 90° to the lower filter, this way the image in the eyepiece appeared dark with no sample inserted into the FP 5 hotstage. When a sample was allowed to crystallise in the stage, spherulites, which contain macroscopic ordered regions, changed the polarisation of the transmitted light away from the initial direction, causing some to pass through the second filter to the eyepiece. Once focused, spherulites in the sample therefore appeared white, compared to darker amorphous or uncrystallized regions. This microscope was used to check whether spherulites were uniformly distributed, and also to estimate crystallisation times from observations of spherulitic growth.

2.6.3 Zeiss reflection microscope

Etched sample surfaces were imaged in reflection using a Zeiss large universal optical

microscope, the sample being illuminated from above. The microscope employs the differential interference contrast (Nomarski) method of imaging; light from the lamp is split into two plane-polarised beams by a Wollaston prism, each being slightly displaced laterally at the sample plane. Reflected light is then re-combined and contrast is then due to the phase difference introduced between the two beams which is due to the surface topography of the sample. This image is then magnified by conventional optics.

This microscope was routinely used to check samples for microtome damage, which if excessive could cause replication and imaging problems later on, and to qualitatively examine sample morphologies, specifically to find areas of interest on samples for detailed examination by electron microscopy.

For some types of observation the Nomarski method is much more sensitive at picking up topological variations, however it was difficult in practice to obtain systematic data for comparisons with this method, since the amount of contrast generated depends upon the way the sample is mounted and it's orientation with respect to the polarisation direction. Furthermore a poor depth of field meant that a painstaking sample alignment procedure was necessary for photography to ensure all of the sample area of interest was in focus. Since sample preparation for SEM was relatively straight forward, and more importantly, systematic data could be obtained using this method, that did not depend critically upon the way the sample was set up, this was used instead for characterising morphology. TEM was then used for more detailed examination, and details of both of these methods follow.

2.6.4 Scanning electron microscopy

Conventional optical microscopes suffer from relatively poor resolution, limited to around the wavelength of the light used (around 500 nm). An electron microscope has an obvious advantage over an optical microscope in that the wavelength of the electrons can be made much shorter than that of visible light. Resolution is theoretically limited by the wavelength of the electrons used, although in practice the optics of the particular microscope used are also important in determining resolution. The wavelength of an electron is related to its energy and accelerating voltage V by the expression;

$$\lambda = \frac{hc}{eV}$$

where h is Planck's constant (6.628×10^{-34}J/s), C is the speed of light in Vacuum (2.997×10^{8} m/s) and e is the electronic charge (1.602×10^{-19}C), data from (21). At a typical operating voltage of 15 KV electrons in the SEM could have wavelength around 0.1 nm, which is far better than visible light.

Samples for SEM examination after etching, were cut with a fresh razor blade, into pieces of about 5mm square and were then mounted onto 10mm diameter aluminium SEM sample holders, using double sided sticky tape. Where several samples had to examined concurrently a 35mm SEM holder was used instead, which could accommodate about 6 such samples. They were then coated with a film of gold (approx 70-150nm thick) under vacuum in an EmScope SC500 sputter coater using argon gas for sputtering. For large samples a small drop of carbon cement placed on one side of the sample, prior to coating, helped to ensure an earthing path for the electrons.

The SEM used throughout was a Philips 515 instrument, electrons are produced by a heated tungsten filament, collimated, and accelerated through a potential difference (5-30 KV) before hitting the sample. The electron beam is scanned across the sample surface and re-emitted electrons are collected by a standard scintillation detector with photomultiplier stages. The detector signal is further amplified electronically and fed to a monitor screen which is scanned identically to the sample. The ratio of the two scanning signals therefore controls the magnification of the instrument and the signal from the detector constitutes the brightness.

Two types of main interactions occur between the electrons and the sample, low energy (10-50 eV) secondary electrons are emitted due to inelastic collisions between the incident electrons and those in the sample, which due to their low energy can only escape from regions near the surface of the sample (22). Elastically backscattered electrons are also produced which due to their higher energy (K eV's) can originate from deep within the sample as well as from the surface. The SEM was used in secondary electron mode throughout to image etched surfaces as required. Contrast mechanisms in the SEM are

complex, since many different interactions occur within the sample. However in secondary electron mode with gold coated samples, contrast is mainly topological, which is as required.

The working distance, between sample and detector, was set by adjusting the sample height, to 6 mm, which seemed to give the best resolution, a larger working distance gave poorer resolution. All samples were imaged at specimen an angle of 40° to the horizontal (detector) plane, with a spot diameter of typically 20 nm [4] and an accelerating voltage of 16 KV.

At low magnification an image was then formed and focused at a fast scan rate (250 lines/frame at 2 ms line time). If the stigmators needed to be adjusted, this was done by finding a circular grain of dust and adjusting the controls until it appeared to stay circular when the focus was adjusted. Focusing on a higher magnification than the one needed ensured that SEM images were crisp and focused prior to photography. The brightness needed for a photograph depended somewhat on the sample and was usually found by trial and error. Pictures are taken on a 35mm camera, built into the SEM, using Jessop black and white Technical Pan film. All pictures were taken at 2000 lines per frame at 32 ms line time, thus to build up a photograph several minutes were required and during this time the camera shutter was held open manually. Scanning at this slow speed improved the signal to noise ratio in the image, but had the cost that the pictures could involve some time to take. Normally in use a compromise was found between ease of viewing and scan speed.

SEM does have one drawback, because the sample itself is placed in the electron beam it can be easily damaged, especially if high accelerating voltages and small spot sizes are used in an attempt to maximise resolution in the SEM. Our samples were routinely damaged if the voltage was above 18 KV at 20nm spot size, this manifested as dark, bland areas in the image.

SEM was unsuccessful on quenched samples mainly due to a lack of relief. In a few cases images were obtained, but even at high voltage and small spot size (an attempt to increase resolution still further) detail was still poor and samples were often damaged before detail could be obtained. Replicas of quenched surfaces were examined by TEM instead.

---

[4] In practice this was the limiting factor on the resolution obtained with the instrument, since 20 nm represents the smallest spatial area of the sample scanned at any one time.

2.6.5 Replication

The technique of replication is a standard technique (23) and involves making an electron transparent carbon copy of an etched surface. Sample morphology can then be imaged under the higher operating voltages found in the Transmission electron microscope without the beam damage that might occur if a sample were to be examined directly. The method described here was used to prepare replicas of etched samples for all the examinations of morphology in the TEM.

The freshly etched surface of the sample to be replicated was wetted by a drop of spectroscopic grade acetone, then a sheet of acetate (Agar Scientific) was carefully placed upon the surface to be replicated. Twenty minutes was allowed for the acetate to harden, after which the sheet and sample were carefully separated, taking particular care not to tear or stretch the acetate sheet.

The acetate impressions was then mounted face up on a slide and coating followed, which was carried out in an Edwards E206A coating system. Two stages are involved; shadowing involved evaporating, under high vacuum, a small amount of a tungsten-tantalum alloy onto the impression at an angle of 35° to the horizontal. The entire surface was then carbon coated from above, with spectroscopic grade carbon, which was evaporated from two rods to give a film 20-40 nm thick. The slide was then removed from the coating unit and small pieces were cut with a fresh razor blade from the resulting replica, which were then laid on 200 mesh hexagonal copper TEM grids, with a drop of acetone.

The acetate sheet was dissolved away by boiling suitable solvents in a dual reflux apparatus and suspending the copper grids in a small basket in the hot solvent vapours. About 2 minutes in butanone, followed by 10 minutes in a mixture of 4 parts dichloroethane to 1 part ethanol, followed by another 2 minutes in butanone was generally sufficient to completely remove the acetate. Extraction time was mainly trail and error, the replicas were examined at frequent intervals in the reflection optical microscope to look for any remaining acetate, which manifested itself as coloured patches. When the replica was clear of acetate it was allowed to dry for 10 minutes, at which point it was ready to place into the transmission electron microscope. Extracting for too long caused replicas to fragment into small sections, which made subsequent examination difficult.

2.6.6 Transmission electron microscopy

The microscope used at Reading is the Phillips EM301. A tungsten filament source is used to provide a collimated beam of electrons to bathe a large area of the specimen, which is placed in a small grid holder. The electron beam, which passes through the replica, is magnified by a further set of magnetic lenses onto a phosphor viewing screen where the morphology is viewed.

Much higher energy electrons (80 KeV) are routinely used in this instrument due to observing a replica rather than a sample directly, therefore much improved resolution over SEM is possible, although this depends on the imaging and contrast mechanisms employed. Resolution and detail are limited by the replica, particularly by the size of the alloy grains used, and by alignment of the beam and apertures. With careful alignment of the microscope and carefully prepared replicas, all aspects of polymer morphology down to lamellar level could be observed with ease. Contrast in the TEM is generated by the shadow placed onto the replica which scatters electrons due to it's high atomic mass, carbon is relatively transparent as far as electrons are concerned. If the replica was made carefully, an accurate representation of the original sample could be imaged, which compared well with optical and SEM examination.

TEM observation was carried out at 80 KV and with a saturated filament, lens currents were controlled automatically, however focus and magnification were set manually. Stigmation was adjusted in the same way as the SEM, using a grain of dust, and the focusing had to be readjusted each time the magnification was changed. The objective aperture was put in place to improve the contrast, however all other apertures were left out, this procedure seemed to give the best brightness, detail and contrast. The procedure for starting at the lowest magnification, locating the area of interest then 'zooming in' to the area of interest (gradually adjusting the focusing controls) was followed throughout the use of the TEM.

Photographs of replicas were taken on 35mm high resolution TEM film, using manually set brightness settings and exposure times. Sometimes not all of the acetate sheet was dissolved on the replica even when examination optically suggested it had been. This was manifested as dark patches in the TEM images, however re-extraction of such replicas normally cured the problem to an acceptable degree.

2.7 Electrical testing system and procedure

A standard electrical testing procedure was used throughout (24), based upon the general consideration laid down in the ASTM standard D149-87 (10,25,26). The sample for testing was immersed in Dow Corning 200/20cs silicone fluid, between opposing 6.3 mm diameter steel ball bearings and a 50g load applied to the upper electrode (total mass on upper electrode 56g) [5]. The lower electrode is connected to earth and an increasing A.C voltage at preset ramp rate (R Volts/sec) was applied to the upper electrode, until the sample failed. All experimental parameters are computer controlled and appropriate data logged automatically. The ball bearings were changed after about every 10 tests, this was sufficient to avoid pitting, which could be detected optically on the surfaces of the ball bearings after about 15 tests, and which could cause rather low values of breakdown voltage to be recorded.

Figure 2.2 shows the main components of the testing equipment used throughout these investigations. The dashed line shows those components which are at high voltage and are therefore enclosed in a mechanically interlocked steel mesh safety cage. The computer, via a D/A card, controls the amplitude of a signal generator (Black Star 'Jupiter') which then drives a fibre optic link. The output of the link drives a Citronic PPX 900 power amplifier, which increases the 3 volts or so on the input to around 70 volts. The amplifier output feeds two transformers, which can generate up to 30 KV. When a sample fails a voltage is generated across the resistor R, which the relay detects and cuts off the signal to the power amplifier, thus reducing the voltage to zero. The relay remains tripped until it is manually reset after inserting the next sample.

Feedback is essential to maintaining the voltage level and is provided by a tap on the isolation transformer. This feeds back to the computer via isolation components and a Keithley model 175A digital multimeter, which is used as a analogue to digital convertor which then feeds the r.m.s amplitude information back to the computer.

---

[5] It was found that having this extra mass on the upper electrode was very important. Without it the measured electrical values were unexpectedly high, this was thought to be due to a film of oil between the ball bearings and the sample. The results from this 50g load correlate with those for a 500g load, it is therefore the conclusion that with the 50g load applied no film of oil existed and that the electrical values are a true representation of the sample properties.

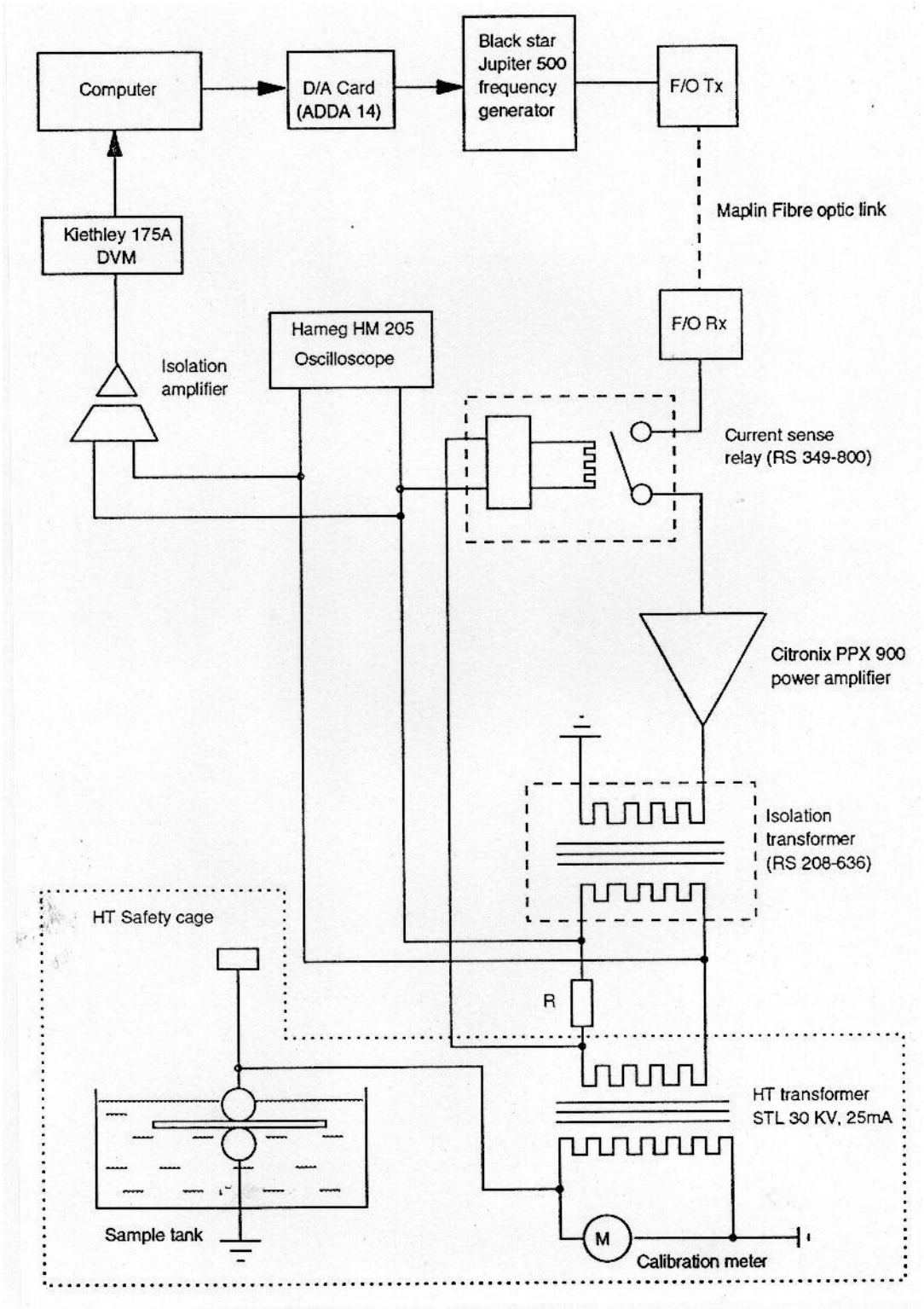

Figure 2.2: Schematics of equipment used for electrical breakdown testing.

The small meter inside the high voltage cage is used initially to calibrate the system, it is connected to the HT transformer via a high impedance probe (1:100). Calibration is software controlled and involves manually adjusting the output voltage (10,15, 20 and 23 KV), which the computer then uses to correlate the voltage generated at the sample (as indicated by the yellow meter) with the input it is receiving back from the multimeter.

The isolation components (fibre optic link and isolation amp.) protect the computer from possible voltage spikes which are generated when a sample failed, otherwise it could be destroyed.

The system was found to operate reliably and give a clean sinewave for A.C frequencies between 40-80 Hz and with ramp rates from 0 (constant voltage test) up to 100 V/s. The maximum sample thickness was found to be 150 microns for PE specimens, as the system did not work reliably above about 25 KV as severe distortion of the waveform occurred, with introduced harmonics. A warm up time of 1 hour was required prior to calibration which needed to be carried out each day when the system was in use and also on changing the A.C frequency. Disk samples could have about 5 tests performed on each before electrical flashover becomes a problem, mainly due to adjacent breakdown holes.

Twenty electrical tests were performed on each batch (any given morphology) of samples to enable their electrical strength and standard error to be assessed, initially using a normal distribution. With 5 tests uncertainty in the measurements due to experimental scatter was about ±35 KV/mm, with 15 tests this reduced markedly to around ±7 KV/mm, which could be improved a little (±5 KV/mm) by going to 20 tests. After this the improvement was slight (ie: ±4 KV/mm for 35 tests) and the time involved in gaining this extra accuracy was considered unnecessary.

2.8 REFERENCES

1) A.S Vaughan, Polymer 1992, **33**, 2513

2) S.R Hu, T Kyu and R.S Stein, Jour. Poly. Sci. part B 1987, **25**, 71

3) D.R Norton and A. Keller, Jour. Mat. Sci. 1984, **19**, 447

4) J.M Rego-Lopez and U.W Gedde, Polymer 1988, **29**, 1037

5) M. J Hill and P.J Barham, Polymer, **34**, 2975

6) J. Martinez-Salazar and M.S Cuesta, Polymer 1991, **32**, 2984

7) A.Gustafsson, PhD Thesis, Royal Institute of Technology, 1993

8) R.G Alamo, J.D Londono, L. Mandelkern, F.C Stehling and G.D Wignall, Macromolecules 1994, **27**, 411

9) J.H Mason, IEEE Trans. Electr. Insul. 1991, **26**, 318

10) D. Fournier and L. Lamarre, Proc. DMMA, IEE Conf. Pub. 363, IEE, London, 1992, p330

11) H.C Miller, IEEE Trans. Electr. Insul. 1993, **28**, 512

12) R.D Naybour, IEEE trans. Electr. Insul. 1978, **13**, p59

13) J.J Janimak, submitted to J. Mat. Sci., June 1995

14) A. H Windle, personal communication

15) R. J Young and P. J Lovell in 'Introduction to Polymers', Chapman and Hill, London, 1991, p 322.

16) R. H Olley and D.C Bassett, Polymer 1982, **23**, 1707

17) R. H Olley and D.C Bassett, Proc. R. Soc. Lond. A 1978, **359**, 121

18) A. M Freedman, D.C Bassett and R.H Olley, J. Macromol. Sci.-Phys. 1988,
B27, 319.

19) D.C Bassett in 'Crystallisation of Polymers', ed. M. Dosiere, Kluwer Academic, Netherlands, 1993, p107.

20) D.C Bassett in 'Principles of Polymer Morphology, Cambridge University Press, 1981

21) 'The Open University Science data book', ed: R. M Tennant, Oliver and Boyd, Edinburgh, 1989.

22) R. Hessel and B.Gross, IEEE Trans. Electr. Insul. 1992, **27**, 831.

23) J.H.M Willison and A.J Rowe in 'Practical methods in Electron Microscopy', Vol.8-'Shadowing and freeze etching techniques', ed. A.M Glauent, North Holland, Amsterdam, 1980.

24) C. K Ku and R. Leipins in 'Electrical Properties of Polymers', Hanser, Munich, 1987.

25) A Gustaffson and U.W Gedde, Proc. Nordic. Insul. Symposium, Vasteres, 1992.

26) L.A Dissado and J.C Fothergill in 'Electrical degredation and Breakdown in Polymers', ed. G.C Stevens, Peter Peregrinus, London, 1992.

CHAPTER 3- THE EFFECTS OF MORPHOLOGY ON ELECTRICAL STRENGTH

3.1 Introduction

The work described here sets out to examine systematically the effects of morphology on electrical strength in a single polyethylene blend. The polyethylene blend was made from varying ratios of Rigidex 140/60 (BP chemicals) linear polyethylene (LPE) and 4901 (Borealis Chemical) branched polyethylene (BPE) prepared by the solvent blending technique. By making use of the control of structural parameters that is achievable in polymer blends, it was possible to study systematically and independently, the influence that morphology has on the electrical strength of polyethylene.

A range of morphologies could be grown within an invariant matrix (constant interspherulitic molecular composition), thereby eliminating spurious effects on electrical strength due to defective material being rejected from growing spherulites. Here, the effect of changing the LPE content and thermal treatment conditions are reported and the effects of spherulitic size and spherulitic number density are examined in detail.

The concept of introducing an inorganic filler into polyethylene needs to be investigated as it has been suggested that fillers may have a detrimental effect on the electrical strength of commercial materials (24-26). Two types of filler particles were incorporated into the 4901 branched polyethylene by melt mixing, zinc oxide (ZnO) and alumina (Al_2O_3) which were measured by the percentage volume of the filler particles.

3.2 Preliminary Studies

Before embarking on any detailed investigation, a number of preliminary studies were performed. Although dissolution in xylene has been used extensively as means of preparing polyethylene blends (1-8), the likely effect of this procedure on both the structure and, more critically, the electrical properties of the resulting materials was first investigated. This was accomplished by comparing the virgin BPE with the same polymer which had been put

through a blending procedure in xylene and recovered.

Samples of both materials were then melt pressed and quenched. No significant structural differences were revealed by DSC or microscopy. Also, the electrical strength of the virgin BPE was unaffected by the dissolution process (virgin BPE, breakdown strength 130 ± 5 KV/mm; xylene processed BPE, 128 ± 4 KV/mm). Similar conclusions have been reported in other studies (9, 10). A similar comparison was made between virgin 4901 and that which had been put through the melt mixing procedure detailed in chapter 2. The electrical strength of the melt mixed material was determined as 128 ± 5 KV/mm, which is not significantly different from the virgin material.

Next, blends with 7% LPE were prepared by solution blending and recovered. Pieces were melt pressed and then crystallised isothermally in the Mettler hotstage, within the temperature range 110-128°C. Crystallisation times were deduced by examining the samples in situ as crystallisation was occurring. When crystallisation was judged to be complete the samples were quenched. These were then etched in permanganic reagent, mounted and then examined by SEM. Figure 3.1 shows the range of morphologies which could be produced by isothermal crystallisation as imaged by SEM.

Two definitive morphological regimes were seen. At temperatures above about 118°C, the observed morphologies were based upon compact, sheaf like, lamellar aggregates whereas, below this temperature, increasingly open banded spherulites were seen, however the transition between these regimes is not abrupt. In all samples, these structural entities were uniformly distributed throughout. On the basis of the results described above, isothermal crystallization at 115°C and 124°C were chosen to be representative of open spherulitic and compact sheaf-like inclusions respectively.

Two samples were melt pressed and quenched, one of the blend and one of 4901, but little detail could be resolved by SEM. This uniform morphology was also chosen for further investigation as it represented a third type of morphology in the blend. Four further quenched samples were chosen with 5% and 30% by volume of filler particles for investigation. Small samples of these were melt pressed and a uniform distribution of filler could be obtained easily as deduced by optical observations.

Quenched samples and samples isothermally crystallised at 115 and 124°C were then chosen for further investigations from blends with 1%, 3%, 7%, 10%, 15%, 20% and 30%

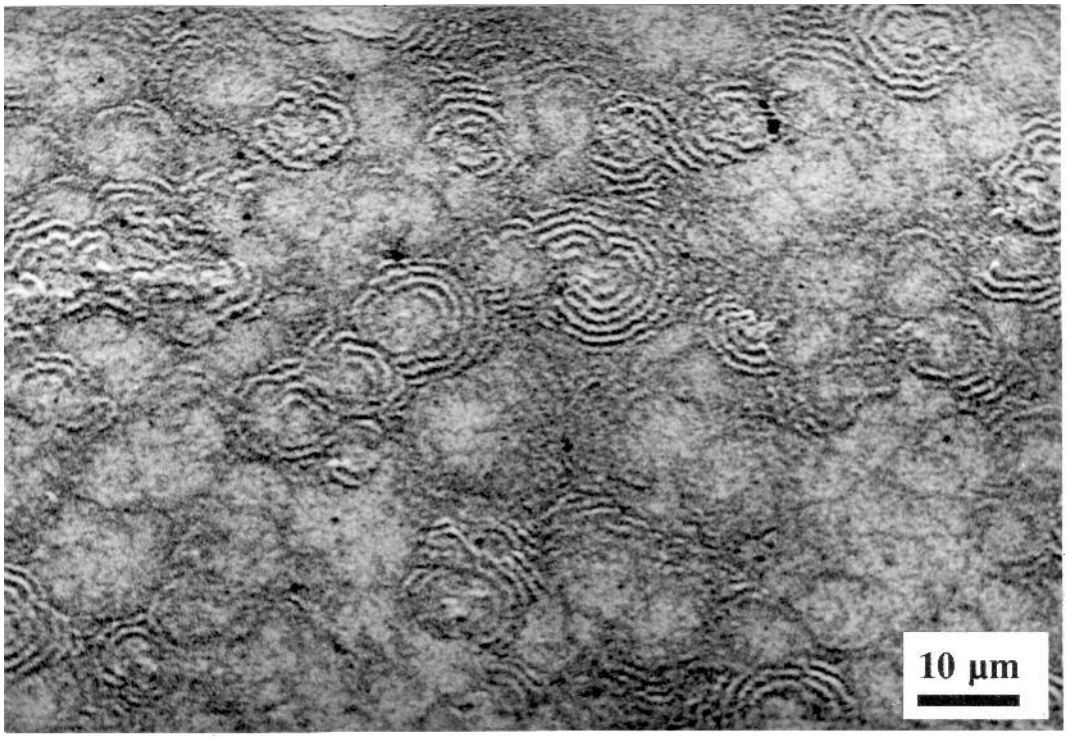

Figure 3.1(a): Banded morphology in the 7% LPE blend crystallised at 105°C.

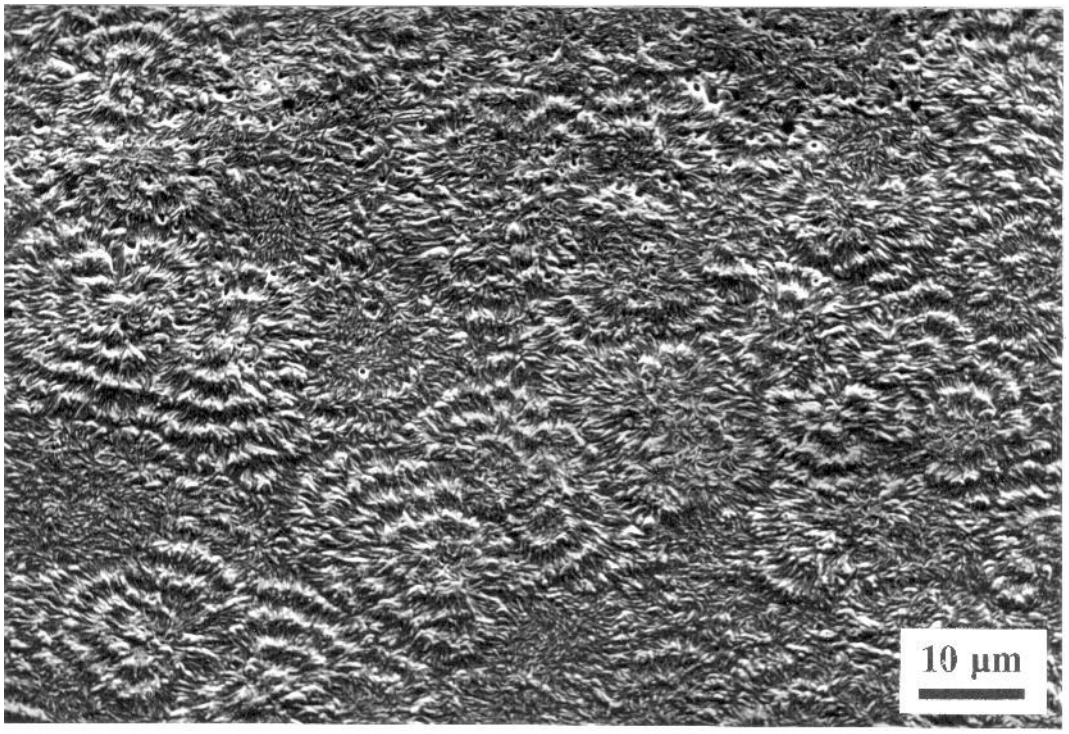

Figure 3.1(b): Larger banded spherulites, crystallisation at 115°C.

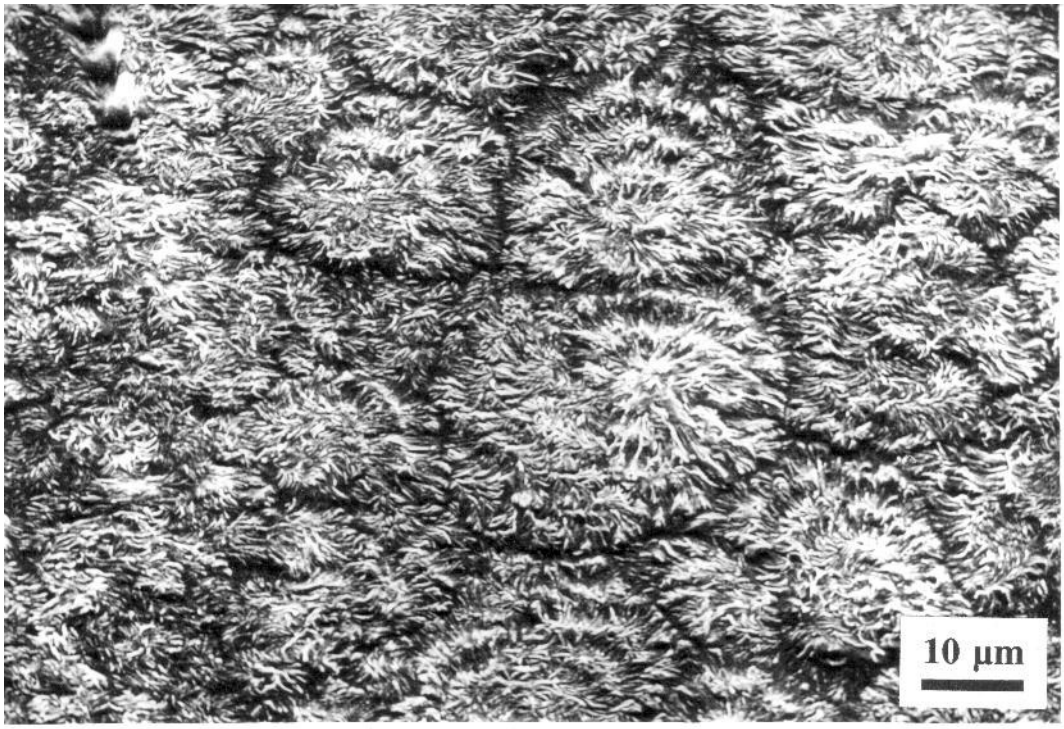

Figure 3.1(c): Transitional morphology-banded lamellar aggregates, 118°C.

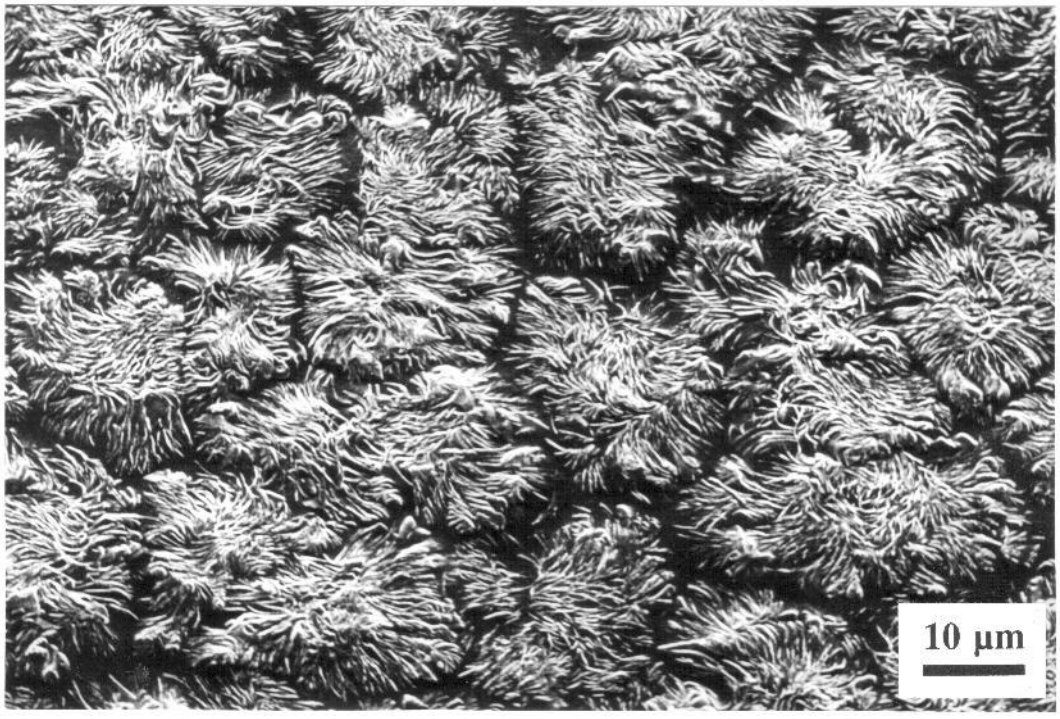

Figure 3.1(d): More compact lamellar aggregates, crystallisation 120°C.

Figure 3.1(e): Small lamellar aggregates, 7% LPE blend crystallised at 124°C.

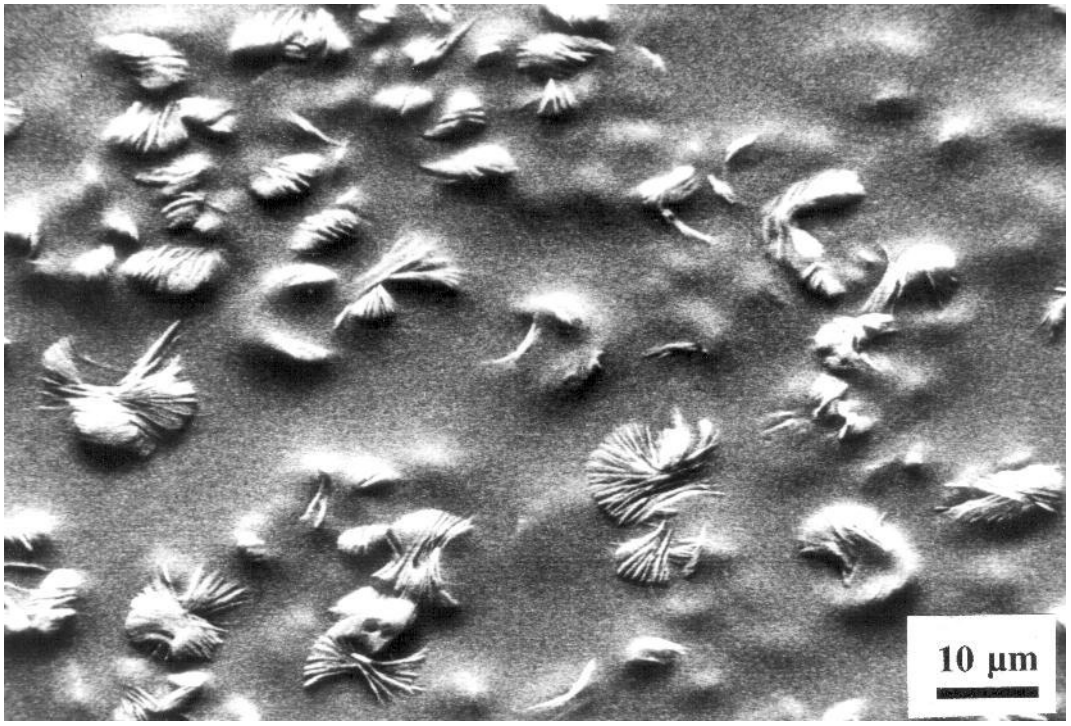

Figure 3.1(f): Very small lamellar aggregates, crystallised at 126°C.

LPE content. For simplicity the blends will be referred to as follows; BPA T/C where BPA signifies the blend of 140/60 in 4901, T signifies the crystallisation temperature in °C and C the % LPE content. For instance a blend of 10% 140/60 in 4901 isothermally crystallised at 124°C was labelled BPA 124/10 whereas one with 1% 140/60 in 4901 which had been quenched straight after melting was labelled BPA Q/1. Filled samples are indicated by the nature of their filler and its volume percent in the blend; ZnO 5 means quenched 4901 with 5% zinc oxide, whereas ALO 30 means quenched 4901 containing 30% by volume of alumina particles. All samples of filled 4901 were melt pressed and then immediately quenched.

3.3 Differential Scanning Calorimetry

Crystallization Behaviour. Before any samples could be prepared for detailed investigation, it was necessary to quantify the time for maximum crystallisation of the linear component; visual estimation of crystallisation times were not considered sufficient for a detailed study. The graph in figure 3.2(a) shows the crystallisation time as a function of blend composition and temperature, as judged from the DSC isothermal crystallisation exotherms. This shows that blends prepared at higher crystallisation temperatures, or those with lower LPE contents require longer crystallisation times. Qualitatively, this general form of behaviour is in line with expectations (1-4) and, assuming that the time for maximum crystallisation at each temperature is inversely related to the crystallisation rate, the measured crystallisation times are not inconsistent with secondary nucleation theory (11), figure 3.2(b).

Although, the minimum time for "complete" linear crystallisation varies with composition, for simplicity and reproducibility it was decided to adopt crystallisation times of 45 minutes at 115°C and 4 hours at 124°C. This is sufficient to ensure maximum LPE crystallisation in all cases. This procedure also has the advantage of allowing any stress or compositional variations associated with crystallization to relax prior to quenching (12-14).

Melting behaviour. Figure 3.3(a) shows the DSC melting behaviour of quenched samples as a function of linear content. Two peaks are seen in all the blends in line with previously published data (1), the upper peak being relatively sharp, whereas the lower exhibits a

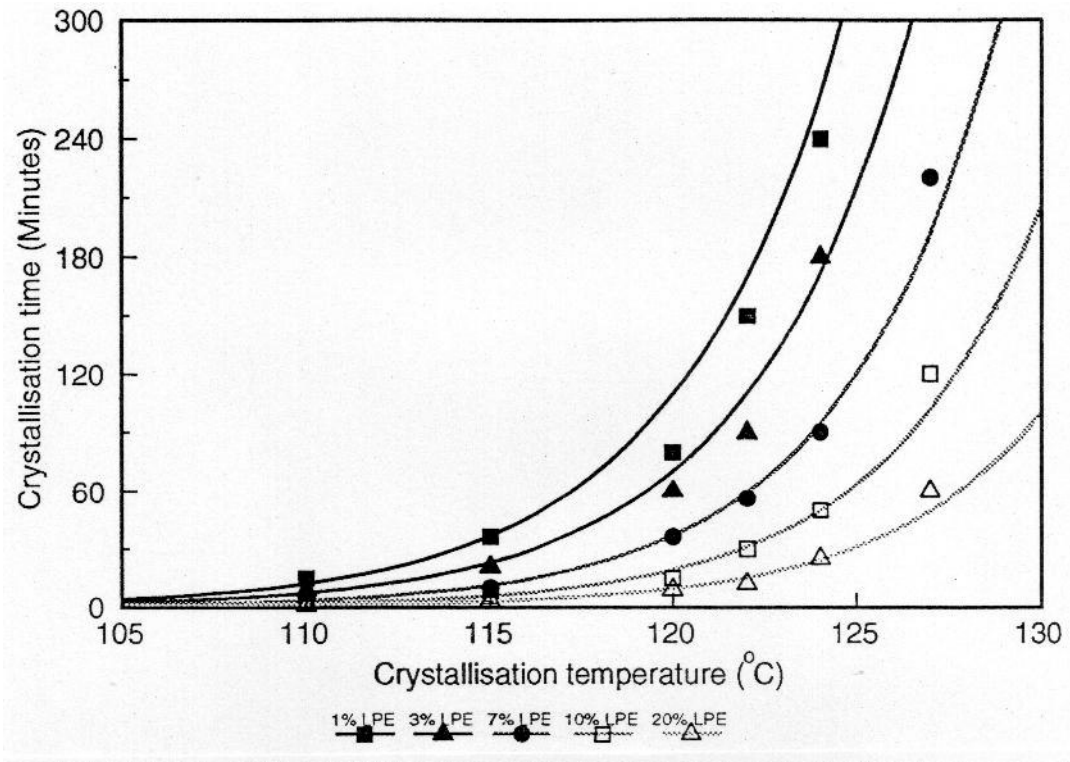

Figure 3.2(a): Crystallisation times of various BPA blends.

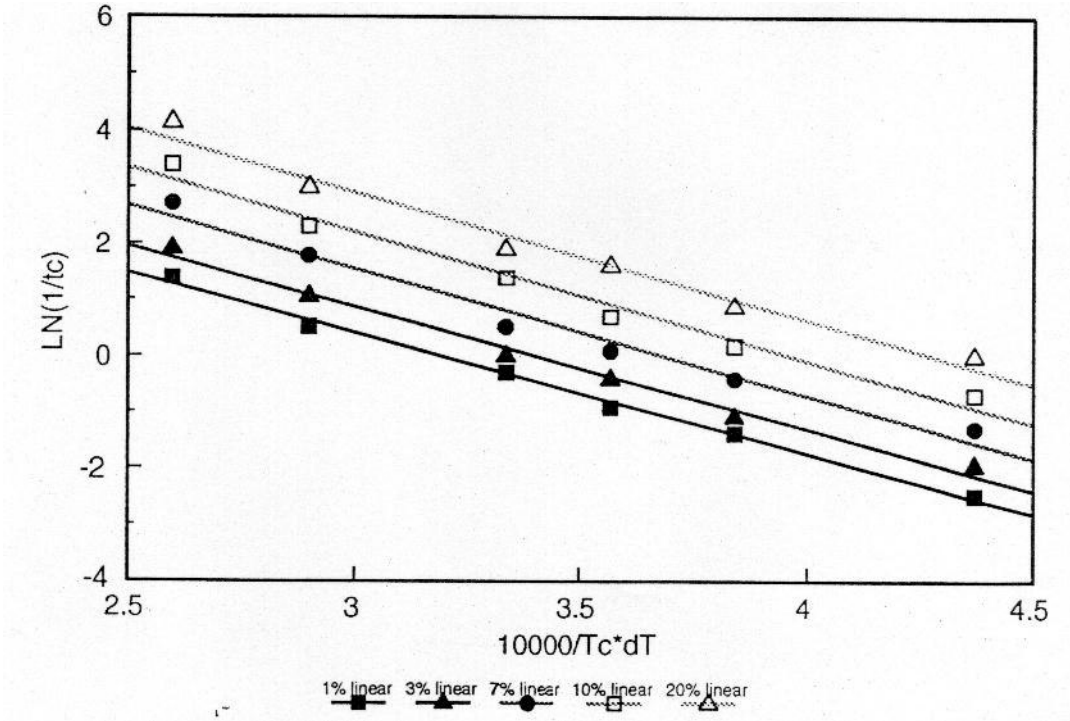

Figure 3.2(b): Alternative plot of crystallisation times in BPA blends.

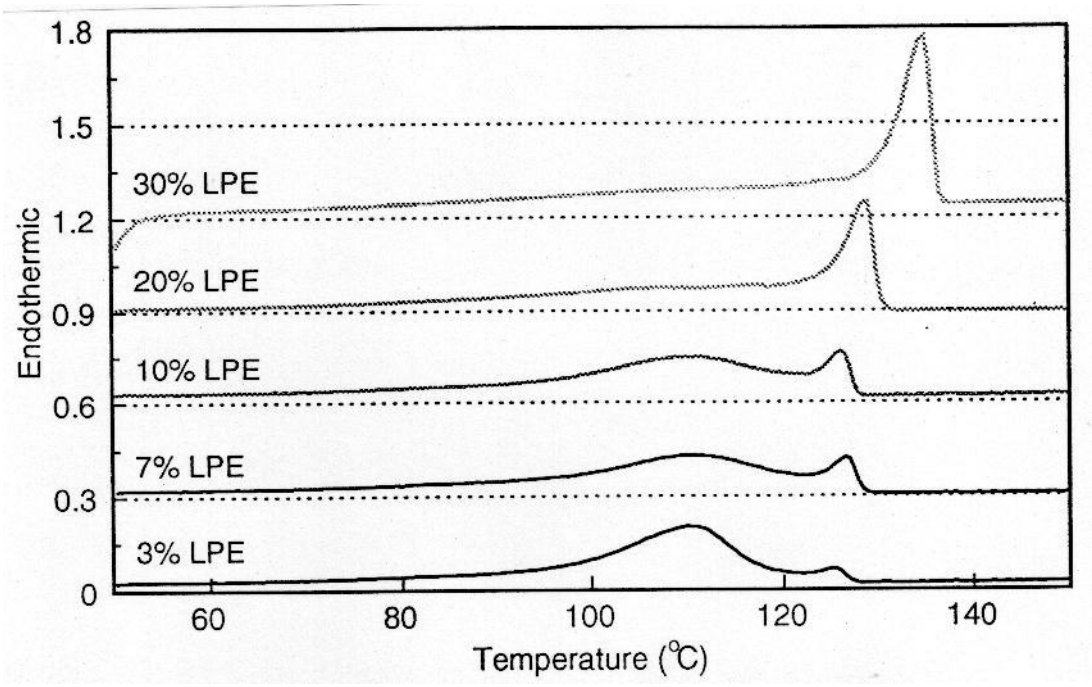

Figure 3.3(a): DSC melting behaviour of quenched BPA blends.

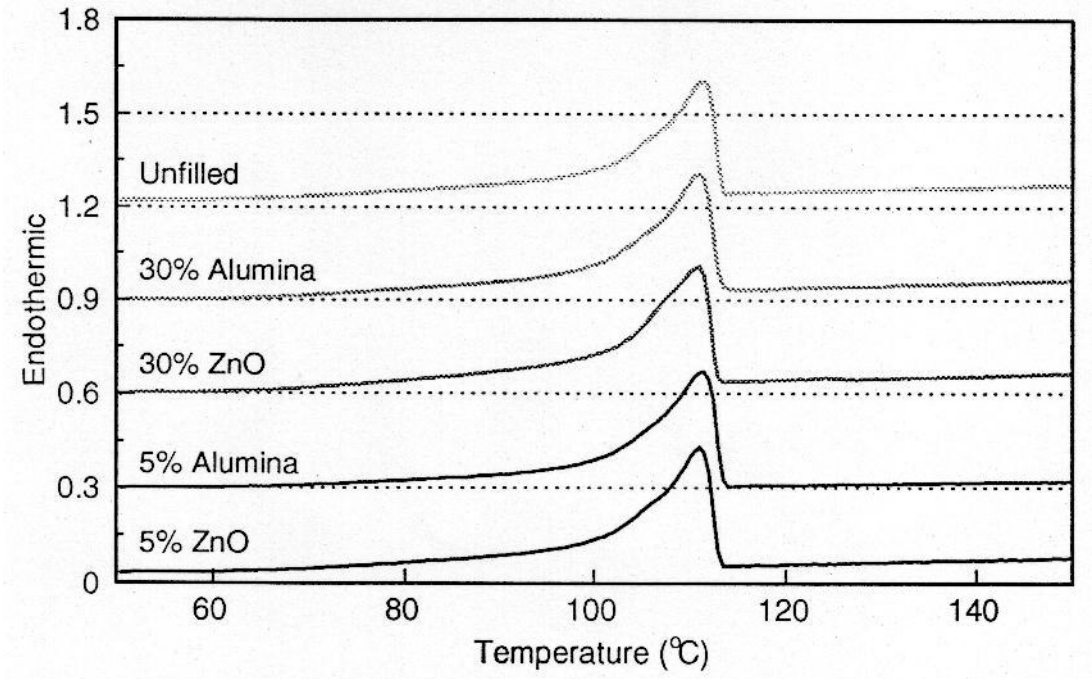

Figure 3.3(b): Melting behaviour of filled and unfilled 4901.

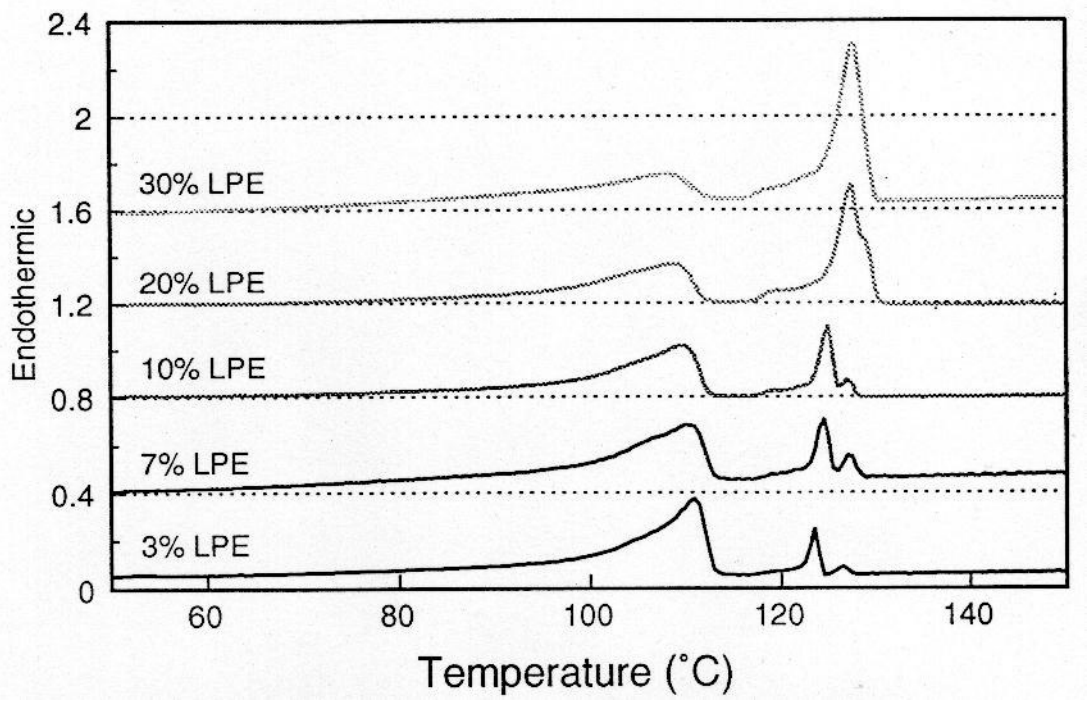

Figure 3.4(a): Melting behaviour of BPA blend after crystallising at 115°C.

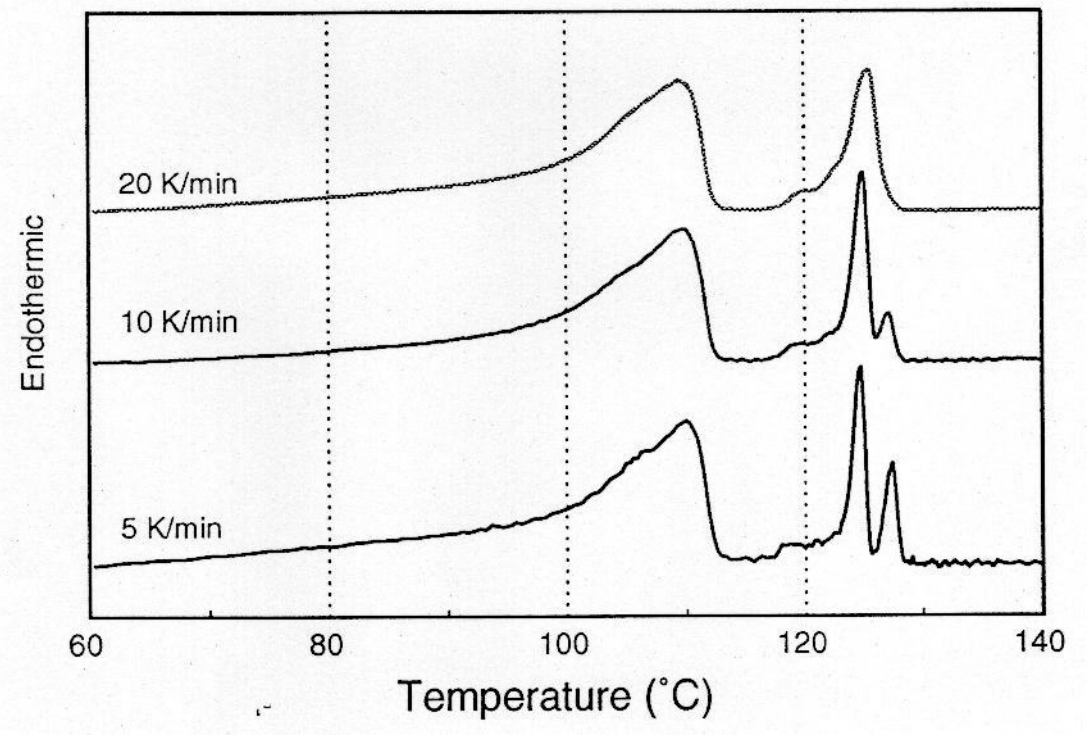

Figure 3.4(b): Scan rate dependence of DSC data for BPA 115/10.

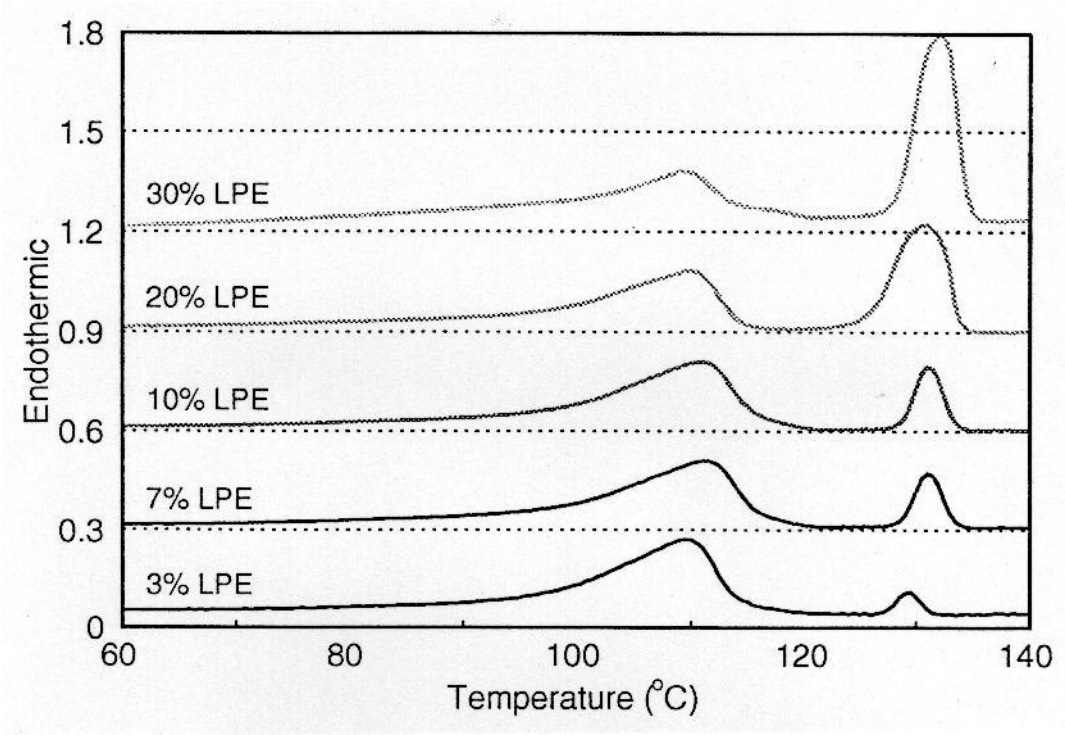

Figure 3.5: Melting behaviour of BPA after crystallisation at 124°C.

long tail extending towards room temperature. In all the blends, the lower peak maximum is situated at a temperature close to that of the pure BPE, and this feature is therefore associated with lamellae composed *principally* of branched molecules. Subsequently, this lamellar population will be referred to as the BPE-rich phase. Similarly, the higher melting peak is *principally* associated with linear material (LPE-rich phase). In the 4901 only a single peak is observed (fig. 3.3(b)), no noticeable change in melting temperature occurred due to the incorporation of filler particles.

In the samples crystallised at 115°C (figure 3.4(a)), the higher temperature peak is generally much narrower and the peak area much higher than in the comparable features shown in figure 3.3(a). The enthalpy of this peak is such that it provides strong evidence of co-crystallization of the linear material *and* the more linear fractions of the BPE. The corresponding melting temperature increases somewhat with blend linear content, from 123 to 127°C and, in addition, at least one subsidiary peak is observable. The magnitude of the highest temperature peak is found to be dependent upon the DSC scan rate (see figure 3.4(b)) and this feature can therefore be attributed to a population of co-crystals that are richer in LPE and which can therefore anneal during scanning. The BPE-rich phase seems to be very similar to that formed on quenching.

Figure 3.5 shows the DSC data obtained from the blends crystallised at 124°C. The composition and melting point of the BPE-rich lamellae are invariant as seen in both previous cases, but the peak corresponding to the LPE-rich phase is now wider and is singular, in contrast to the samples crystallised at 115°C. The area of this peak is lower than that of the corresponding endotherm seen in the 115°C samples, and the melting temperature is around 130°C, i.e. the two peaks are more widely separated. Thus, crystallization at 124°C gives two very different lamellar populations, as would be anticipated, and also leads to less co-crystallisation.

In all three cases the LPE peak can be seen to get larger as more LPE is added, and the BPE peak smaller, calculations confirm that this is simply due to the increased mass of LPE and decreased mass of BPE and is not a result of compositional variations which may be due to rejected defective molecules from growing spherulites. For any given temperature of crystallisation the compositions of both phases remain constant, the only variable being the masses of materials present.

All the DSC traces described above are similar to those reported in the literature and it can therefore be concluded that the materials considered in this study are not atypical. However, perhaps the most important point to note from these results is that there is no evidence to suggest that the BPE-rich phase in any of the sample sets varies to any appreciable degree with thermal treatment or blend composition. Only the LPE-rich phase is seen to vary with the crystallisation conditions, in all cases the BPE-rich phase appears very similar to the pure 4901. Thus, on the basis of DSC data, the prime objective of this study can be achieved; various morphologies can be grown within an invariant matrix. Furthermore spherulites in say BPA 115/1 and BPA 115/20 are essentially made up of material of the same composition.

3.4 Detailed morphological Examination

The morphology of the blend systems considered here were, again, similar to those reported elsewhere in the literature and a selection of typical examples are included.

Crystallisation at 115°C. Figure 3.6 shows SEM micrographs of samples crystallised at 115°C. BPA 115/3 (figure 3.6(a)) contains open banded spherulitic structures (LPE-rich) which are about 20 μm in diameter and which are separated from each other by regions of quenched matrix (BPE-rich). If the linear content is increased, as in figure 3.6(b) (BPA 115/15), then the spherulites become more compact, somewhat larger and impinge upon one another such that the banded texture becomes space filling, if we add 30% linear polyethylene (BPA 115/30) the morphology remains very similar (fig 3.6(c)). Figure 3.7 shows the microstructure of some samples crystallised at 115°C, as revealed by TEM. Figure 3.7(a) shows immature banded spherulites in BPA 115/3, clearly here the growth of the spherulites has been limited by the amount of LPE available. Figure 3.7(b) shows BPA 115/7, in which well ordered lamellae in the more mature banded spherulites can be seen, together with the more random lamellar orientations in an adjacent, apparently non-spherulitic region. Figure 3.7(c) shows the morphology of BPA 115/20 in which the spherulites are much better developed. In this micrograph, banded spherulitic structures can be seen together with an apparently less ordered region (A). However, even here no variation of lamellar thicknesses is apparent and the lamellae do show orientational

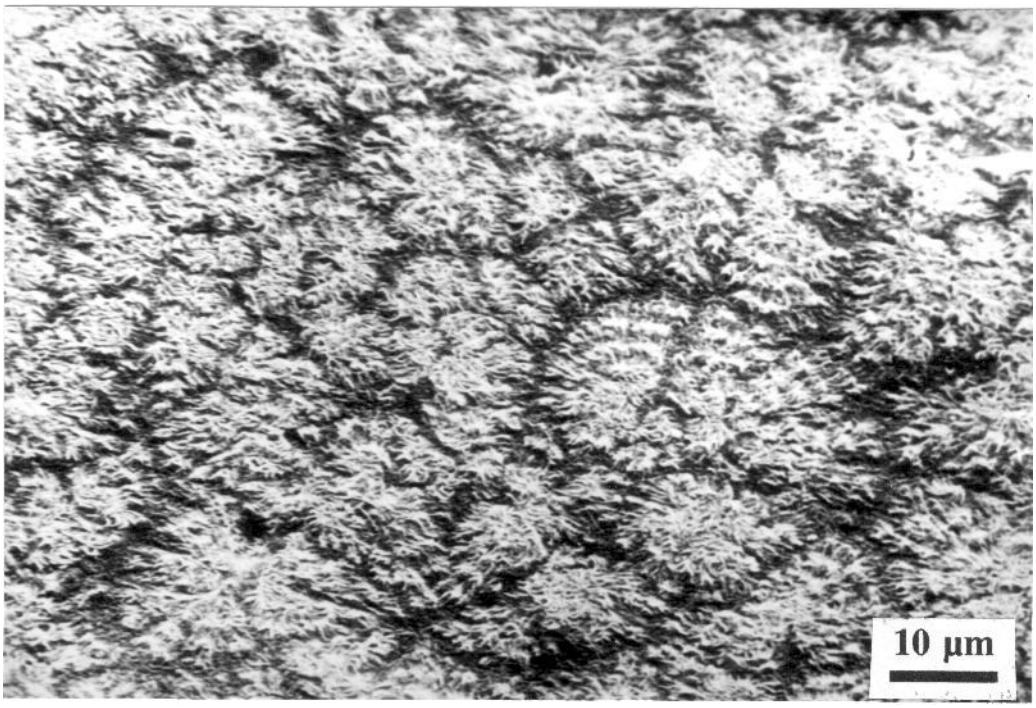

Figure 3.6(a): Immature banded spherulites in BPA 115/3.

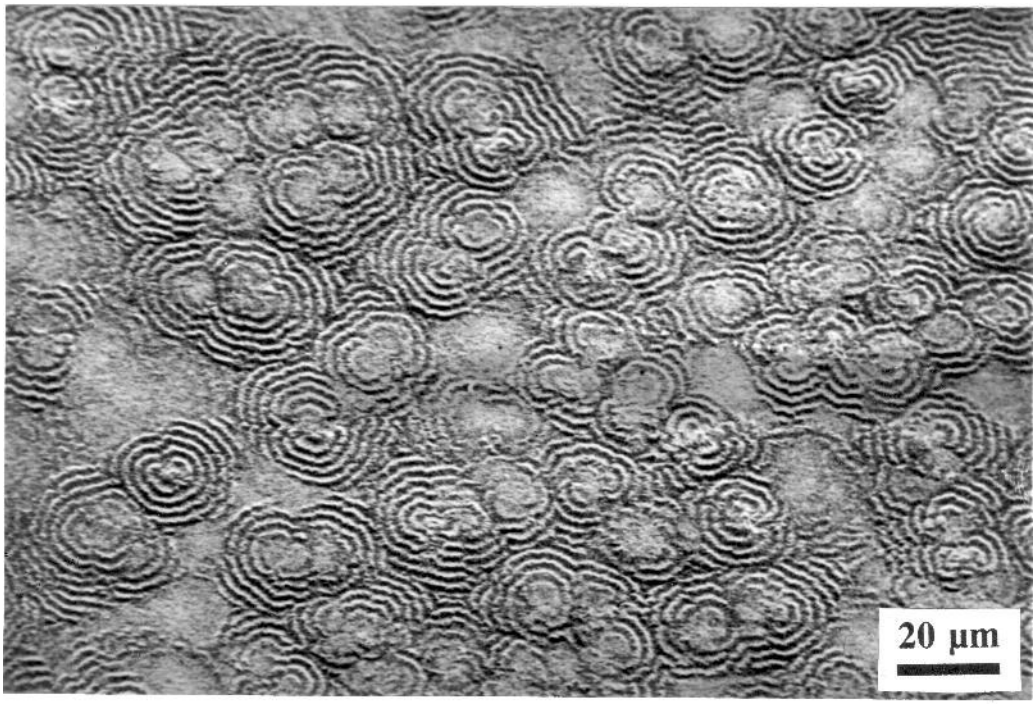

Figure 3.6(b): At higher LPE contents the banding becomes more apparent, BPA 115/15.

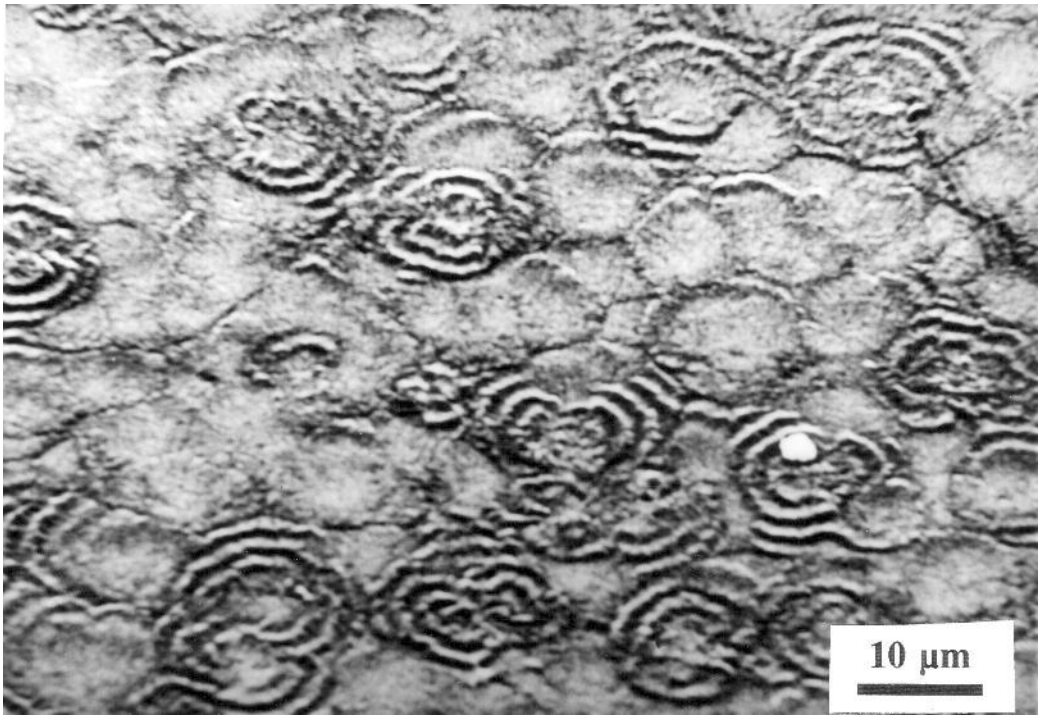

Figure 3.6(c): Similar banded morphology in BPA 115/15 is seen in BPA 115/30.

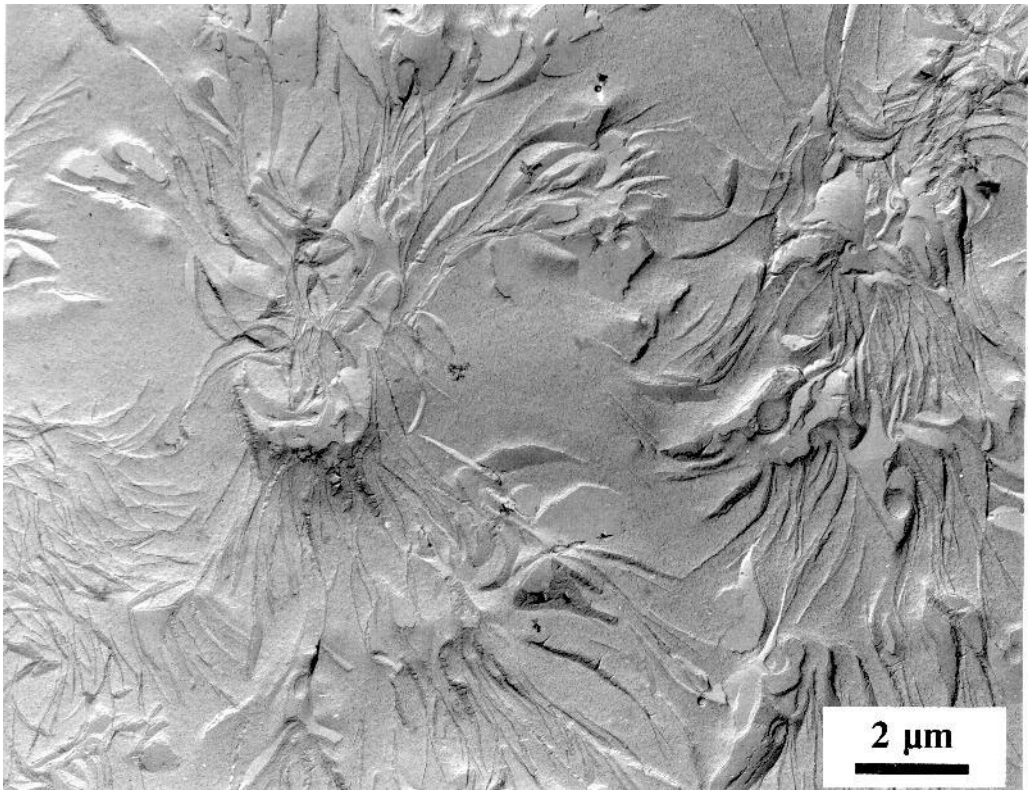

Figure 3.7(a): Clearly the growth of the banded spherulites has ceased due to a lack of crystallisable material in BPA 115/3.

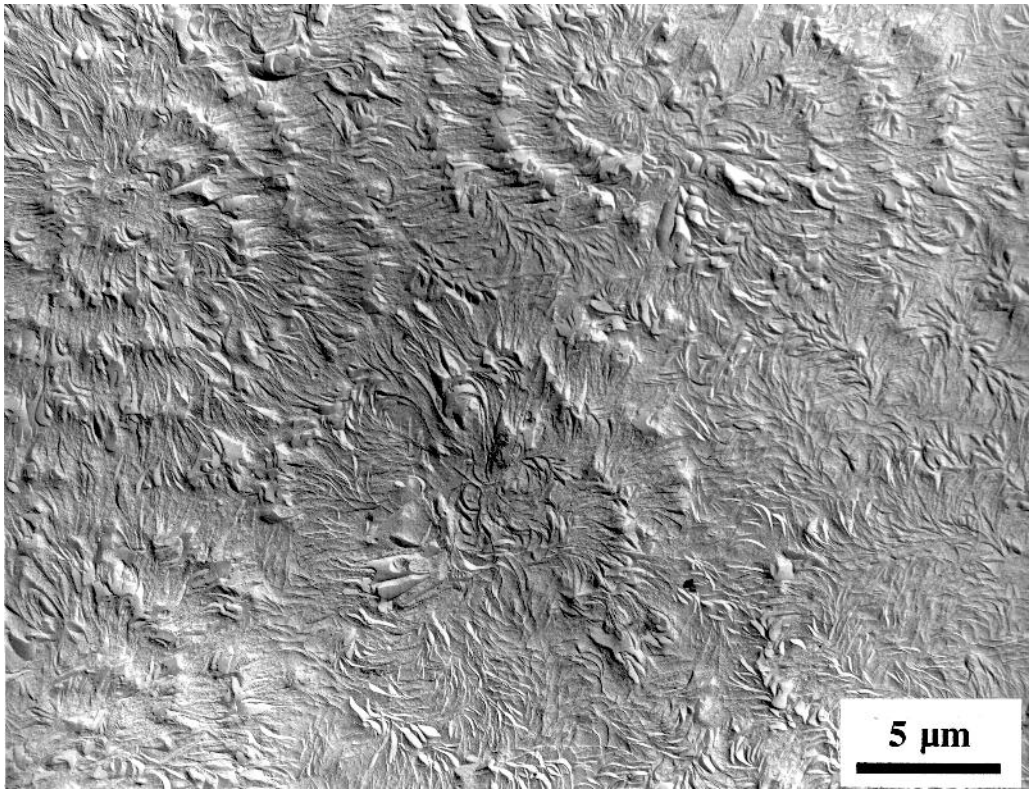

Figure 3.7(b): In this blend with 7% LPE, banded spherulites are much better developed.

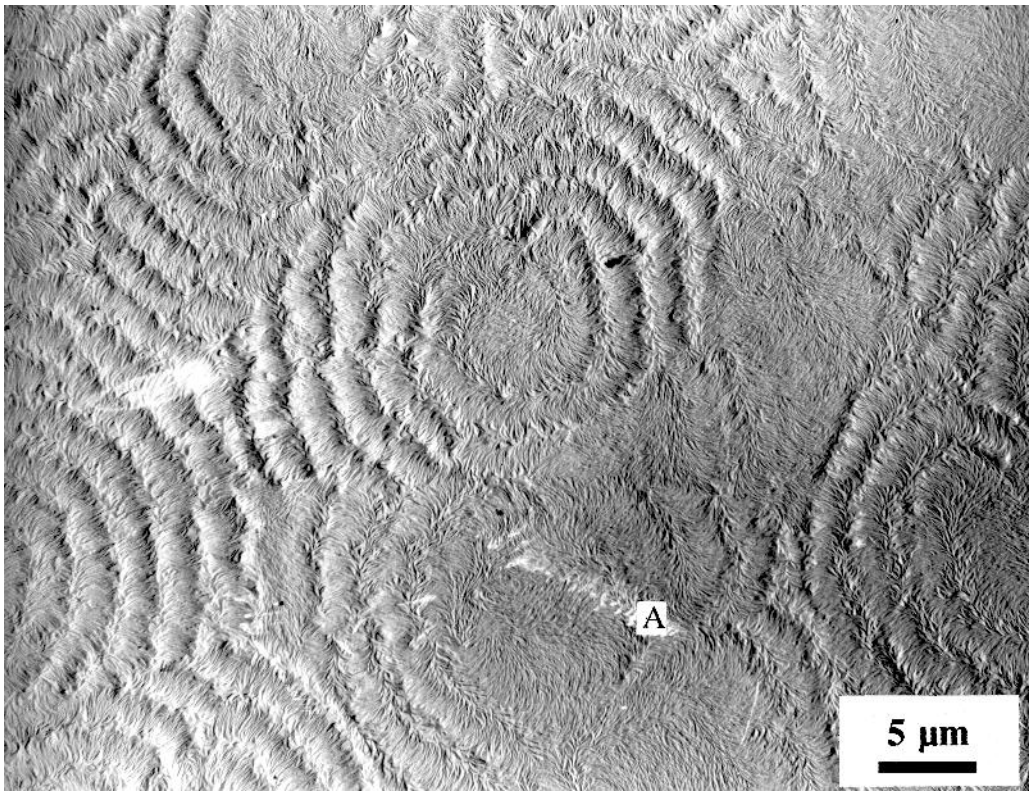

Figure 3.7(c): In BPA115/20 the whole system is composed of a space filling lamellar array.

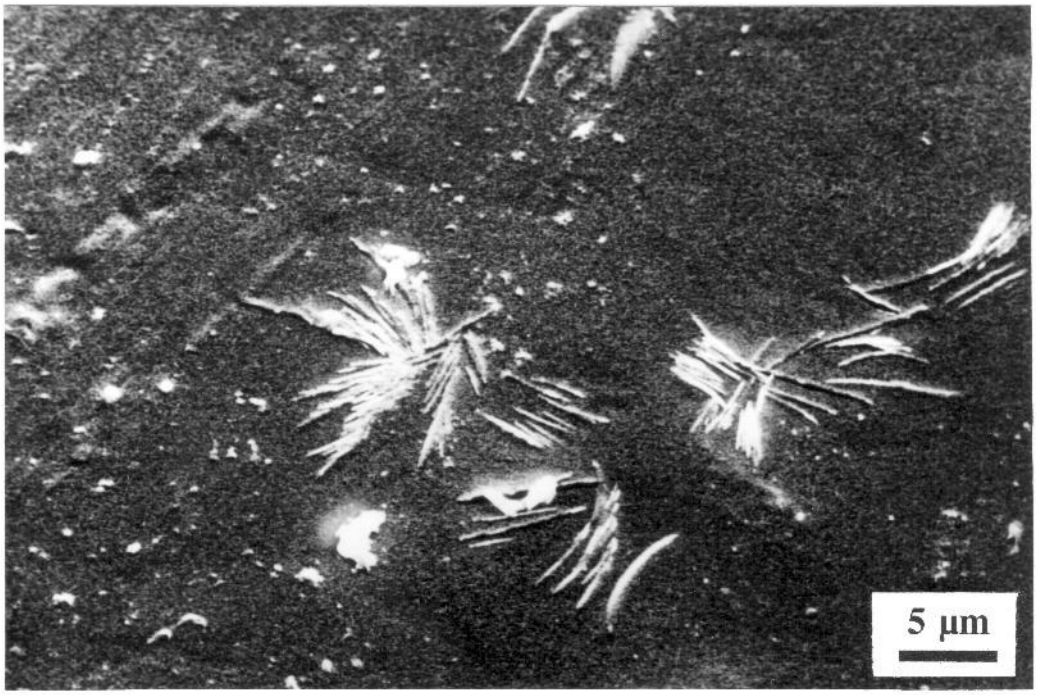

Figure 3.8(a): In BPA 124/1 isolated lamellar aggregates are formed.

Figure 3.8(b): In BPA 124/20 the aggregates have grown to a greater extent.

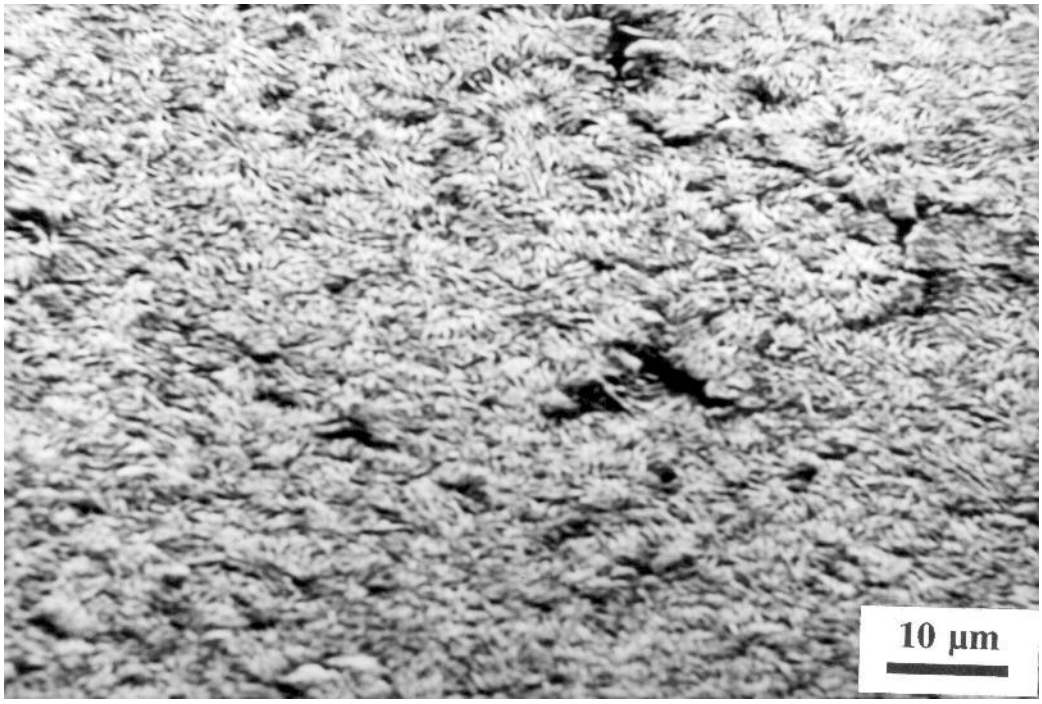

Figure 3.8(c): BPA 124/30 contains so much LPE that individual lamellar aggregates cannot be distinguished yet boundaries are still evident.

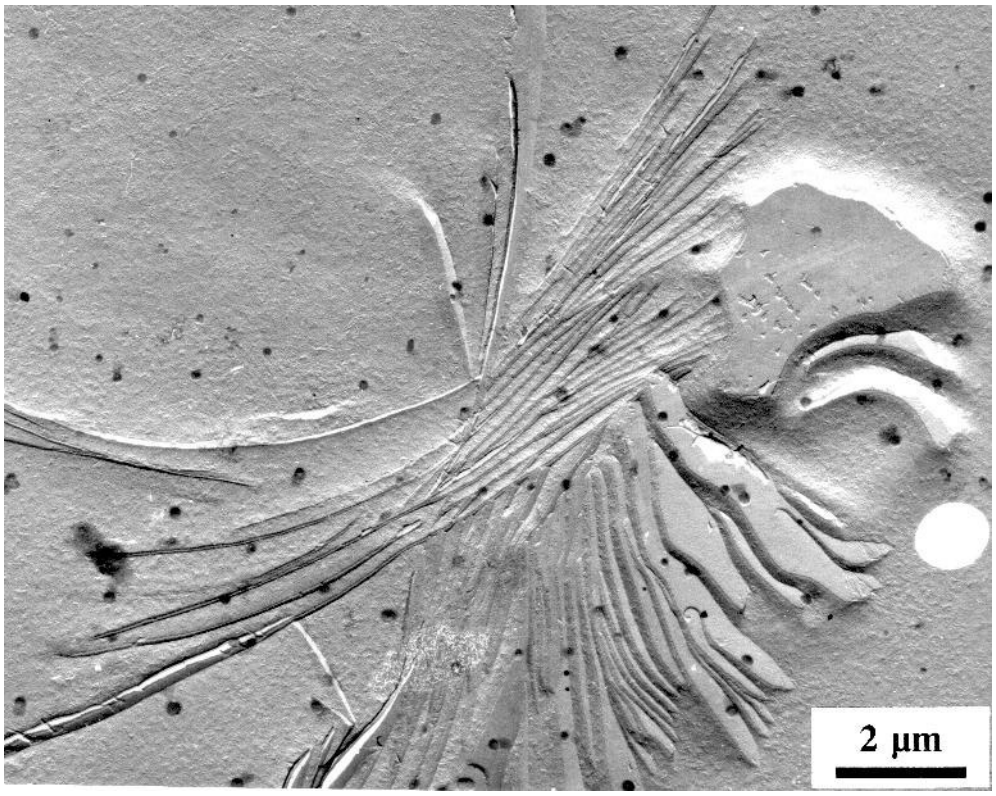

Figure 3.9(a): TEM micrograph of simple aggregate in BPA 124/1.

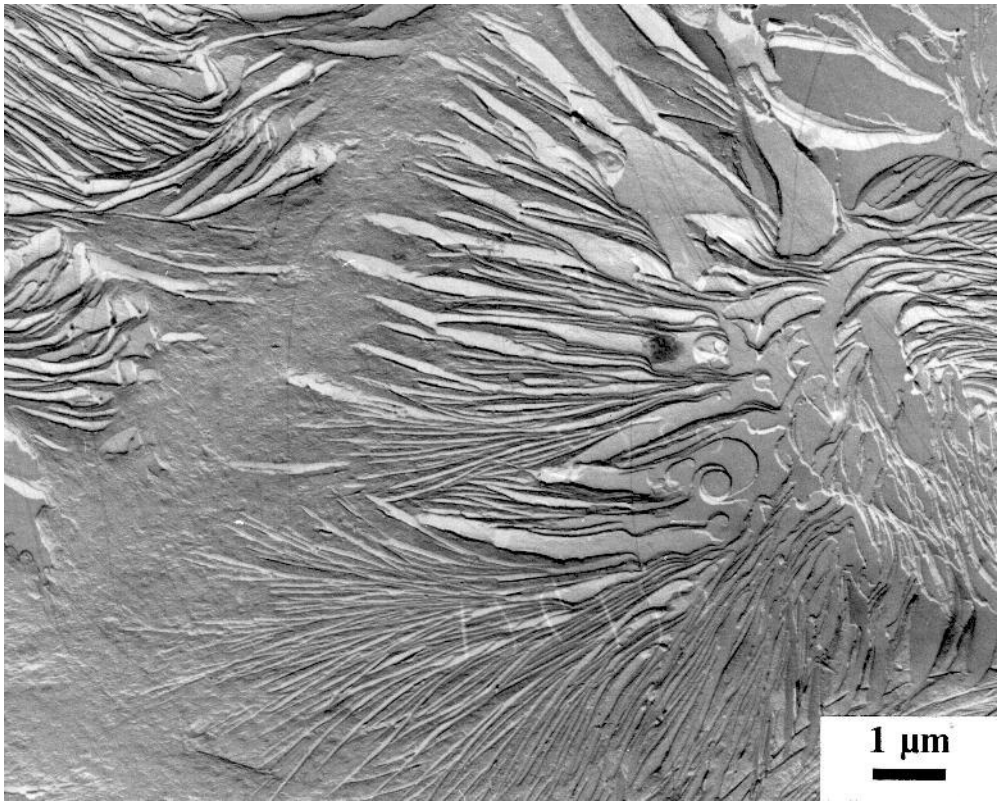

Figure 3.9(b): Complex aggregates are formed in BPA 124/20.

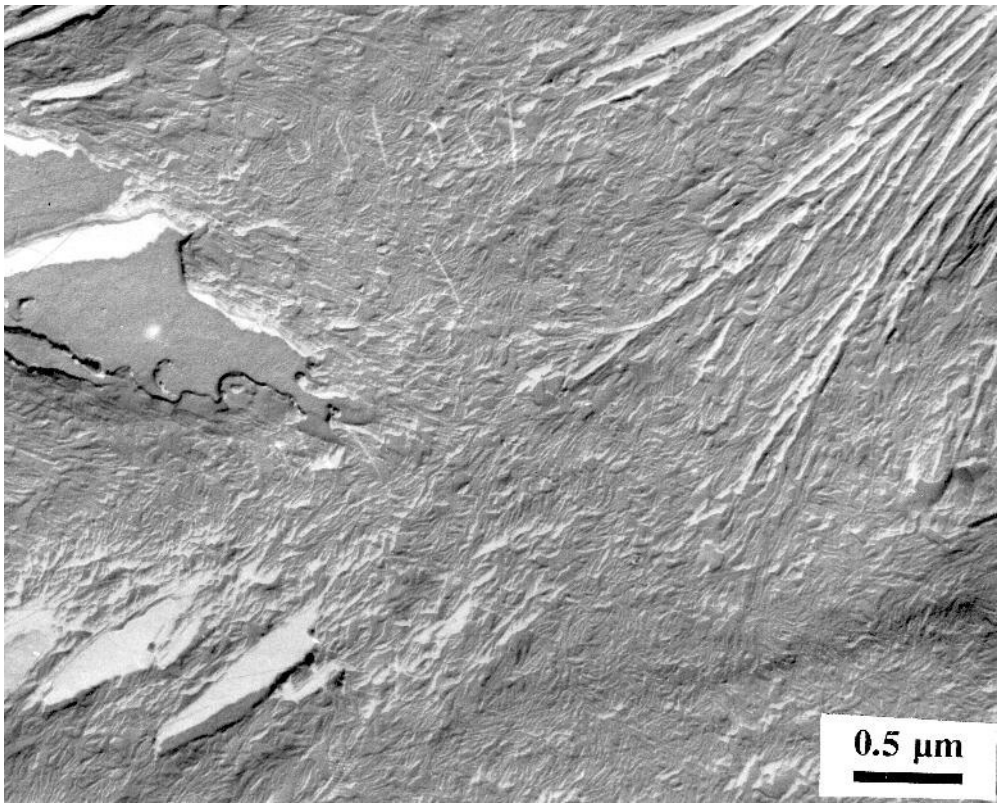

Figure 3.9(c): Detail of inter-spherulitic region in BPA 124/20.

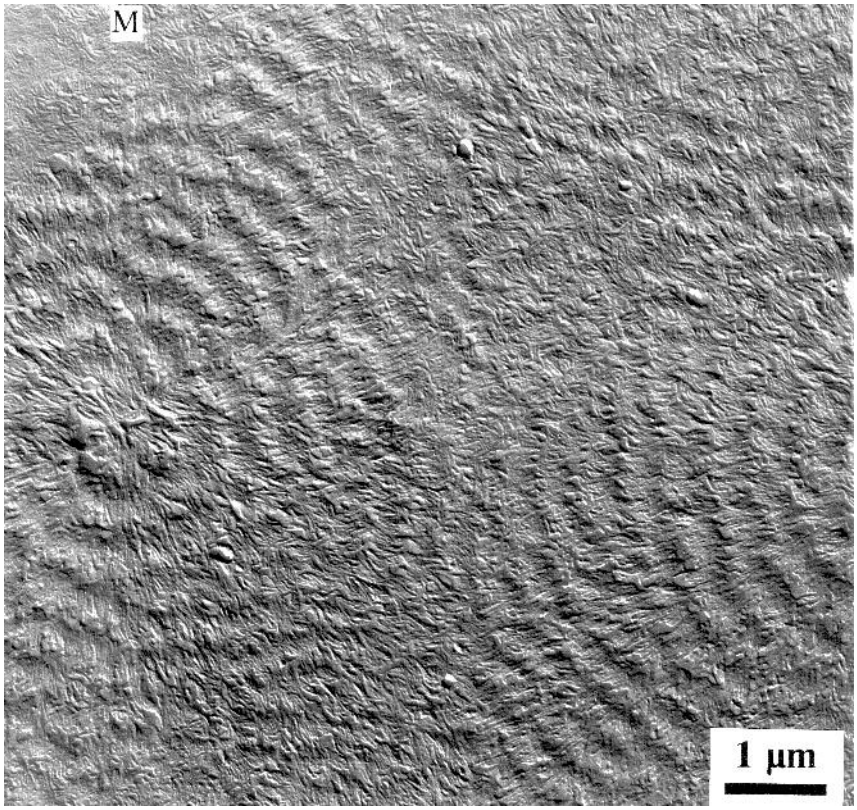

Figure 3.10(a): BPA Q/7 showing fine banded texture.

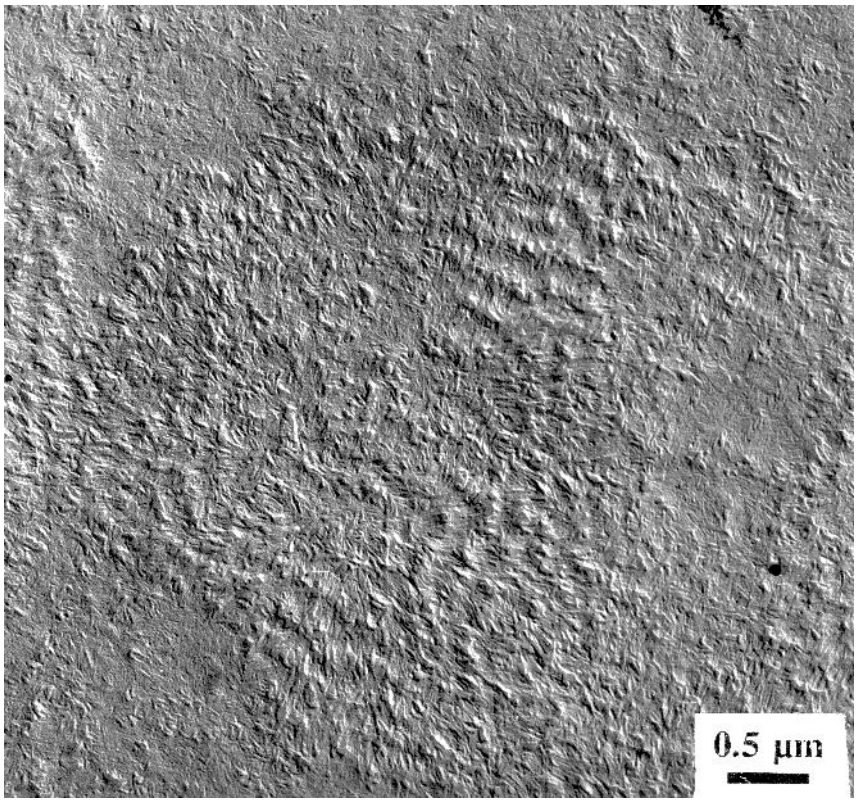

Figure 3.10(b): A similar morphology forms in BPA Q/0.

correlations, unlike in BPA 115/7, where the lamellae were randomly oriented between spherulites. So, region A is likely to correspond to another spherulite viewed radially, so supporting the SEM observations of a space filling interpenetrating set of spherulites, without any distinct `matrix'. In this case, the BPE-rich phase is located between individual LPE-rich lamellae.

Crystallisation at 124°C. The morphology is based upon more compact LPE-rich inclusions (see figure 3.8) which, at low linear contents, (1%) are isolated (figure 3.8(a)). Again, on increasing the percentage of LPE, these inclusions become larger and more numerous, such that in BPA 124/20 they almost impinge (figure 3.8(b)). However, even at this composition, distinct boundary regions are still evident (compare figures 3.6(a) and 3.8(b)), even at 30% LPE content the spherulites are somewhat larger, yet such boundary regions still exist (fig 3.8(c)). Figure 3.9 shows some samples crystallised at 124°C, as revealed by TEM. An immature spherulite made up of a few large lamellae in BPA 124/1, surrounded by a BPE-rich matrix made up of very small lamellae, is shown in figure 3.9(a). Figure 3.9(b) contains a TEM micrograph showing larger, more mature structures in BPA 124/20. Figure 3.9(c) shows, at a higher magnification, the distinction between the thicknesses of the lamellae within a spherulite and those located in the BPE-rich matrix. Unlike the BPA 115/20 samples, clear interspherulitic regions still exist even at this relatively high linear content and the same is true at 30% LPE content (figure 3.8(c)).

Quenching. SEM examination of quenched blends was not revealing and therefore only TEM data is shown here. Figure 3.10(a) (BPA Q/7) shows the typical banded spherulitic texture obtained on quenching. In this micrograph two textures can be seen; well developed banded spherulites of diameter 10 microns are present together with areas where there is no evidence of lamellar aggregation into large scale structures (M). Similar local variations in morphology have previously been interpreted as providing evidence of liquid-liquid phase separation. No noticeable variation in structure or spherulitic nucleation density was seen with LPE content. Such spherulites were not generally seen in the matrix of the isothermally crystallised blends, in most cases there was simply no room for them to grow, however in low LPE blends crystallised at 124°C only a few banded spherulites were ever seen in the matrix, certainly no where near as many as in the quenched blends. Figure

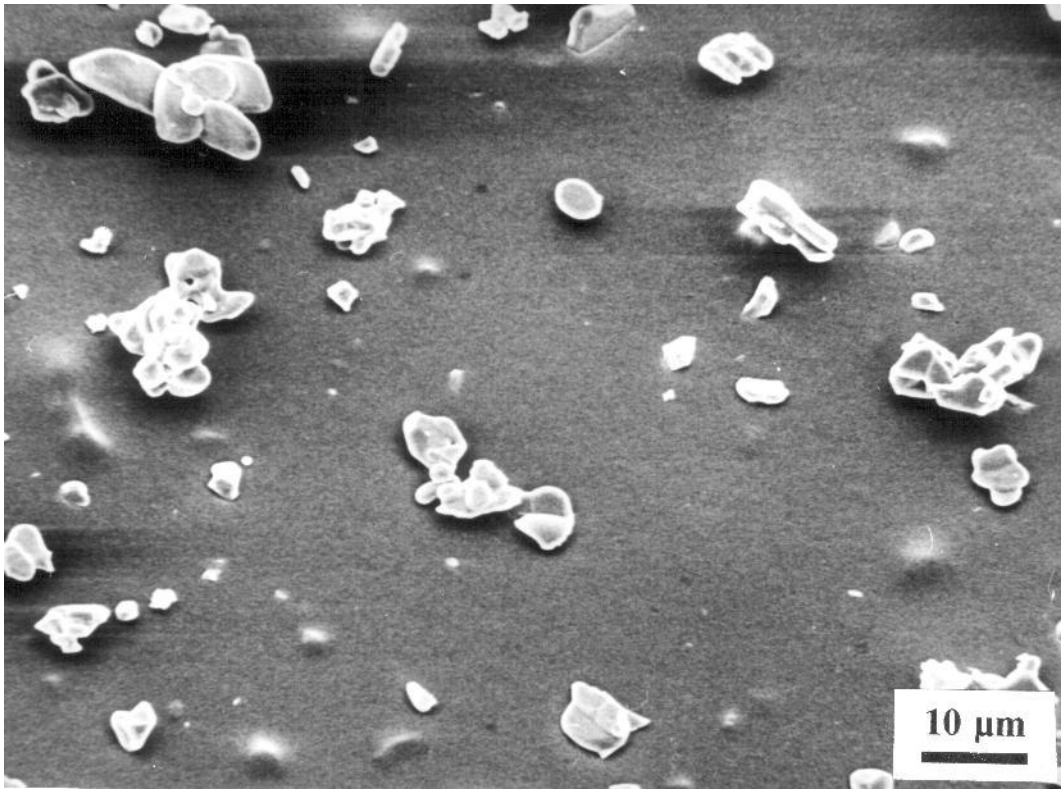

Figure 3.11(a): Filler particle distribution in 4901 containing 5% alumina.

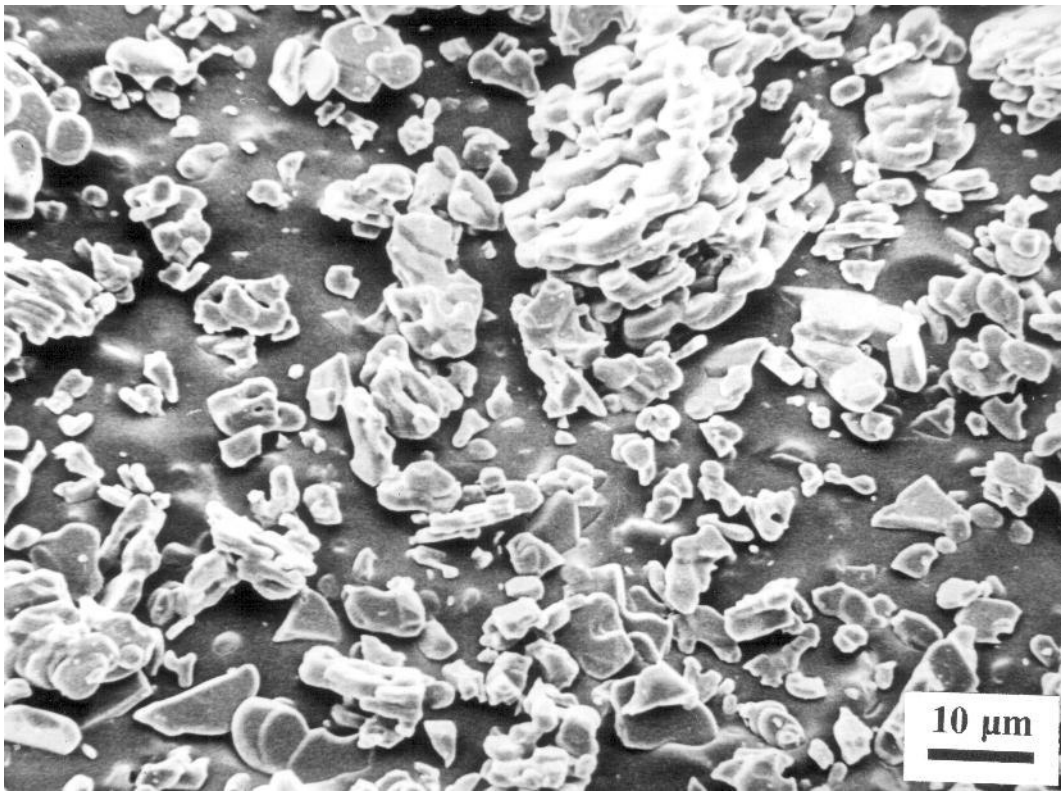

Figure 3.11(b): Particle distribution in 4901 containing 30% alumina filler.

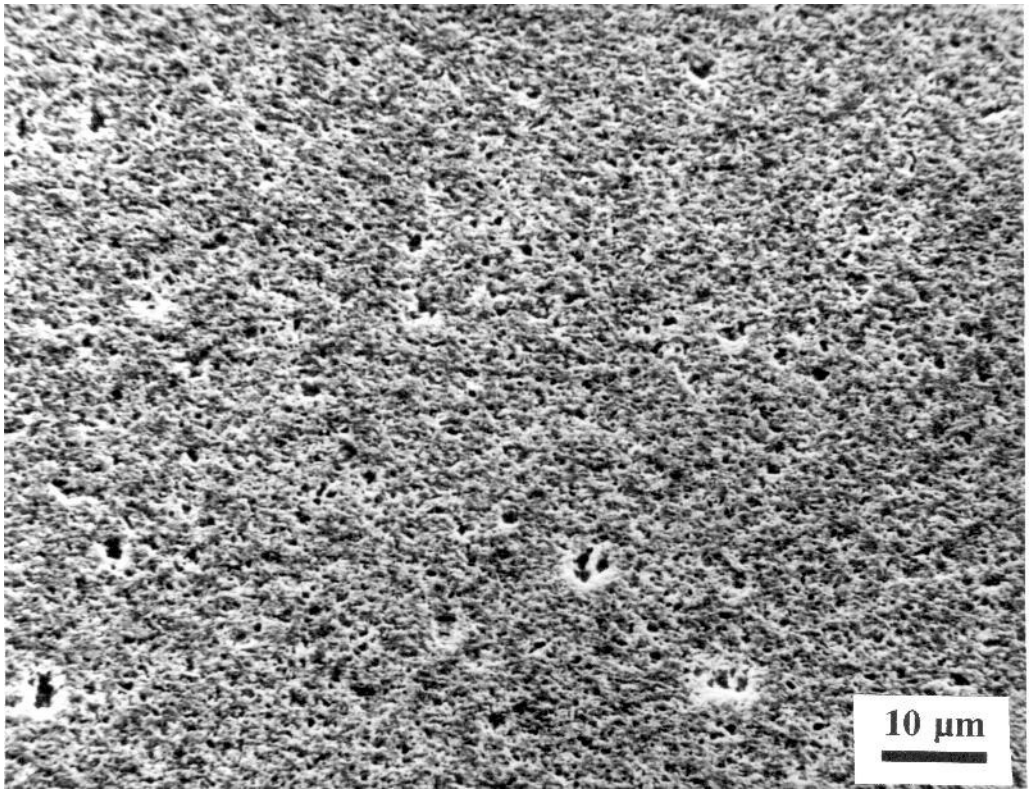

Figure 3.11(c): SEM micrograph showing finer zinc oxide particles in ZnO 5.

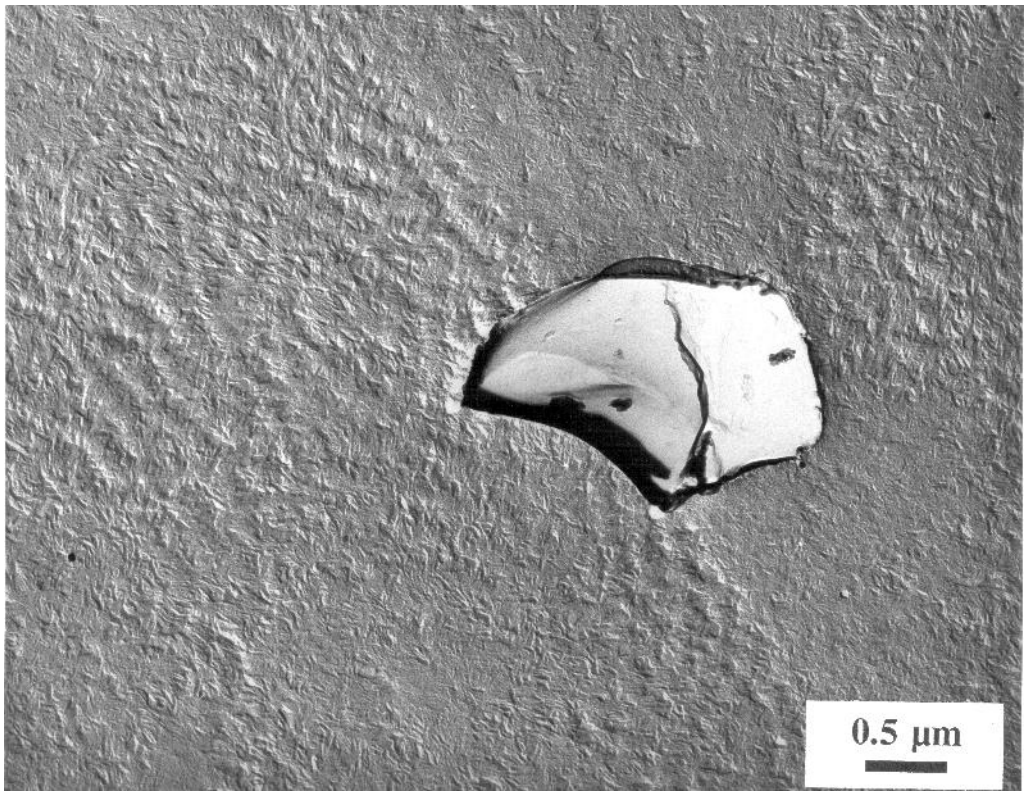

Figure 3.11(d): TEM detail of filler particle and surrounding morphology in ALO 5.

3.10(b) shows the morphology of the BPE material 4901 in the absence of LPE, similar spherulites were observed. Although here similar variations in local morphology were not found, the spherulitic population was very similar to that seen in the quenched blends.

Filled 4901 samples. Figure 3.11(a) and 3.11(b) are SEM micrographs which contrast the differences in alumina filler concentrations in AlO 5 and AlO 30, clearly in the 4901 sample containing 30% filler by volume, filler particles frequently touch. Zinc oxide particles are much finer than alumina particles, so they incorporate into the material to give a much more uniform texture, this is shown for 30% zinc oxide content in figure 3.11(c). One important concern was whether the particles would act as nucleating sites for spherulites in the polyethylene, however TEM observation could only be performed on alumina filled samples since the etchant did not reveal lamellar texture in the zinc filled materials. One suggested reason for this behaviour was that the zinc oxide may be having a detrimental chemical effect upon the etchant used (15). However it is clear from those materials which could be examined by TEM, that the particles do not nucleate spherulites, in fact the morphology of the 4901 is hardly changed at all away from the filler particles (figure 3.11(d)).

To sum up. The morphological results described above correlate well with the DSC data, and with other studies reported in the literature (1-8). We observe, generally, that for isothermally crystallised samples, the size of the linear rich structures increase with linear content. It is therefore apparent, particularly in the case of isothermal crystallisation at 124°C, that spherulitic growth is limited by the amount of available crystallisable material in the volume of melt in which the LPE-rich structure is growing. Also the amount of space available for a spherulite to grow becomes important with high linear concentrations, this is seen particularly well in the BPA 115/20 and BPA 115/30 samples which show a similar morphology, despite the addition of extra LPE. In the quenched samples, the number and size of banded spherulites do not show any definite trends; the morphology does not vary appreciably over the blend composition range considered here and is very similar to that found in the 4901 material. Although the composition of the BPE rich matrix in the isothermally crystallised samples was similar to 4901 from the point of view of the DSC data, morphologically this was not true.

Filled systems show a spatially uniform distribution of irregularly shaped particles in a matrix essentially made of 4901, this is confirmed by DSC data and by TEM. However in

the ZnO filled samples the situation is less clear, with regards to the structure of the BPE matrix.

3.5 Electrical Test Results

Electrical ramp tests were then performed at a ramp rate of 50 volts/second using 50 Hz A.C voltage on samples of 75 microns in thickness using the procedure and equipment described in chapter 2.

Figure 3.12(a) shows the average breakdown strength of the blend systems described above. The branched polymer 4901 was found to give an average strength of 129 KV/mm and in the analysis that follows, we shall take this as a reference point with which to compare each of the blends. In all cases, appreciable scatter was observed in the results and therefore 95% confidence limits were calculated from each data set. In all the materials, the resulting confidence interval was of the order of 5 KV/mm but, despite this uncertainty, it is, nevertheless, still possible to identify general trends in the data sets. In the case of the samples crystallised at 115°C (open banded spherulites), the electrical strength increases markedly with the proportion of LPE in the blend, up until a point, the effect of going from 20% LPE to 30% LPE is small; a somewhat smaller increase is also seen in the samples crystallised at 124°C (sheaf-like inclusions). Conversely, in the quenched materials, the electrical strength is largely independent of composition. Compared with the BPE alone, a clear improvement is seen in properties above about 7% linear in the samples prepared at 115°C whereas, in those prepared at 124°C, an improvement could be said to occur above about 17% LPE. At compositions below about 7% linear polymer, both data sets show a similar reduction in electrical strength. A similar reduction in electrical strength occurred in the case of the filled 4901 (fig. 3.12(b)). Here average values have been used for ease of calculation, however these compare well with those calculated using a Wiebull fitting program (figure 3.12c).

Thus, whereas morphologies based upon well distributed, small spherulites, or filler particles, lead to a reduction in breakdown strength, space filling spherulitic structures can improve substantially the electrical strength of the material.

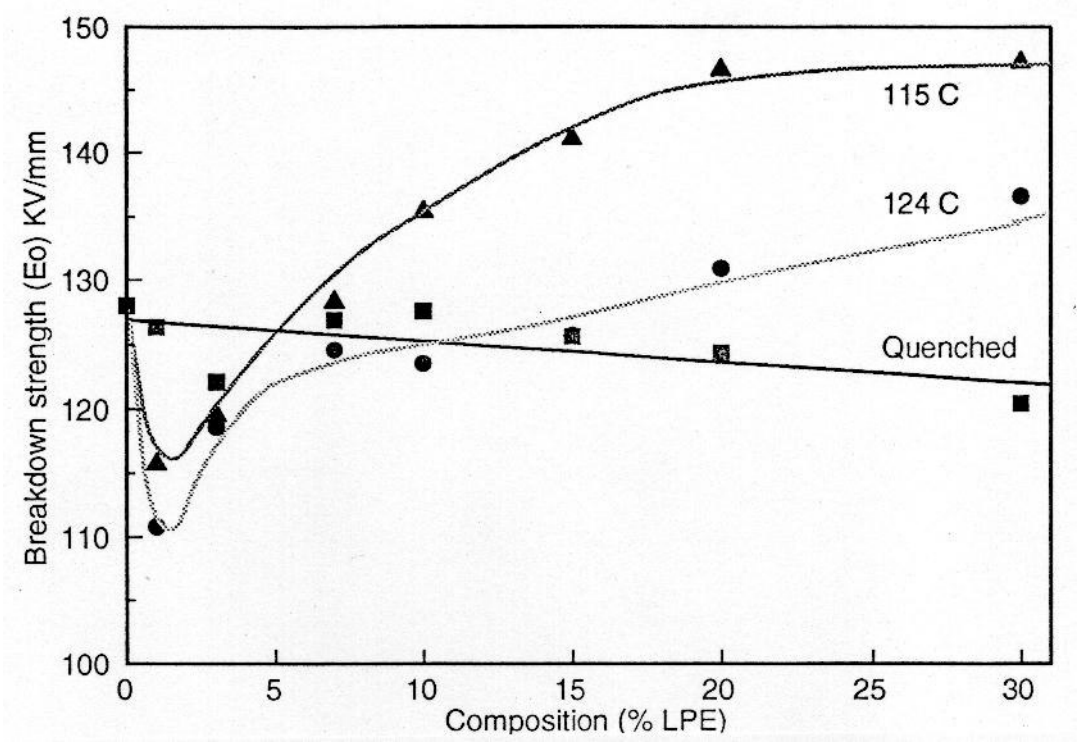

Figure 3.12(a): Electrical strength as a function of blend composition.

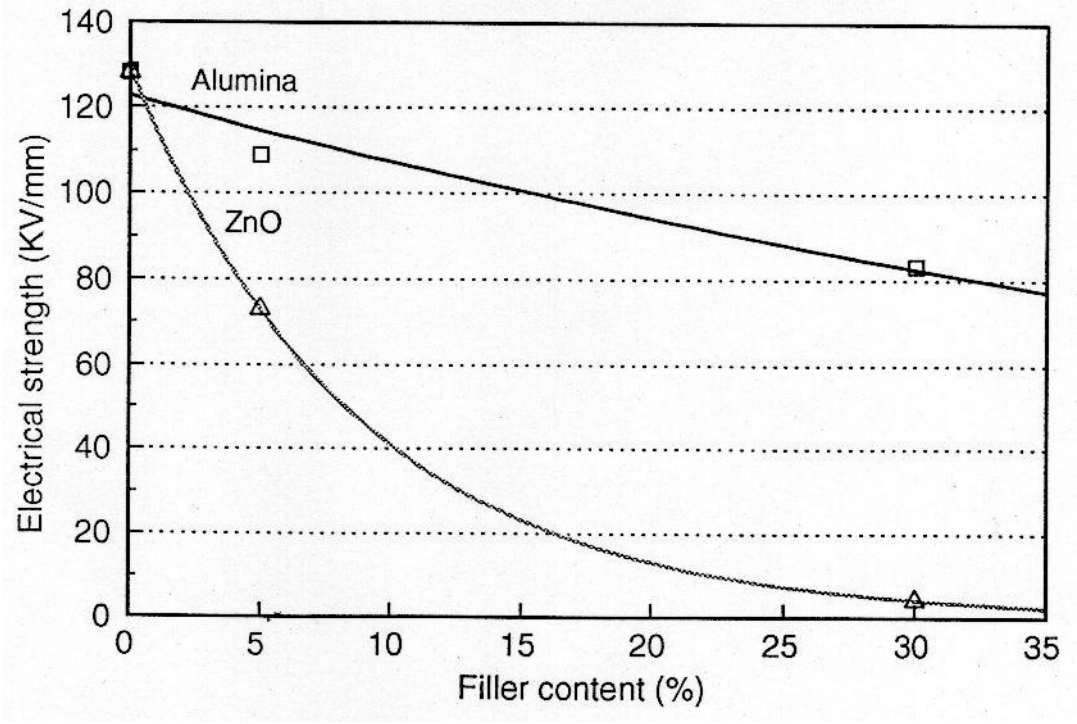

Figure 3.12(b): The effect of filler particles on the electrical strength of 4901.

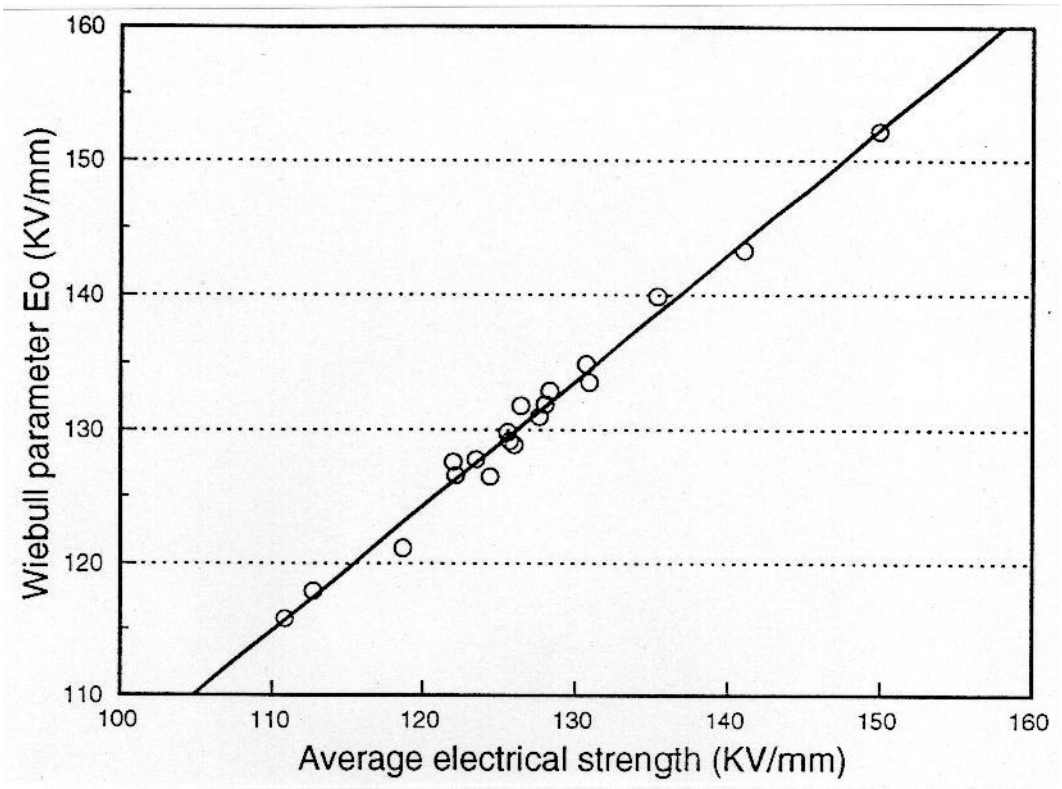

Figure 3.12(c): Comparison of Wiebull and average methods for determining electrical strength.

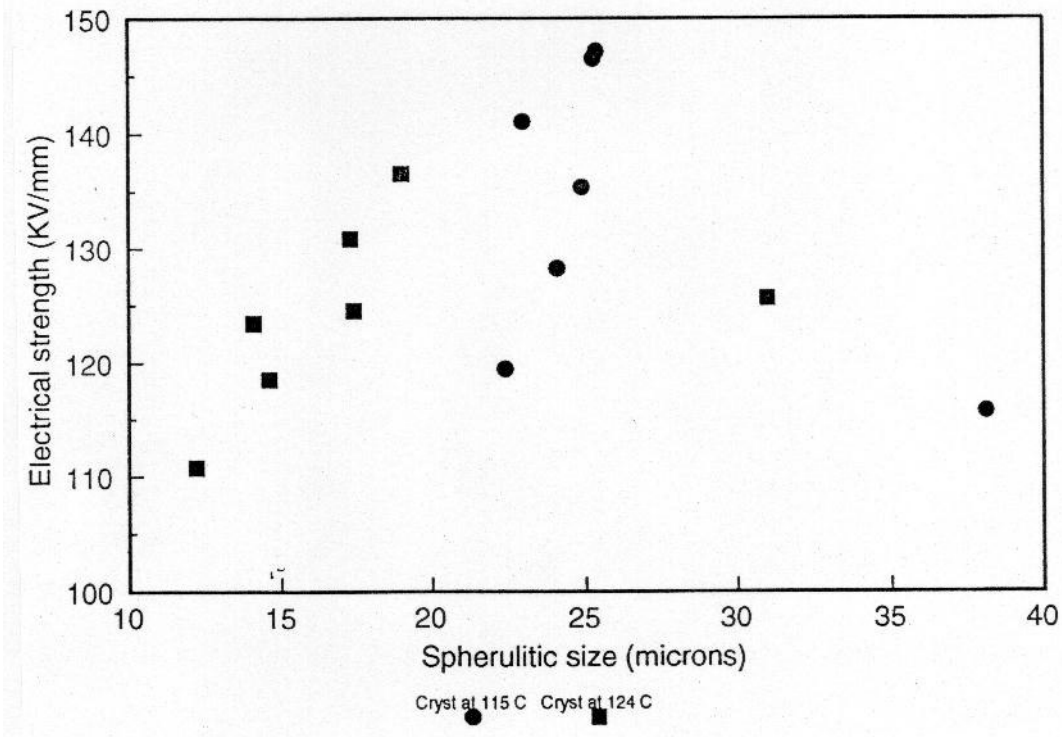

Figure 3.13(a): Dependence of electrical strength on spherulitic diameter.

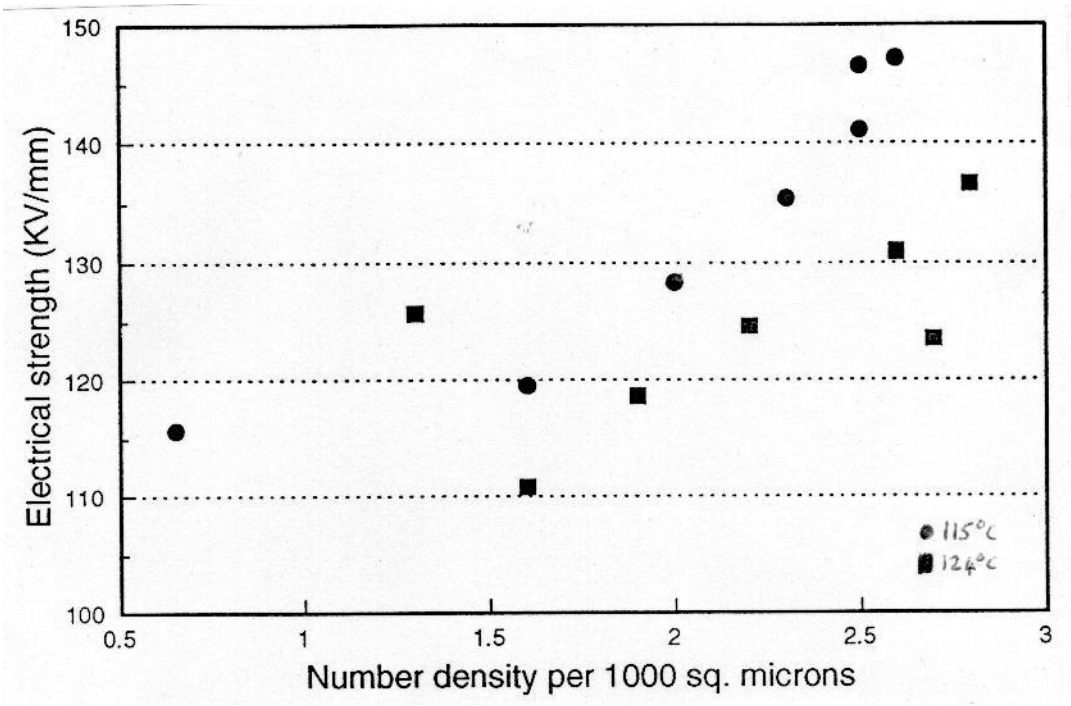

Figure 3.13(b): Dependence of electrical strength on nucleation density.

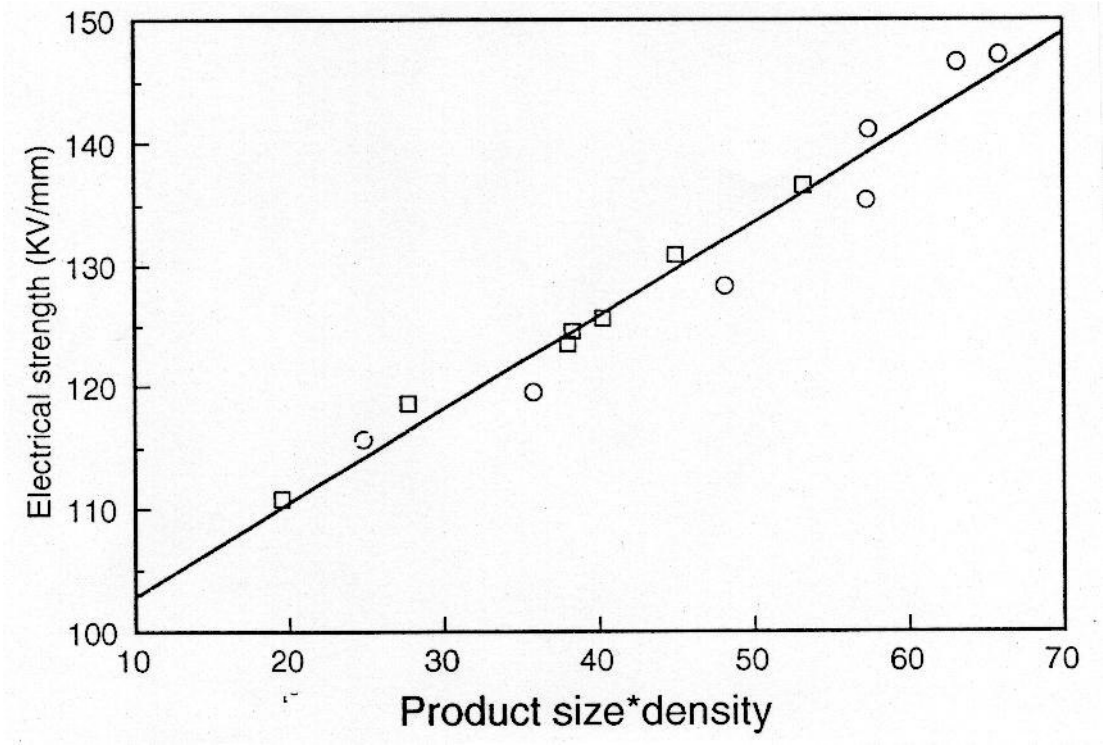

Figure 3.13(c): Dependence of electrical strength on nucleation density and spherulitic diameter.

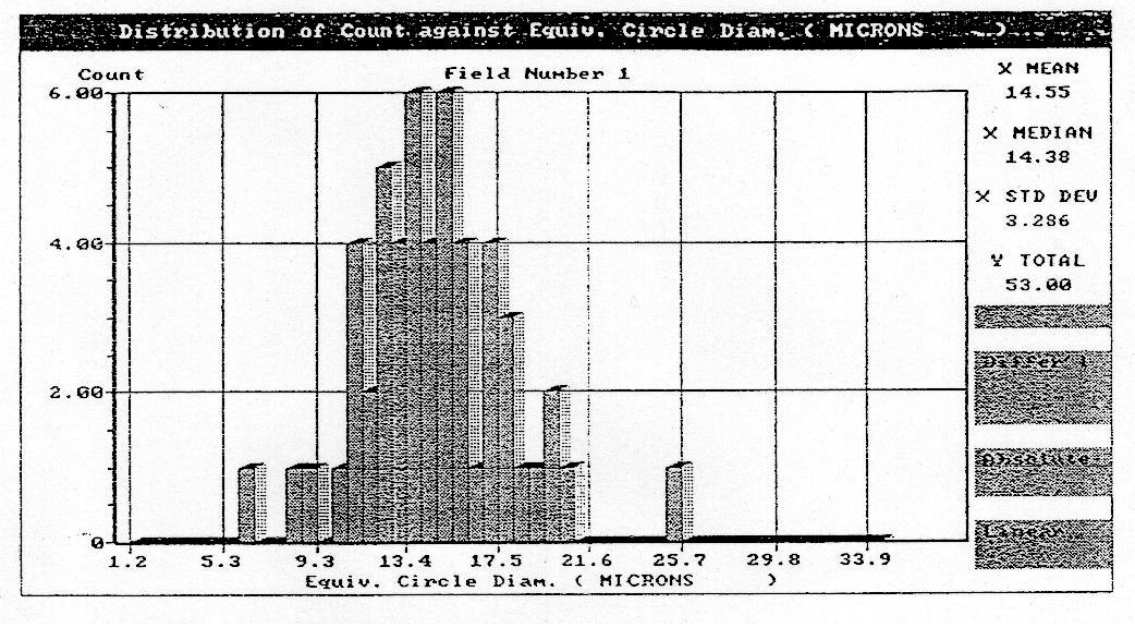

Figure 3.13(d) Histogram of spherulitic diameters in BPA 115/3.

3.6 Electrical strength and spherulite size

It was difficult to image the quenched blends in the SEM, and they did not show any significant variation in electrical strength, so this discussion is limited to the isothermal samples only. Figure 3.13(a) shows the average spherulitic diameter d, as measured by the Quantimet system, (details see chapter 2) plotted against the electrical strength of the corresponding blend and no trend is evident. Again when the number of spherulites per unit area, N_a, is plotted against electrical strength (fig 3.13(b)) no trend is evident. Figure 3.13(c) is a plot of the product of the two variables N_a and d against electrical strength. A linear dependence is observed with both blends displaying the same trends, despite clear differences in crystallisation behaviour and the microstructure of spherulites in each case. It is therefore clear that *both* the size and number density of spherulites is important in determining electrical strength of these materials and examining either parameter on their own leads to inconclusive results, here it is plain that the *nature* of the spherulites is unimportant.

Figure 3.13(d) shows a typical histogram of spherulitic size in one SEM picture - showing that the procedure yields meaningful results.

The primary conclusion here is that spherulites are quite clearly influencing the electrical strength, but the question is how. To do this we have to examine electrical trees and how spherulites might influence their growth.

3.7 Electrical tree observation

Some attempts were made to try and examine electrical trees in our samples to see how they are influenced by a well defined spherulitic population, but it was difficult to predict the moment before a sample might fail as the times to failure were so short and the scatter in the data was so large. Several attempts were made to image trees from pre-failure samples but it was not possible to see where they were in the sample (so that sectioning and examination could be performed) through the semi-opaque samples, this was further complicated by their small size, being limited to the thickness of the samples (70 microns). Waiting for a sample to fail and then examining the trees was also tried but to no avail,

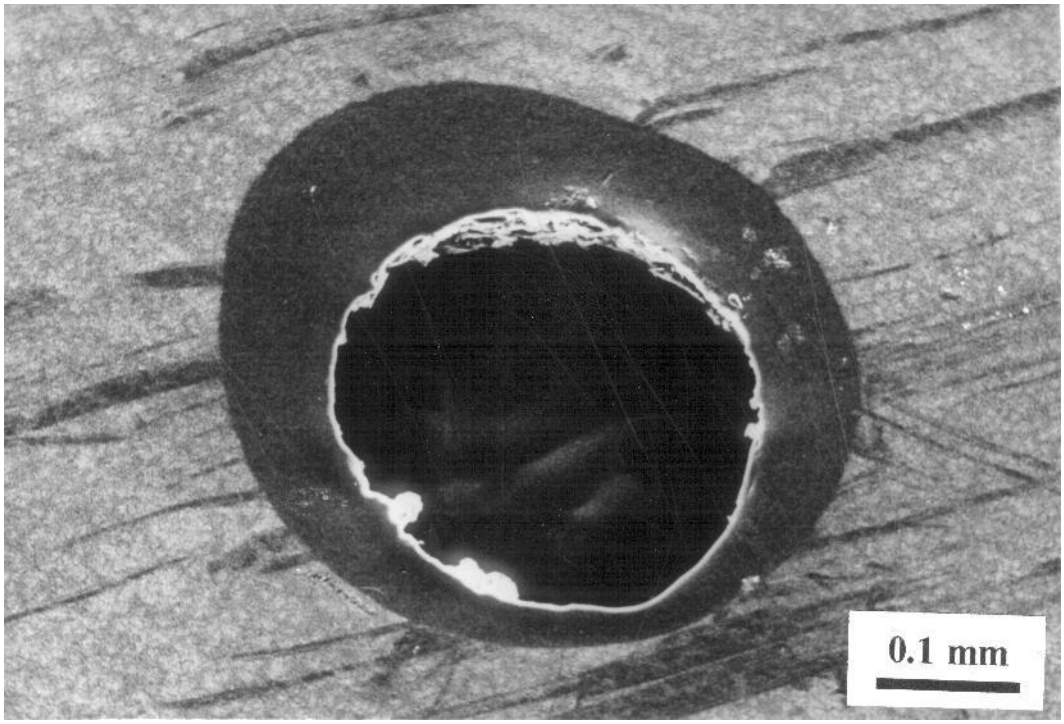

Figure 3.14(a): Melted hole in BPA 124/10 after a breakdown event, showing an adjacent region of quenched material and the surrounding spherulitic morphology.

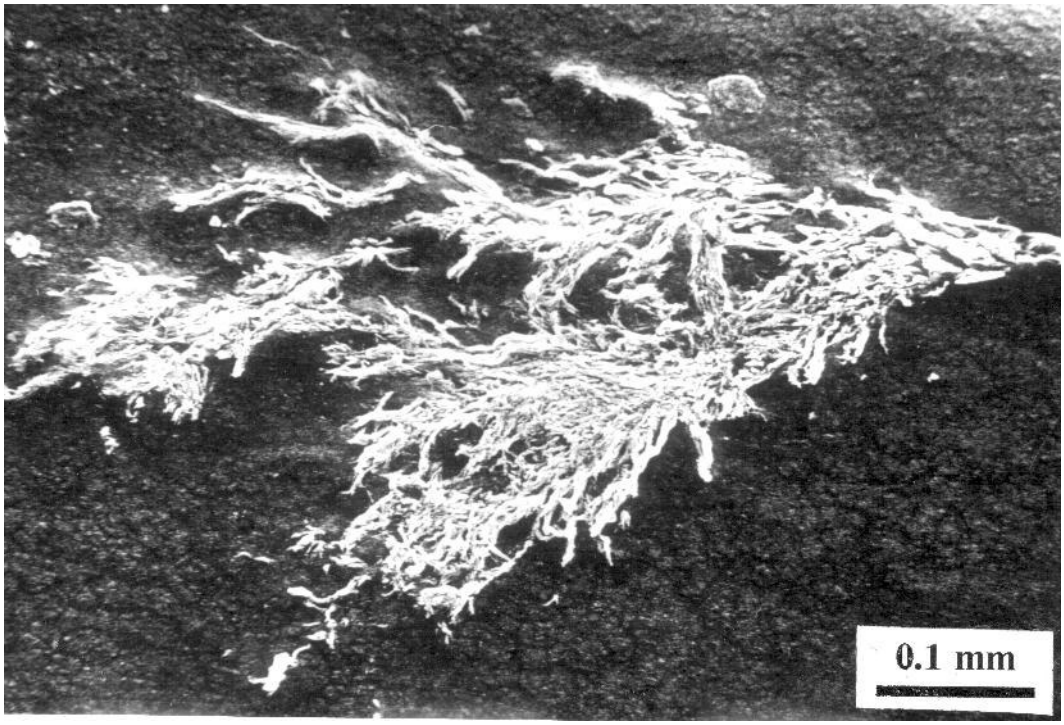

Figure 3.14(b): Electrical tree grown in BPA 124/10.

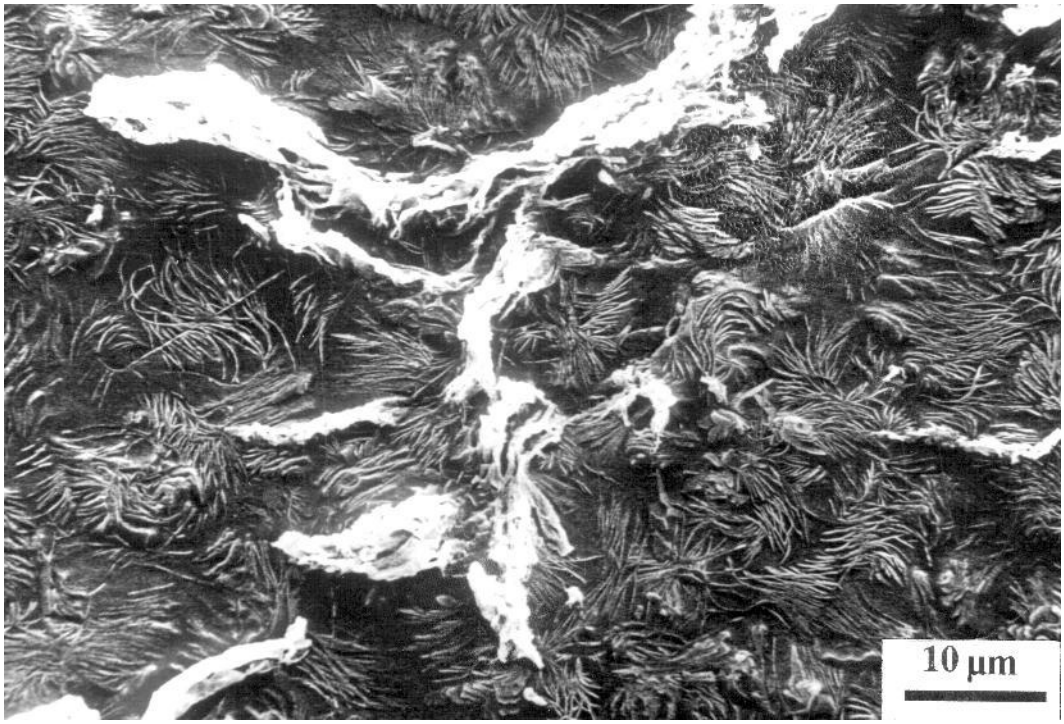

Figure 3.14(c): Although the tree is a 3 dimensional structure this example shows the tree clearly avoiding spherulites.

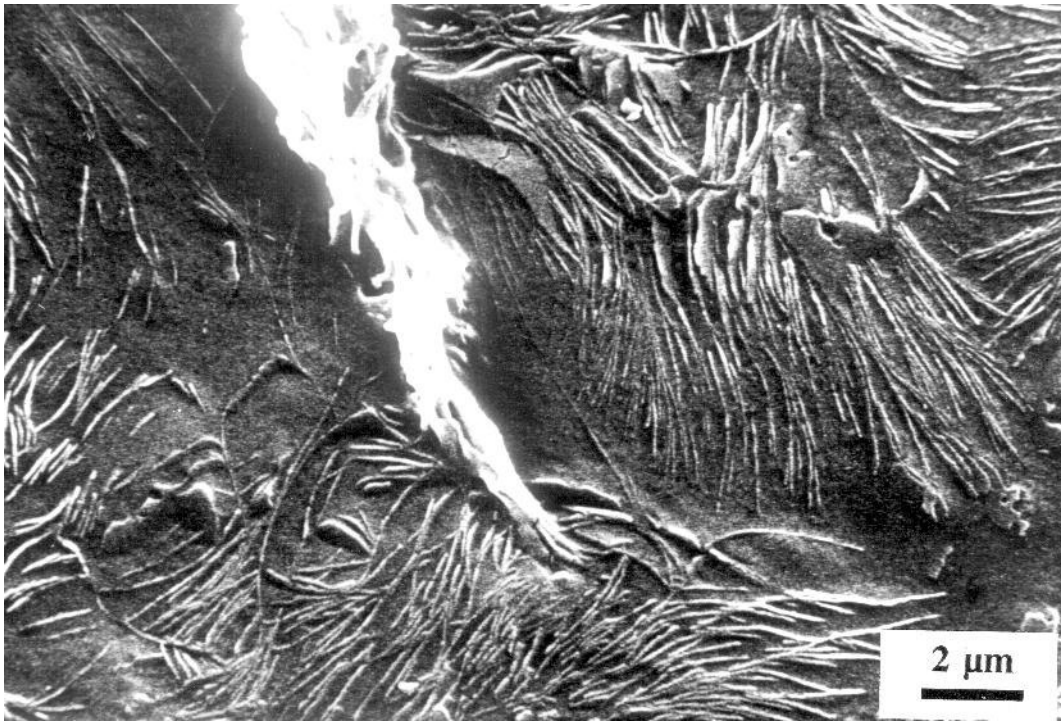

Figure 3.14(d): This section of the tree has impinged into a spherulite and growth may have stopped.

since any trees are destroyed by the final discharge (which exceeded 5mA-even with the trip set to its most sensitive setting) to leave a melted hole (figure 3.14(a)). So instead, to gain such understanding and some idea of tree growth patterns, a larger tree was needed so it could be located easily and imaged. To carry out this operation and to get a bigger tree the electrode separation needed to be much larger than 70 microns. A small block of the blend BPA 124/10 was prepared, this sample was then subjected to 5.8 KV for a total of 105 hours between 0.5 mm diameter (radius of curvature at tip 0.1mm) opposing needle electrodes spaced 2 mm apart, after which a tree was clearly visible in the material, which grew from the earth electrode. The electrodes were then removed and the tree filled with LR White medium grade acrylic resin (The London Resin Co. Ltd), which was allowed to diffuse into the tree channels for 48 hours. The LR white was then cured for 12 hours at 60°C under nitrogen, after which the sample was cut open with a microtome, etched and mounted for SEM examination.

In figure 3.14(b) the general pattern of the tree grown in BPA 124/10 is shown, it shows a multiply branched structure. A closer examination confirms that the tree follows a tortuous path generally avoiding the spherulitic regions (fig 3.14(c)). Figure 3.14(d) shows a vivid example of a tree branch, which has impinged into a spherulite, and growth has apparently halted. Despite the necessarily different growth conditions, this tree grown in a typical material shows many of the features typical of electrical trees (16, 17). In conclusion we see a well defined multiply branched structure which primarily grows between the spherulites. Where branches impinge onto spherulites, growth either ceases or the branch is deflected by the spherulite. Clearly, spherulites *do* influence growth patterns of electrical trees.

3.8 Discussion

3.8.1 Crystallisation

Although the crystallisation behaviour with temperature does follow the general precepts of secondary nucleation theory, the variation of crystallisation time with linear content deserves some discussion on its origins and causes. Blends with lower LPE content take significantly longer to crystallise at a given temperature than those with higher LPE

contents, this effect is thought to be due to a `dilutant' effect of the BPE on the LPE. In blends with high concentrations of BPE are present it is thought that this `defective' material becomes entrapped at growth fronts (19) and as a consequence the crystal growth rate decreases. This sort of behaviour has been reported in polystyrene mixtures diluted with benzophenone (18) and also in isotactic/atactic polystyrene blends (19).

3.8.2 Spherulitic influence on electrical breakdown data

To explain the results it is necessary, first, to consider current understanding of the factors that may influence the breakdown behaviour of a polymer.

During an electrical breakdown event, the energy dissipated locally is substantial and, for this reason, it has been argued that morphology can only ever play a minor role in influencing electrical strength (10,20). Conversely, detailed TEM studies of electrical tree *initiation* by TEM have suggested that, in the earliest stage of development, the tree does not grow in the direction of the maximum electric field but, rather, tends to develop parallel to the neighbouring lamellae, in regions of low crystallinity (16,17). In fact it was found that spherulites of various diameters had 'intrinsic electrical strengths'[6] of somewhere between 3-4 times that of the surrounding material (21), spherulites are therefore unlikely to be weak points favoured by tree growth.

A space filling network of lamellae would serve to deflect the growing tree away from the direction of maximum electric field and, as a consequence, the breakdown strength *is also* affected by the spatial distribution of lamellae (22). In view of this, it is easy to see why a space filling spherulitic texture results in a higher electric strength. In polyethylene blends, spherulites are composed of an array of linear-rich lamellae separated by regions of more defective material. Electrically, such a morphology effectively constitutes an interpenetrating array of planar barriers which, on the basis of the above evidence, serve to inhibit the propagation of an electrical tree. An increase in LPE content from 20% to 30% had little effect on the degree of space filling and that the morphologies of these systems were very similar so the electrical strength does indeed seem to be connected *directly* with

[6] Here the term could be somewhat misleading as all one can do is measure the time to failure across a specified region of material under a certain voltage stress. Precise details of the testing procedure were not given.

the amount of space filling, which reaches a saturation value at around 20% LPE content. This simply implies that it not possible to fit in more than a certain amount of lamellae into the available volume. In all these cases of space filling spherulites, there is little or no matrix material for the tree to grow in, therefore the electrical trees must go through such regions. In this case the tree growth rate is likely to be decreased.

However, this type of breakdown via interspherulitic regions is often attributed to molecular fractionation effects [22,23]. In view of the results presented here, this explanation seems unlikely in the case of polyethylene blends and, therefore, ideas such as mechanical discontinuities at spherulite boundaries or microvoiding as a consequence of the stresses associated with specific volume changes that occur during crystallization are more attractive in explaining the apparent 'weakness' of interspherulitic regions.

3.8.3 Effects of particulates and small spherulites

However, it is not so easy to explain why a distribution of filler particles and particularly small spherulites should result in reduced electrical strength.

It is well appreciated that contaminant particles will inevitably become incorporated into high voltage insulation during commercial manufacturing processes and, therefore, many studies have been performed to examine the influence of inclusions on dielectric breakdown (23-25). In 1988 Morshuis et al (26) reported on a comparative study of the effects of a range of metallic, biological and mineral particles and concluded that glass was most deleterious in high voltage applications. In the absence of any supporting data, this surprising result (the stress enhancement in the vicinity of a metallic inclusion should be far more severe than those arising from the permittivity mismatch between polyethylene and glass) was attributed to void formation as a consequence of debonding at the interface between the matrix and the inclusion. Morphological examinations of the two types of filler particles would seem to suggest that voiding around their edges is certainly possible. Although no direct evidence for voiding was found on the basis of indirect surface replicas, it is hard to believe that such inorganic filler particles could be points of electrical weakness in themselves, so this idea of voiding is more favourable.

In the case of linear polyethylene inclusions within a branched polyethylene matrix

however, this explanation seems implausible. However, other arguments, based upon differential coefficients of expansion, the specific volume changes associated with crystallization, permittivity mismatches, etc. also seem inappropriate to these systems. In all the quenched blends the spherulitic population was well developed and the same was true of the 4901 BPE material, all had similar electrical strength, this points to an extremely important conclusion. Provided variations in composition do not affect the morphology, morphological rather than compositional factors are key in influencing electrical strength.

However the absence of significant populations of such spherulites, within the matrix material in the isothermally crystallised blends, could be responsible for the fall in electrical strength, observed at low linear contents. DSC results suggested that little compositional change in the matrix was occurring with LPE content, and therefore the reason for this effect must be morphological. This idea can only be reinforced by our conclusion that morphological, and not compositional, changes are responsible for changes in electrical strength.

The reason why few banded spherulites form in the matrix of these blends under these treatment conditions is that there is either no space for them to grow, or the LPE rich spherulites could be drawing in the available crystallisable material from the BPE during crystallisation. The absence of these spherulites in the matrix could be influencing its electrical strength, which could then be causing the drop in overall electrical strength seen at low linear contents. By changing the BPE material for one with a lower electrical strength, we can check whether this variable can influence the electrical strength of the blend in which it is used.

Further work is needed to verify these two important conclusions, this work forms the basis of chapter 4.

3.8.4 Effect of analysis method on electrical breakdown data

So far all electrical data has been expressed in terms of simple averages and standard errors have been calculated from the Normal distribution. In electrical engineering in particular, it is general practice to quote values calculated according to the Weibull distribution (29, 30). The Weibull distribution is thought to reflect the failure processes occurring in electrical

insulation better than a Normal distribution. Calculating values according to Normal distributions is easy and simple to do, however it may suffer from drawbacks; one worry was that results may be an artefact of this method of calculation of mean electrical strength values rather than using the full Weibull distribution.

We have processed most of the data generated in this chapter, through a commercially available standard Weibull fitting program and figure 3.12(c) compares the Weibull average electrical strength with the average values as calculated using a simple normal distribution. As a result of the good linearity of these data sets it is concluded that the results calculated using simple averages lead us to the same conclusions as the Weibull values and the results are therefore not a spurious product of using an inappropriate calculation method.

3.9 Conclusions

1) It is clear that blending has considerable potential as a scientific expedient for exploring structure/electrical property relationships and as a technological means of preparing enhanced polyethylene insulation materials. In this work, breakdown strength has been used as a measure of performance, but the results concur with those reported by Nitta & Funayama [27] who measured inception voltages, rather than breakdown strength, in a number of polyethylene blends. Although no details of materials or processing routes were provided in their paper, a similar general improvement in the performance of blend with increasing linear content was reported.

2) On the basis of the results described above, it is clear that solvent and melt blending are valid procedures for the preparation of polymer blends that do not lead to detrimental effects, as far as electrical strength measurements are concerned. Subsequent data is not therefore an artifact of included solvent, extracted molecular fractions or included impurities, all which could lead to spurious results.

3) We have shown how blending can be used to produce two phase morphologies with, constant composition interspherulitic matrix. When crystallised isothermally, larger spherulites can form at higher LPE contents which can raise the electrical strength.

4) Quenching blends led to very similar morphologies irrespective of LPE content and the electrical strength was similarly invariant within experimental error. This means that

molecular or compositional variations in isolation do not influence electrical strength.

5) It has been possible for the first time to deconvolute the role of the spherulitic morphology in influencing dielectric breakdown from that of the impurity rich, defective interspherulitic regions. The small variations in the matrix composition that do occur are unlikely to be important, since quenching shows that the actual linear content has little bearing on electrical strength, provided the morphology remains unchanged. With this deleterious effect removed it is clear that morphological rather than compositional variations are key at controlling dielectric breakdown.

6) Detrimental effects were seen in low linear content blends, over their quenched counterparts, where only a few small spherulitic structures were present. This general form of behaviour was similar for both isothermally crystallised blend systems. This effect, although needing support from additional research, could be associated with a lack of banded spherulites in the BPE matrix, as seen in the isothermally crystallised systems.

7) Filled systems showed a similar decrease in electrical strength and morphological examination does not discount the possibility of voiding at particle interfaces being responsible for this detrimental effect.

8) The space-filling open banded spherulites gave the greatest increase (noted above 7%) in electrical strength, but it reaches a maximum around 20% LPE content, whereas compact spherulites which did not interpenetrate had less of an effect (not notable until about 17% LPE). Assuming that the general failure route is through the growth of an electrical tree (28-29), the above results suggest that in space filling morphologies electrical trees are seeing interspherulitic regions with many lamellae incorporated. This highly crystalline material is thought to have a higher intrinsic dielectric strength (11, 21).

9) If the linear content is chosen to be high and the sample is crystallised to increase the size and number of the spherulites that are present, a significant improvement in electrical strength can be obtained over the branched material alone. This could have wide ranging implications for cable manufacturers, if a commercially viable production route can be devised.

10) More detailed examination of electrical treeing is required to understand fully the role spherulites have upon electrical breakdown behaviour. However, practical difficulties mean that this cannot be done easily in the thin samples considered here. Electrical trees can be

grown much slower in thicker samples, permitting observation at leisure, which is a better approach to adopt. This is outside the scope of the current academic study.

3.10 References

1) P.J. Barham, M.J. Hill and C.C.A Rosney, J. Mater. Sci. Letts. 1988, **7**, 1271.

2) M.J. Hill, P.J. Barham, A. Keller and C.C.A. Rosney, Polymer 1991, **32**, 1394.

3) M.J. Hill and P.J. Barham, Polymer, 1992, **33**, 4891.

4) M.J. Hill, P.J. Barham and A. Keller, Polymer 1992, **33**, 2530.

5) S.R. Hu, T. Kyu and R.S. Stein, J. Polym. Sci. B 1987, **25**, 71.

6) J.M Rego-Lopez, M.T Conde-Braha, B. Tenselius and U.W Gedde, Polymer 1988, **29**, 1045.

7) D.R. Norton and A. Keller, J. Mater. Sci. 1984, **19**, 447.

8) A.S Vaughan, Polymer, 1992, **33**, 2513.

9) A. Gustafsson and U.W Gedde, Proc. Nordic Insulation Symposium Vasteras, 1992, p8.4:1.

10) W.L. Wade, R.J Mammone and M. Binder, Polymer 1993, **34**, 1093.

11) J.D Hoffman, G.T Davis and J.I Lauritzen, in `Treatise on Solid State Chemistry', vol.3, Crystalline and Non-crystalline Solids, ed. N.B.Hannay, Plenum, New York, 1976, p497.

12) H.D Keith and F.J Padden, J. Appl. Phys. 1964, **35**, 1270.

13) J.R Dryden, J. Mater. Sci. Letts. 1987, **6**, 1129.

14) D. Patel and Bassett, D.C., Proc. R. Soc. Lond. A 1994, **445**, 577.

15) R. H Olley, personal communication.

16) N. Hozumi, T. Okamoto, H. Fukagawa., Jap. J. Appl. Phys. 1988, **27**, 1230.

17) N. Hozumi, M. Ishida, T. Okamoto and M. Fukagawa, IEEE Trans. Electr. Insul. 1990, **EI-25**, 707.

18) J. Boon and J.M Azcue, Jour. Polym. Sci. A-2 1968, **6**, 885

19) G. S. Y. Yeh and S. L Lambert, Jour. Polym. Sci A-2 1972, **10**, 1183

20) W. Golz, Colloid and Polym. Sci. 1985, **263**, 286.

21) S. N Kolesov, Polym. Sci. USSR. 1980, **21**, 1993.

22) T. Okamoto, M. Ishida and N. Hozumi, IEEE Trans. Electr. Ins. 1989, **EI-24**, 599.

23) R. Jocteur, E. Favrie and H. Auclair, IEEE Trans. Power Apparatus and Systems 1977, **PAS-96**, 513.

24) C. Laurent and E. Kay, J. Appl. Phys. 1988, **64**, 336.

25) T. Nensi, A. E Davies, A.S Vaughan and S. G Swingler, Ann. Report of Conf. on Electrical Insulation and Dielectric Phenomena (IEEE, Victoria, BC, 1992), p.493.

26) P.H.F Morshius, F.H Kreuger and P.P Leufkins, IEEE. Trans. Elect. Ins. 1988, **EI-23**, 1051.

27) Y. Nitta and M. Funeyama, IEEE. Trans. Elect. Ins. 1978, **E1-13**, 130.

28) P. Fischer, in `Electrical Properties of Polymers', ed. D.A Seanor, Academic Press, New York, 1982, p319.

29) C.C Ku and R. Leipins in `Electrical Properties of Polymers', Hanser, Munich, 1987.

30) C. Chauvet and C. Laurent, IEEE Trans. Electr. Insul. 1993, **28**, 18.

CHAPTER 4 - EFFECTS OF MOLECULAR COMPOSITION ON ELECTRICAL BREAKDOWN BEHAVIOUR

4.1 Introduction

In the previous chapter, the effect on dielectric breakdown of varying the composition of blends of linear (LPE) and branched polyethylene (BPE) was described. By suitable processing routes, a range of morphologies was produced and it was demonstrated that the structural features had a marked influence on the macroscopic electrical strength of the system, as gauged by short term ramp testing. In particular it was seen that the spherulitic texture, rather than molecular or processing conditions determined electrical strength. In this study the same three regimes of behaviour are considered. Isothermal crystallisation at temperatures above the maximum melting temperature of the BPE (~113°C), was employed to grow various lamellar aggregates, principally composed of LPE, within an effectively invariant matrix of branched polymer. Below about 118°C these were composed of space filling banded spherulites, whereas above this temperature they took the form of compact lamellar aggregates. In this way, morphological parameters could be varied independently of other effects associated with rejection of defective molecular fractions during crystallization, stresses at spherulite interfaces etc (1). Materials containing well developed spherulitic structures were found to have improved properties, a conclusion which contradicts previous results (2-7) where, in less well controlled materials, spherulitic development was found to lead to a reduction in electrical strength.

The effect of quenching from the melt was also examined in chapter 3. In these systems, the observed morphology was found to be independent of melt composition, and the electrical strength was, similarly, largely invariant. Although this result strongly suggest that it is morphology rather than molecular composition that determines the electrical breakdown strength of a polymer, as measured by ramp testing, in reality the range of compositions studied (1-30% LPE) was not large, and the effect of changing the molecular architecture was not examined.

The work described below was therefore undertaken to test further the principal conclusion

from chapter 3; namely that morphological rather than molecular factors are responsible for the electrical strength of a semicrystalline polymeric insulator. This was achieved by systematically changing each component in a series of binary blends of a 10% linear polyethylene (LPE) in a branched ethylene based copolymer (CPE). In this way, the effects of molecular mass, branch type, branch content etc could be examined in materials where morphological factors remained largely invariant. Crosslinking, the process of linking together polymer chains to form a network, is important to cable manufacture, here the exact effects of crosslinking are examined by use of an ethylene vinyl silane copolymer. Such materials have the advantage that they can be crosslinked very easily following the crystallisation process, or left in an uncrosslinked state, thus allowing a direct comparison of the effects of crosslinking on electrical strength. Here we take six new blends, two of which involve replacing the original LPE (Rigidex 140/60) with one of higher molecular weight and the other four involve replacing the original BPE (Borealis 4901) with various ethylene based co-polymers.

In all, eight polymers were used, and available data is listed in Table 4.1. From these, the required binary blends (see table 4.2) were prepared by dissolution in xylene, a procedure which results in representative morphologies (8,9) and reliable breakdown data (10,11). In accordance with the previous convention, samples will subsequently be referred to using the following notation; BPX T/C. In this, X specifies the materials used (see Table 4.2), T indicates the thermal treatment (isothermal crystallization at 124°C or 115°C, or quenching) and C gives the proportion of linear polyethylene (always 10% in this study).

4.2 Preliminary studies

The branched polymer 4421 can be crosslinked after crystallisation. This can be accomplished simply by immersing the specimens for 6 hours in a water bath held at 90°C, as prescribed in the manufacturers instructions. This process was verified on some samples of pure 4421 which had been quenched following melt pressing. Crosslinking was subsequently verified by solvent extraction in boiling xylene. The gel component was recovered and, after vacuum drying, about 35% of the initial sample mass remained. As a control, a sample which had not been crosslinked was also subjected to this procedure; as

expected no gel was recovered. Crosslinking was also attempted for 16 hours at 90°C but no more gel component could be extracted.

4.3 Differential Scanning Calorimetry

Crystallisation behaviour. The times taken to crystallise the eight blends isothermally are shown in table 4.2, for the two isothermal conditions. Despite the wide differences in materials used and bearing in mind the uncertainty in finding the point at which the samples had completely crystallised, the times were very similar from blend to blend.

Melting behaviour. Figure 4.1 shows 3 sets of DSC traces, one for each of the crystallisation conditions considered. Most of the blends followed the general behaviour of the BPA blend (as discussed in chapter 3), so only one trace is shown of the blends following this behaviour. This shows the typical melting behaviour of PE blends (12), phase separation of LPE from BPE occurs leading to two distinct lamellar populations, however exceptions occurred in 3 of the 8 blends.

Quenched blends. Figure 4.1(a) shows a selection of melting traces from quenched blends. Most of these traces contain two distinct features, a relatively sharp peak at ~125°C together with a broad endotherm extending from ~120°C to below 90°C. The higher of these two transitions corresponds to lamellae composed principally of linear material, whereas the broad endotherm is associated with a distribution of lamellae containing low molecular mass linear polymer together with the BPE. However, whether this bimodal lamellar distribution is associated with liquid-liquid phase separation (LLPS) prior to quenching (12-14) or molecular segregation during crystallization itself (liquid-solid phase separation; LSPS) (15) is unclear, solely on the basis of such DSC data.

The blend BPD Q/10 displays a very different melting behaviour. In this material, the two features described above overlap to such an extent that the melting transition appears almost singular in form. This difference in behaviour stems from the molecular architecture of the branched copolymer M1, which contains only 9.6 butyl branches per 1000 carbon atoms (16). As such, this polymer is capable of forming thicker (ie higher melting) lamellar structures than the other BPE materials considered here. Indeed, the melting temperature

data included in Table 4.1 further supports this assertion. The blend BPI also shows a similar single peak, this is not surprising as the melting temperatures of the two components is so similar (123 and 133°C) that both components effectively crystallise as one component. The opposite case is observed in BPH, where the melting temperatures are so dissimilar that no interaction at all occurs between the components resulting in two very separated peaks, whereas in most of the other systems described there is always some co-crystallised material situated between the peaks.

Crystallisation at 115°C. Traces from the samples crystallized at 115°C are shown in figure 4.1(b) and, once again, the BPD and BPI blend are anomalous. In all of the other systems the crystallization temperature (115°C) is higher than the melting temperature of the branched component, such that co-crystallization is of only secondary importance, as evidenced by the well separated, well defined peaks that are observed in these cases. In BPD 115/10 and BPI 115/10, however, the crystallization temperature is below that at which lamellae of copolymer M1, and to a greater extent copolymer 2H376, are stable and, hence, extensive co-crystallization occurs, leading to multiple peaks in the case of BPD, and in BPI, where both components effectively crystallised together. In contrast the BPH 115/10 system shows two well separated peaks, which points at no co-crystallisation between the components in this blend. This is not surprising, noting the differences in their melting temperatures (table 4.1).

Crystallisation at 124°C. The melting behaviour of the 124°C crystallized materials is shown in figure 4.1(c). Qualitatively, all the traces appear similar, apart from BPI, all contain two distinct transitions, a high temperature LPE peak plus a broad endotherm which corresponds principally to the BPE component of the blend. The singular nature of the higher temperature peak (cf. figure 4.1(a)) implies that *extensive* co-crystallization does not occur at 124°C, in line with expectations (12). However, it should be noted that whilst the pure HO20-54P has a peak melting temperature that is somewhat higher than the other LPE grades (138°C as opposed to 133°C; Table 4.1) this is not manifest in the blend. This suggests that the lamellae formed in the blends are not the same as those that develop in the absence of branched molecules and this may indicate a degree of co-crystallization

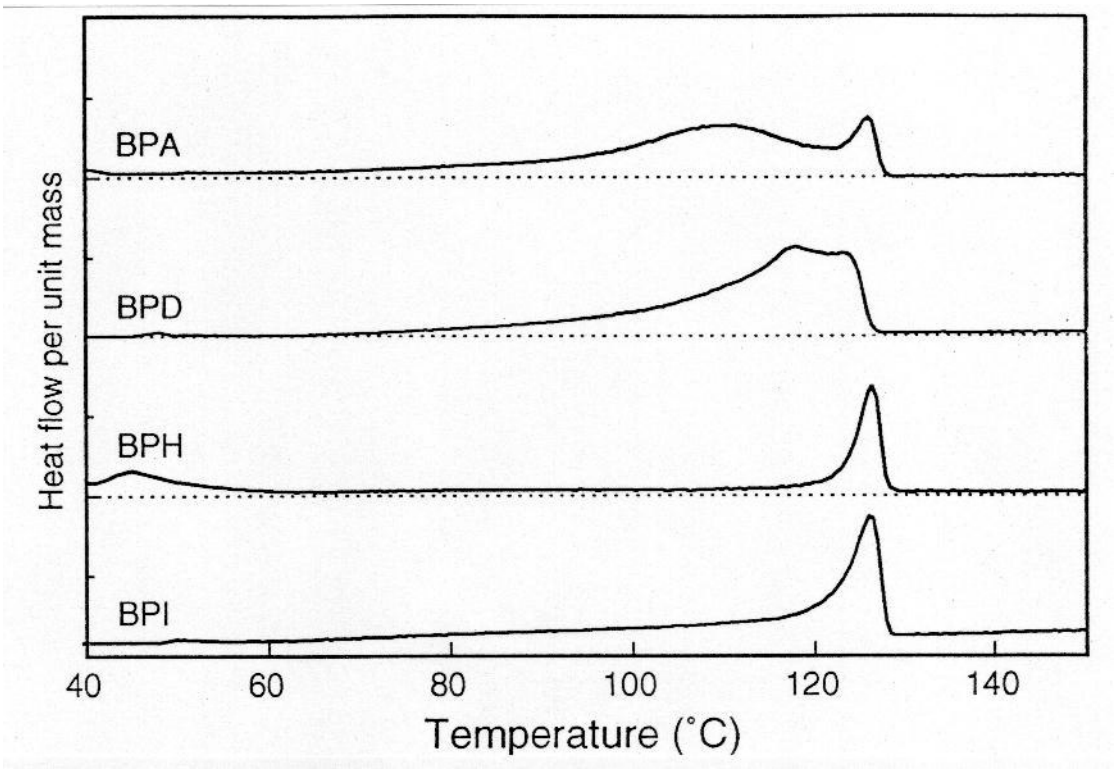

Figure 4.1(a): Melting behaviour of some quenched blends.

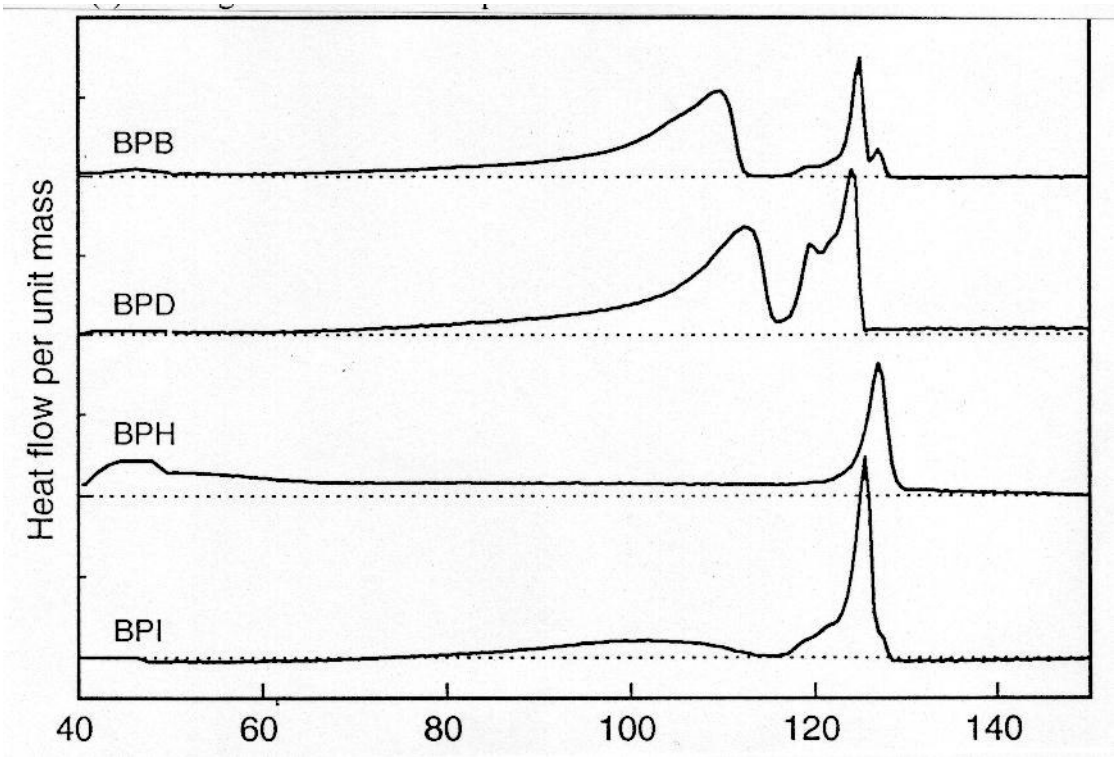

Figure 4.1(b): Melting behaviour of some blends following crystallisation at 115°C.

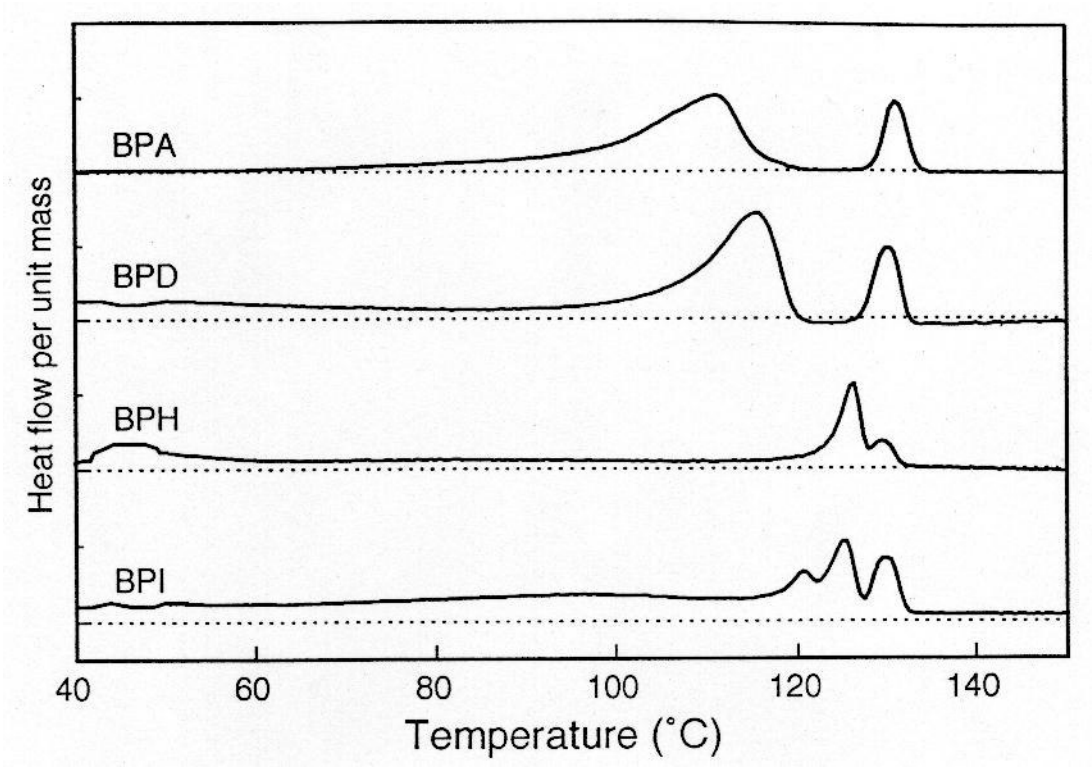

Figure 4.1(c): Melting behaviour of blends after crystallisation at 124°C.

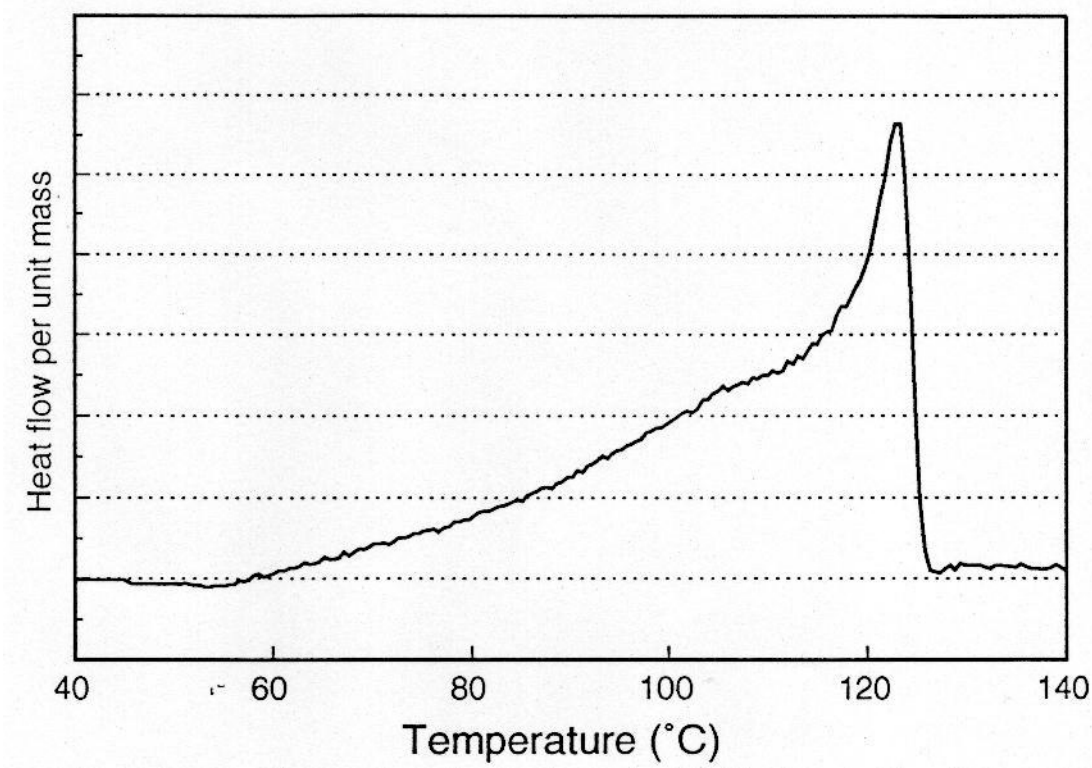

Figure 4.1(d): The co-polymer 2H376 shows an unusually wide melting endotherm.

occurs even at this high temperature. Some comment ought to be made in the case of the multiple peaks observed in the BPI blend. The crystallisation temperature, 124°C in this case allows much of the 2H376 to crystallise (fig 4.1(d)), whereas in all other cases the branched copolymer remains molten. However not all of the 2H376 can crystallise at this temperature, only the most perfect of molecules can crystallise together with the 140/60. These co-crystals are represented by the peak at around 127°C, whilst the higher temperature peak (near 131°C) represents material rich in 140/60 which can readily crystallise. The lower temperature endothermic peak (near 122°C) represents the rest of the material, which can only crystallise on quenching.

4.4 Morphology

The morphologies seen in the blend systems considered here were generally similar to those described previously in chapter 3, so we will concentrate primarily on the cases where differences in structure occurred.

SEM examination. After crosslinking, the BPG blend retains its original morphology; the example shown in fig 4.2(a) is of BPG 115/10 which shows a banded spherulitic texture, typical of crystallisation at this temperature and identical to BPF 115/10. BPB 124/10 was found to contain unusually large lamellar aggregates (fig 4.2(b)), compare with the usual microstructure imaged in BPC 124/10 (fig 4.2(c)).

TEM examination. Two types of morphology existed in samples that were quenched. In those blends which showed a double DSC melting peak after quenching the morphology was of segregated banded spherulites, like that shown in figure 4.3(a) which is of BPF Q/10. This is evidence therefore of liquid-liquid phase seperation in the melt which gives rise to domains of LPE rich material, which then crystallise quickly on quenching to give a characteristic morphology (12-14). In the blend BPI Q/10 (figure 4.3(b)), and also noted in BPD Q/10, a uniform lamellar morphology is obtained with no spatial variations in texture, indicative of a miscible melt.

In blends crystallised at 115°C two exceptions occurred to the expected banded spherulitic texture, here illustrated in BPA 115/10 (figure 4.4(a)). In blend BPD 115/10,

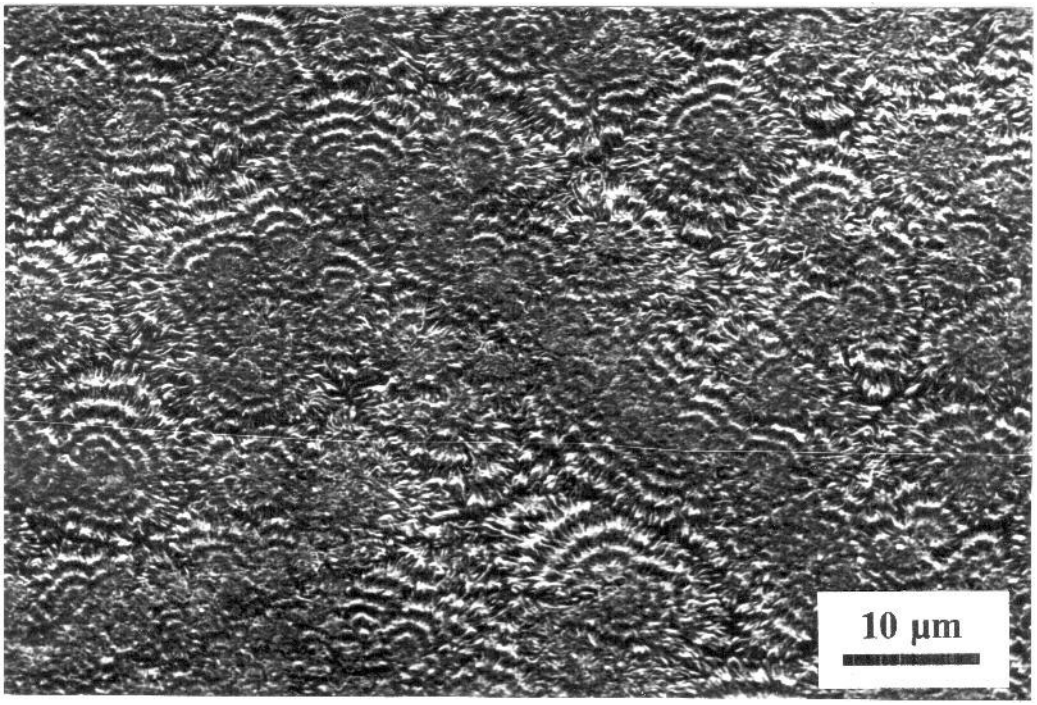

Figure 4.2(a): Banded texture is retained after crosslinking BPF 115/10.

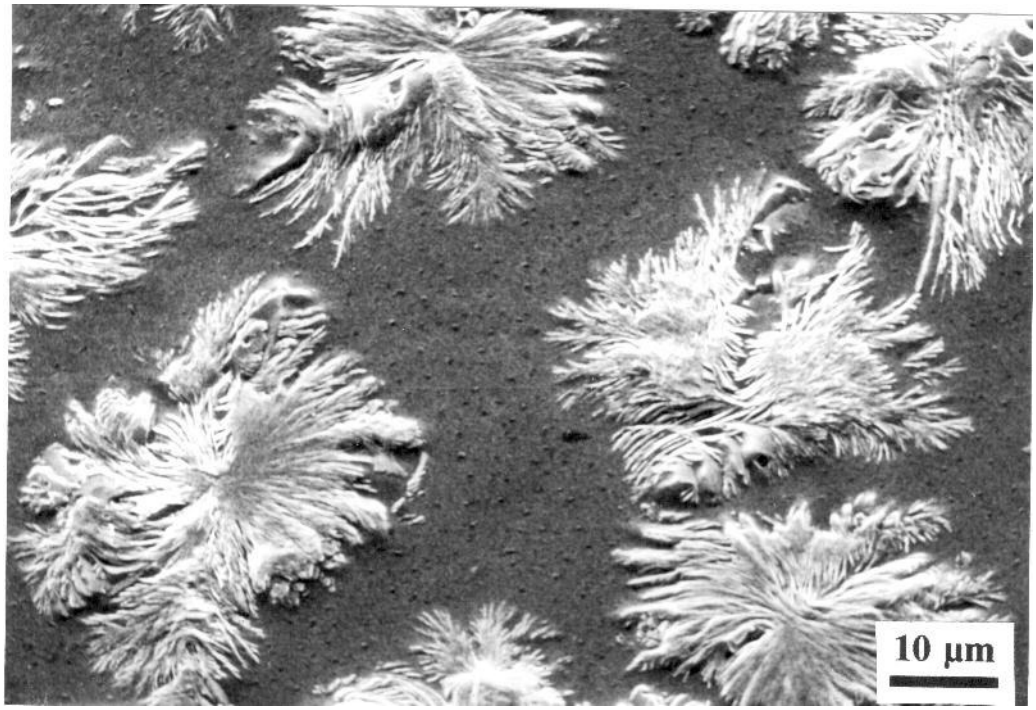

Figure 4.2(b): BPB 124/10 showing unusually large lamellar aggregates.

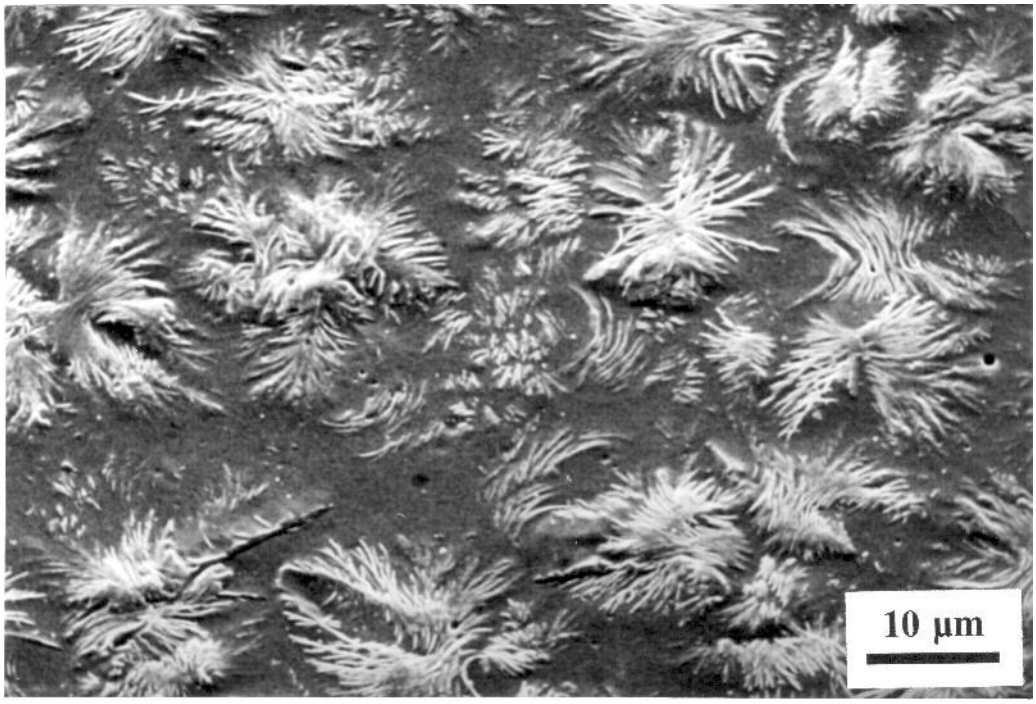

Figure 4.2(c): Typical lamellar aggregates in BPC 124/10.

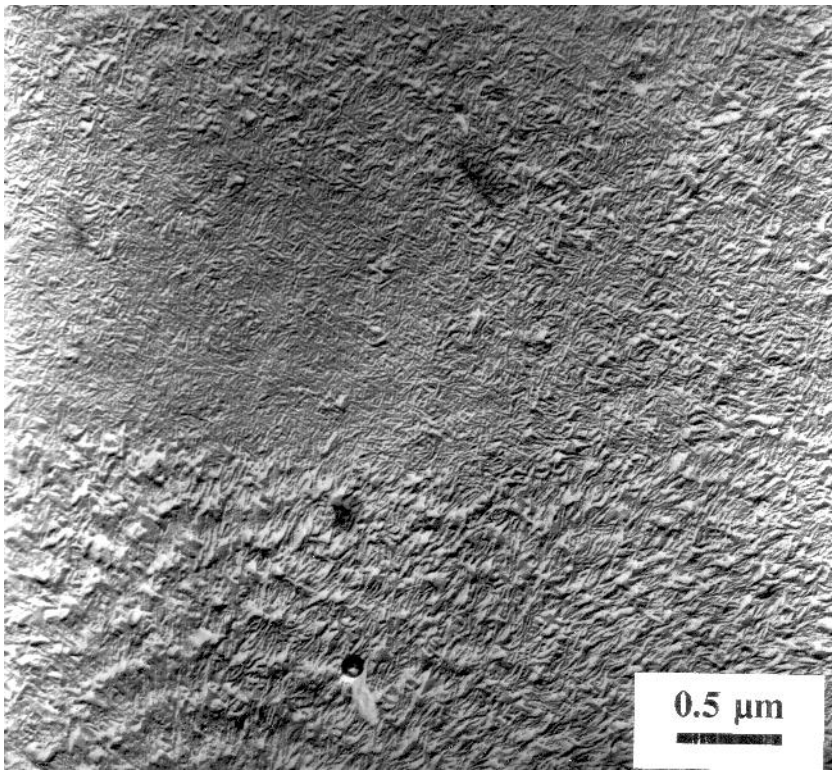

Figure 4.3(a): Segregated microstructure of BPF Q/10.

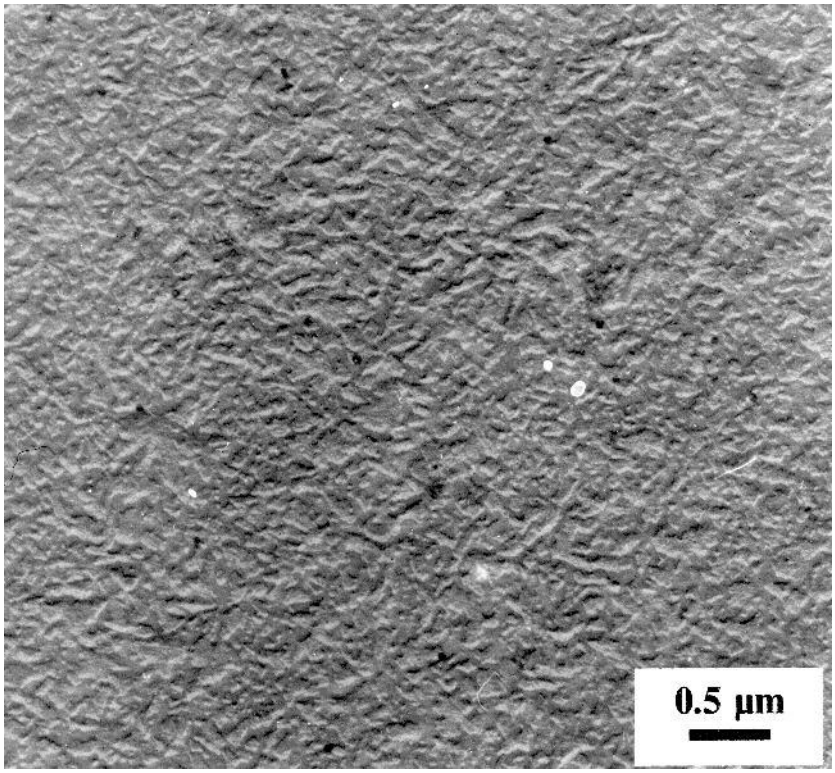

Figure 4.3(b): Uniform microstructure of BPI Q/0.

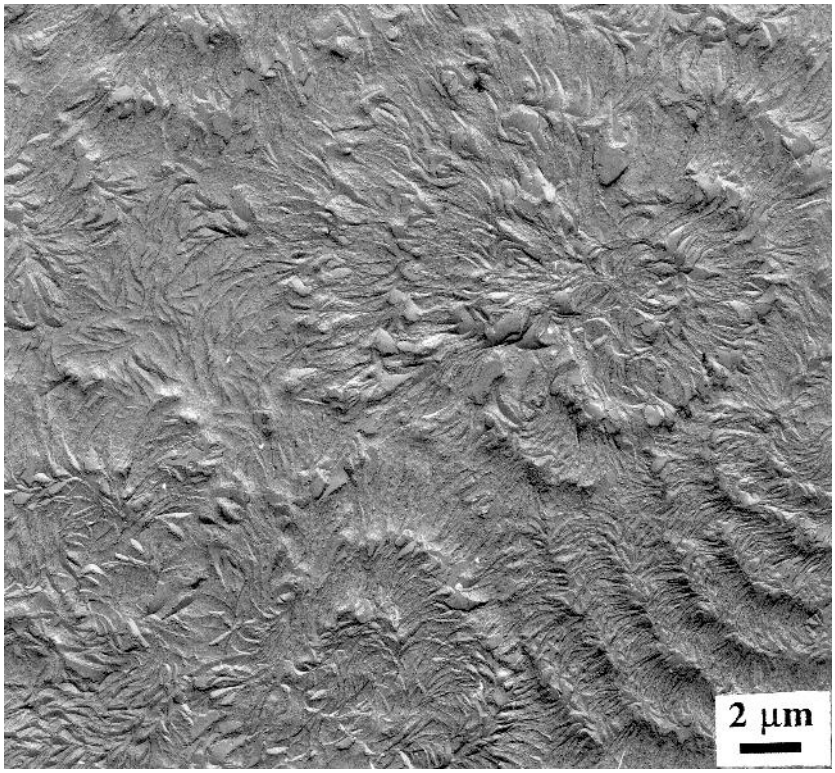

Figure 4.4(a): Typical space filling banded morphology in BPA 115/10.

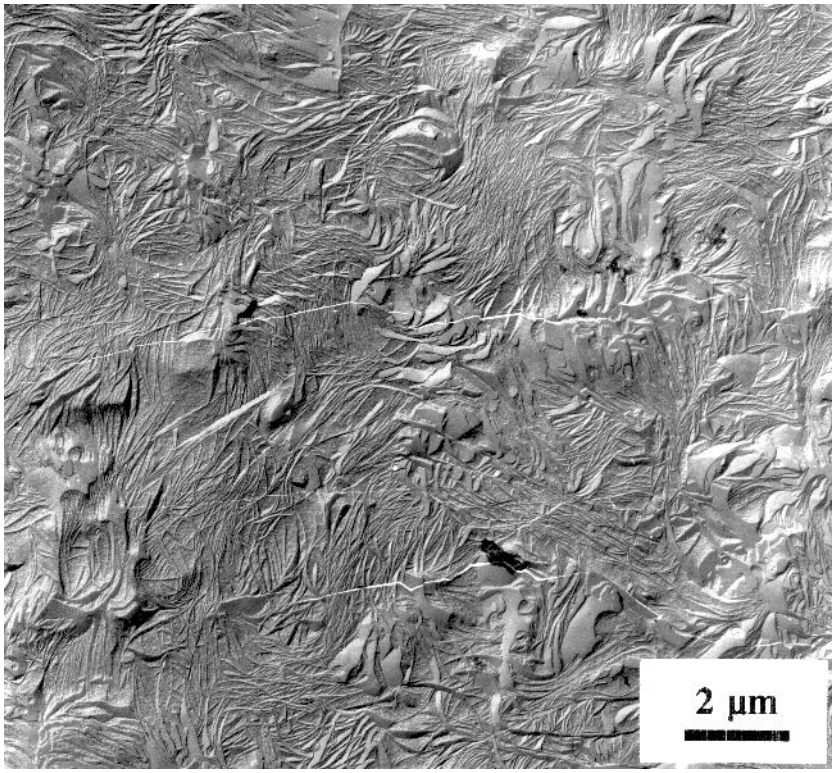

Figure 4.4(b): Uniform texture of randomly oriented lamellae in BPD 115/10.

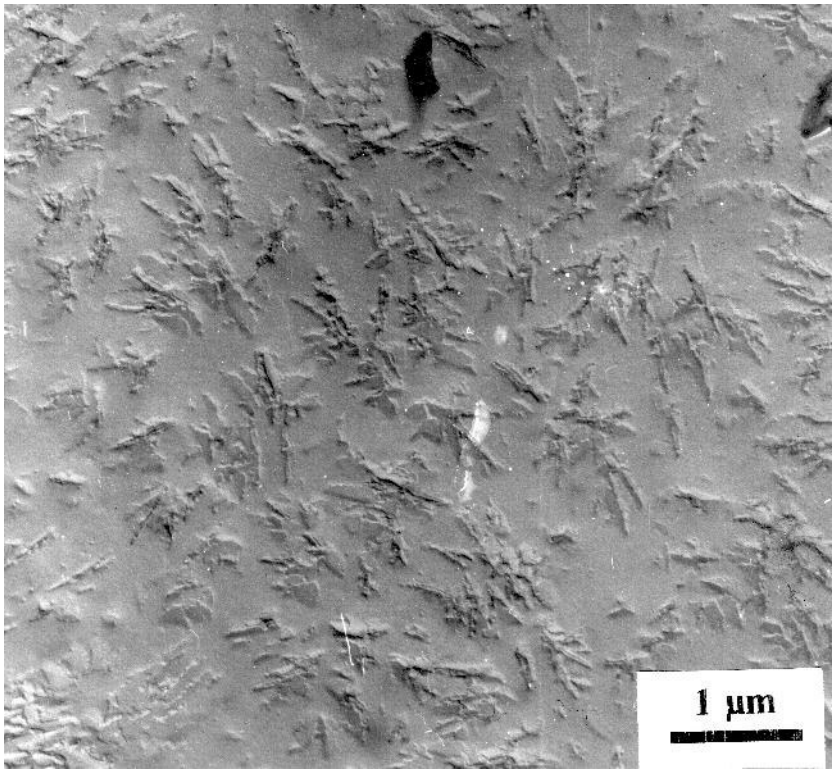

Figure 4.4(c): Lamellar aggregates are formed instead in BPH 115/10.

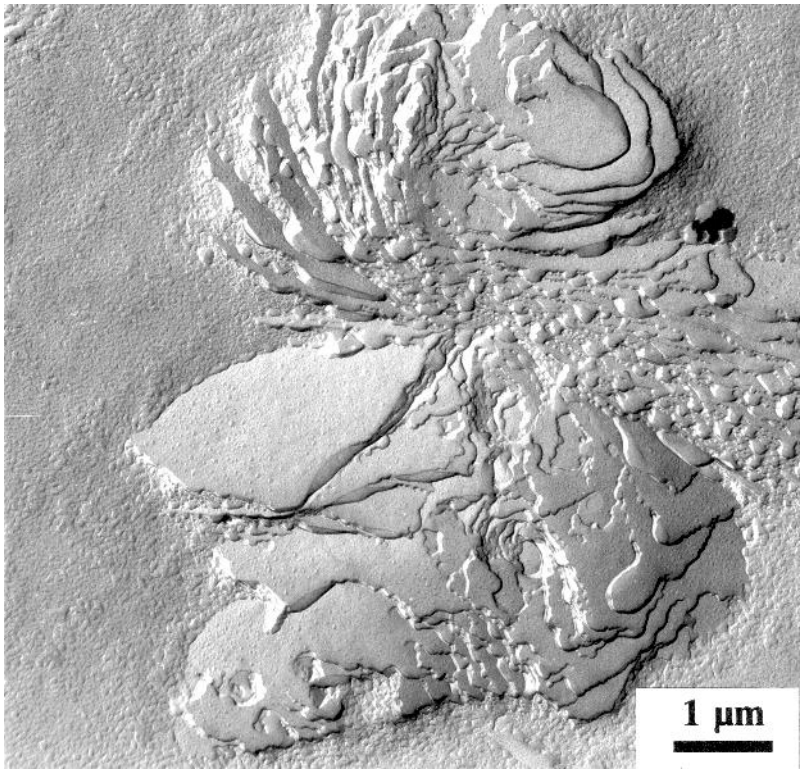

Figure 4.5(a): Detail of lamellar aggregate in BPD 124/10.

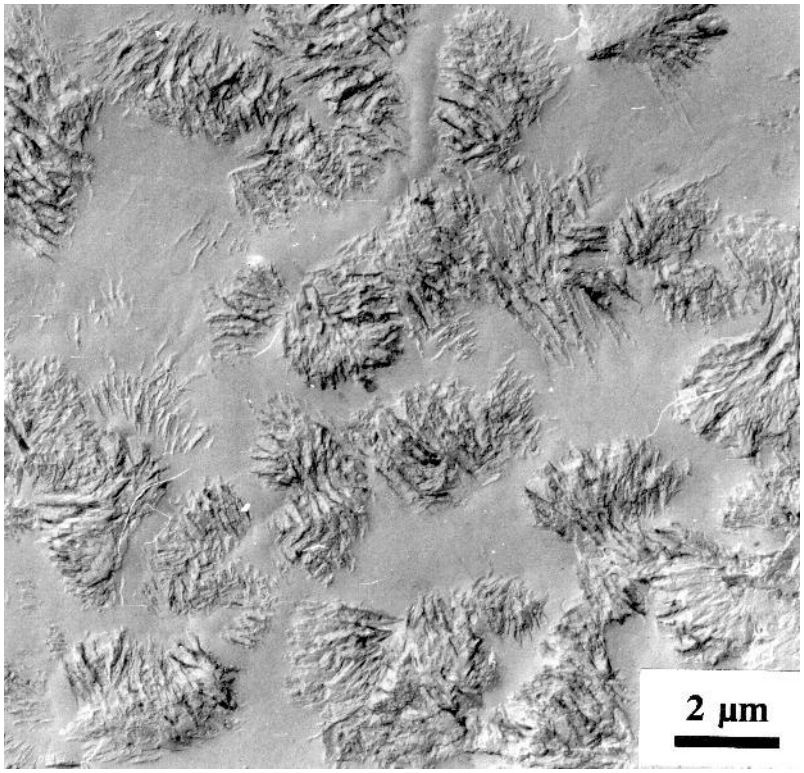

Figure 4.5(b): Very small lamellar aggregates in BPH 124/10.

which showed much co-crystallisation as deduced by DSC, a uniform texture composed of randomly oriented lamellae was obtained, with no evidence of banded spherulites (fig. 4.4(b)). This morphology is interesting when compared with BPI Q/10 (fig 4.3(b)), which also showed a uniform microstructure. This implies that in both these systems little or no segregation of LPE and BPE rich phases in the melt is occurring, yet the DSC trace of BPD 115/10 (fig. 4.1(b)) shows two peaks.

In BPH 115/10, which according to DSC, had two very different lamellar populations a morphology composed of individual groups of isolated lamellae was obtained (fig. 4.4(c). The absence of domains indicates that crystallisation is occurring from a miscible melt, however liquid-solid phase separation occurs on crystallisation to leave this characteristic morphology. Here the matrix, composed of the co-polymer, showed no noticeable lamellar texture, presumably because the more linear sequences in the co-polymer have been drawn out during crystallisation and have been incorporated into growing spherulites.

When blends were crystallised at 124°C to completion, most followed the general morphology of lamellar aggregates of around 10 microns in diameter, as shown in figure 4.5(a), which is of BPD 124/10. In BPH 124/10 a somewhat similar morphology, composed of small (2 micron diameter) isolated lamellar aggregates was seen in a matrix of the co-polymer (fig. 4.5(b)), this suggests that at this temperature some segregation of BPE from LPE must be occurring to give the domain structure.

Most of the systems that were examined do correspond to the general pattern described in chapter 3; quenching produces a banded texture that has spatial variation, crystallisation at 115°C generally produces LPE rich open banded spherulites and crystallisation at 124°C produces lamellar aggregates about 10 microns across. A number of deviations from this scheme are summarised below;

a) In quenched systems, where the DSC melting trace is singular (BPD and BPI), a spatially uniform morphology was obtained. In these cases liquid-liquid phase separation is not occurring in the melt, which would otherwise give a domain structure.

b) In BPD 115/10 there is an absence of banded spherulites, instead an arrangement of randomly oriented lamellae is seen, this could be taken as evidence of crystallisation from a

miscible melt.

c) In BPH 115/10 aggregates of a few lamellae in a matrix of the co-polymer are seen, which are in some respects similar to the sort of structures obtained usually by crystallising at 124°C.

c) In BPB 124/10 unusually large lamellar aggregates, of diameter around 30 microns formed.

d) In BPH 124/10 unusually small (2 microns diameter) aggregates were seen.

Crosslinking did not affect the morphology of the BPG systems when compared to their uncrosslinked (BPF) counterparts.

None of the isothermally crystallised samples crystallised at 124°C, where well defined regions of BPE existed, showed any significant degree of banding within the BPE rich phase, unlike the majority of quenched blends where banded spherulites of 10 microns diameter were detected. On the whole the morphology of the quenched blends were very similar to the morphology of the co-polymers used, in the case of BPH, however, the co-polymer had a uniform texture, which was replaced by a texture of lamellar aggregates in a uniform matrix when LPE was added (figure 4.4c). This sort of behaviour is indicative of crystallisation from a miscible melt.

4.5 Electrical Test Results

Electrical ramp tests at 50 Volts/second at an A.C frequency of 50 Hz were performed on melt pressed samples of each of the blends and the co-polymers used to formulate those blends. Electrical samples were of thickness 75 ± 1 μm, twenty tests were performed for each system and the average electrical strength was calculated on the basis of these results. 95% confidence intervals on these measurements were ±5 KV/mm in each case.

Figure 4.6 contains a chart showing the average electrical strength of blends BPA through to BPG. This chart shows generally that the same overall trends are observed in all materials, namely that the materials crystallized at 115°C have the highest electrical strength, all being within the uncertainty limits of 135 KV/mm. The 124°C materials were

within uncertainty limits of 124KV/mm, with the exception of the R9 blend, which had a strength comparable with one crystallised at 115°C (133KV/mm). However as discussed above this system exhibits a morphology that differs from the others crystallised at 124°C. Thus this increase in electrical strength is a morphological effect; it is not associated *directly* with the molecular composition of this material. Similarity the BPD 115/10 system which had a randomly orientated array of lamellae, rather than a banded spherulitic texture shows the highest electrical strength for any 10% LPE/BPE blend (138KV/mm) although it could be argued that this is within experimental uncertainty. This is expected since this blend contains the most linear of the co-polymers, meaning that the composite blend can be thought of as equivalent to one of the other blends with a somewhat higher LPE content.

The quenched systems all had electrical strength values within uncertainty limits of 128 KV/mm and the co-polymers alone, showed a similar electrical strength of 127 KV/mm, adding linear material and then quenching does not therefore give any advantage over using the branched base materials alone.

Finally crosslinking did not make a difference to the electrical strength or to the trends observed as evidenced by the set of data for the systems (BPF and BPG) containing the ethylene vinyl silane copolymer 4421. The general trends from these systems concur with those in chapter 3.

Figure 4.7 is a chart indicating the electrical strength of the BPH and BPI blends, the electrical strength here differs from that of the other blends significantly due to *the reduced electrical strength of the co-polymer used.*

The morphology of the BPH system was very different to the other blends, and it's electrical strength behaviour reflects this, being of around 88-90 KV/mm, apart from in the case of 124°C samples in which case the electrical strength falls abruptly. This is a system containing isolated small lamellar aggregates, which again concurs with the general results reported in chapter 3.

In BPI the overall morphology was similar to the majority of the blends studied, and the electrical strength of this system follows the same trends. However all values of electrical strength for this system are about 15 KV/mm less than the blends shown in figure 4.6, and this can be attributed to the reduced electrical strength of the 2H376 component.

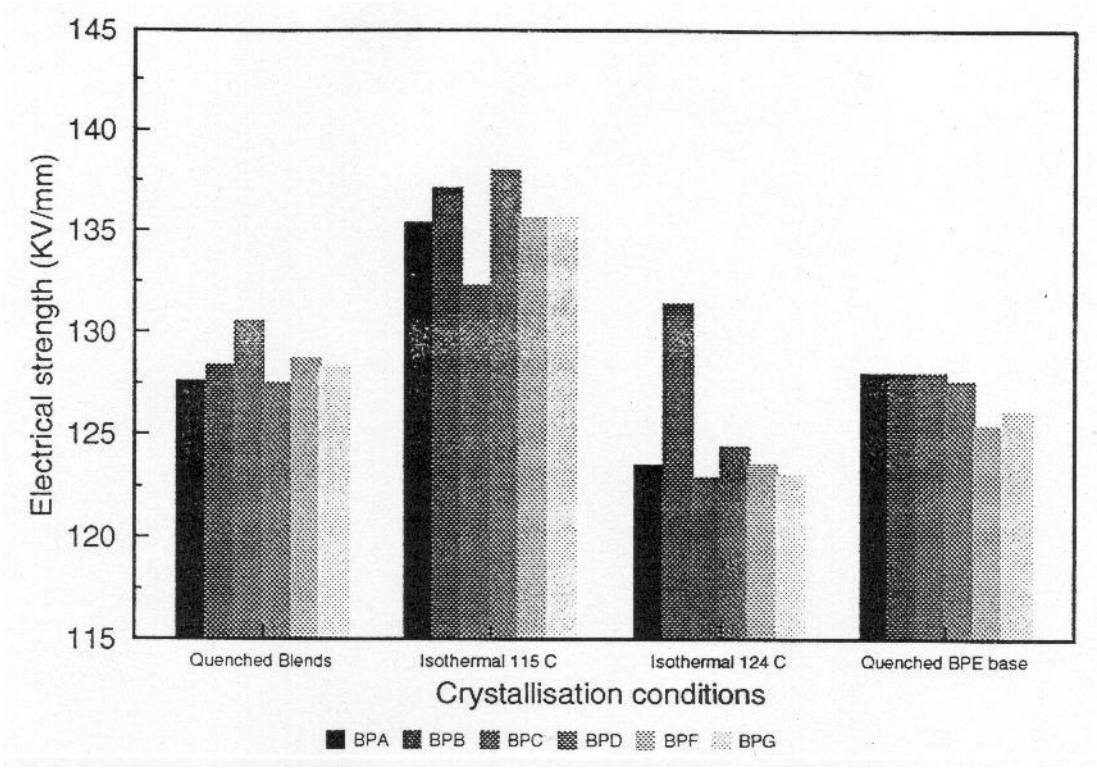

Figure 4.6: Barchart showing electrical strength of blends BPA-BPG

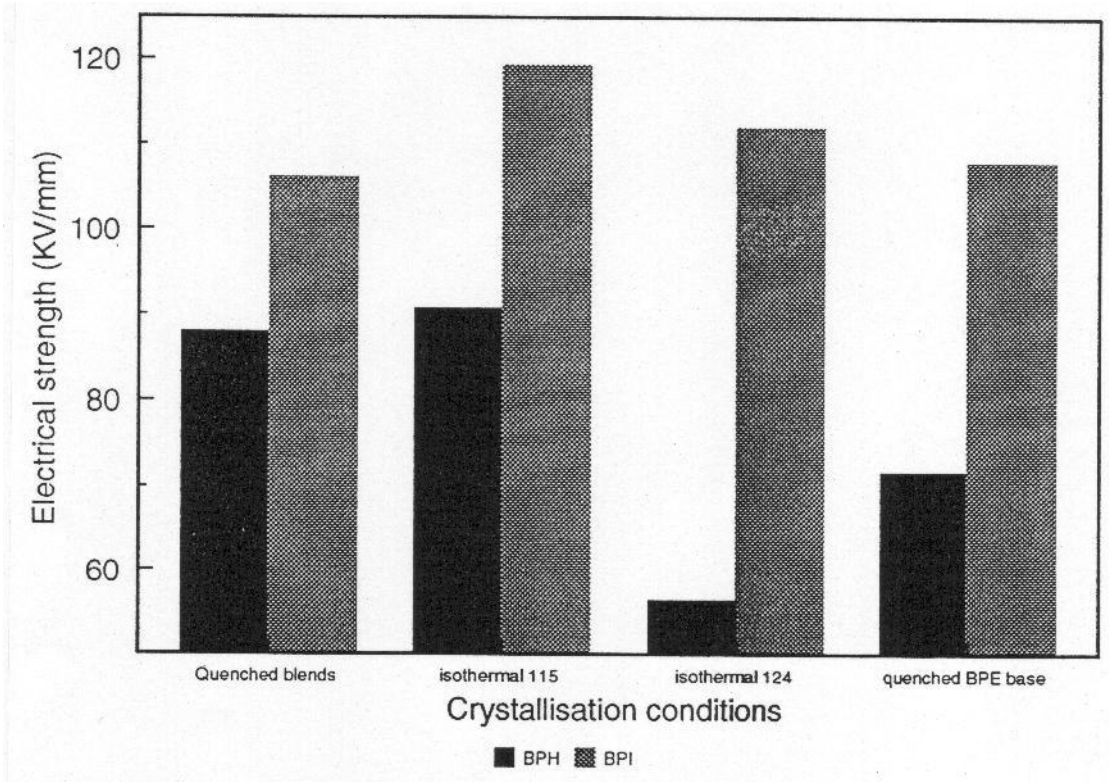

Figure 4.7: Barchart showing electrical strength of BPH and BPI blends.

4.6 Discussion

4.6.1 Comparison of results with chapter 3

It is shown here quite clearly that variations in molecular composition or architecture have little effect on electrical strength, provided the morphology does not change as a result. In chapter 3 we supposed that the spherulites and lamellae introduced into these samples had a direct effect upon electrical tree growth. Here it was not unreasonable to suppose that the composition of the material through which the tree grows also has some bearing on the rate of tree growth. Also in chapter 3 it was speculated that lack of banding in the BPE matrix, as seen in the isothermally crystallised blends, may be responsible for an overall reduction in electrical strength of the BPE phase, and this was reflected in the blend. It is generally accepted that electrical trees grow through the least dense part of the material (i.e. the BPE matrix) (17) and that the lamellae interposed simply serve as barriers to deflect the tree path. Therefore any reduction in electrical strength of the BPE material should be important.

In this study we have demonstrated that *both* of these factors are important and that these general concepts are at least consistent with the available data. In the BPI blend a systematic decrease in electrical strength occurred due to the reduced electrical strength of the 2A376 copolymer. In BPH the situation was more complex as the matrix morphology and spherulitic size simultaneously changed with temperature, but an overall reduction in electrical strength as a result of the 2722 copolymer was nevertheless found.

There are many variables to consider when trying to assess which co-polymer will give the highest electrical strength. Thermal history, molecular variability and processing conditions could serve to change the microstructure of the co-polymer involved; in chapter 3 we showed that the best insulating blend could also be one of the worst by a simple change in processing conditions! To say that an LLDPE may have a higher electrical strength than a VLDPE just because it contains `more linear molecules' is a rash conclusion to draw without additional data. Here this conclusion was tested by measuring the electrical strength of the co-polymer used in each of the blends directly and in each case where the electrical strength of the co-polymer was reduced the electrical strength of the blend was also, systematically by the same amount.

The conclusion here is clear, provided that changes in molecular architecture do not result in a change in morphology then the electrical strength of a polyethylene blend does not depend on molecular factors. These results are at variance with some studies (18,19), which report that electrical strength increases with molecular weight, other studies (20) seem to connect an increase in electrical strength with density. However, no definitive morphological data was given in any of these publications, so it is difficult to compare results.

4.6.2 What sort of morphological variations influence electrical properties?

The scale of such morphological changes required to influence electrical strength has to be quite severe as in the case of BPB 124/10 where the spherulite size increased dramatically. When the sizes and number density of such spherulites were analysed in the same way as was done in chapter 3, the increase in spherulitic diameter was found to be *directly responsible* for the enhanced electrical strength. In the case of BPD 115/10, the effect was more subtle and resulting in just a slight increase in electrical strength. Certainly, the types of changes required to influence the electrical strength could be resolved by SEM.

4.6.3 Effect of crosslinking

Finally some mention must be made of the result found by crosslinking the BPF blend, namely that it resulted in no difference in electrical strength. The chemistry of the silane crosslinking reaction is detailed in chapter 1. The morphology of the materials did not change as a result of crosslinking, due to the low temperatures involved in the crosslinking process. This being the case it is not difficult to see why crosslinking did not lead to a difference in electrical strength and concurs with studies into peroxide cured EPDM where the electrical strength was not dependent upon the crosslink density of the rubber (21).

4.5 Conclusions

1) A wide variety of different blend systems have been considered here in determining the

effects of molecular composition on electrical strength. Three crystallisation conditions were chosen to generate a wide range of morphologies, quenching gave rise to banded spherulites, isothermal crystallisation at 115°C gave rise to open banded spherulites, whereas crystallising at 124°C generated compact lamellar aggregates.

2) Results from most of the blends concur in that changing the components used to make up the blends makes little difference to the electrical strength, except where the morphology is changed. These general results support those in chapter 3.

3) Significant changes in microstructure are needed to influence electrical strength, such as seen in BPB 124/10, where the spherulitic diameter increased and directly caused the increased electrical strength. A small change was detected when the BPD 115/10 system was composed of a uniform space filling texture instead of banded spherulites as in most of the other systems.

4) The electrical strength of a blend could also be altered if the electrical strength of its branched co-polymer changed, as in the case of the 2722 and 2H376 used to make the blends BPH and BPI. These represent two examples of this behaviour, the electrical strength was lowered by the same amount regardless of crystallisation conditions. This certainly suggests that features in the BPE (such as banded spherulites) could be important in influencing the electrical strength of the composite system.

5) In the BPH system, the morphology was very different, lamellae collected together in clusters. For lower crystallisation temperatures LPE rich lamellae were embedded uniformly in the matrix, after crystallisation at higher temperatures small sheaves were produced. This is indicative of crystallisation from a miscible melt and these small sheaves were detrimental to electrical performance, as seen in chapter 3 with blends of low LPE content.

6) Crosslinking the samples after preparation had no effect on their morphology or electrical strength and is significant as good electrical performance can be combined with the good mechanical properties yielded by crosslinking.

7) These results support the conclusions of chapter 3, namely that morphological rather than molecular considerations primarily determine electrical behaviour. The general result that the electrical strength of the branched matrix can change the electrical strength is to be expected if failure is due to treeing, as described in chapter 3.

8) It is very conceivable that the drop in electrical strength at low LPE contents seen in chapter 3, is not therefore a result of stress enhancement or voiding but is rather more a consequence of the loss of banding of the BPE matrix material when isothermally crystallised as a blend. This work confirms that the electrical strength of the BPE material is important in influencing the electrical strength of the blend as a whole.

4.6 References

1) B. V. Ceres and J. M. Schultz, J. Appl. Phys. 1984, **29**, 4183.

2) S. N. Kolesov, IEEE Trans. Electr. Insul. 1980, **I5**, 382.

3) S. N. Kolesov, Polymer Science USSR 1980, **21**, 1993.

4) S. N. Kolesov, Elektrichestvo 1970, **9**, 84.

5) H. Wagner, IEEE Trans. Electr. Insul. 1978, **13**, 81.

6) M. Ieda, IEEE Trans. Electr. Insul. 1980, **15**, 206.

7) T. Kyu, S.-R. Hu, and R. S. Stein, J. Polym. Sci.: Part B: Polym. Phys. 1980, **25**, 89.

8) J. M. Rego Lopez and U. W. Gedde, Polymer 1989, **30**, 22.

9) C. Puig, Ph. D. Thesis, University of Bristol 1994, p.78.

10) A. Gustafsson and U. W. Gedde, Proc. Nordic Insulation Symposium (Vasteras 1992) **8.4**:1.

11) W. L. Wade, R. J. Mammone and M. Binder, Polymer 1993, **34**, 1093.

12) M. J. Hill, P. J. Barham, A. Keller and C. C. A. Rosney, Polymer 1991, **32**, 1385.

13) P. J. Barham, M. J. Hill, A. Keller and C. C. A. Rosney, J. Mater. Sci. Letts. 1988, **7**, 1271.

14) H. H. Song, R. S. Stein, D.-Q. Wu, M. Ree, J. C. Philips, A. LeGrand and B. Chu, Macromolecules 1988, **21**, 1180.

15) R. G. Alamo, J. D. Londono, L. Mandelkern, F. C. Stehling and G. D. Wignall, Macromolecules 1994, **27**, 411.

16) J.A.Parker, D.C.Bassett, R.H.Olley and P.Jaaskelainen, Polymer 1994, **35,** 4140.

17) N.Hozami, T. Okamoto and H.Fukagawa, Jap. Jour. Appl. Phys. 1988, **27**, 1230.

18) K.Amakawa, T.Moriachi, T.Yoshida and Y.Inuishi, J. Inst. Elect. Engrs. of Japan 1964, **84**, 129.

19) P.H.H Fischer and K.W Nissen, IEEE Trans. Electr. Insul. 1976, **11**, 37.

20) M. Farkh, Hoang-The-Giam, R.El Hayani, Bul Al, B. Dalle, J. Perrett, C. Simon and J. Berdala, J. Appl. Phys. 1989, **22**, 566.

21) E.C Hsu, IEEE Trans. Electr. Insul. 1978, **13**, 110.

Table 4.1: Polymers used in this study

Polymer	Type	M_w	M_n	T_m
140/60	Linear high density	53,000	16,000	133
Rigidex 9	linear high density	170,000	11,300	133
Ho20-54p	Linear high density	312,000	33,000	138
4901	Branched low density	76,800	11,300	113
M1	Linear low density	84,600	18,900	118
4421	Ethylene-Vinyl Silane	98,400	14,200	109
2722	EPDM co-polymer	92,500	14,700	45
2H376	VLDPE	67,900	12,000	128

Table 4.2: Blends and crystallisation data

Blend	Made from...	tc at 115°C (min)	tc at 124°C
BPA	10% 140/60 in 4901	5-8	40-50
BPB	10% R9 in 4901	3-6	45-55
BPC	10% HO20-54p in 4901	3-7	40-50
BPD	10% 140/60 in M1	8-10	45-55
BPF	10% 140/60 in 4421	6-8	35-38
BPG	Crosslinked BPF	as BPF	as BPF
BPH	10% 140/60 in 2722	3-8	35-42
BPI	10% 140/60 in 2H376	2-4	25-32

M_w, M_n data obtained by GPC analysis (Rapra Technology LTD, Shawbury, Shropshire, SY4 4NR), thermal data obtained by DSC.

CHAPTER 5 - EFFECT OF SAMPLE PREPARATION AND MEASURING TECHNIQUES ON ELECTRICAL BREAKDOWN DATA

5.1 Introduction

In chapter 3 the effects of adding a proportion (1-30%) of linear polyethylene to a low-density polyethylene was described. By suitable processing routes, a range of morphologies was produced and it was demonstrated that the resulting structural features had a marked influence on the macroscopic electrical strength of the system, as gauged by short term ramp testing. The invariant electrical strength of quenched samples where only the composition changed and not the morphology, suggested that morphological rather than compositional factors are responsible for influencing the electrical strength of a polycrystalline polymeric insulator.

In chapter 4 we systematically changed the materials used to formulate the blends and found that, provided the morphology remained constant, then the molecular composition was irrelevant as far as the electrical strength was concerned, supporting the conclusions of chapter 3. A change in spherulitic size was seen to have a great effect upon measured electrical strength, whereas more subtle changes such as a different conformation of lamellae in such systems had little effect on behaviour. Also changes were seen when the electrical strength of the BPE base material changed, in such cases the electrical strength of the blend changed similarly, for all crystallisation conditions. Examination of an electrical tree showed that it followed a tortuous path, generally avoiding regions of high crystallinity.

The solution blending route has thus been found to generate consistent and reliable data in line with currently accepted ideas, however in an industrial application, where many tons of blend need to be produced, this is clearly not a viable route. So far we have looked at melt blending briefly in chapter 3, as a means of incorporating inorganic filler particles into a branched polyethylene, and we showed that this preparation technique gave reliable results in line with previous work. However a melt mixed blend has not as yet been studied in detail. Reports of a comparison between solution and melt blending (1) concluded that melt

blending yielded an increased nucleation density, with smaller but more numerous spherulites generated. Clearly such results, based on our previous work, may be somewhat worrying as a difference in the morphology can influence the electrical strength. However it is instructive to study and compare blends of the same type but prepared using different methods. For this investigation two blends were examined, both of which have been characterised in detail in chapter 3, for the solution blending preparation route. Blends composed of 10% and 20% 140/60 in 4901 branched polyethylene were prepared by the melt mixing procedure discussed in detail in chapter 2. These two blends are labelled throughout as BPA T/C M where T is the isothermal crystallisation temperature and C is the % LPE content. M signifies a melt mixed system, as opposed to previous solution blended systems. Therefore a blend of 10% 140/60 in 4901 crystallised isothermally to completion is labelled BPA 115/10 when prepared by solution blending, whereas the melt blended equivalent would be labelled BPA 115/10 M.

The breakdown data, discussed previously, was based upon 75 micron sample thicknesses whereas cable insulation thicknesses and service conditions are very different from those encountered in the short term ramp testing used here. Here the effects of varying three parameters on measured electrical breakdown strength are examined.

Sample thickness. The effect of sample thickness on breakdown behaviour has been studied in some detail (2-6), these reports all conclude a reduction in electrical strength occurs with increased sample thickness, thus it is extremely important to characterise these effects properly in our blends. Although some attempts have been made to explain these effects by stipulating an increased amount of contaminants in thicker films as being the cause of decreased electrical strength, the true reason remains unclear.

Voltage ramp rate. The effect of ramp rate on measured electrical data has attracted less interest (7,8) possibly due to less widespread use of AC ramp testing. In one case (7), under AC ramp tests, the electrical strength was reported to increase with the voltage ramp rate, whereas for DC tests Leda (8) reported the opposite case. The origins of these effects are therefore unclear.

AC frequency. In AC breakdown tests the effects of frequency on measured electrical data have also been investigated in some detail (9,10), both reports concluded that the measured electrical strength generally decreased with applied frequency. Mason puts this effect down

to increased frequency of micro-discharges in tree channels (9).

However in all these studies the morphology of the specimens used was not characterised fully, so on the basis of these studies, it is difficult to say whether these aforementioned effects are due to morphological changes, local field enhancement, voiding etc.

These three effects are explored here in two very different systems, both of which have been examined previously and characterised in detail in chapter 3. One being the superclean low density polyethylene 4901, with a breakdown strength that is typical of conventional cable insulation materials (127 KV/mm), denoted BPA Q/0, and a blend of 4901 and 20% linear polyethylene which, through isothermal crystallisation at 115°C has an enhanced strength (147 KV/mm), denoted BPA 115/20. This blend was prepared by the solution method discussed in chapter 2.

5.2 Differential scanning calorimetry

Melting behaviour All of the aforementioned blends have been analyzed in detail in chapter 3, apart from the new melt mixed blends, so we need to discuss these here, particularly to compare the effects of preparation route on crystallisation and melting behaviour. Both materials were crystallised at 115°C for 45 minutes, 124°C for 4 hours or simply quenched.

Figure 5.1 compares the DSC melting behaviour of the two blends prepared by the two different routes for a scan rate of 10 K/min. Both show two peaks corresponding to BPE and LPE rich material as discussed in detail in chapter 3. Blends prepared using both methods show dual DSC peaks, however the melt mixed blends in particular show other subsidiary peaks, which can be associated with enhanced populations of co-crystals. This is particularly evident after quenching or crystallisation at 115°C, and is particularly pronounced in the 10% blend (figure 5.1(a)).

Crystallisation behaviour. The minimum time for crystallisation (t_c) was determined by DSC, it is clear that the crystallisation behaviour depends on the sample preparation route as shown in table 5.1. Melt mixed blends crystallise isothermally in much less time than their solution blended equivalents. Provided that the electrical strength of the melt mixed blends is not reduced, this is a considerable advantage.

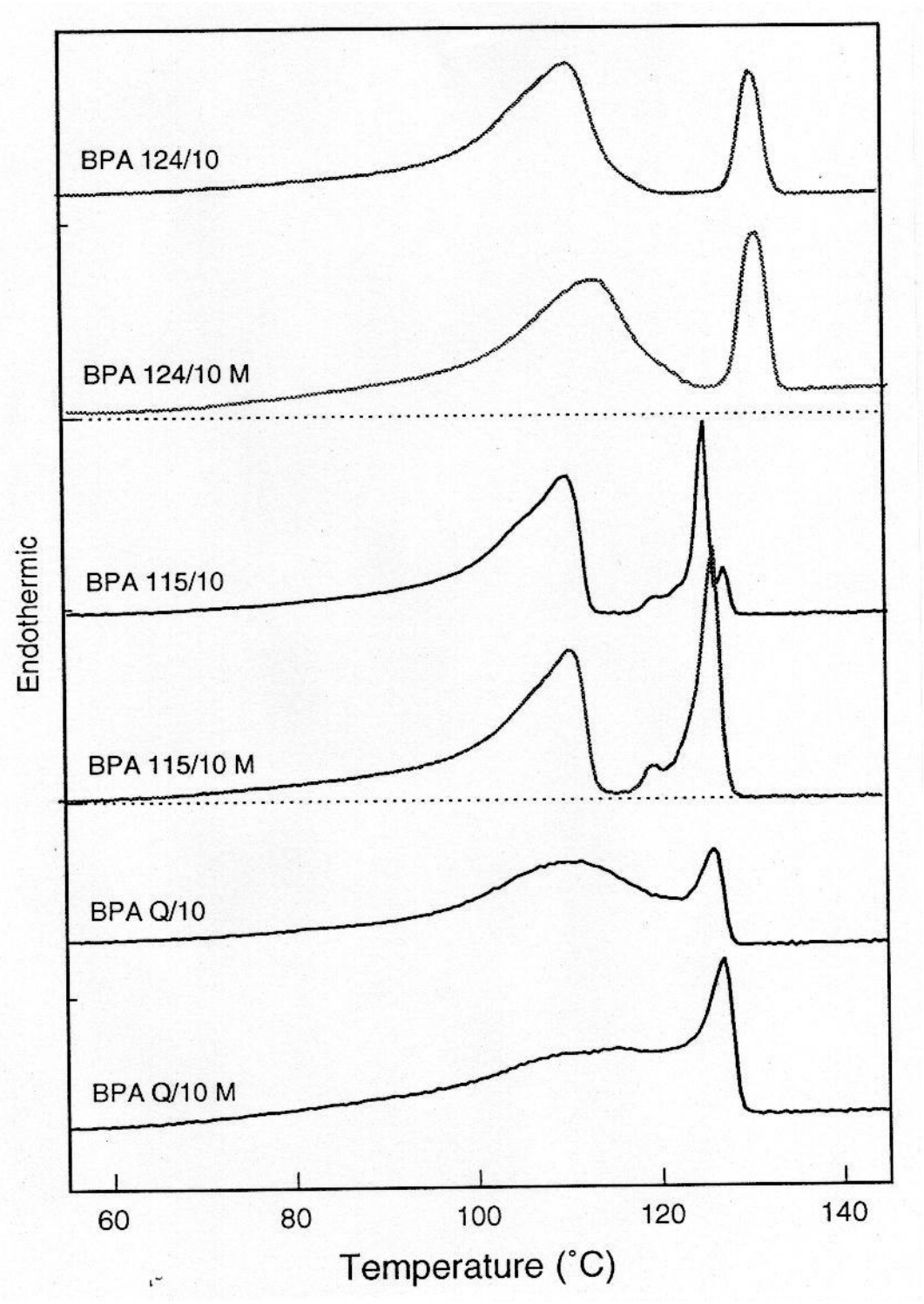

Figure 5.1(a): Melting behaviour of melt and solution mixed 10% LPE blends

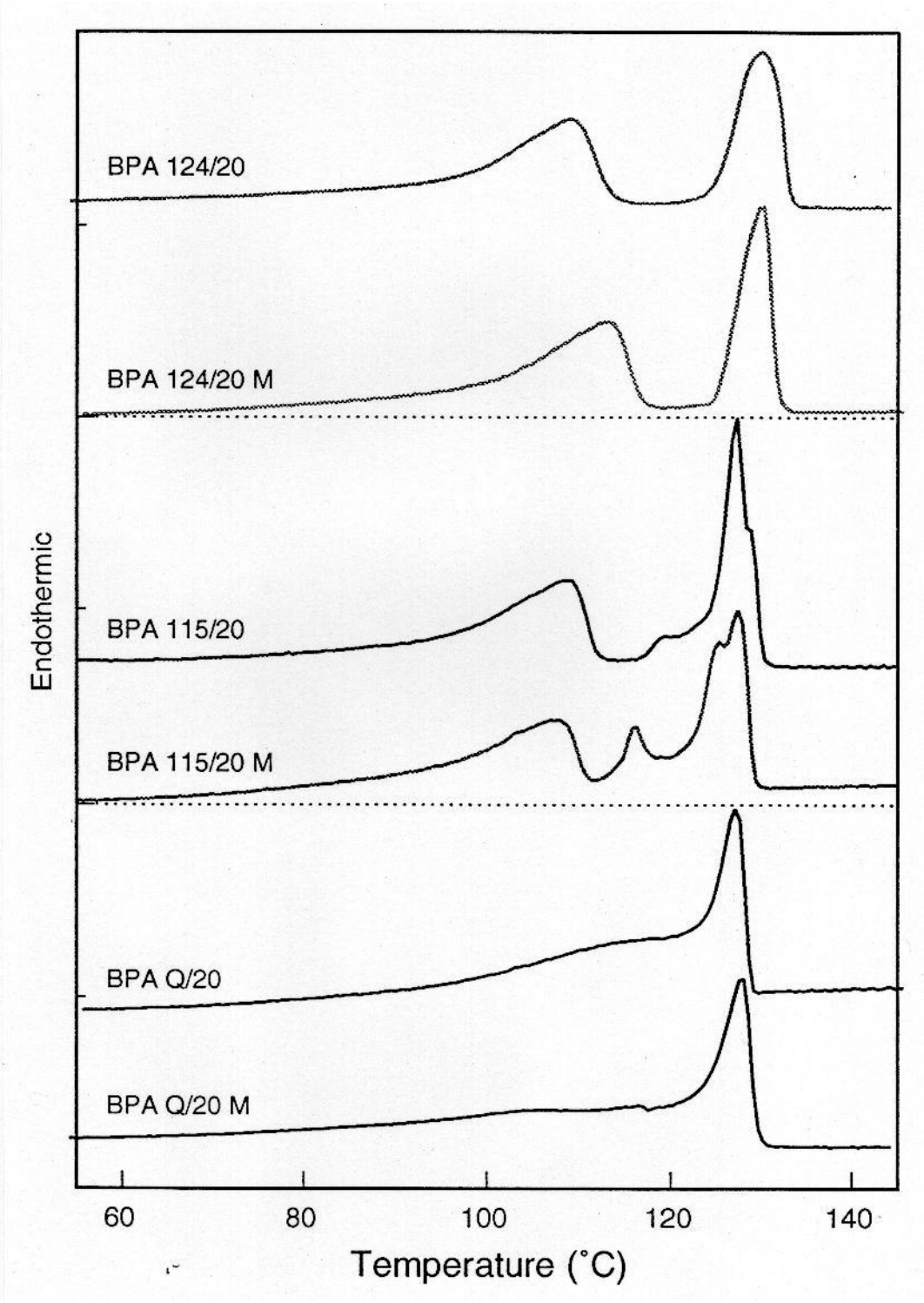

Figure 5.1(b): Melting endotherms of 20% solution and melt mixed blends.

LPE content	Preparation route	t_c at 115°C (mins)	t_c at 124°C (mins)
10%	Solution	6-10	45-50
	Melt	2-4	10-12
20%	Solution	3-6	15-25
	Melt	1-3	6-8

Table 5.1: Crystallisation times of melt mixed and solution blends.

5.3 Morphology

Solution blended samples. Figure 5.2 shows the morphologies present in the two solution blended materials which were chosen to determine the effects of test conditions on measured electrical data. Both of these systems have been discussed in detail in chapter 3, but are included here for completion. Figure 5.2(a) shows the morphology of the samples made from BPA Q/0, a continuous banded texture made of many fine lamellae is evident. In the blend sample (BPA 115/20), a morphology made of two different types of region is shown in figure 5.2(b). Banded spherulites which show ordered lamellae and regions between, which show a uniform texture. The lamellae in the second sample are larger and better developed than those in BPA Q/0, these correspond exactly with the results discussed in chapter 3.

Both micrographs are of carbon replicas prepared from etched surfaces of disks prepared for electrical testing. Examining these samples straight from electrical disks, rather than preparing separate samples for morphological studies, justifies our previous conclusion that the melt pressed samples prepared previously were a valid representation of the morphology of the disks prepared for electrical testing. A further check was made to see if the morphology was adversely affected by sample thickness, particularly in thin samples. No adverse effects of this nature were seen in the randomly chosen set of samples examined. Morphologies are therefore well defined, consistently reproducible, and are not an artefact, for example of sample thickness.

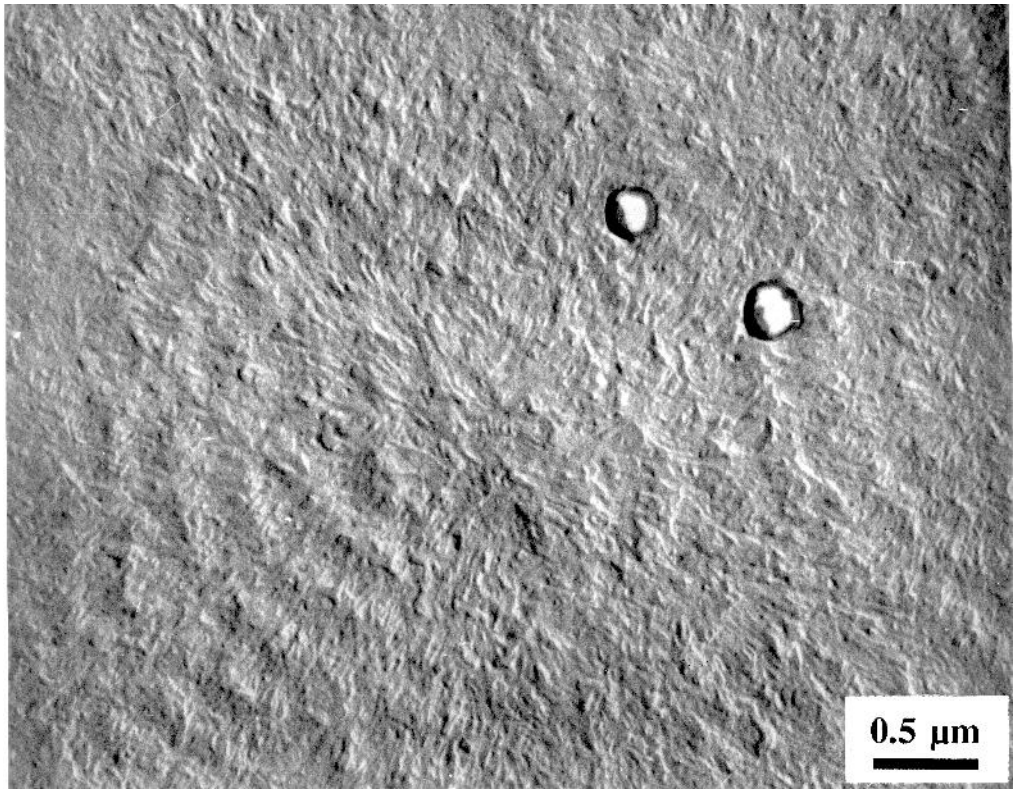

Figure 5.2(a): Fine scale banded texture of BPA Q/0.

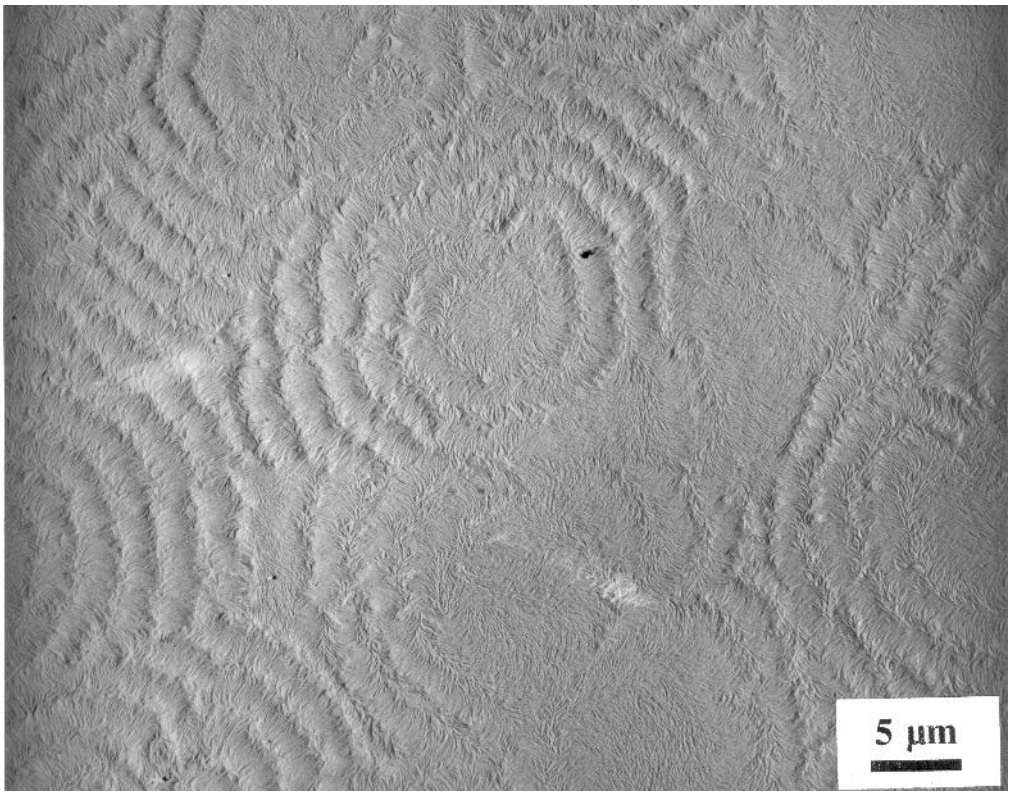

Figure 5.2(b): Coarser space filling lamellar structure in BPA 115/20.

Melt vs solution blending SEM micrographs comparing samples made from solution and melt mixed blends are contained in figures 5.3 to 5.5. Figure 5.3 compares the morphology of solution blended BPA 115/10 with the melt blended equivalent. The banded spherulites are smaller and more numerous in the latter case (being about 9 microns in diameter in BPA 115/10 M as compared to 25 microns in BPA 115/10). The same general behaviour occurs in the BPA 115/20 blends (figure 5.4). Although the individual spherulites in the melt mixed blends are less distinguishable than those in solution blended systems, there are between 1.5 and 2 times the number of spherulites per unit area in the melt blended samples, this corresponds with a 2 to 4 fold increase in the number of nucleation sites per unit volume in the melt blended materials.

When crystallised at 124°C, a similar result of smaller, and more numerous lamellar aggregates in the melt mixed materials is observed. Figure 5.5 demonstrates this in the BPA 124/20 samples. The quenched samples were imaged by TEM, as SEM was not revealing. Figure 5.6 shows a typical banded texture from BPA Q/20, comparing melt and solution cases. The lamellar texture shows very little change with blend preparation route, however once again the spherulites are more numerous in the melt mixed case. The increased co-crystallisation seen in melt mixed blends does not appear to affect the morphology to a great extent. However reduced crystallisation times, due to increased nucleation density, could result in increased populations of co-crystals in the melt mixed blends, as inferred by DSC. In this case less time is available for liquid-solid phase segregation whilst spherulites are crystallising, which means that much more BPE material is incorporated into growing lamellae.

Table 5.2 contains estimated values of the nucleation density N_a and sizes of spherulites in the isothermally crystallised samples. In each case the figures in brackets are for the equivalent melt blended systems. The product $N_a d$ was found to be important in determining the electrical strength of such systems (see chapter 3). It is clear that this value does not change significantly with blend preparation route, therefore we might expect the electrical strength to be independent of blend preparation route, despite the differences in crystallisation habits.

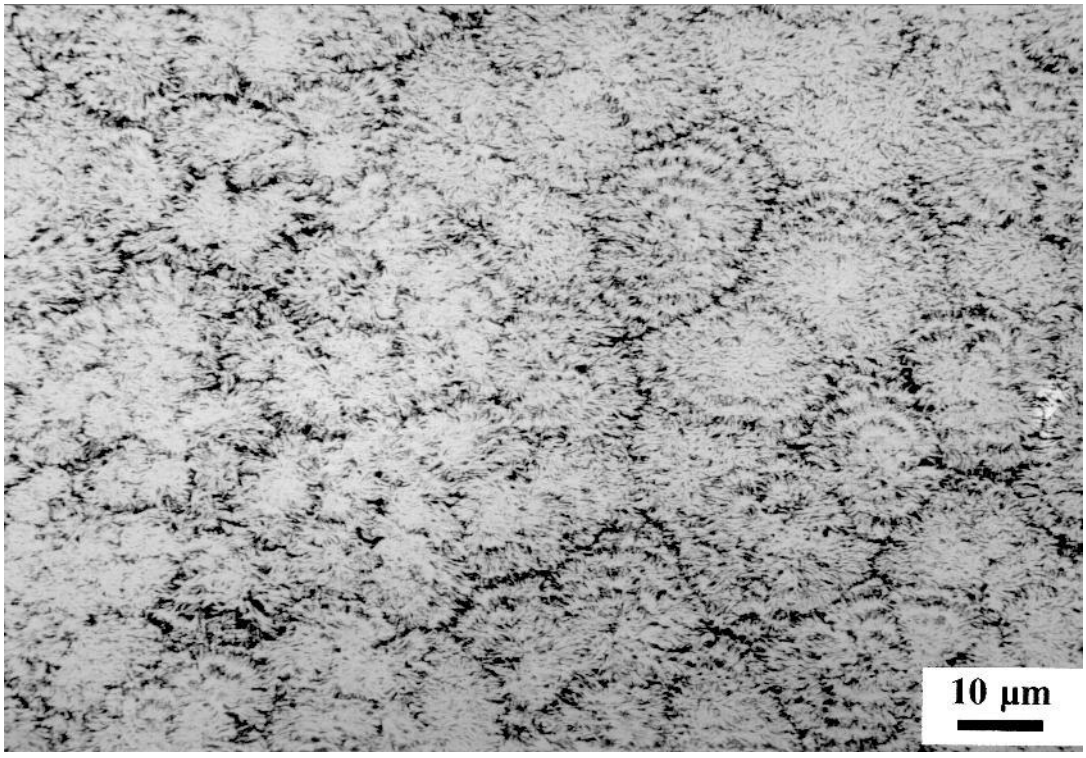

Figure 5.3(a): SEM micrograph of BPA 115/10 showing banded texture.

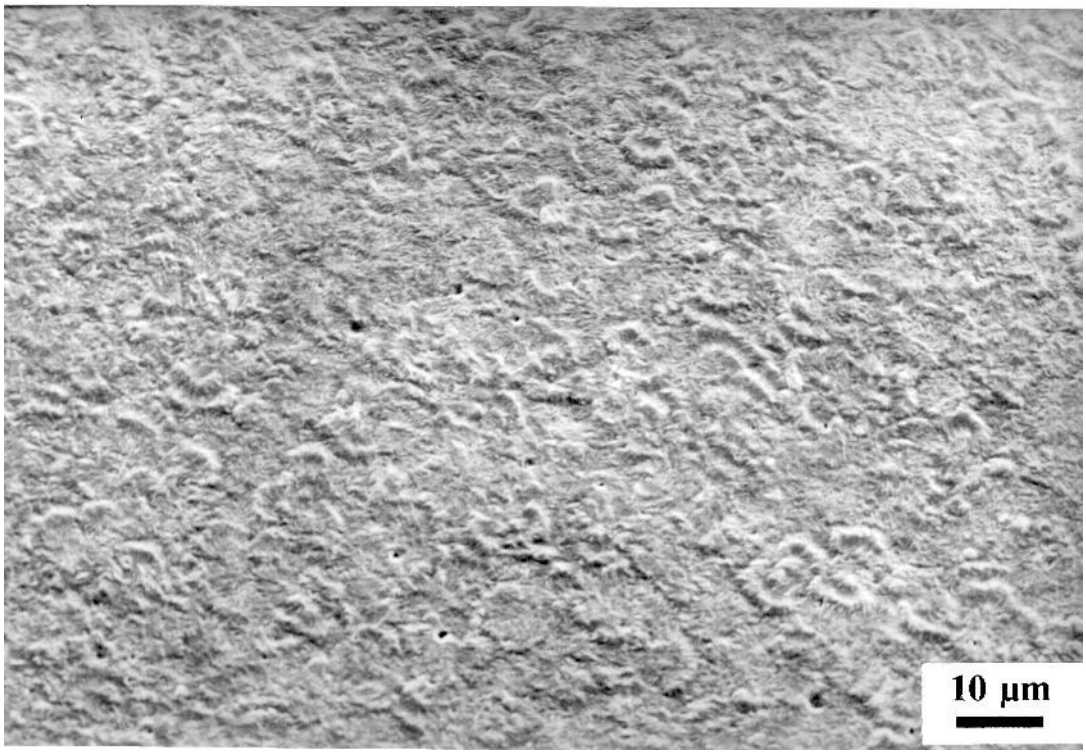

Figure 5.3(b): Morphology of BPA 115/10 M.

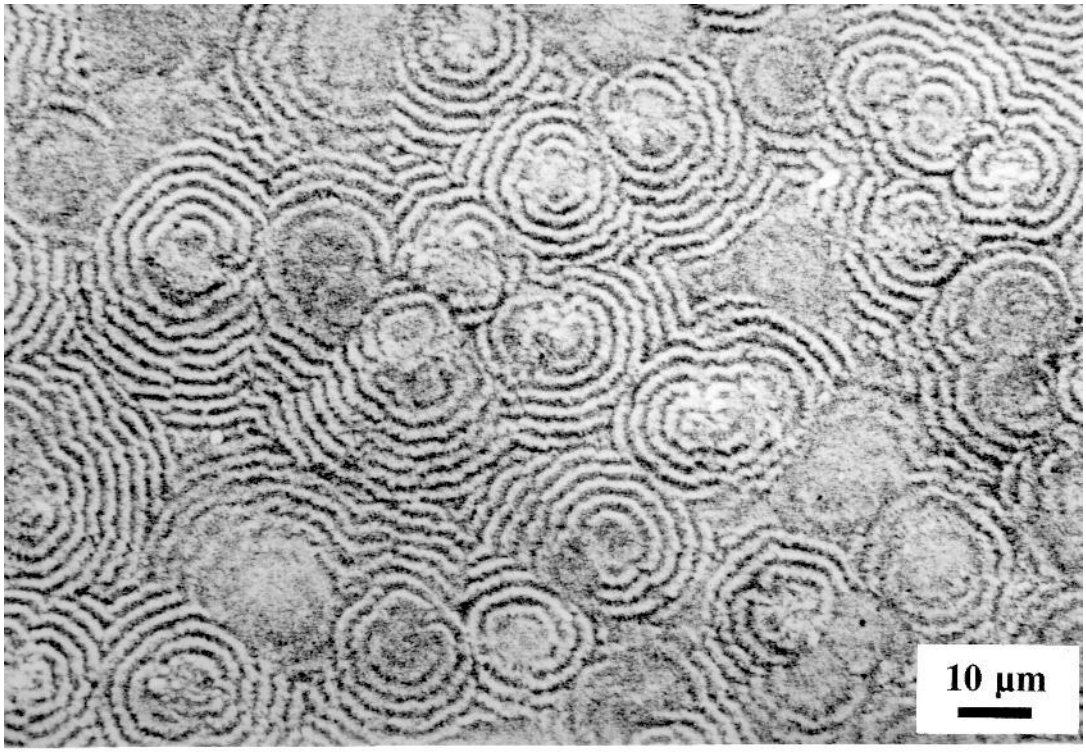

Figure 5.4(a): Banded spherulitic texture in BPA 115/20.

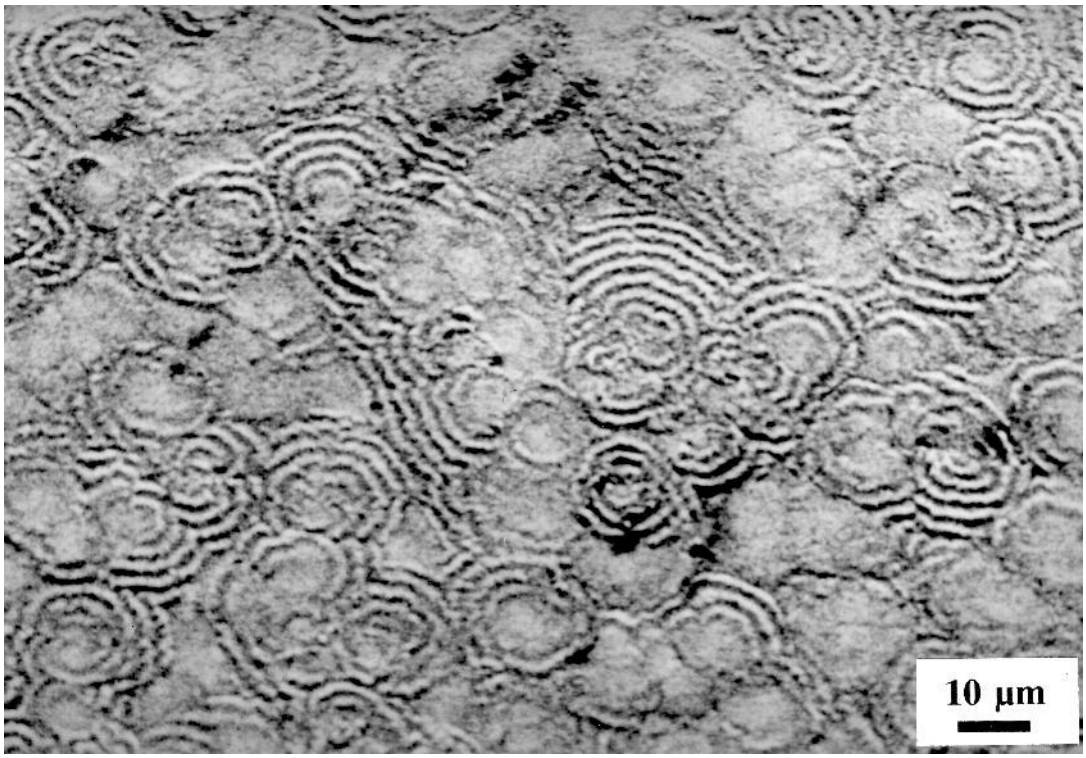

Figure 5.4(b): Morphology of BPA 115/20 M.

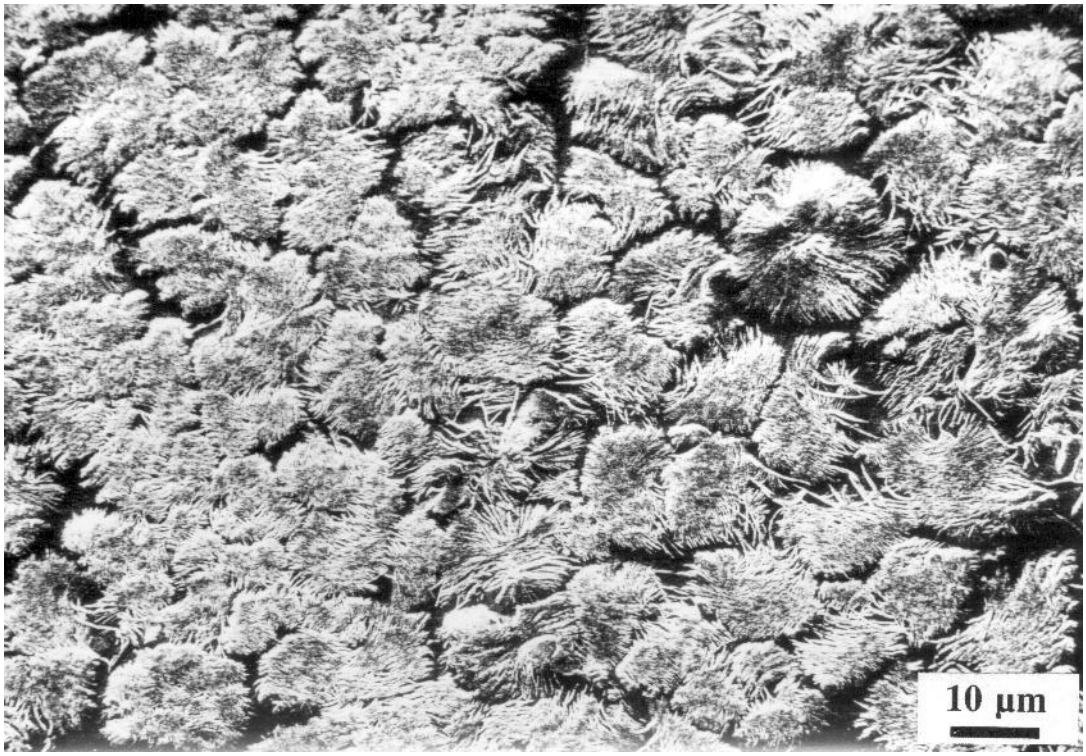

Figure 5.5(a): Large lamellar aggregates in BPA 124/20.

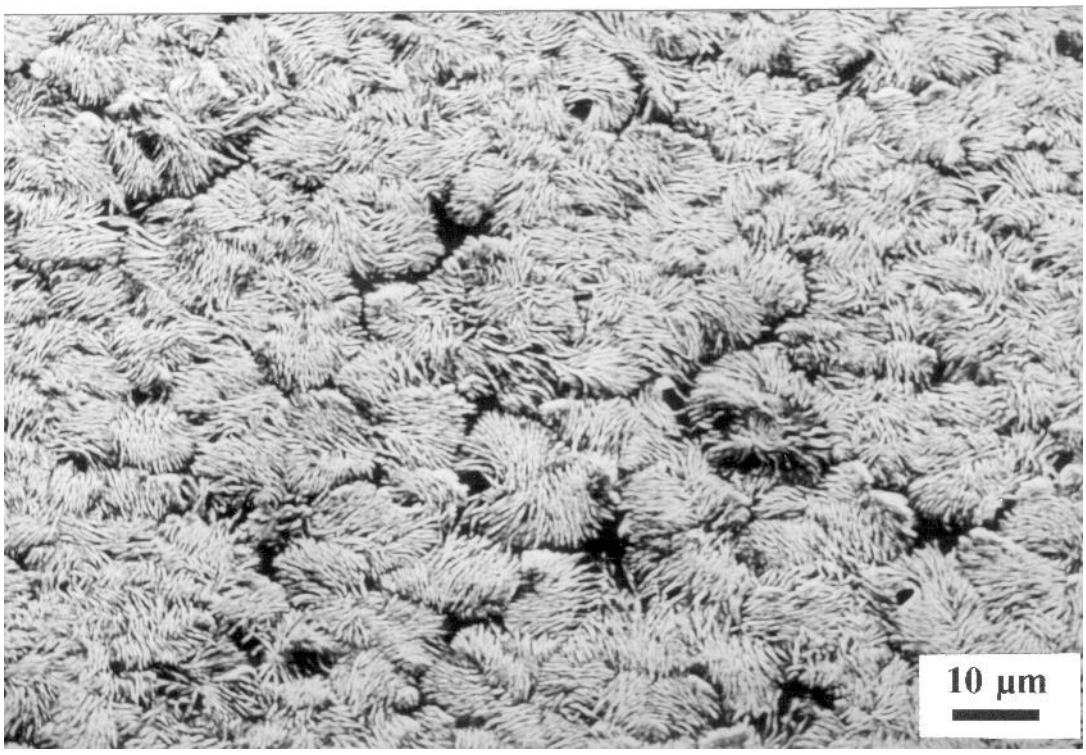

Figure 5.5(b): Smaller aggregates in BPA 124/20 M.

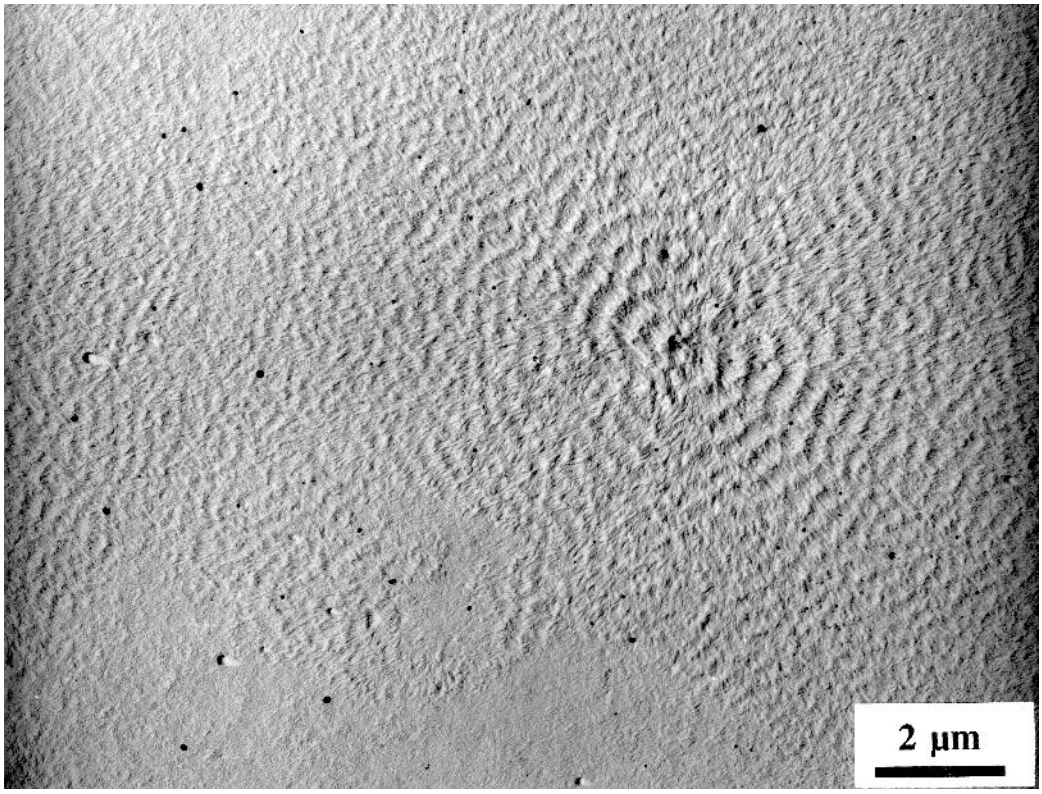

Figure 5.6(a): Banded texture of BPA Q/20.

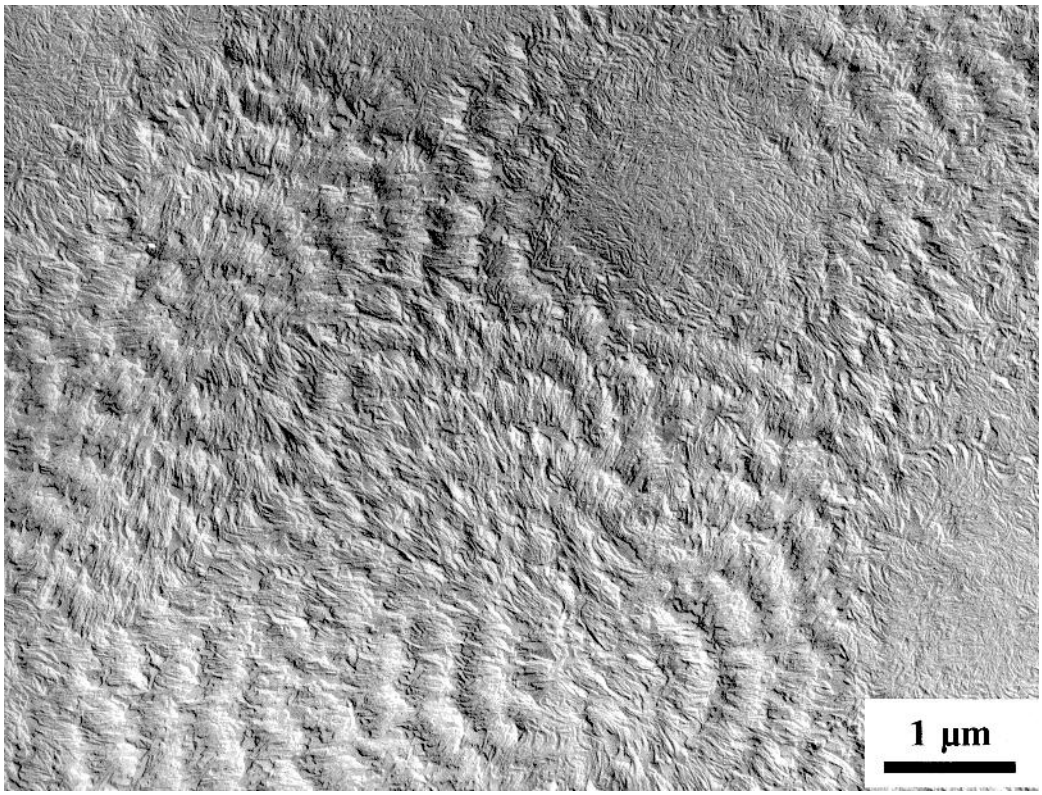

Figure 5.6(b): Banded spherulites are more numerous and smaller in BPA Q/20 M.

Blend	N_a (per 1000μm^2)	d (μm)	N_ad
BPA 115/10	2.3±0.3 (4.8±0.6)	25±3 (13±2)	57±10 (62±11)
BPA 124/10	2.7±0.2 (4.5±0.3)	14±1 (9±2)	38±4 (40±9)
BPA 115/20	2.5±0.2 (3.7±0.4)	25±2 (18±3)	63±7 (67±13)
BPA 124/20	2.6±0.2 (4.9±0.5)	17±1 (10±2)	45±4 (49±11)

Table 5.2: Nucleation density and spherulitic size in solution blended and melt mixed blends. Values for the latter preparation route are in brackets.

5.4 Electrical test results

Thin film samples were prepared with nominal thickness 75 microns and tested at 50Hz. A ramp rate of 50 Volts per second was used throughout in line with the standard breakdown testing procedure discussed in chapter 2. Figure 5.7 contains a bar chart comparing the electrical strength of the melt blended and solution blended systems, as can be seen the electrical strength is *unchanged* by the melt blending preparation route, despite the morphological differences described previously.

Then, further samples were prepared from solution blended materials and tested at various ramp rates and AC frequencies as determined by the limitations of the test equipment. Figure 5.8(a) shows the dependence of measured electrical strength in BPA Q/0 on sample thickness and ramp rate used for testing. Electrical strength falls with increasing sample thickness and with decreasing ramp rate. Figure 5.8(b) shows very similar trends in the sample BPA 115/20, which has a generally higher intercept for all ramp rates, but shows the same thickness and ramp rate dependence.

Figure 5.9 shows how the measured electrical strength changes with AC test frequency, both the curves have the same gradient, therefore the effect of frequency on electrical breakdown data does not depend on sample morphology in the limited range of frequency considered here. These results concur with previous studies (2-7, 9-10) and show that in a system of well defined morphology, that reported effects of testing conditions on

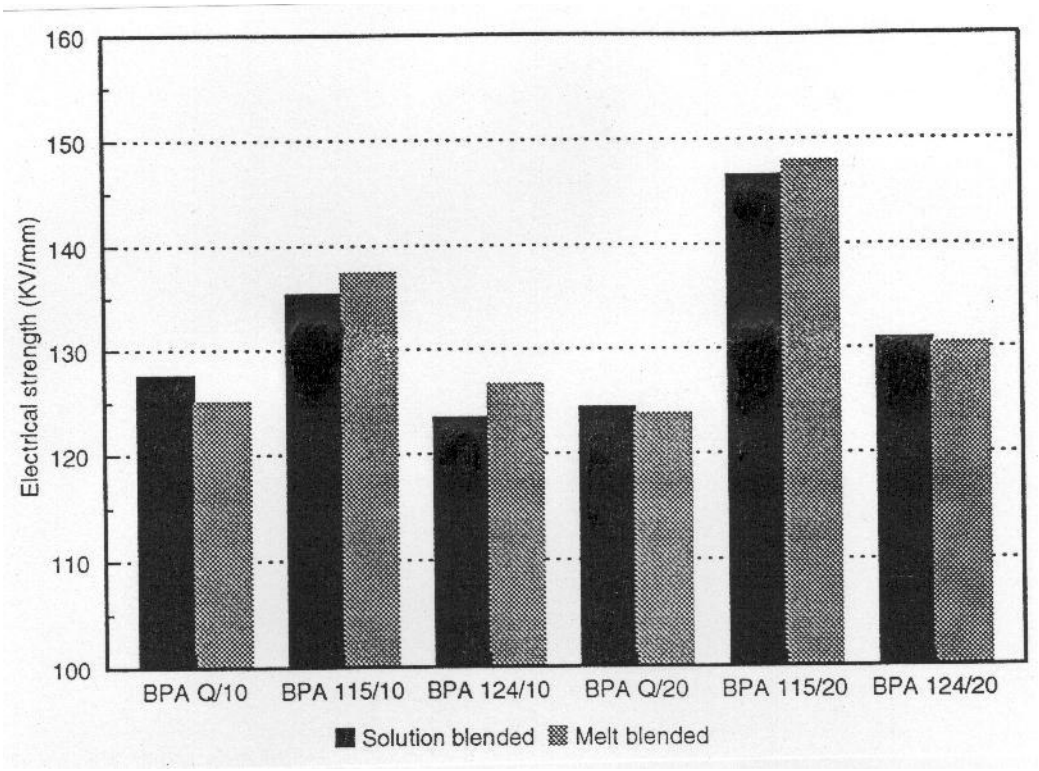

Figure 5.7: Effect of blend preparation route on electrical strength.

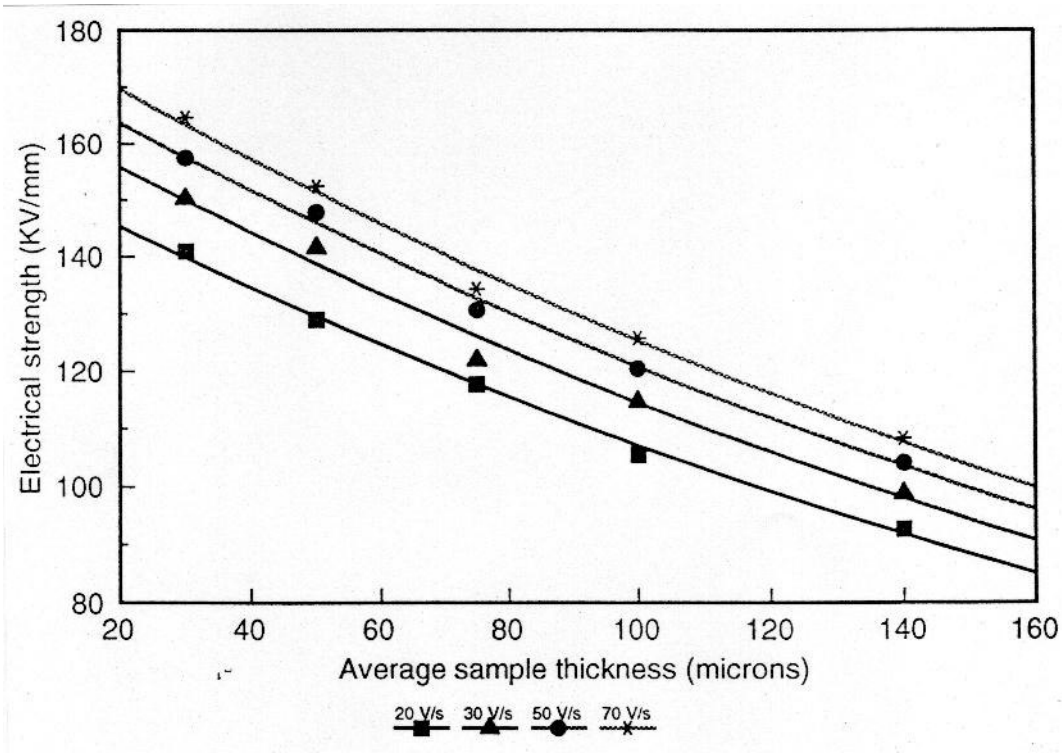

Figure 5.8(a): Effect of ramp rate and sample thickness on electrical strength of BPA Q/0.

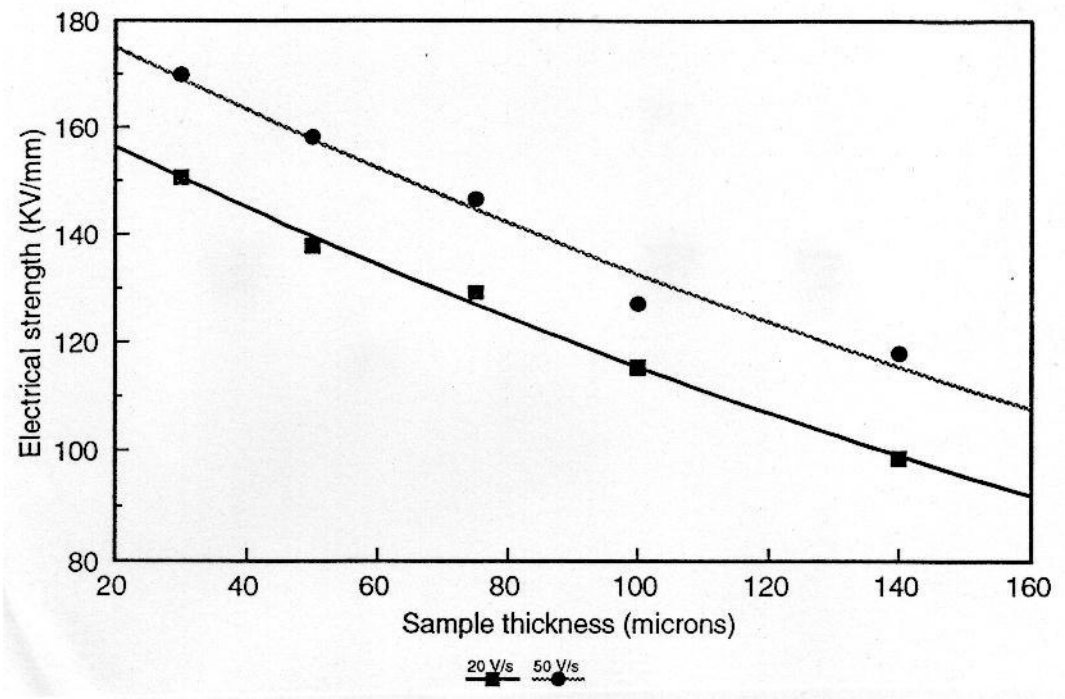

Figure 5.8(b): Effect of sample thickness and ramp rate on electrical strength of BPA 115/20.

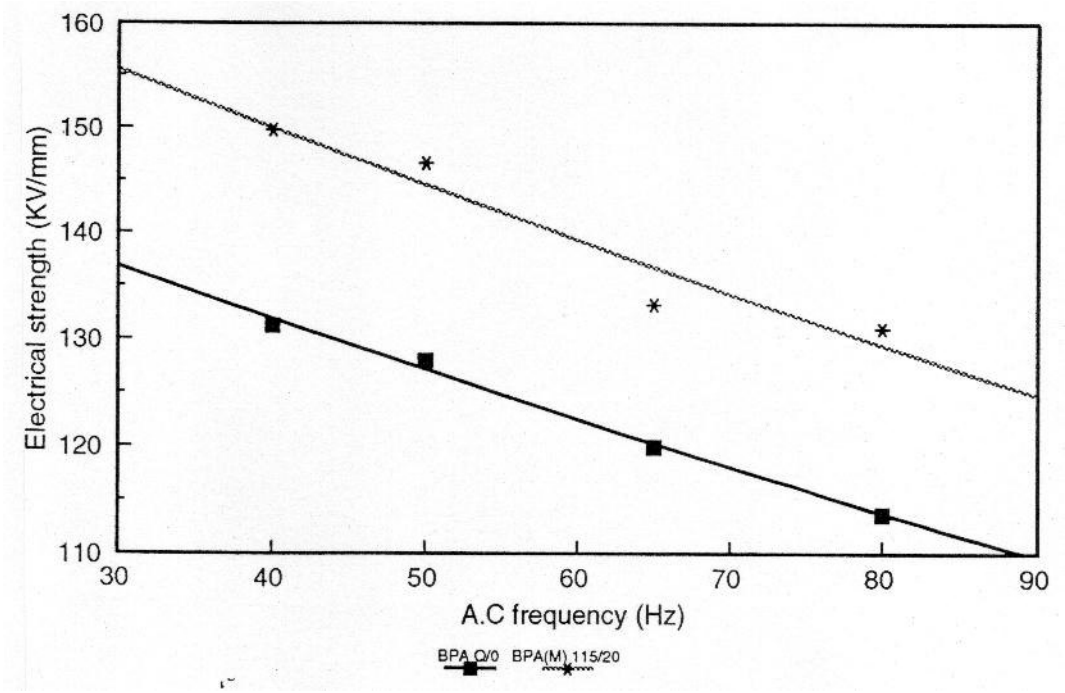

Figure 5.9: Effect of test frequency on electrical strength in both blends.

breakdown data are not an artefact of spurious changes in morphology with sample thickness, included solvent, impurities etc.

5.5 Discussion

5.5.1 Melt mixing Vs solution blending

It is clear from the breakdown data that the melt blending procedure, despite changing the morphology resulted in no change in the electrical strength, the high electrical strength of the BPA 115/20 blend could be reproduced in a melt mixed blend. The spherulite sizes and spherulitic nucleation density were estimated from SEM micrographs and it was found that the product of these quantities did not significantly depend on blend preparation technique. On the basis of the results of chapter 3 this would suggest that electrical strength is independent of blend preparation route, this was confirmed by electrical tests. This result also implies that impurities are not removed by dissolution or introduced by melt mixing therefore the results are independent of impurity effects.

DSC data shows that the composition of the two lamellar populations (LPE and BPE rich) did not depend on the way in which the blend was prepared. It was clear from morphological data that a higher nucleation density reduced the crystallisation time in these samples simply because more spherulites could then grow simultaneously, hence the available crystallisable material is used up more quickly.

Melt mixing would tend to cause local alignment of molecules (due to the shear fields experienced during mixing) and thus favour nucleation (1), this is clear despite the molecular relaxation that would occur during the degassing procedure. Another less likely explanation could be nucleation around contaminant particles, however there is no direct evidence to support the idea that melt mixed blends contain any more contaminants than solution mixed blends.

5.5.2 Discussion of effects of test conditions on measured data

The relationship between these quantities is not a simple one and it would be very

dangerous to try and extrapolate the data to real cable systems without additional data. Some attempts to try to quantify these effects in detail have made use of modified forms of the Weibull equation (11-13) adapted for differing test conditions. Here we have carried out a simple Weibull analysis including the effects of thickness and ramp rate, the relevant Weibull equations are given in Chen and Liepins p 336 (12).

The Weibull distribution is usually expressed in terms of the probability P_f of a sample failing at a given constant field E;

$$P_f = 1 - \exp[-(\frac{E}{E_c})^{a+b}] \qquad 1$$

where E_c and (a+b) are equivalent to the mean and variance in the normal distribution. The `life law' is commonly used to relate time of failure to applied voltage stress, where C is a constant, and can be written;

$$t_c = C^{-1/a} E^{b/a} \qquad 2$$

The `hazard function' h(t), expresses the proportion of samples failed at time t as;

$$h(t) = a t_c^{-a} t^{a-1} \qquad 3$$

The Weibull equation can be defined also in terms of the hazard function;

$$P_f = 1 - \exp[\int h(t) dt] \qquad 4$$

For tests where the voltage is a function of time, this expression is a more usefull starting point than equation 1. We can substitute for h(t) in equation 4 using equation 3 and rewriting h(t) in terms of E using equation 2.

$$P_f = 1 - \exp[\int a t^{a-1} C E^b dt] \qquad 5$$

To integrate this expression we must have everything in terms of t, this is simplified in a

ramp test since;

$$(\frac{dE}{dt})t = E \qquad 6$$

substituting this expression into 5 and integrating yields;

$$P_f = 1 - \exp[-\frac{ca}{a+b} t^{a+b} (\frac{dE}{dt})^b] \qquad 7$$

and writing all in terms of E, with reference to equation 4 yields;

$$P_f = 1 - \exp[-\frac{ca}{a+b} E^{a+b} (\frac{dE}{dt})^{-a}] \qquad 8$$

but since

$$\frac{dE}{dt} = R/D$$

$$P_f = 1 - \exp[-\frac{ca}{a+b} (\frac{D}{R})^a E^{a+b}] \qquad 9$$

On comparing equation 9 with 1 it is clear that;

$$E_c{}^{a+b} = \frac{a+b}{Ca} (\frac{R}{D})^a \qquad 10$$

since both equations must be equivalent. Finally taking logarithms to linearize, gives the final expression that;

$$\mathrm{LN}(E_c) = \frac{1}{a+b} \mathrm{LN}(\frac{a+b}{Ca}) + \frac{a}{a+b} \mathrm{LN}(\frac{R}{D})$$

The Weibull equation can therefore apparently give us thickness and ramp rate dependence of measured electrical strength data, as we can see E_c (or the mean electrical breakdown

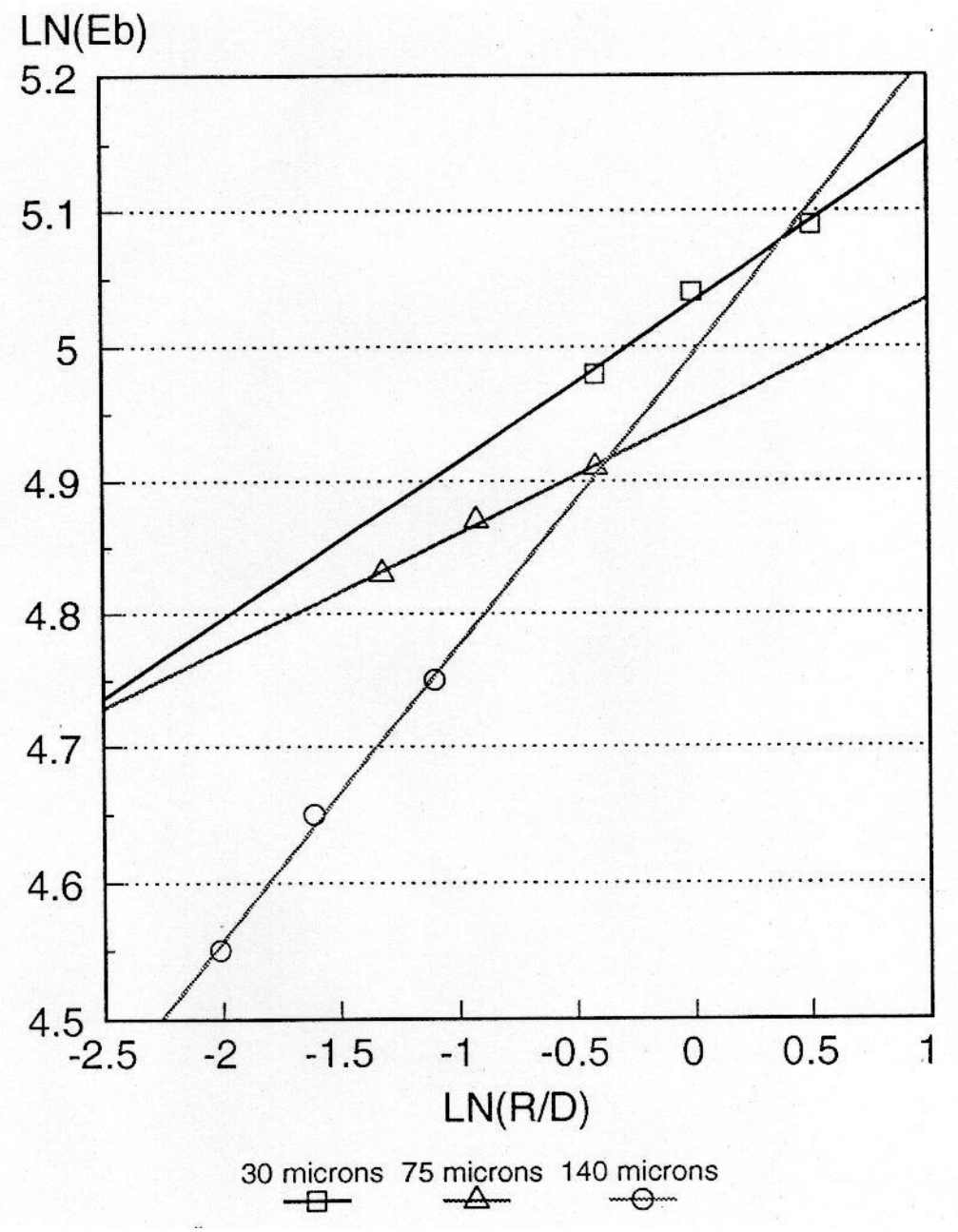

Figure 5.10: Weibull type plot of some electrical strength data from BPA Q/0.

strength) depends upon both R and D. So, if Weibull is adequate at explaining our observed trends, then a plot of LN (E_c) against LN (R/D) should yield a straight line for our results. Weibull fits were calculated for some of the experimental data from BPA Q/0 using a commercial fitting program and the resulting data plot is shown in figure 5.10. As can be seen quite clearly the points do not all fall on a straight line but the gradients and intercepts still depend on D and R. This clearly shows that this analysis is, unfortunately, too simplistic an explanation for what is occurring here.

However, the conclusion is clear; it is very important to specify the testing conditions and geometry precisely when reporting electrical breakdown results. Much of the confusion surrounding electrical breakdown measurements could then be removed if a single standard testing methodology and geometry were to be adapted, particularly for academic studies where meaningful comparisons need to be made.

5.6 Conclusions

1) Changing the sample preparation methods from solution blending to melt mixing generally increased the nucleation density and reduced the size of the spherulites developed. As a result, the crystallisation times of these blends are reduced.

2) The product of nucleation density and spherulite diameter was shown, in chapter 3, to be connected with electrical strength. This product and the actual electrical strength data did not depend upon how the blend was prepared.

3) We have seen a clear dependence of electrical strength on both ramp rate and sample thickness in two very different systems. The dependence of electrical strength on these two quantities was the same even though two systems with very different morphologies were compared. A Wiebull analysis was not sufficient to explain such dependencies of electrical strength on these two parameters.

4) The trends reported in the previous chapter (ie: increased LPE content increased electrical strength) are seen in thicker samples. However extreme care must be exercised in extrapolating these type of short term tests to long term service conditions. Nevertheless trends seen are in line with the literature and are not a result of morphological changes with thickness, included impurities etc.

5) The AC test frequency used also has an effect upon the measured value of electrical strength in short term ramp testing. This is thought to be due to increase frequency of micro-discharges during tree growth (10) and was again independent of morphology.
6) From these results it is clear that when any electrical testing is performed it is important to specify the testing conditions accurately and in detail, as they can affect the measured results. Much of the confusion surrounding meaningful comparisons of electrical data, particularly in academic studies, could then be removed if one standard testing methodology and geometry were to be adopted.

5.7 References

1) A.Gustafasson and U.W Gedde, Nordic insulation symposium, 8.4.

2) P.H.H Fischer and K.W Nissen, IEEE Trans. Electr. Insul. 1976, **11**, 37.

3) J.H Mason, IEEE Trans. Electr. Insul. 1991, **26**, 318.

4) R. Lovell, IEEE Trans. Electr. Insul. 1976, **11**, 110.

5) J. Artbauer and J. Griac, IEEE Trans. Electr. Insul. 1970, **5**, 104.

6) B. Helgee and P. Bjellheim, IEEE Trans. Electr. Insul. 1991, **26**, 1147.

7) D.M. Tu, W.B. Liu, G.P Zhuang, and Z.Y. Liu, IEEE Trans. Electr. Insul. 1989, **24**, 589.

8) M. Leda, IEEE Trans. Electr. Insul. 1980, **15**, 206.

9) J.H Mason, IEEE Trans. Electr. Insul. 1992, **27**, 1213.

10) W. Pfeiffer, IEEE Trans. Electr. Insul. 1991, **26**, 239.

11) Chen C Ku and R Liepins, Electrical properties of Polymers, Hanser 1987.

12) D A Seanor, Electrical properties of polymers, Academic press 1982.

13) Alun Vaughan, Personal communication.

CHAPTER 6 - EFFECTS OF MECHANICAL DEFORMATION ON ELECTRICAL BREAKDOWN BEHAVIOUR.

6.1 Introduction

In chapter 3 the effects of varying the LPE content in a binary LPE/BPE blend were discussed as a way of improving the electrical performance of such materials. In chapter 4 it was concluded that morphology, rather than molecular composition, was the dominant factor influencing electrical strength. A significant improvement over BPE alone could be achieved by adding LPE and crystallising under conditions to maximise lamellar space filling. The random array of lamellar barriers caused by space filling increased the electrical strength of such systems. Chapter 5 showed that the increase in performance achieved by doing this is not an artefact of the sample or testing procedure but could be related to real systems, and as such has potential commercial significance. Another important aspect, related to applications of these materials is mechanical deformation.

The deformation of polyethylene is a complex process and has been extensively studied, by cold drawing (1-4). The spherulitic structure, in the absence of mechanically induced orientation, contains randomly oriented lamellae. When this structure is deformed, an onset of orientation has been reported to occur beyond the first yield point. X-ray data suggests that lamellae begin to tilt toward the direction of draw, adopting a fibrillar nature at higher strains which eventually leads to macroscopic necking. The number of explanations as to the microscopic processes occurring during deformation are many and numerous; the lamellae have been reported to separate, tilt and to undergo lamellar slip (5). Early work was on homogeneous samples, specially prepared to confirm particular mechanisms (1,2,6). Most studies have not attempted to relate structural changes to the stress-strain curve, only a few real time experiments have been carried out (4, 7-10) but these results generally concur with the majority of the work which has been carried out by deforming samples and then examining subsequently. Recent work has confirmed the existence of double yield points (11-13); the first is associated with onset of crystalline orientation, whereas the second is attributed to a break up of the crystalline structure. A useful model was developed at

Reading (14) for the existence of both yield points, based on morphological as well as X-ray data. Here, the material was viewed as a network of lamellar crystals held together by entanglements arising principally from chain branches, which can not be incorporated into the crystals during crystallisation. Up to the first yield point, these entanglements are stretched elastically and recovery is possible, then, below the second yield point these chains become disentangled, the second yield point marking the onset of permanent plastic deformation and the annihilation of the network. In a later paper, the same authors (15) examined the effects of deformation rate and annealing. Higher draw rates led to more pronounced deformation of the banded spherulites, and annealing after cold drawing led to reduced residual strain and recovery of the original morphology.

Melt drawing is recognised as a way of giving a polymeric material improved tensile strength (16) as a result of linear shish kebab structures which are formed under crystallisation (17). A more thorough treatment of deformation in polyethylene is given in (18) where the effects of orientation (brought about by mechanical tension) are investigated. In this case the draw ratio was 9.5:1 and fibrillar morphologies were produced as a result of the mechanical deformation. In (19) it was shown that similar morphologies could be generated by mechanical deformation and that the tensile properties changed with LPE content in binary LPE/BPE blends. In HDPE (20) it was reported that voids about 80nm in diameter could be produced by mechanical drawing. An interesting viewpoint is given in (21), where the tensile yield stress of a wide range of polyethylenes was found to be dependent on their crystal thickness, and therefore the conclusion was that the amorphous regions simply serve to transmit load onto the crystals. The exact mechanical properties, and particularly the stress/strain behaviour, was highly sensitive to crystal thickness and to temperature. In (22) fracture toughness of LLDPE was investigated and it was found that this mechanical property was sensitive to the amount of phase segregation in the LLDPE samples investigated and a similar conclusion was found in binary PE blends (23) where mechanical properties depended on the nature of the blend considered.

In all these cases it is quite clear that deformation influences morphology in a very profound and significant way, and as such warrants investigation. However, the electrical strength of drawn materials is an area which has not been studied extensively. An early paper (24) looked at the effects of mechanical compression and extension; it was reported

that the electrical strength of both of the materials considered could be increased by mechanical compression and reduced by mechanical extension. Although a detailed examination of the mechanical properties of these materials is interesting in its own right, this investigation primarily concentrates on the consequences of mechanical deformation on electrical properties.

6.2 Preliminary work

6.2.1 Materials

Here we concentrate on the effects of mechanical deformation on *morphology and electrical behaviour* in a branched polyethylene material (4901), and a blend composed of 10% LPE (Rigidex 140/60) in 4901 branched polyethylene.

Three very different morphologies were chosen for this investigation, which differed essentially only in their crystalline structure, each had constant composition BPE matrix, and one material had no added crystalline LPE.

The three morphologies considered are shown in their undeformed state in figure 6.1. Quenched 4901 (BPA Q/0) shows a uniform banded texture. Crystallising the blend isothermally at 115°C (BPA 115/10 M) gives rise to open banded spherulites, and crystallisation at 124°C (BPA 124/10 M) gives rise to compact lamellar aggregates. The designation `M' after the blends means that they were prepared by melt mixing so as to yield sufficient quantities for this investigation.

6.2.2 Comparison of dumbbell and thin film samples

Since it is clear that the mechanical behaviour of a polymeric material depends upon the time scale of the experiment (15), higher draw rates will cause more changes within the material, for a given extension, than a lower draw rate. Since this effect could complicate this investigation, a draw rate of 10 mm/min was chosen and adhered to throughout.

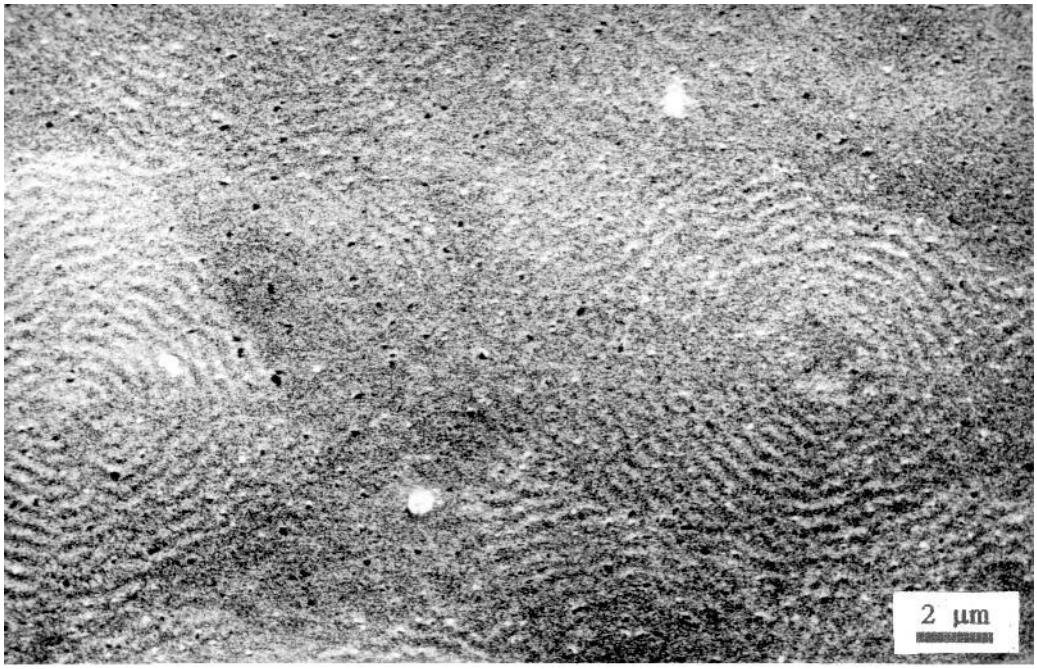

Figure 6.1(a): Banded spherulitic texture in BPA Q/0.

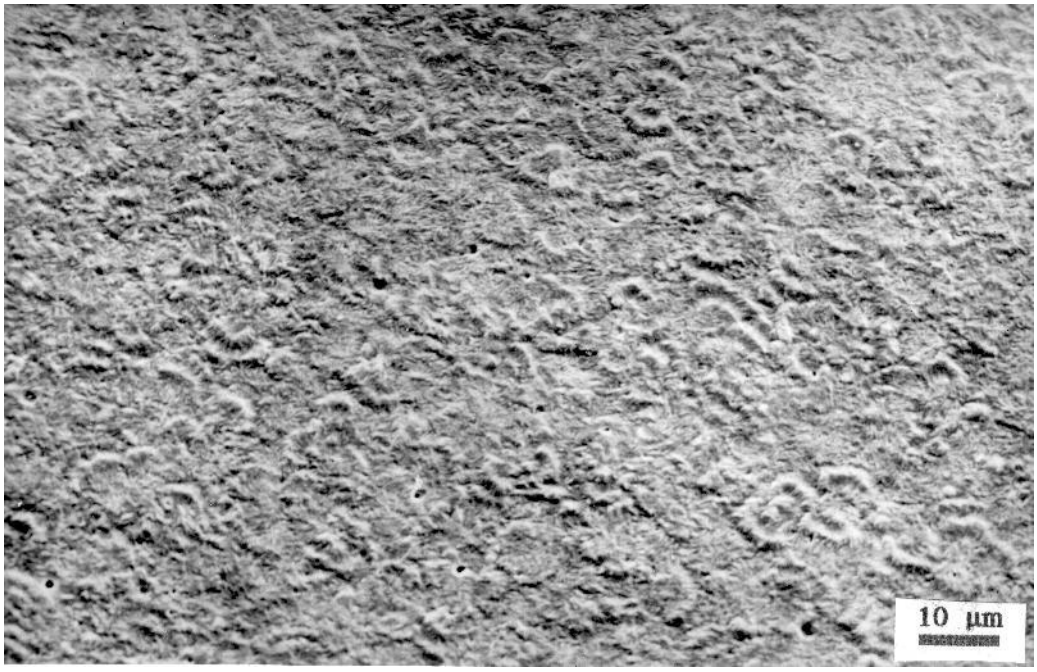

Figure 6.1(b): Open banded spherulites in BPA 115/10 M.

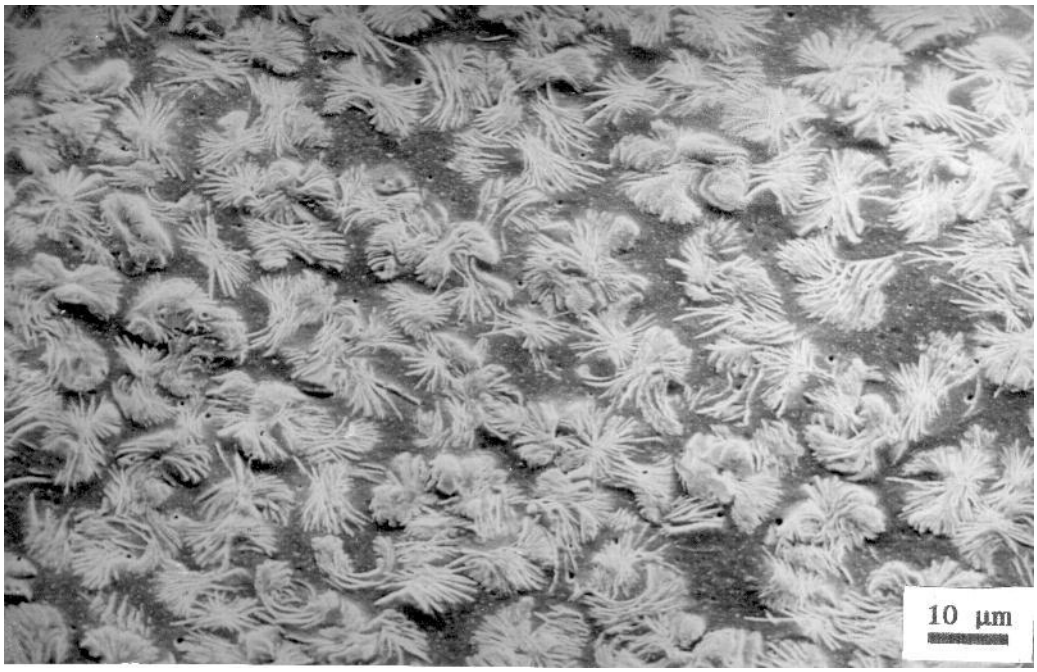

Figure 6.1(c): BPA 124/10 M showing compact lamellar aggregates.

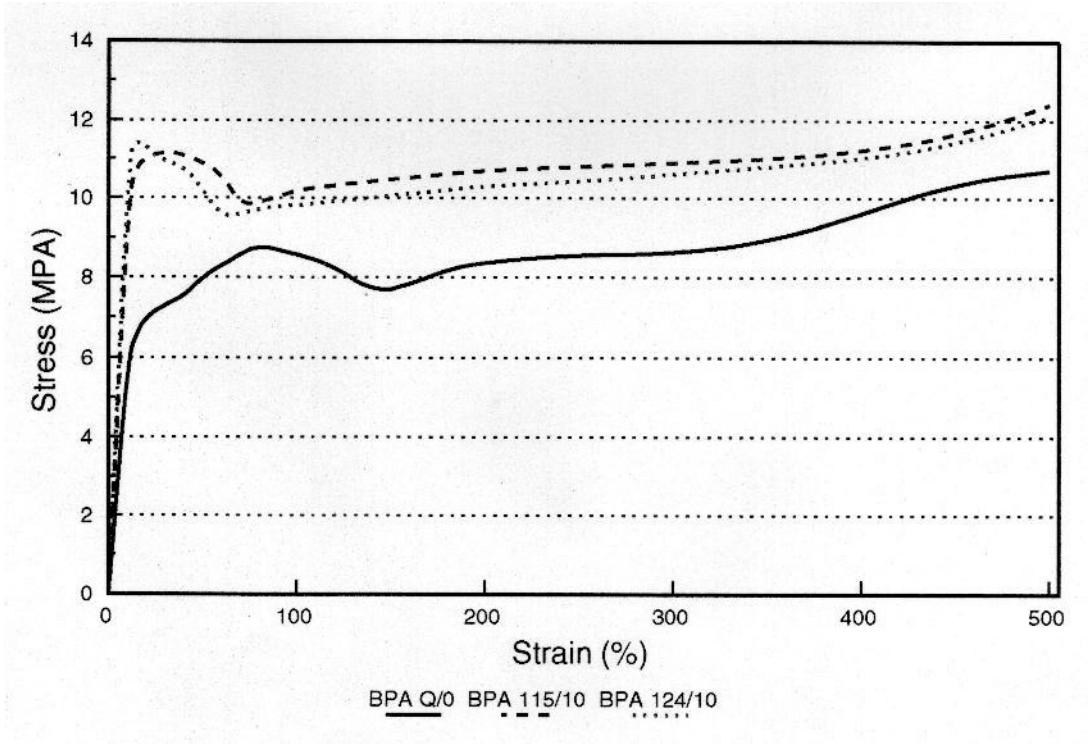

Figure 6.2: Stress-strain relationships in all three materials.

Dumbbell shaped samples were used for morphological investigations, due to the ease with which these samples could be prepared for examination, whereas electrical testing necessitated thin film samples. Up to 100% strain, it was found that the stress-strain properties of films and dumbbell samples were identical. Above this strain, the film samples had a tendency to tear and therefore electrical testing was restricted to strains up to 100%. Furthermore, above this strain the thickness of the films decreased significantly as necking occurred, and as discussed in chapter 5 this could affect the electrical results. Clearly such effects on electrical data due to sample thickness are unwanted in this investigation.

6.2.3 Stress-strain curves

Figure 6.2 shows the stress-strain curves for all three systems considered, details of the experimental procedure are contained in chapter 2. The mechanical properties are very different for each material. In BPA Q/0 the first yield point is located at about 20% applied strain, followed by a gradual rise to a maximum stress of 8.5 MPa at 100% strain. The second yield point is located at around 120% strain as this is where necking first occurs. The BPA 115/10 M blend behaves very differently; the first yield point is located around 15% strain with a flat region following this. The maximum stress is higher here than in BPA Q/0, however, necking occurs more readily in this system, and first occurs at 80% strain. The BPA 124/10 M blend again behaves differently. The first yield point is located at a strain of 12%, and there is a peak stress of 11 MPa at 15% strain, after which the stress drops off rapidly and necking then occurs around 65% applied strain. It is therefore clear from these stress-strain curves that crystalline morphology significantly affects mechanical properties, this is in line with the literature (19, 23).

6.2.4 Relaxation behaviour

Figure 6.3 shows a series of `hysterisis loops', the applied strain was increased to 20%, at 10 mm/min, and then decreased at the same rate until the stress was zero. The graph clearly shows that appreciable plastic deformation occurs in each sample, even at the low strains

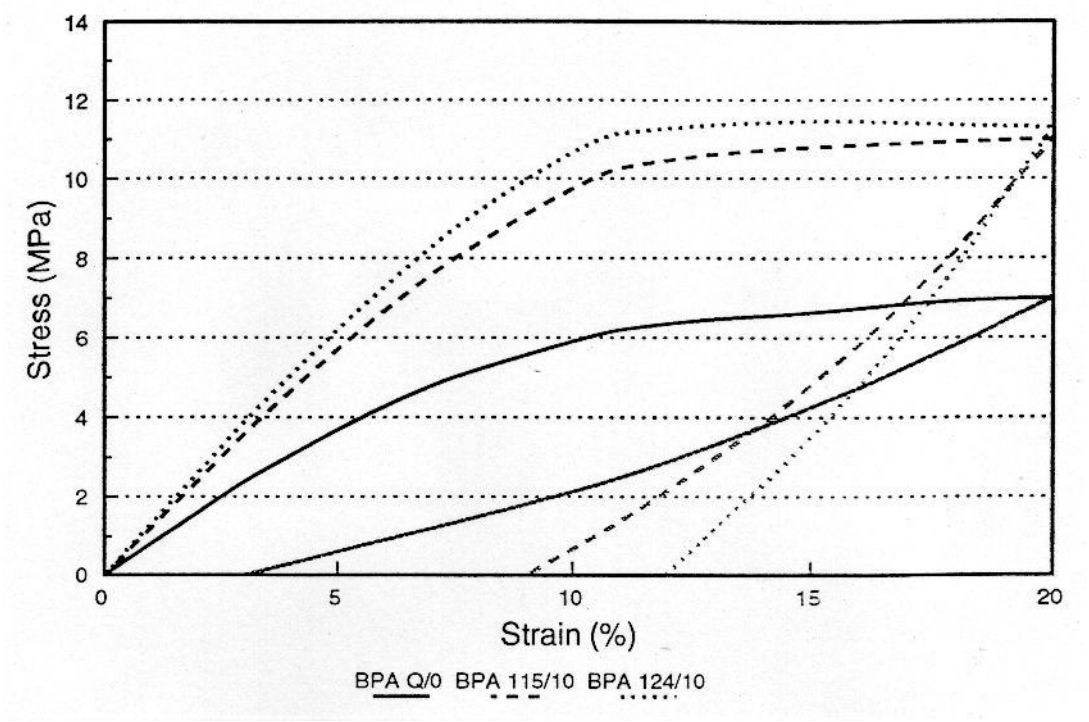

Figure 6.3: Hysterisis loops for all three materials and 20% strain.

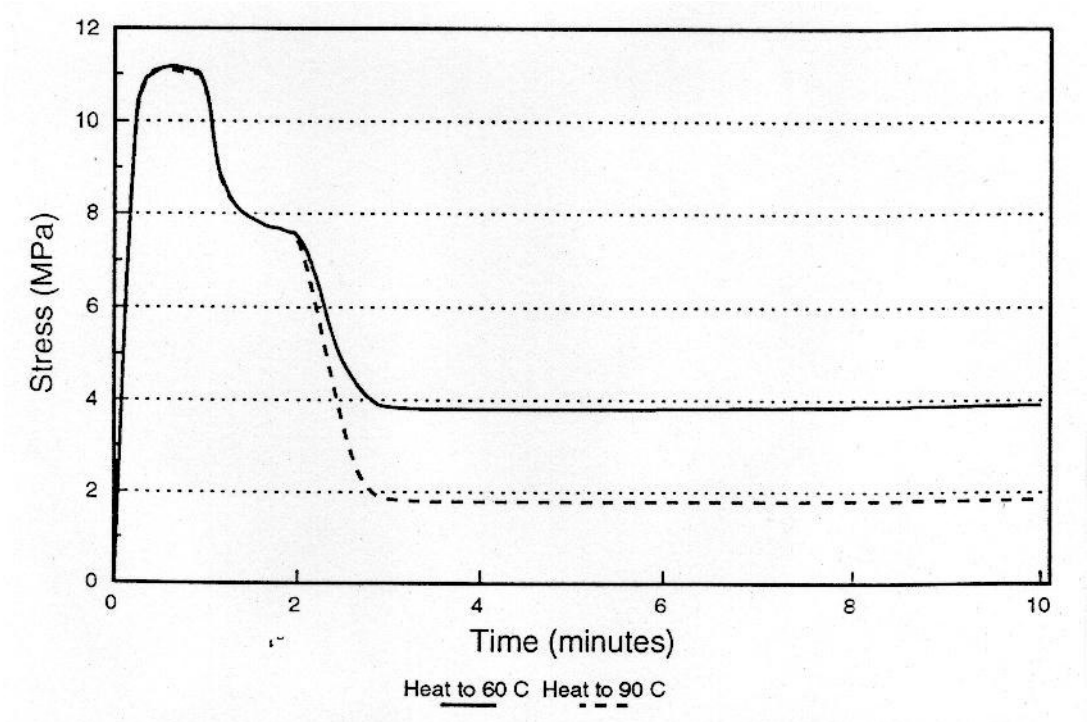

Figure 6.4: Stress relaxation at constant strain in BPA 115/10 M, 50% strain.

considered here. BPA Q/0 showed around 3% residual strain immediately after testing, BPA 115/10 M had 9% and BPA 124/10 M showed 12%. So the last system, which has compact lamellar aggregates, showed a higher degree of plastic deformation than the BPA Q/0 system which was more elastic.

By heating a sample under constant strain (50%), the stress in the sample dropped. This typical behaviour is shown (figure 6.4) in BPA 115/10 M. At room temperature an immediate drop in stress occurred as soon as 50% strain was reached, which then remained. A further drop in stress could be obtained by heating the sample to 60°C at time t=2 minutes, the stress was reduced from a peak stress of 11 MPa to 3.9 MPa. By heating a similar sample to 90°C, the stress was reduced to just 1.8 MPa. The stress did not increase once the heat was removed at t=4 minutes and the relaxation remained even when the sample had cooled.

Increasing the temperature of a material increases its entropy (amount of disorder), which would have two effects. In disordered amorphous regions this would result in an increase in entanglements and a contraction of the structure, increasing the apparent stress for fixed strain. Crystalline regions, which are ordered initially, would become less ordered and expand. In these samples heating causes an expansion of the sample (decrease in measured stress), therefore, on the basis of this data, the latter effect is dominant. At elevated temperatures partial melting of the crystallites could be occurring.

6.2.5 Practical experimental procedure

Clearly relaxation occurs after straining, especially at elevated temperatures. Etching and replicating a sample for detailed TEM work involves timescales of a few days, clearly samples would relax significantly during this time and invalidate any results obtained. Therefore if dumbbell samples were not needed for X-rays or DSC, which were carried out immediately following straining, the samples were sandwiched between sheets of a block copolymeric elastomer. This has the effect of 'freezing in' the permanent deformation induced. Under these conditions reproducible TEM replicas could be obtained after 4 hours permanganic etching, which several weeks later retained their morphology. Obtaining consistent electrical data was more of a problem, and the standard procedure of performing

5 tests on each sample did not work. The samples relaxed during the hour spent testing, which caused the electrical data to change significantly. To overcome this problem, only two electrical tests were carried out on each thin strip of material immediately following deformation. This allowed minimum time for the sample to relax during the electrical test procedure. Provided this was done, molecular relaxation had an insignificant effect on the electrical data obtained. For this investigation, due to the large number of samples required by the modified electrical test procedure, strains of 20%, 50% and 100% were chosen for this investigation. These represent, approximately, points below the first yield point, between the first and second yield points, and near the second yield point.

6.3 Results

6.3.1 Differential scanning calorimetry

Samples were subjected to DSC analysis immediately following deformation. It is clear from the previous data that during the DSC run the sample in question could anneal during scanning. Therefore DSC analysis cannot be relied on to provide data about the possible morphologies after straining. However should permanent damage to the sample occur, the DSC will pick this up if it is not recoverable during the scan, for this reason DSC runs were taken of some samples after deformation.

Figure 6.5(a) shows DSC melting endotherms, as a function of mechanical strain. In BPA Q/0, the endotherms do not change significantly even after 100% strain. On the basis of this data the BPE does not appear to be permanently affected by the applied deformation even after 100% strain.

A different effect occurs in both blends, the peak corresponding to the LPE rich phase is significantly reduced following 100% strain (figure 6.5(b)), this implies that crystals are being mechanically broken up. The effect of this strain is more pronounced in the subsidiary peak of co-crystals and is so severe the peak almost disappears.

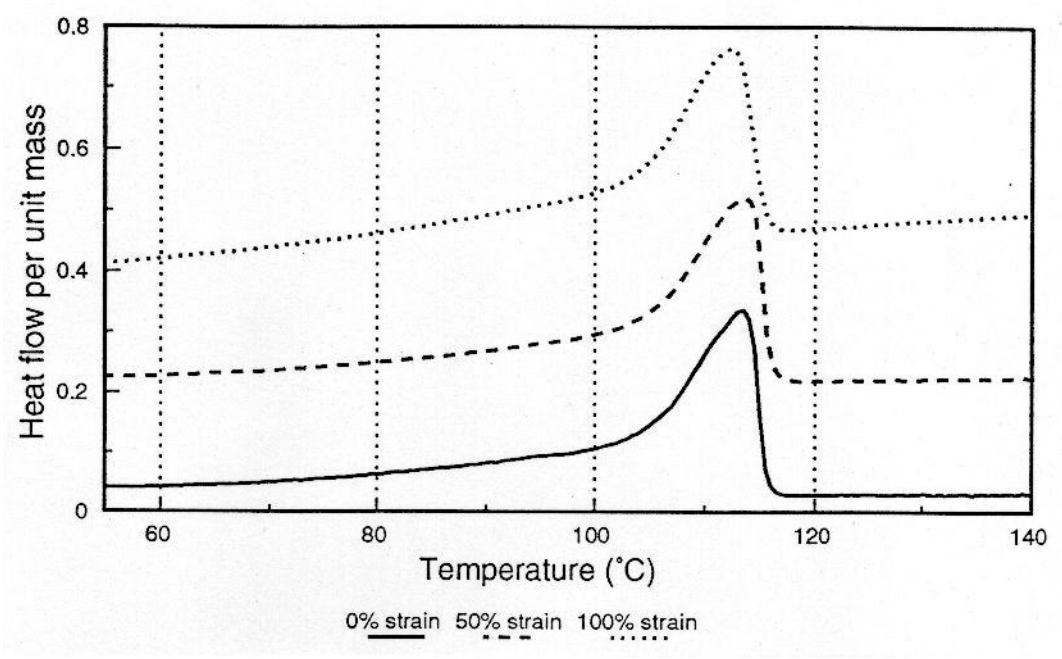

Figure 6.5(a): DSC melting behaviour of BPA Q/0 for various strains.

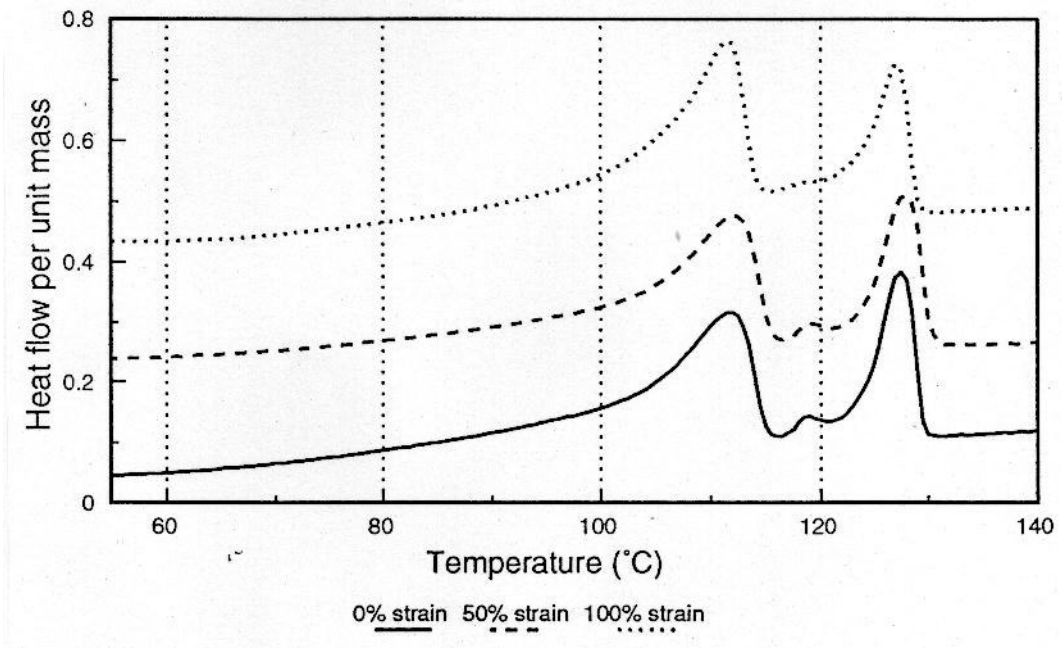

Figure 6.5(b): Melting behaviour of BPA 115/10 M.

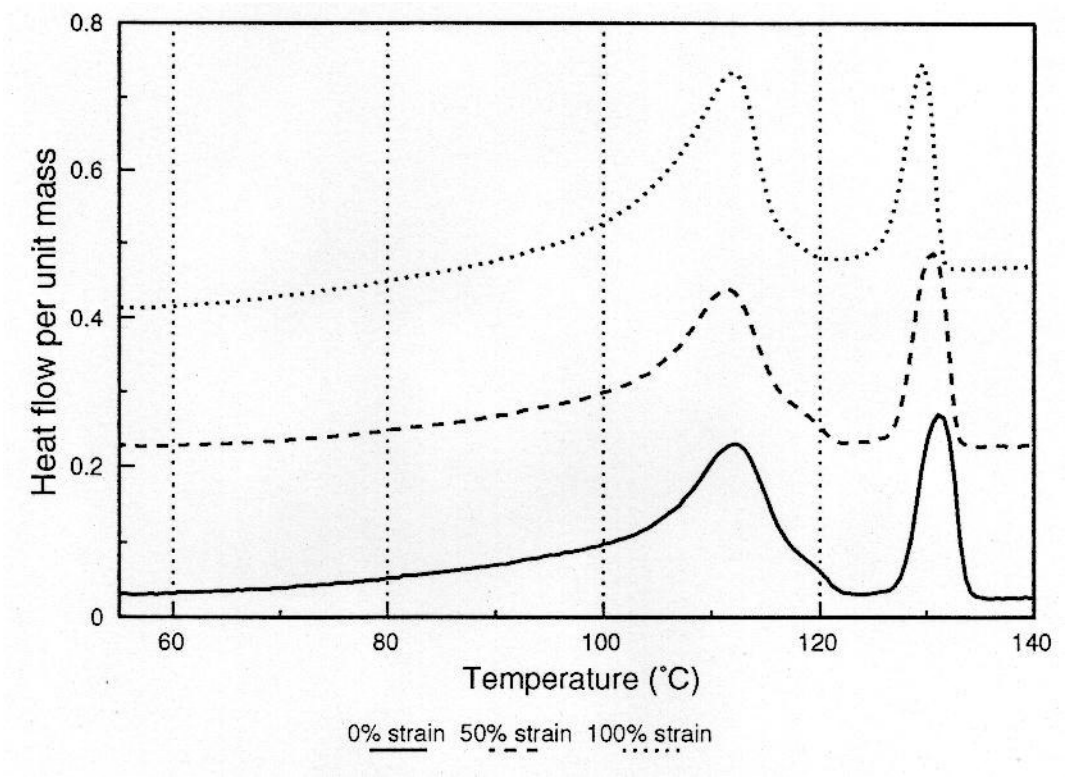

Figure 6.5(c): Melting endotherms of BPA 124/10 M for various applied strains.

Figure 6.5(c) shows this effect in BPA 124/10 M, here a co-crystal shoulder located to the right of the BPE peak disappears at 100% strain. It is clear from this data, that for a strain of 100%, permanent damage is occurring, principly in the crystalline regions, the amorphous material can be viewed as elastic, transmitting the strain onto the crystals. This is in agreement with the ideas discussed in the literature (15, 21).

6.3.2 Morphological examination

The morphology of all three materials from 0-100% strain was considered, wide angle (WAXS) and small angle (SAXS) X-ray scattering patterns were taken to supplement the TEM data. The arrow on the figures indicates the draw direction and the scattering patterns have been lined up to correspond with the micrographs in all cases.

BPA Q/0 (figure 6.6). We can see that even at low strains the spherulites become clearly deformed, elongating in the direction of the draw axis. Some evidence for lamellar

orientation is seen, particularly in figure 6.6(b) (50%). At a strain of 100% the spherulites are completely destroyed, to be replaced by a uniform texture of lamellae which appear to show a cross-hatched pattern (6.6(c)). These observations are supported by the X-ray data which shows marked orientation of lamellae perpendicular to the draw direction, the extent of which increases with strain.

BPA 115/10 M. The behaviour of this blend is shown in figure 6.7 and is generally very similar to that in BPA Q/0. At 20% strain (fig 6.7(a)) spherulites show some elongation along the draw direction, although somewhat less than in BPA Q/0. The X-ray scattering patterns are similar in both cases (cf. fig. 6.6(a) and fig. 6.7(a)). At 50% strain spherulites are clearly deformed and figure 6.7(b) shows regions where lamellae are primarily oriented perpendicular to the draw direction `a' as supported by the X-ray data. The final result of deformation is a uniform texture of lamellae such as figure 6.6(c).

BPA 124/10 M. Micrographs of this system are shown as figure 6.8. There is little evidence that individual aggregates are deformed as a whole, unlike the previous examples, but that lamellae are affected on an individual basis. Figure 6.8(a) shows that deformation of lamellae within aggregates occurs even at 20% strain and the type of deformation experienced by a lamellae appears to depend on it's orientation with respect to the draw axis. Deformed lamellae appear curved where they happen to be aligned obliquely to the draw axis `b', elongated when aligned along the draw direction `c' and separated when aligned perpendicularly `d'. This observation suggests that such lamellae may be elastically deforming at low strains, and this is borne out by reference to figure 6.8(b), which clearly shows buckling and twisting of lamellae within an aggregate which gives a ridged effect. Figure 6.8(c) shows the final stage of this deformation process, for 100% applied strain. In this case former aggregates of lamellae appear to be completely broken up into individual lamellar fragments, which can be clearly seen in this TEM micrograph.

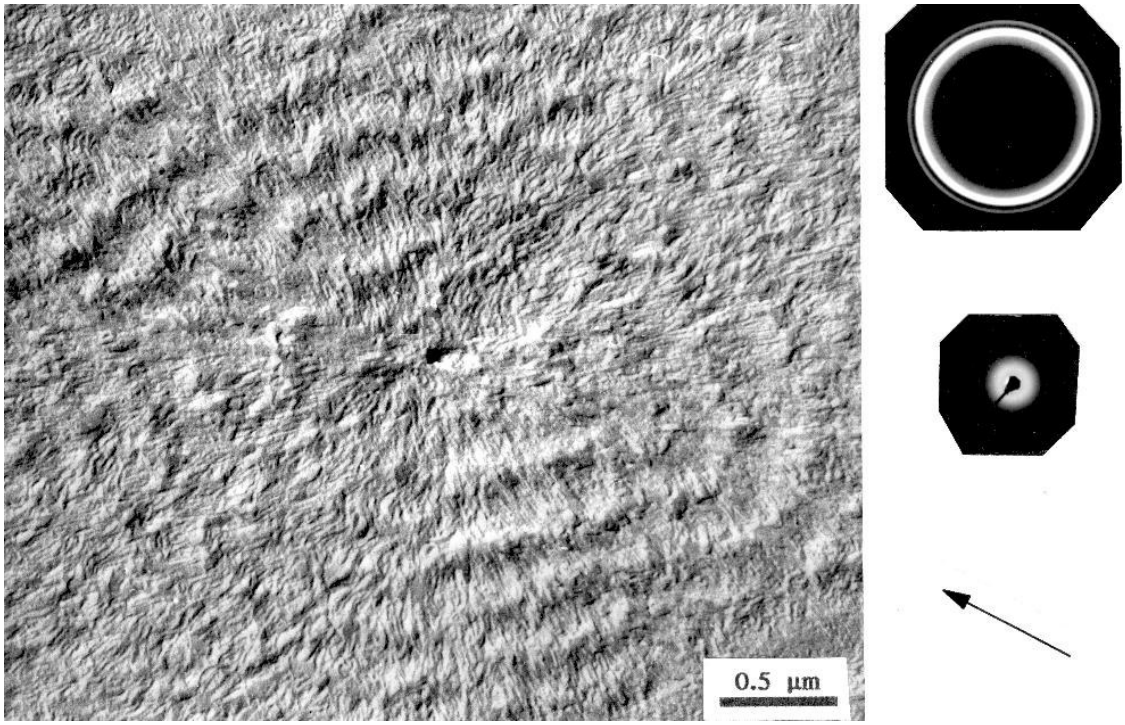

Figure 6.6(a): Banded spherulites in BPA Q/0 showing clear elongation.

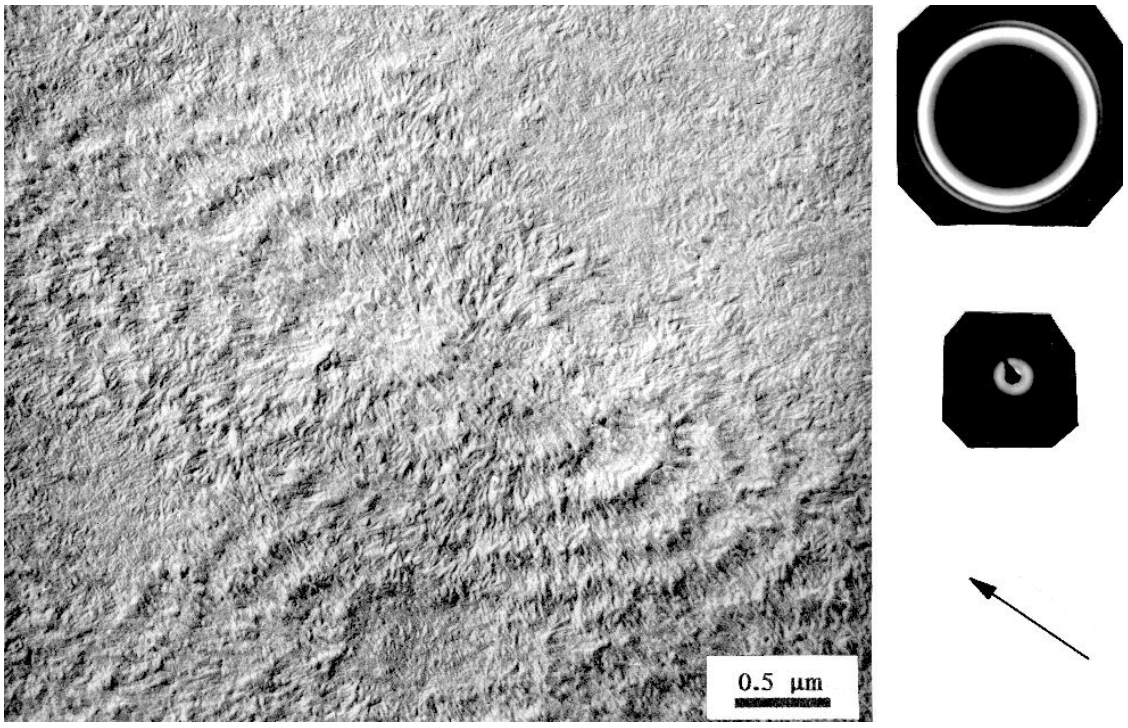

Figure 6.6(b): Further elongation occurs after 50% applied strain.

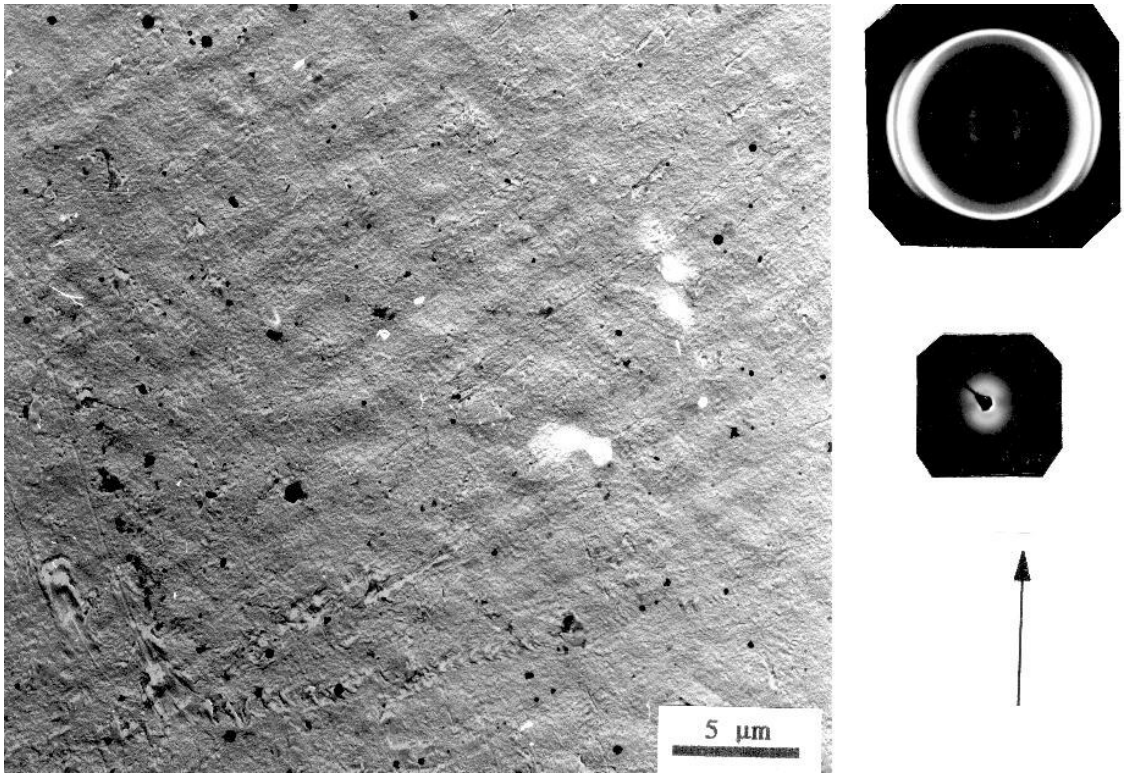

Figure 6.6(c): BPA Q/0 after straining to 100% showing uniform lamellar texture.

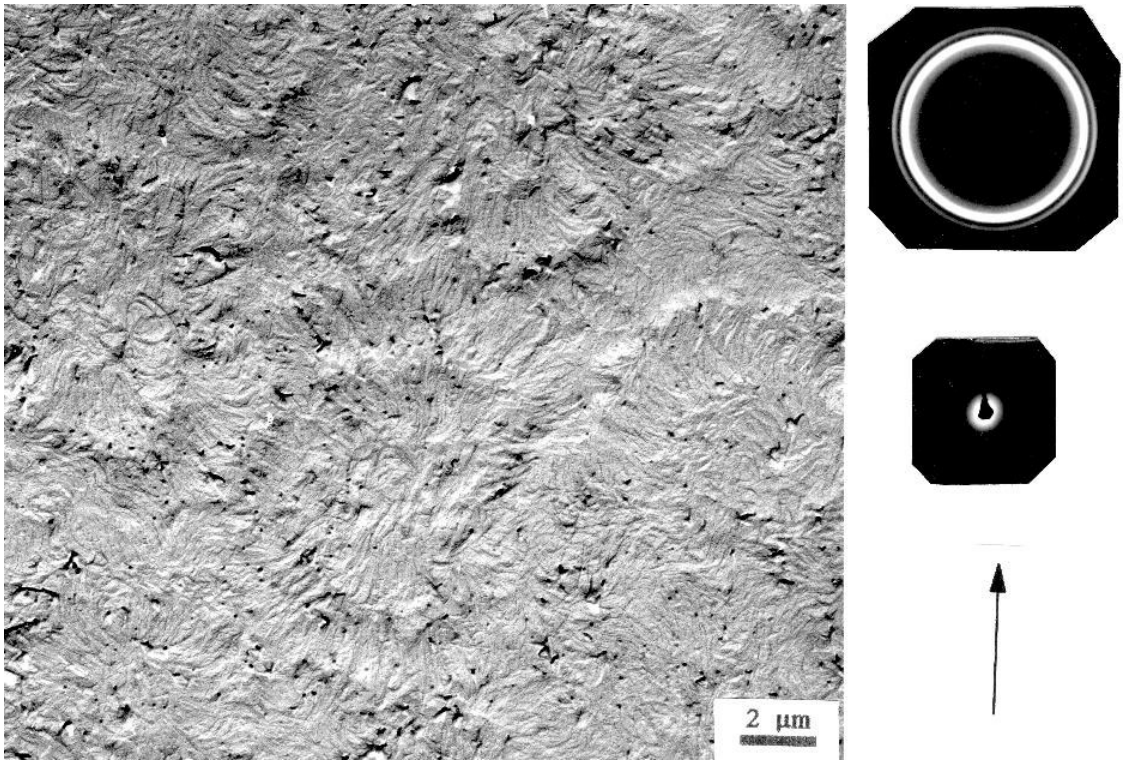

Figure 6.7(a): Evidence of spherulitic deformation in BPA 115/10 M, 20% strain.

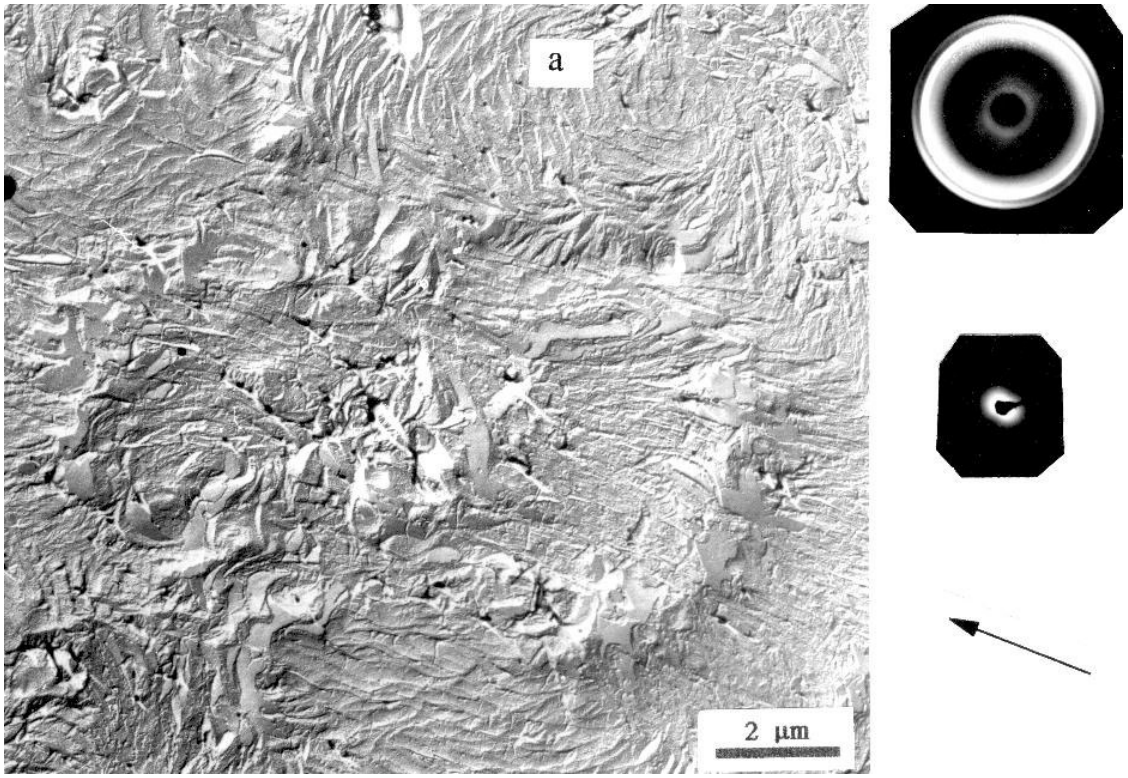

Figure 6.7(b): Regions of oriented lamellae in BPA 115/10 M after 50% strain.

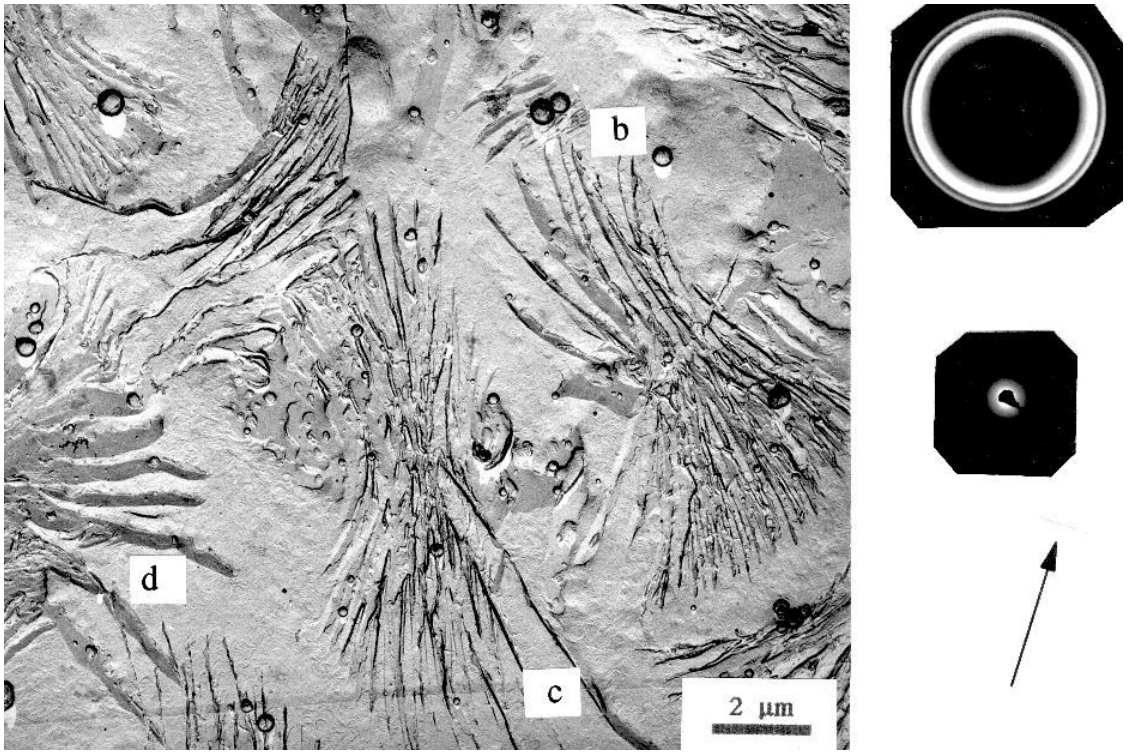

Figure 6.8(a): Lamellar aggregates in BPA 124/10 M showing deformation, 20% strain.

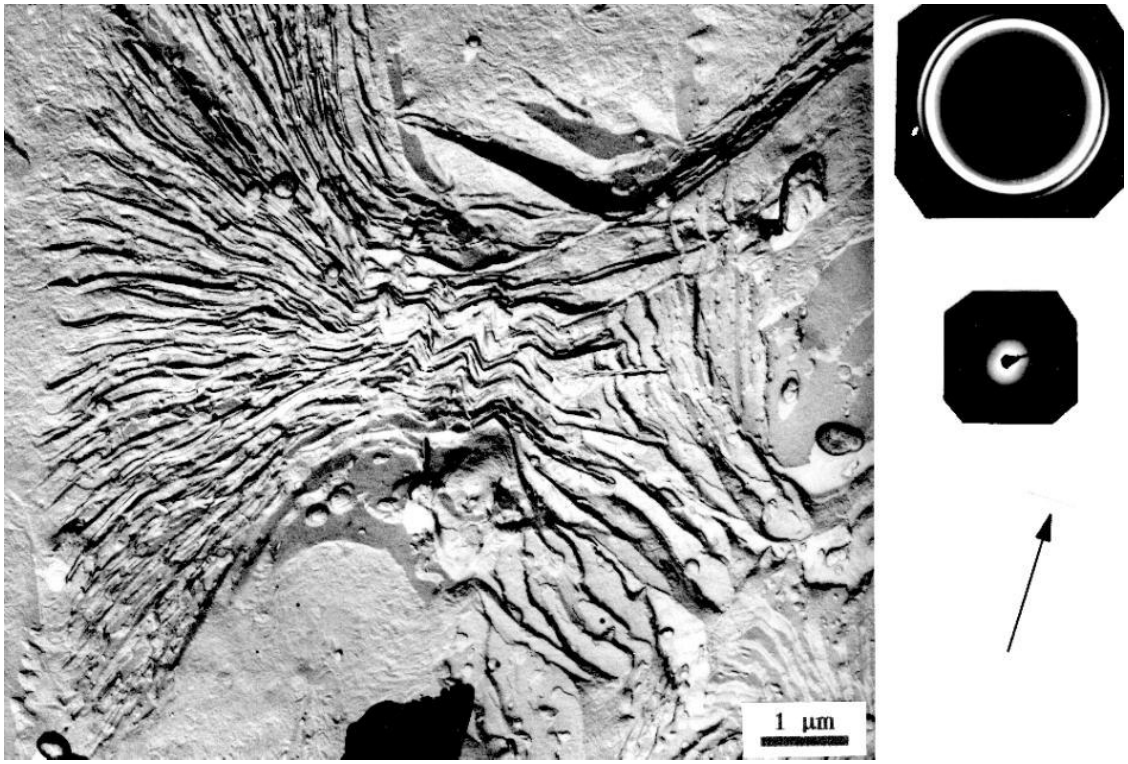

Figure 6.8(b): Lamellae appear ridged in BPA 124/10 M after 50% strain.

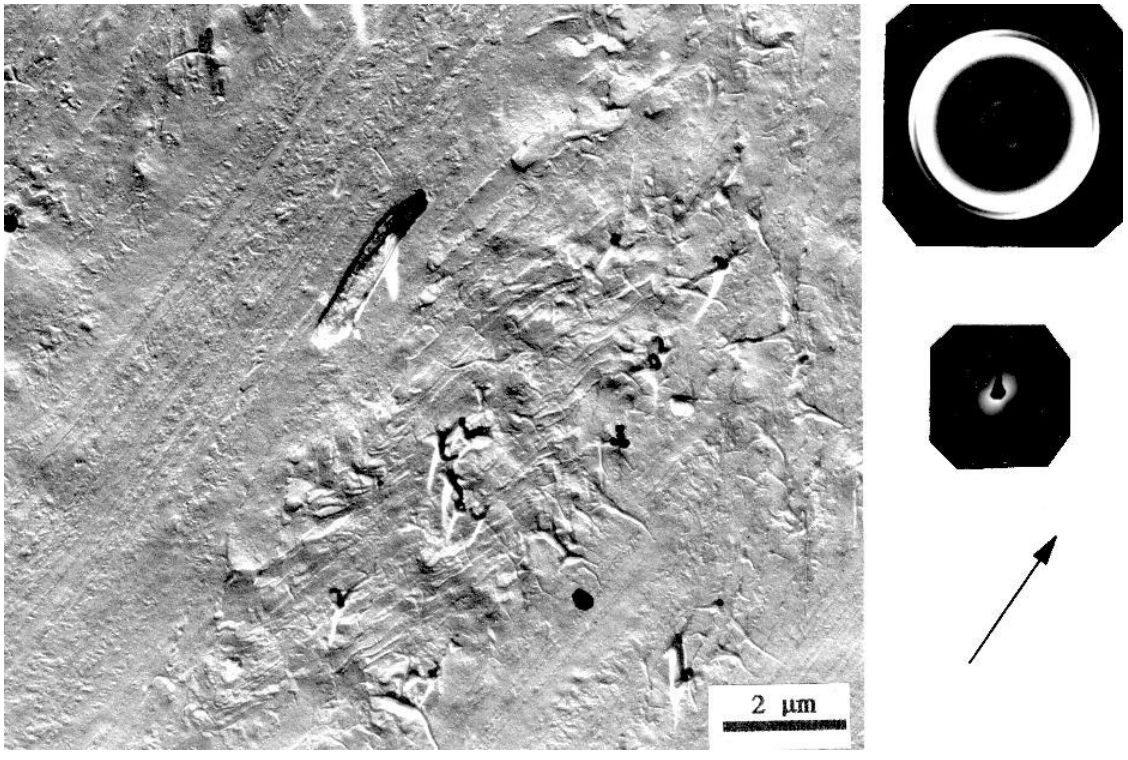

Figure 6.8(c): Complete fragmentation of lamellae in BPA 124/10 M, 100% strain.

In all these cases, although the compact aggregates are affected by the applied strain in a markedly different way from the banded spherulites, the crystalline morphology is affected even for relatively small strains. X-rays are clearly good for seeing, quantitatively, average crystalline orientation, whereas TEM is good for seeing details of the exact effects deformation has on morphology. In conjunction with DSC data it is clear that deformation is having a large effect primarily on the crystals; at low strains crystals re-orient and appear to elastically deform, whereas after 100% strain a completely different sample morphology is apparent, corresponding with the changes in the DSC data at this strain.

6.3.3 Electrical test results

Strips of material of thickness 70 microns were tested for electrical strength at a ramp rate of 50 Volts per second using 50 Hz AC voltage. Since the thickness of the samples decreased somewhat with applied strain these small effects on electrical strength were compensated for using the data in chapter 5. For example the thickness decreased from a nominal 70 microns at 0% strain to 62 microns at 100% strain, a change of 5-6 KV/mm in the measured electrical strength. The 95% confidence interval is ±4 KV/mm on all data.

Figure 6.9 shows the thickness corrected electrical strength of these systems as a function of applied mechanical strain. As discussed in chapter 5 the sample crystallised at 115°C has highest electrical strength of the three systems. At high strains the electrical strength of all three materials appears to tend towards the same minimum (110 KV/mm) for each of the systems considered here. The bulk of the reduction in electrical strength occurs at small strains, up to 50%. The materials containing banded spherulites (BPA Q/0 and BPA 115/10 M), showed an electrical strength which decreased approximately exponentially with applied strain. BPA 124/10 M displayed a much more linear decrease. Figure 6.10 shows the effect of annealing BPA 115/10, after deformation to 50% strain, for the time periods indicated. Clearly in this case the reduction in electrical strength brought about by deformation is reversible. At room temperature much of the electrical strength is regained in a few days, however at 60°C the electrical strength is restored in a matter of minutes. The annealing behaviour was very similar for the other two systems.

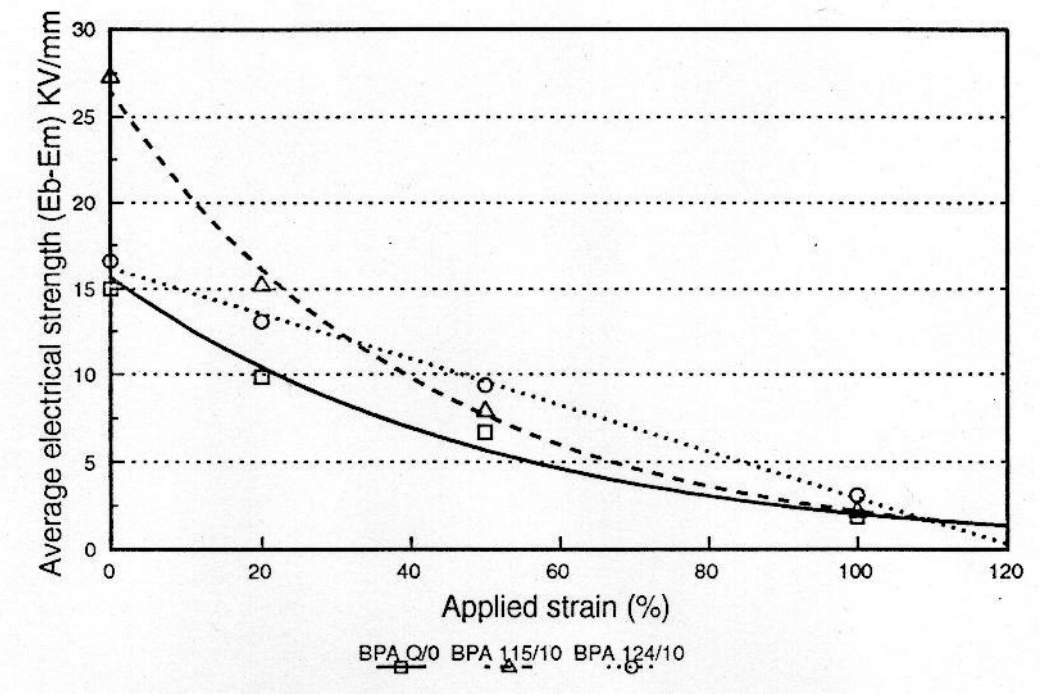

Figure 6.9: Electrical strength as a function of mechanical strain.

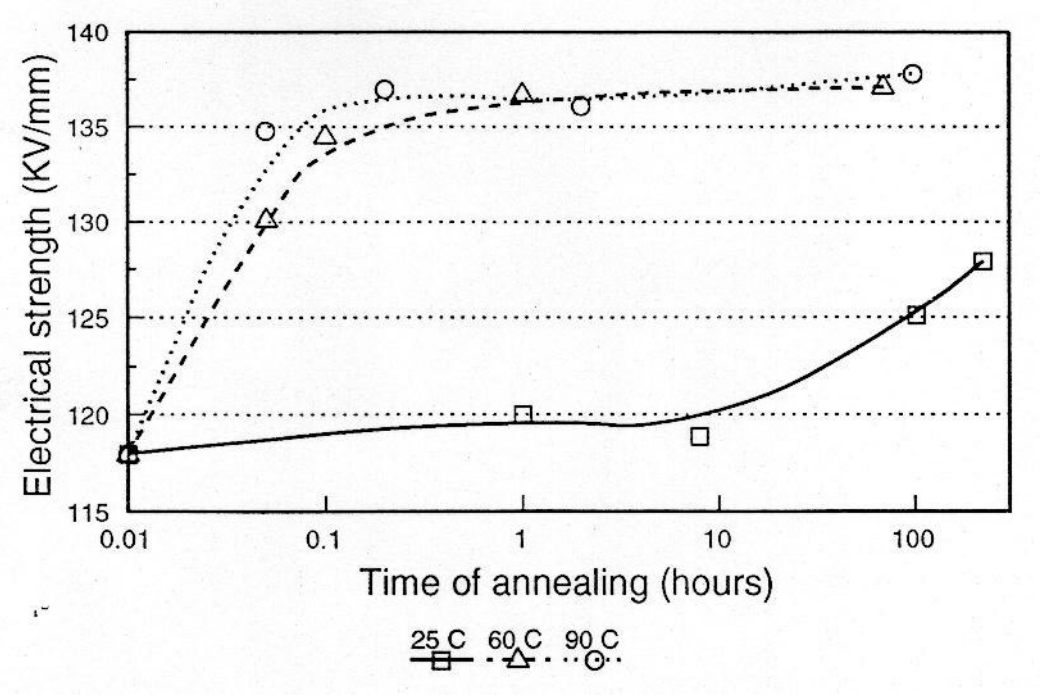

Figure 6.10: Effect of annealing on electrical strength in BPA 115/10 M, 50% strain.

Samples subjected to 20 and 50% strain could be annealed quickly back to full electrical strength, however annealing was not possible with samples subjected to 100% strain. No amount of annealing, even at 90°C, could restore the electrical strength of such materials. Although a detailed study of the morphology of annealed samples was not performed in this investigation, the literature (15) supports a return to the original morphology is possible by annealing, provided the initial strain does not exceed the second yield point.

6.3.4 DMTA analysis

We have seen that from DSC, TEM and X-ray scattering that profound changes occur to the crystallites even at small strains. DMTA provides complimentary information concerning molecular relaxations. In particular the glass transition is of interest in probing possible void formation as has been proposed (20). Mechanically induced voiding could be responsible for the reduction in electrical strength upon mechanical strain seen here. The glass transition corresponds to the onset of chain motion, were microvoids present in the material these would represent free space in the material which may cause a depression in glass transition temperature.

Figure 6.11(a) is a graph showing the parameter Tan-delta (see chap. 2) as a function of temperature in BPA Q/0 M for strains of 0%, 50% and 100%. There is no significant change in any of the transitions observed. The situation is somewhat more complex in the case of the blends, which both show the behaviour illustrated in figure 6.11(b) for the same strains. The peak near -115°C corresponding to the glass transition has not changed even after 100% strain, however the magnitude of the ß transition (at around -5°C) has increased somewhat for 100% strain. This transition is usually associated with motion at branch points or small chain segments (25), however in a multi-phase system, like a polymer blend, the exact meaning of such a change is difficult to interpret and is beyond the scope of the current investigation. DMTA data is inconclusive at showing whether voiding is responsible for the loss of electrical strength seen in this study. This could mean that voids are not present, or instead it could mean that DMTA is not sensitive enough to detect such changes.

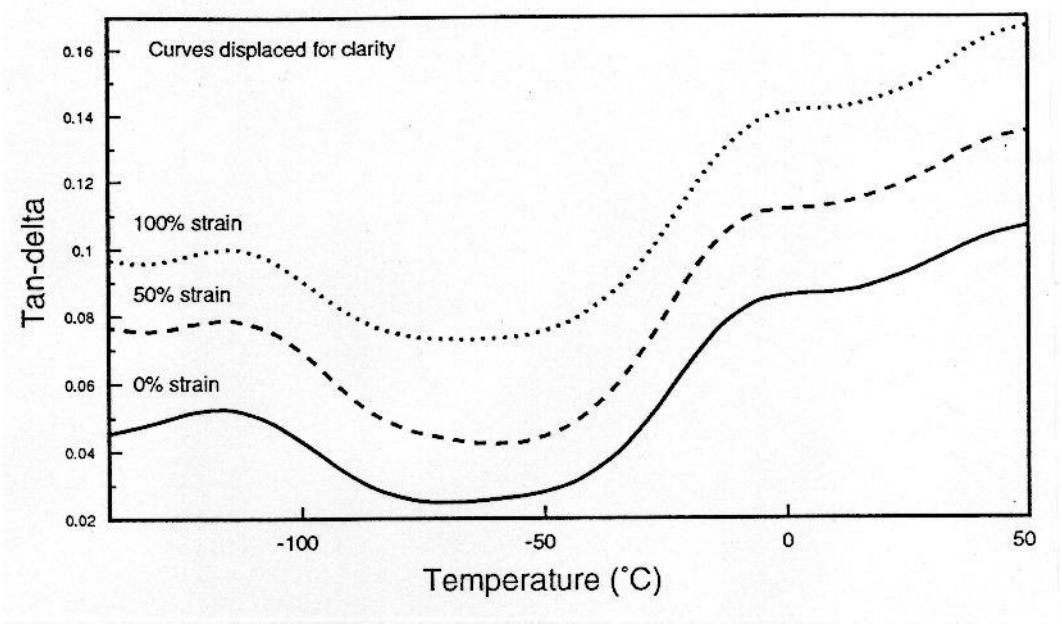

Figure 6.11(a): DMTA data from BPA Q/0.

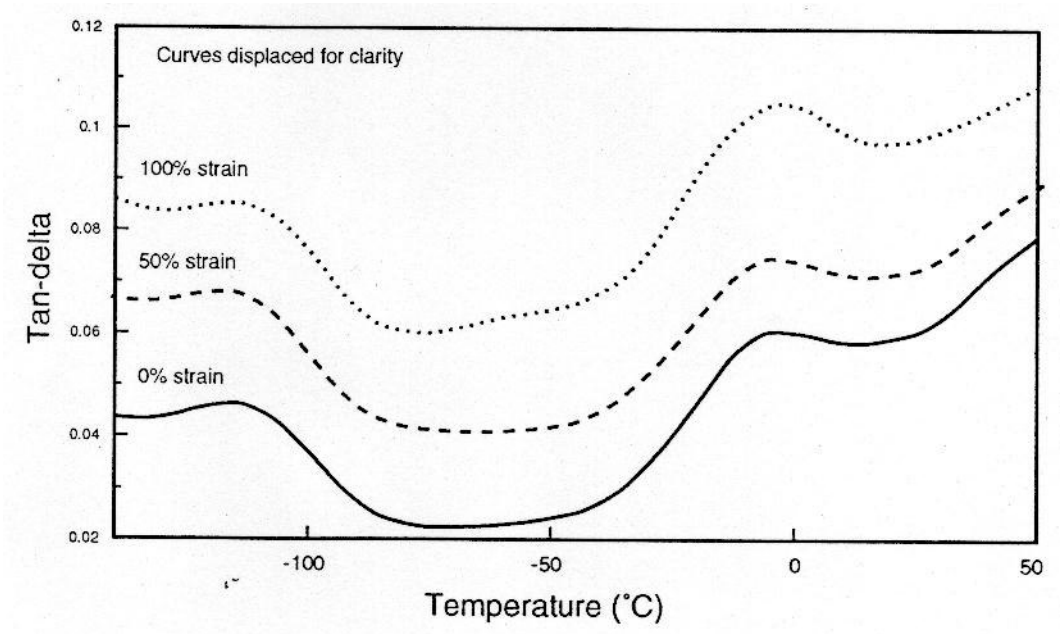

Figure 6.11(b): DMTA data from BPA 124/10 M.

6.4 Discussion

It is clear from these results that mechanical deformation, even in a limited set of polyethylene blends as here, is a very interesting and complex subject. In this investigation we have seen that mechanical properties are affected by the crystalline structure of the materials considered. In any investigation of mechanical deformation relaxation following straining is clearly a major problem, but it can be overcome through careful procedures. In this set of blends several hours were required for relaxation to set in at room temperature, as demonstrated in figure 6.10. This at first may contradict the findings when electrical data was taken, in that electrical results started changing after just thirty minutes of testing. Considerable heating of both sample and immersion oil occurs during electrical testing, this is due to the electrical tests themselves and the surrounding equipment. This could explain why the samples prepared for electrical testing annealed quicker during the tests.

In a practical application deformation of cables would be of no consequence provided the deformation was not too severe. The typical operating temperature of a cable might be around 90°C, at such temperatures any loss in electrical strength due to deformation would be quickly annealed out.

The DMTA work is inconclusive as far as rejecting the possibility of void formation, therefore the cause of loss of electrical strength due to mechanical strain is unclear. A morphological reason for a loss of electrical strength, such as change of spherulitic shape, or changes in lamellar orientation is more favourable in the light of the results from chapter 3, particularly at small strains. Wether voiding is significant at high strains is unclear based on the available data.

The morphologies seen after 100% strain are somewhat similar in all three materials considered, so this might be an explanation of why the electrical strength tends towards the same value for all three systems considered. In this regime morphologies are not unlike those reported in the literature with fragmented lamellar clusters being the final result of deforming the spherulites in the blend. In the BPA 124/10 M system buckling and fracture of individual lamellae is apparent, as well as physical separation of lamellae. The effects of such high strains are quite severe and the irreversibility of the effect (even after heating at 90°C) suggests that this type of structural damage, rather than being a temporary effect, is

permanent in the sense that it can be never removed by annealing. This conclusion is supported by DSC data which showed a permanent change in the LPE phase after straining to 100%.

6.5 Conclusions

The effects of mechanical deformation on polymeric insulators are quite profound even at low strains, the effects can be usefully divided into two regimes;

1) 20 and 50% strain (well below second yield point). Straining a sample results in a definite plastic deformation which remains for some hours after the deforming strain is removed. By annealing the deformation can be reduced to nearly zero, and the stress at constant strain tends to decrease (rather than increase). This together with DSC and TEM data, infers that primarily the crystallites are affected by mechanical deformation, rather than the amorphous regions

Most of the reduction of electrical strength occurs in this regime, spherulites change, mainly in shape and X-ray scattering reveals lamellar orientation. This change in spherulitic shape and/or lamellar orientation may be directly responsible for the loss in electrical strength. Subsequent annealing could restore the electrical strength, after several days at room temperature electrical strength was restored, a process which could be accelerated by heating.

2) 100% strain (Generally around the second yield point). DSC data points at permanent crystalline damage in this regime and this is supported by TEM which shows a distinctive change in morphology whereby spherulites are completely destroyed and crystals are broken up. The electrical strength could not be recovered even by annealing at elevated temperatures.

6.6 References

1) A.S Argon and L.Lin, J. Mat. Sci. 1994, **29**, 294.

2) P B Bowden and R J young, J. Mat. Sci 1974, **9**, 2034.

3) A. Peterlin, J mater sci, 1971, **6**, 490.

4) M.E Vickers and H Fischer, Polymer, **36**, 2667

5) A Keller and I Hay, Polymer 1965, **24**, 43.

6) A Keller and D Pope, J. Polym. Sci. 1975, **13**, 533.

7) K Holland-Moritz, W Stach and I Holland-Moritz, Prog. Colloid. Polym. Sci. 1980 , **67**, 161.

8) J Dupias, P legrand, R Seguela and F Rietsch, Polymer 1988, **29**, 626.

9) N A van Aerle and A W M Braam, Macromol. Chem. 1988, **29**, 626.

10) N A van Aerle and A W M Braam, Colloid Polym. Sci. 1989, **189**, 1568.

11) R Seguela and F Rietsch, J. Mat. Sci. Letts. 1990, **9**, 46.

12) B Crist, Polym. Comm., 1989, **30**, 69.

13) R Seguela and O Darrras, J. Mat. Sci. 1994 , **29**, 5342.

14) J.J Janimak and D.C Bassett to be published.

15) J.J Janimak and D.C Bassett to be published.

16) Z Bashir and A Keller, Colloid Polym. Sci. 1989, **267**, 116.

17) I.L Hosier, D.C Bassett and I.T Moneva, Polymer 1995, **36**, 4197. See publications page 214.

18) S.W Tsui, R.A Duckett, I.M Ward, D.C Bassett, R.H Olley and A.S Vaughan, Polymer 1992, **33**, 4527.

19) A.K Gupta, S.K Rana and B.L Deopura, J. Appl. Polym. Sci. 1992, **46**, 99.

20) G.K Elyashevich, E.A Karpov and V.K Lavrentiev, Intern. J. Polymeric. Mater., 1993, **22**, 191.

21) O Darras and R Seguela, J. Polym. Sci. part B, 1993, **31**, 759.

22) A.D Channel, E.Q Clutton and G Cappaccio, Polymer 1994, **35**, 3893.

23) J Rhee and B Crist, J. Polym. Sci. part B 1994, **32**, 159.

24) C.H Park, T Kaneko, M Hara and M Akazaki, IEEE Trans. Electr. Insul. 1982, **17**, 234.

25) Introduction to Polymers, R.J Young and P.J Lovell, Chapman and Hall, London, 1991, 340.

CHAPTER 7 - TOWARDS A COMMERCIAL CABLE INSULANT

7.1 Introduction

The investigation in chapter 3 showed that adding a small amount of linear polyethylene (LPE) to a commercial low density branched polyethylene (BPE) had many advantages. Under carefully controlled conditions, the resulting morphology can be one of open space filling banded spherulites, which results in a considerable improvement in electrical strength, particularly in blends containing more than 15% LPE. Chapter 4 showed that the molecular architecture of the two polymers choosen to formulate the blends, did not make a difference to the electrical strength, provided that the morphology did not change. The electrical strength of such blends, therefore, depends primarily on thier morphology rather than on molecular factors. Considerable changes in supermolecular structure were needed to influence the breakdown results.

Chapter 5 investigated the validity of melt mixing, and it was shown that the good electrical performance was still achieved in melt mixed blends. Measured electrical strength was found to be sensitive to the testing procedure employed, however for comparative tests, results were still meaningful, provided that the same testing procedure was used throughout. Finally chapter 6 dealt with mechanical deformation; mechanical strains did reduce the electrical strength of the three materials considered, and changed their spherulitic structure. However, provided the applied strain was not too high, recovery was possible given sufficient time. In this chapter some aspects concerned with possible commercialisation of cables based upon polyethylene blends are investigated. The blend of 20% Rigidex 140/60 in 4901 (BPA 115/20 M) is a good example of a system exhibiting improved properties, which might be used for enhanced medium voltage cable insulation. This blend was used to investigate three aspects relating to commercialisation, which are detailed below;

Processing window. So far the investigation of the electrical strength of polymer blends has concentrated on three thermal treatment conditions where markedly different morphologies were obtained. Out of these three, a crystallisation temperature of 115°C was found to give enhanced electrical strength. However, in practice, a range of crystallisation

temperatures, over which enhanced properties are exhibited, is more useful than a single temperature. Although the morphology of similar (7% LPE) blends was studied in some detail in chapter 3, as yet, the dependence of electrical strength upon crystallisation temperature has not been examined in detail.

Minimum crystallisation time. In an industrial process the crystallisation time needs to be reduced to the minimum time possible to gain enhanced properties, so as to increase cable manufacturing output. From an academic point of view, the consequences of incomplete crystallisation, on both electrical properties and morphology is of considerable interest. The dependence of these two parameters on crystallisation time was examined at 115°C, a crystallisation temperature where electrical strength is maximised.

Annealing. Mechanical properties of some blend systems were explored in chapter 6, although annealing was shown to remove the effects of mechanical deformation, no longer term tests were performed. The effects of annealing, in air at high temperatures, on morphology and electrical behaviour is of considerable interest. Some work on aged commercial cables has been reported (1, 2), and the XLPE considered was found to have a significantly lower electrical breakdown strength (1) after prolonged service for many years. Analysis of similarly aged failed cables (2) has shown oxidisation and changes of crystallinity, particularly in the regions near the conductor core.

Obviously, a test where exposure of cables to typical operating temperatures (90-120°C near the conductor) (2) for many years is very useful from an industrial point of view, but this kind of test is not feasible for an academic study. However some work has been reported (3-5) where annealing has been performed on an intermediate time scale, more in line with an academic study. Phillips (3) showed that annealing crosslinked polyethylene (XLPE) at temperatures above 98°C could improve the electrical strength, whereas annealing below 98°C reduced the electrical strength. Ishida et al. (4) reported that annealing XLPE between 80-100°C improved the electrical strength. A report by Blacker et al. (5), investigated the effects of annealing specifically on morphology, no significant morphological changes were reported to occur, provided the anneal temperature was below

the melting point of the LDPE used (~114°C). No detrimental effects on electrical strength were reported as a result of annealing, however, no similar work has been done with polyethylene blends. For this investigation an annealing temperature of 105°C was chosen, a temperature high enough to at least approximate conditions near the conductor core (2), yet low enough so that melting and loss of shape of the thin film samples considered did not occur.

7.2 Results

7.2.1 Differential scanning calorimetry

Crystallisation behaviour Figure 7.1 shows the time required to isothermally crystallise the blend considered (BPA T/20 M) to completion as a function of the crystallisation temperature T, as inferred from DSC exotherms. Times ranged from less than a minute for material nominally crystallised at 100°C, to about 20 minutes for complete crystallisation at 124°C. These results concur with the general crystallisation behaviour discussed in chapter 3, although here the corresponding crystallisation times are reduced due to the use of a melt mixed blend (see chapter 5). Figure 7.2 shows the crystallisation exotherm for isothermal crystallisation at 115°C, it is clear that the bulk of the crystallisation occurs in the first minute under isothermal conditions. A small amount of further crystallisation is apparent from the curve, up until time 5 minutes, after which the material is regarded as completely crystallised. This immediately leads to the question of whether crystallisation really requires 5 minutes, or whether just a minute is sufficient to gain the required electrical strength.

Melting behaviour. Figure 7.3 shows a selection of melting endotherms of the BPA T/20 blend crystallised at various temperatures T. For temperatures below ~116°C, some of the more linear fractions of the BPE material can crystallise isothermally, leading to multiple DSC peaks, above this temperature only two main peaks are seen. The thermal behaviour is therefore strongly dependent on the crystallisation temperature chosen.

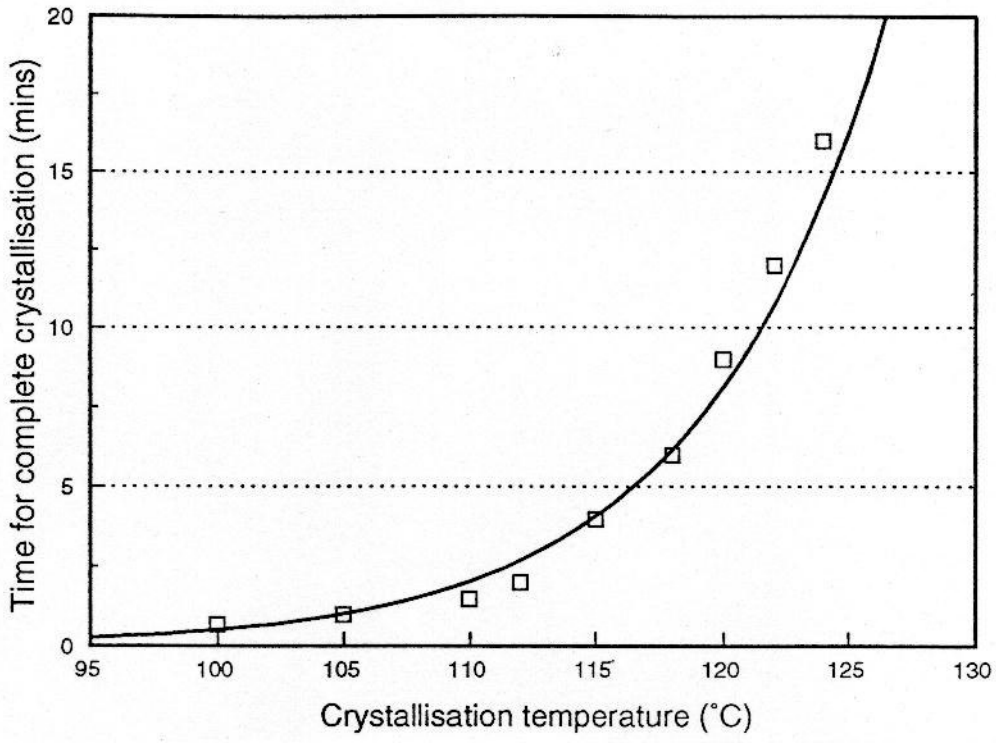

Figure 7.1: Crystallisation times of the blend considered in this investigation.

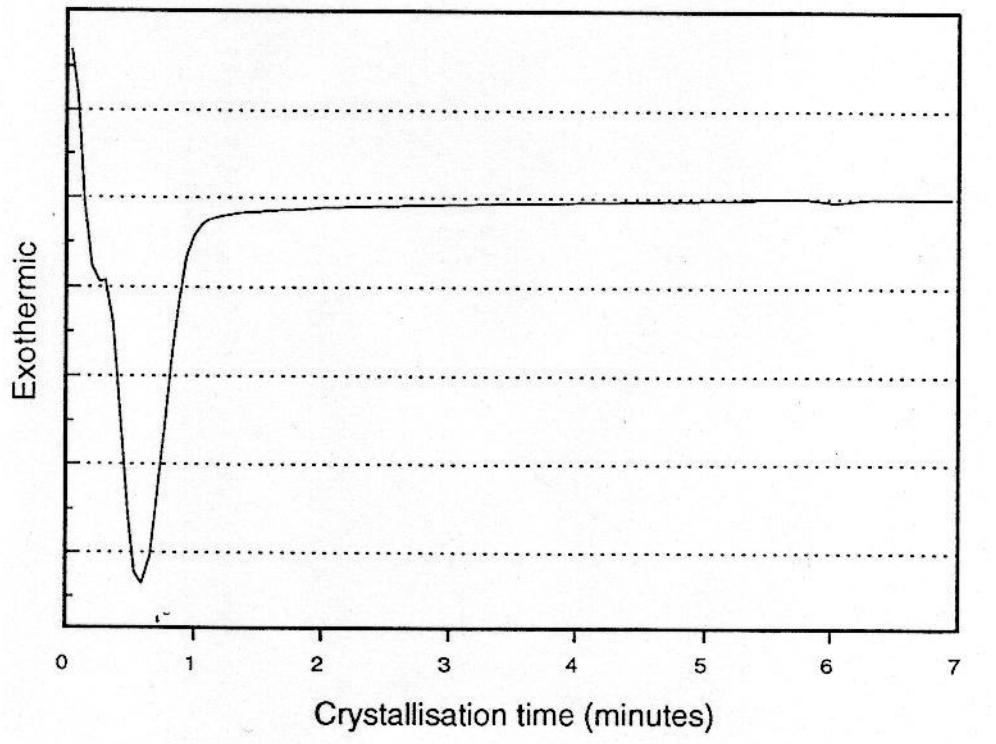

Figure 7.2: Crystallisation exotherm of BPA 115/20 M.

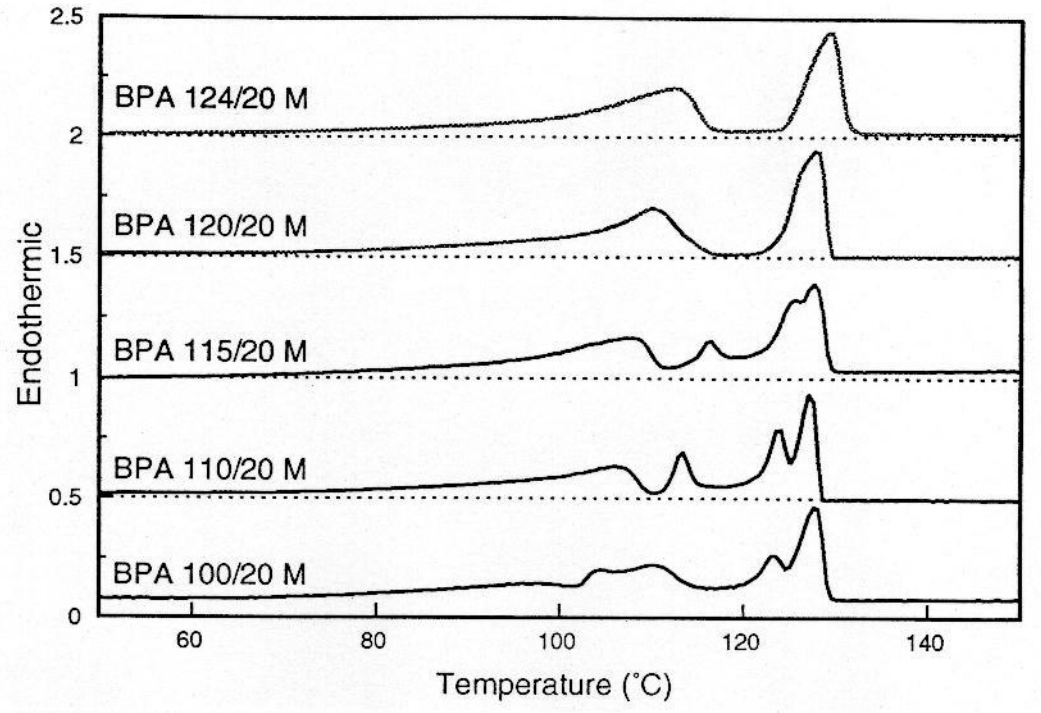

Figure 7.3: Melting behaviour as a function of crystallisation temperature.

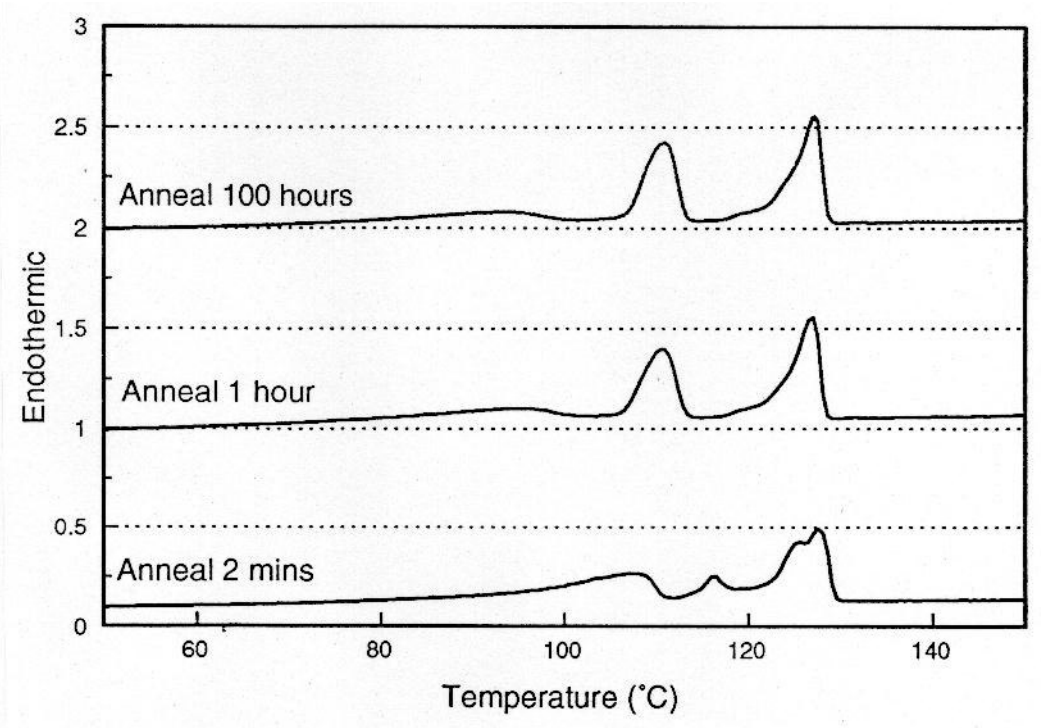

Figure 7.4: Effect of annealing on melting behaviour.

Annealing BPA 115/20 M at 105°C (fig 7.4) changed the DSC melting behaviour. A system with several DSC peaks becomes one with three peaks. Following isothermal crystallisation at 115°C three lamellar populations are established; those rich in LPEcrystallise isothermally to give a lamellar population with a melting point around 128°C, a subsidiary population of more perfect molecules from the BPE, which can crystallise isothermally at 115°C, gives rise to the small intermediate peak, and the rest of the BPE crystallises on quenching. Annealing appears to have had several effects on those crystal populations. The co-crystal population, as well as less perfect LPE crystals, have been allowed to isothermally thicken (6), generating a single peak of more perfect crystals located at ~130°C. At the annealing temperature a substantial fraction of the BPE is molten, therefore further segregation of the BPE has occurred, where more perfect molecules have recrystallised to form a subsidiary population of lamellae with melting point ~110°C, whereas the remaining less perfect BPE molecules crystallise after annealing has been completed. On the basis of this data annealing significantly affects the thermal properties of the blend considered.

7.2.2 Morphological examination

Figure 7.5 shows SEM micrographs of BPA samples crystallised at various temperatures between 100 and 124°C, a range encompassing a wide range of morphological forms (figure 7.5). Despite the multi peak DSC behaviour below ~116°C, the morphology is of space filling banded spherulites right up to around 120°C, where distinctions between spherulites start to become apparent (figure 7.5(f)). Above this temperature, compact lamellar aggregates form (figures 7.5(g) and 7.5(h)) whose size depends on crystallisation temperature. Comparing figures 7.5(a) and 7.5(h) it is clear that the nucleation density of the spherulites is decreasing with temperature, a conclusion not out of line with expectations (7). These morphologies are very similar to the results from a similar 7% blend reported in chapter 3, except here the corresponding spherulites are larger, due to the higher LPE content. It is clear from these results, and those from earlier chapters, that crystallisation temperature primarily influences the *type* of spherulites formed, whereas LPE content primarily influences their *size*.

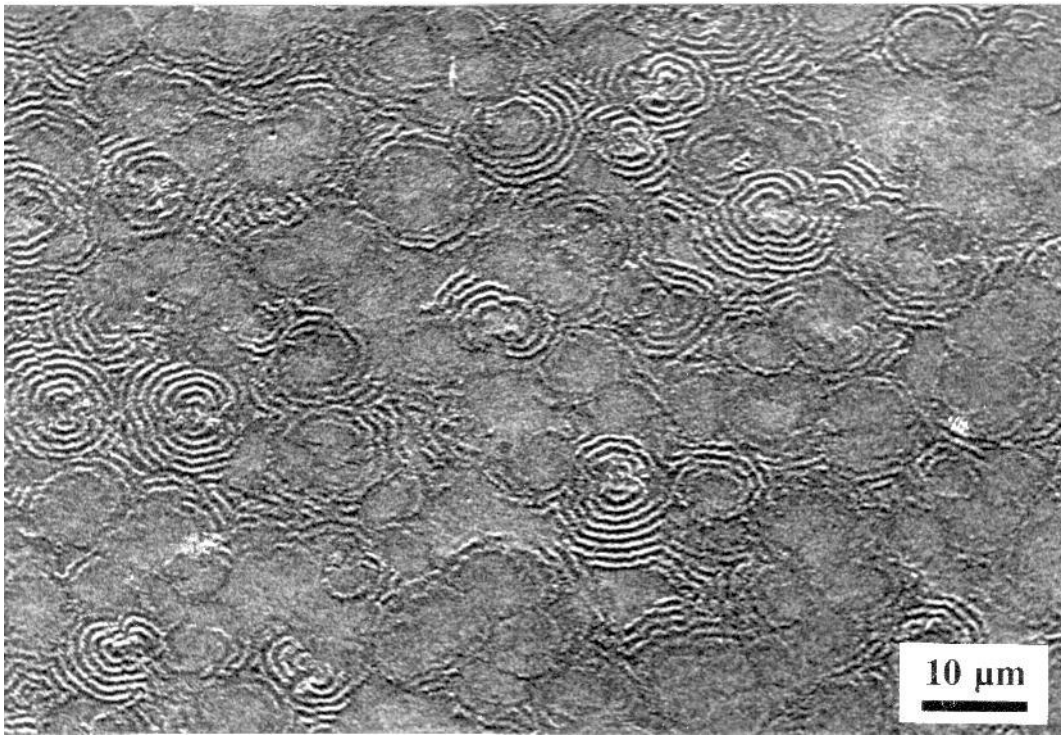

Figure 7.5(a): BPA 100/20 M showing banded morphology with band period ~0.8 µm.

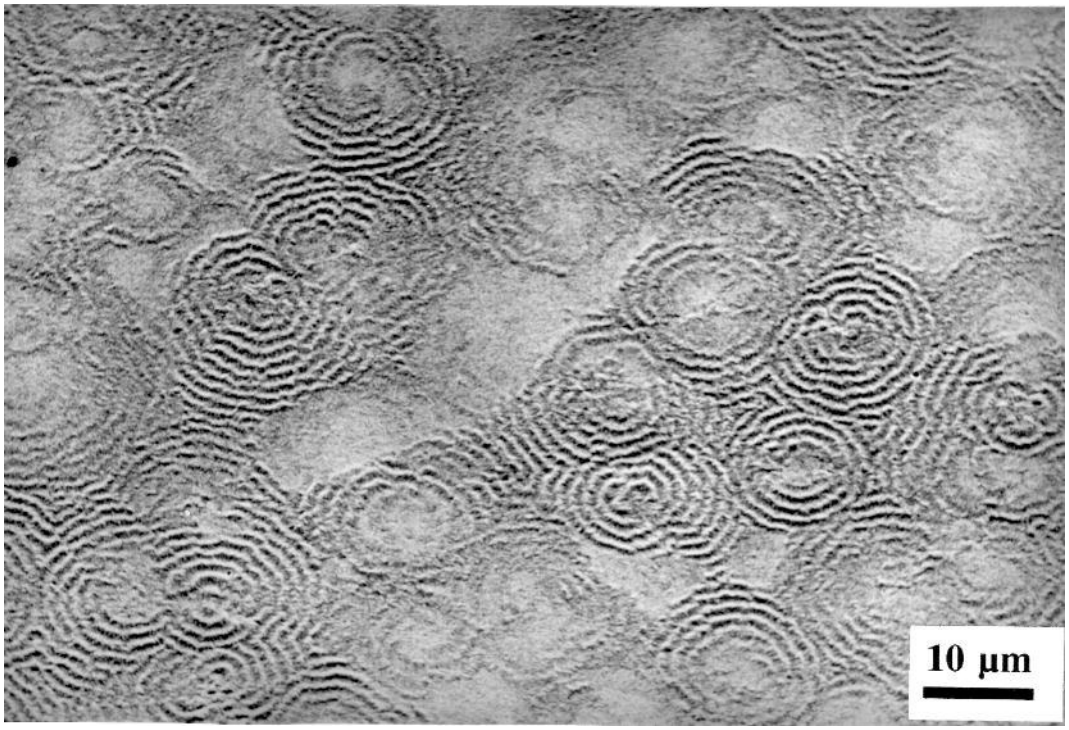

Figure 7.5(b): Crystallisation at 110°C yields spherulites with band spacing ~1 µm.

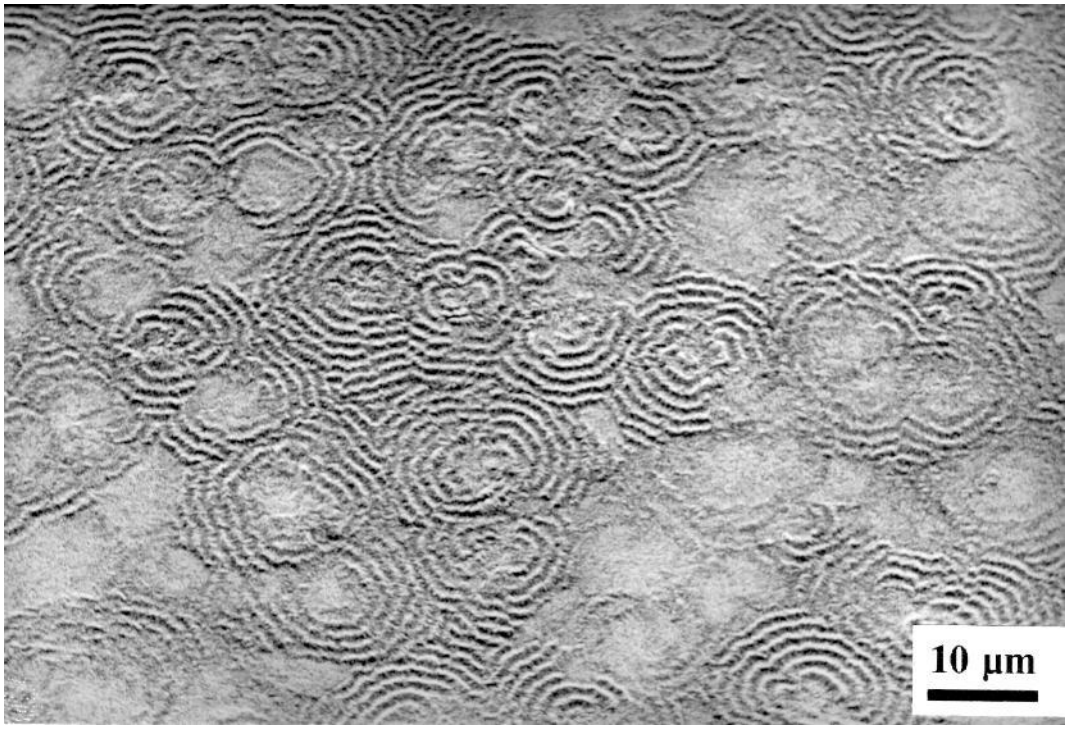

Figure 7.5(c): BPA 112/20 M showing banded spherulites with band spacing ~1.2 µm.

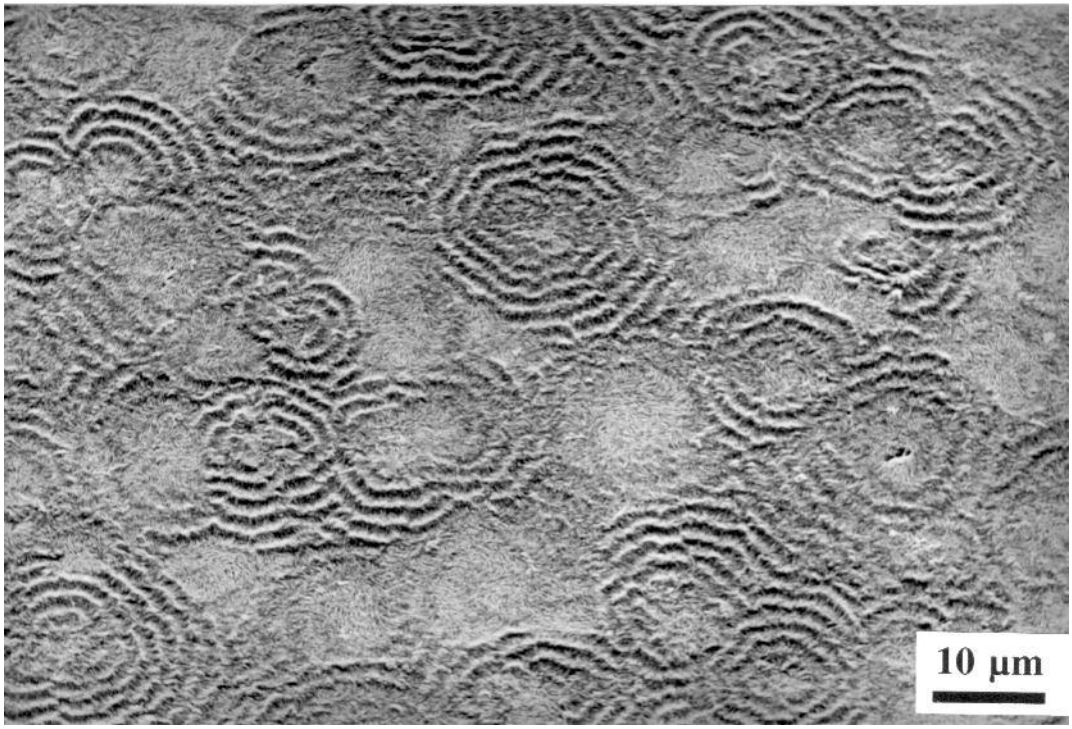

Figure 7.5(d): Similar morphology after crystallisation at 115°C, 1.5 µm band spacing.

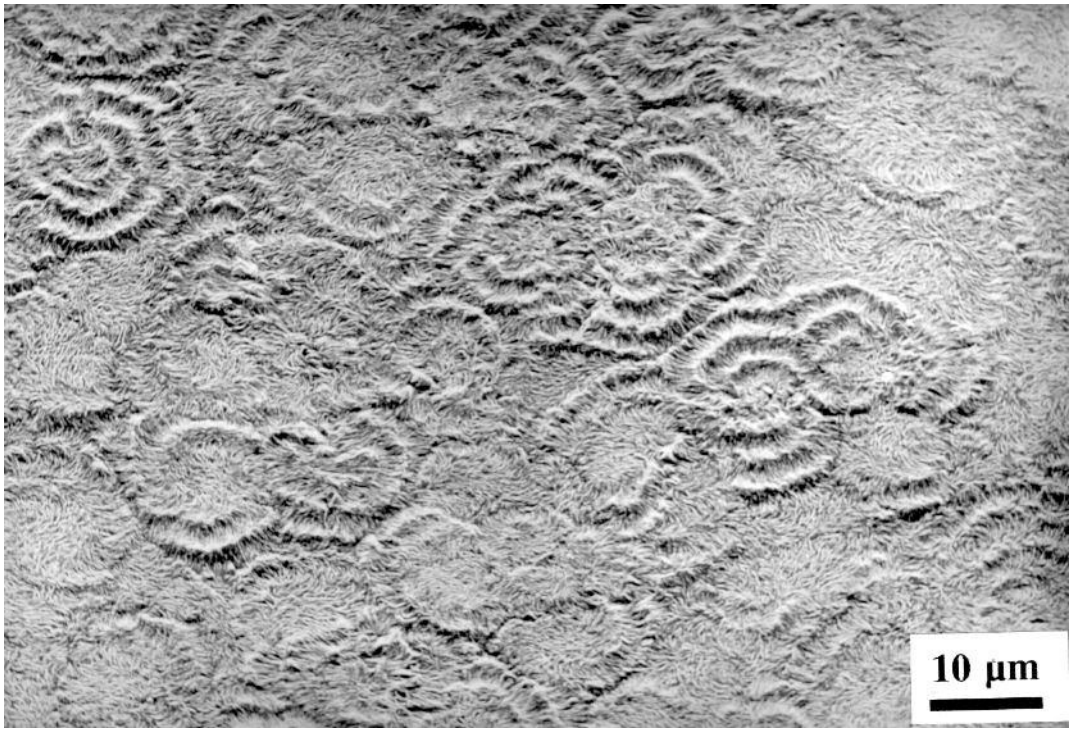

Figure 7.5(e): Banded spherulites with spacing ~2 µm form in BPA 118/20 M.

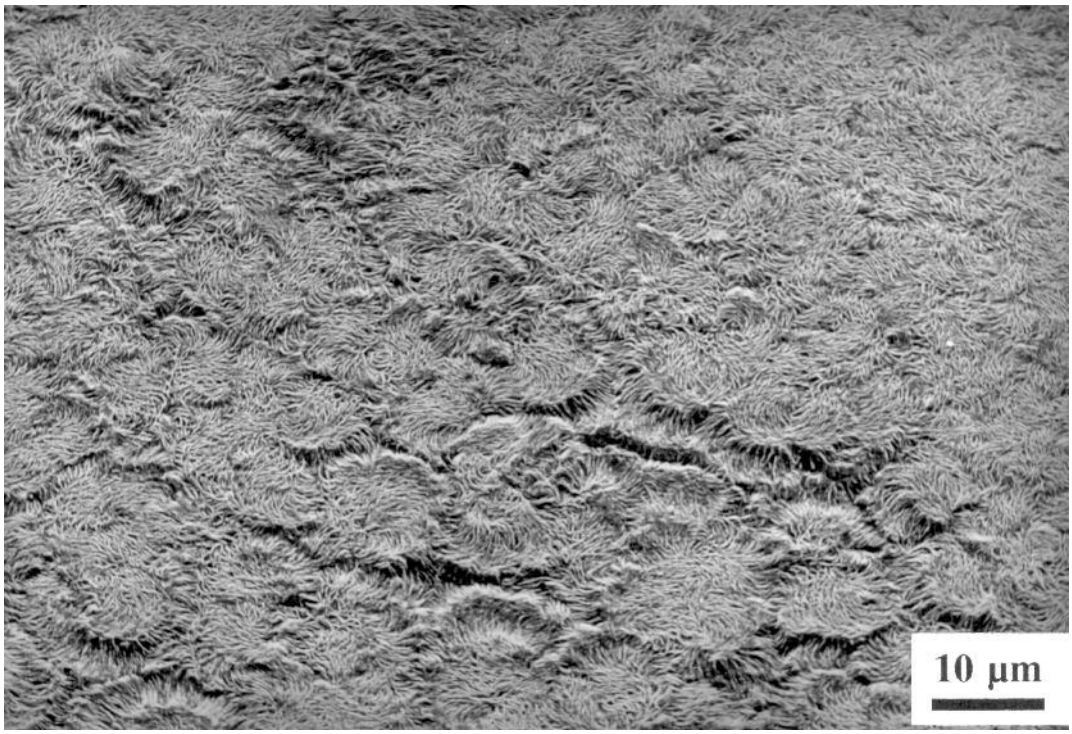

Figure 7.5(f): BPA 120/20 M showing signs of borders between spherulites.

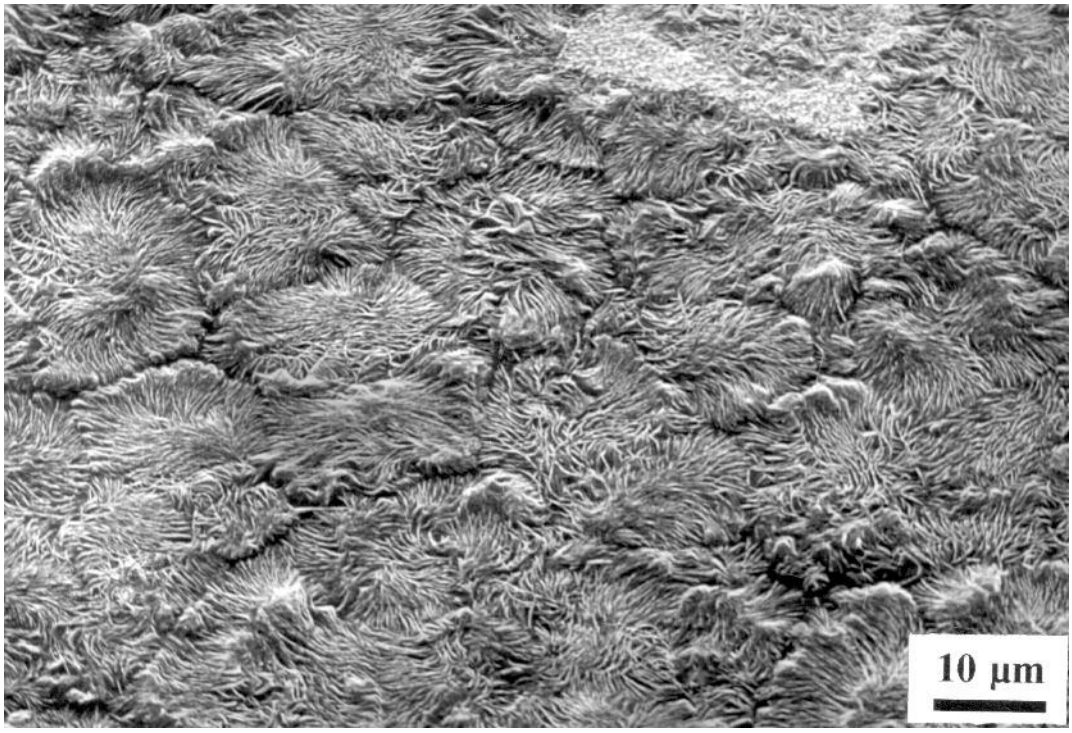

Figure 7.5(g): Lamellar aggregates form in material crystallised at 122°C.

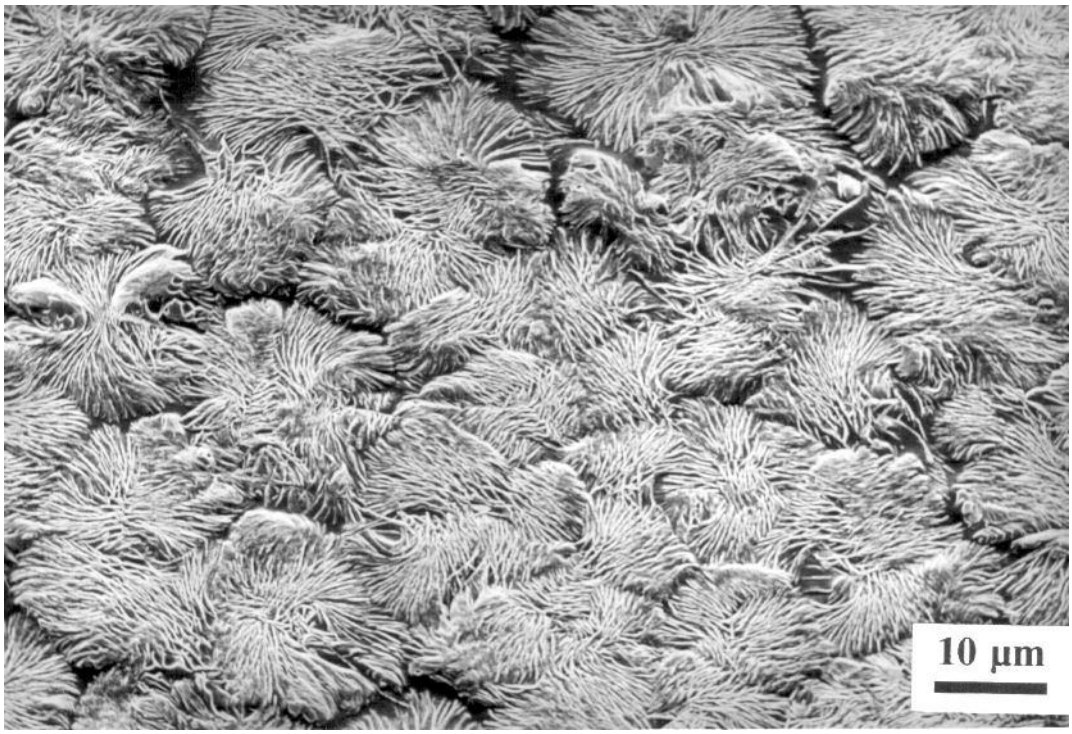

Figure 7.5(h): Compact lamellar aggregates in BPA 124/20 M.

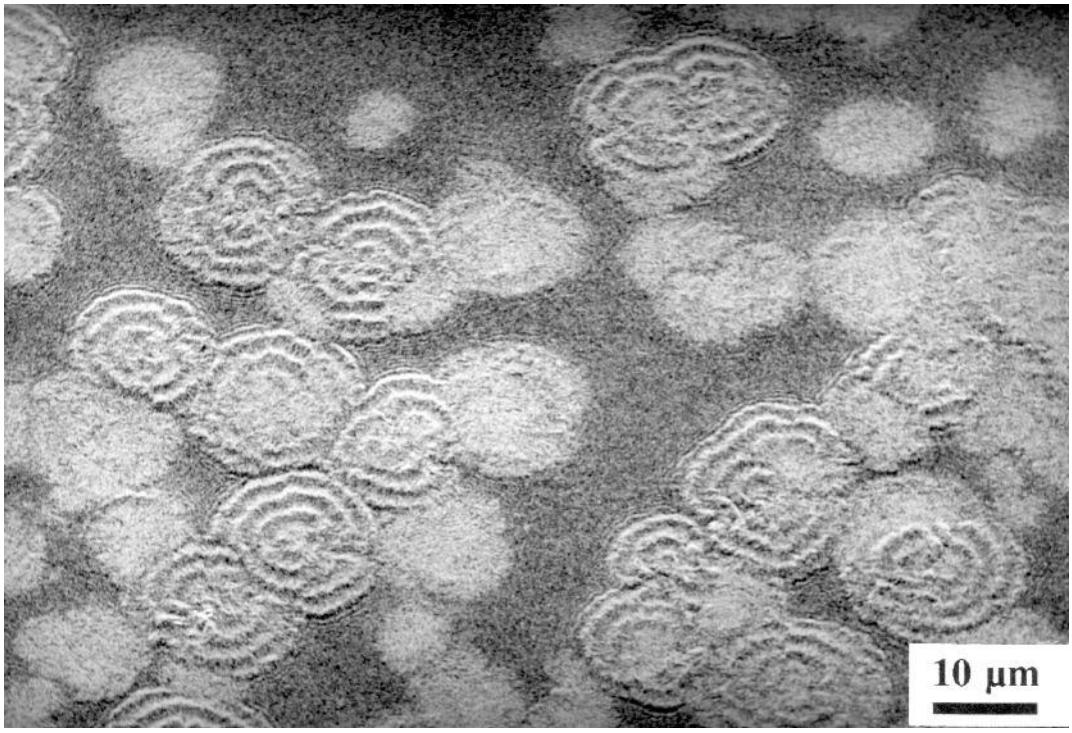

Figure 7.6(a): Incompletely formed banded spherulites in BPA 115/20 M, after just 30 seconds of isothermal crystallisation, surrounded by quench halos.

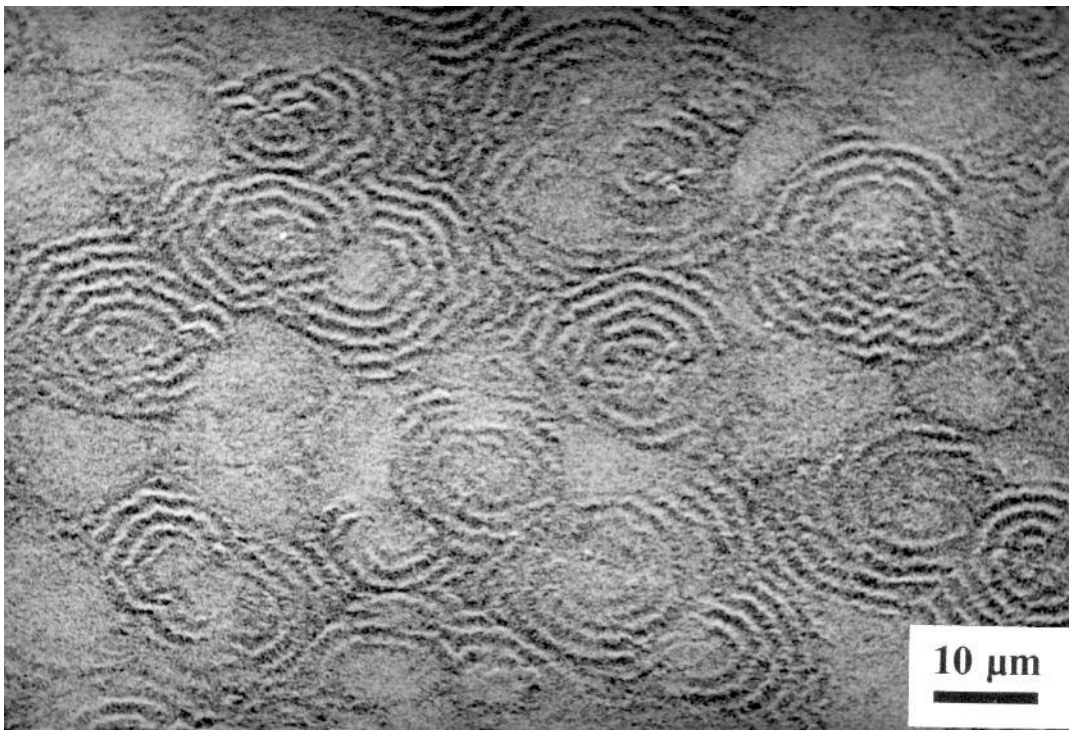

Figure 7.6(b): Crystallisation of BPA 115/20 M for 1 minute yields fully formed spherulites (compare with figure 7.5(d)).

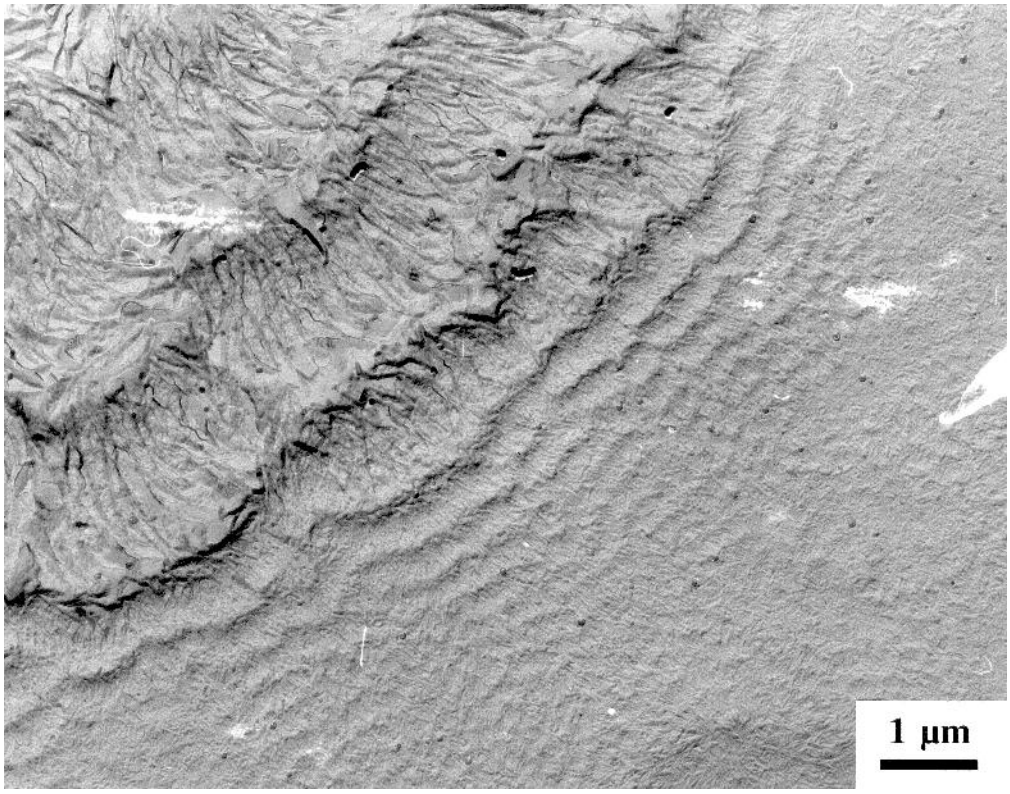

Figure 7.7(a): TEM detail of quench halos in BPA 115/20 crystallised for 30 seconds.

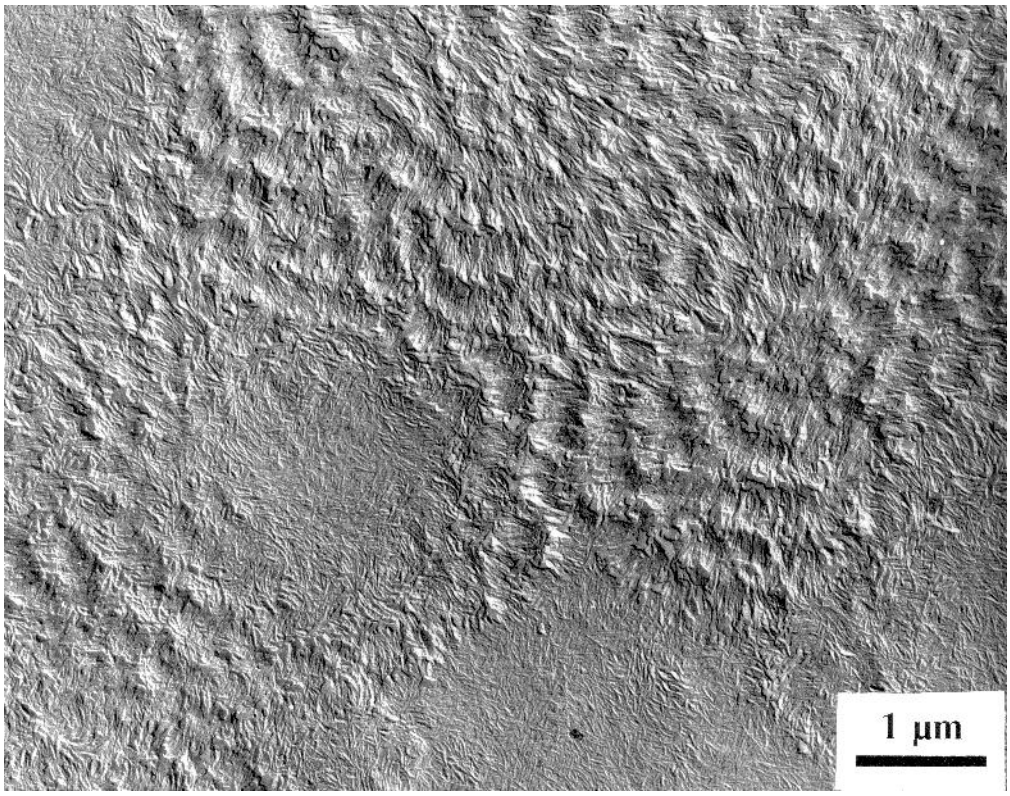

Figure 7.7(b): Similar texture to the quench halos above is shown in BPA Q/20 M.

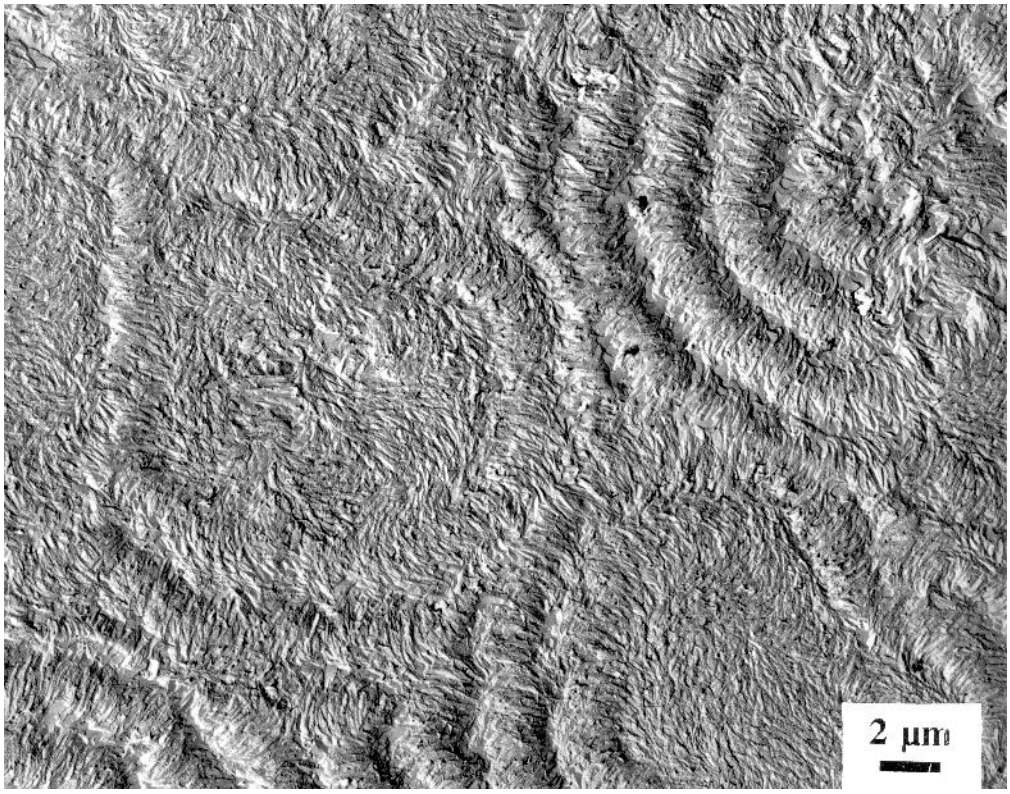

Figure 7.7(c): BPA 115/20 M crystallised for 5 minutes without annealing.

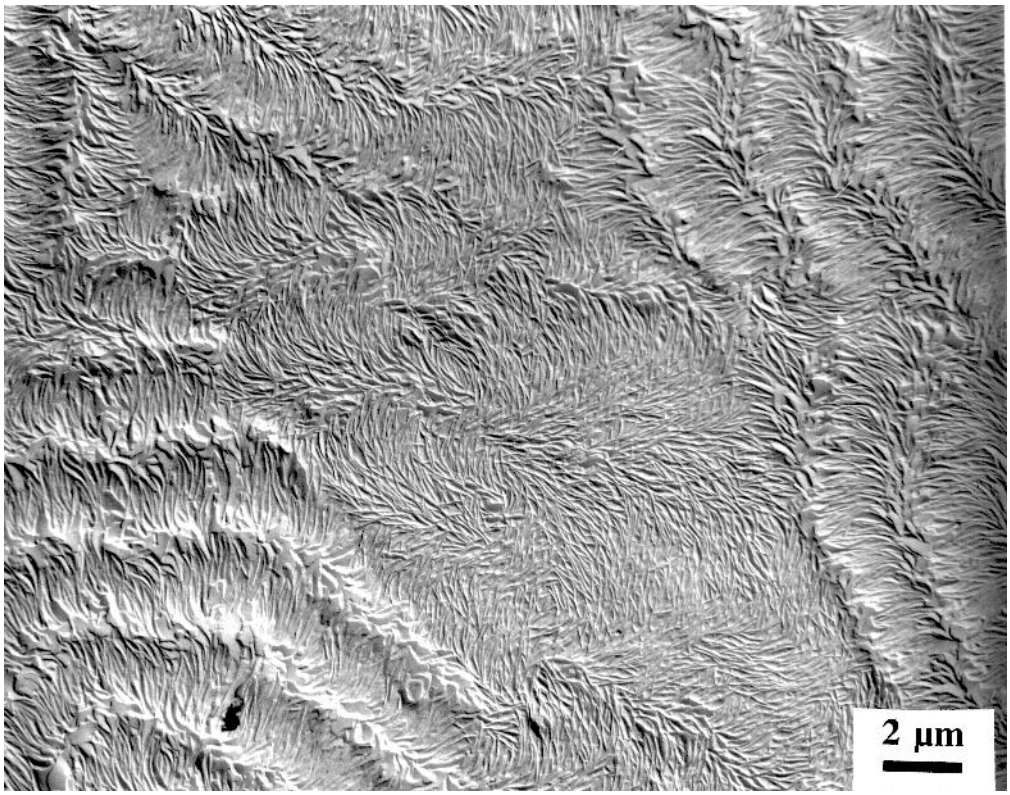

Figure 7.7(d): The same blend, but annealed for 100 hours following crystallisation.

Figure 7.6 shows two SEM micrographs of BPA 115/20 crystallised for 30 seconds and one minute, and then quenched. After 30 seconds banded spherulites have already begun to nucleate, but clear interspherulitic regions are apparent, which appear devoid of larger lamellae (figure 7.6(a). Distinctive banded halos are apparent around the developing spherulites, where their development was arrested by quenching. In figure 7.6(b) no interspherulitic regions are visible, a morphology which compares well with the case when the full 5 minutes crystallisation is allowed (figure 7.5(d)).

The TEM micrographs in figure 7.7 show this more clearly. Figure 7.7(a) shows the morphology after just 30 seconds of crystallisation. The spaces between spherulites are clearly filled with very fine lamellae which have formed on quenching, and the banding around the spherulitic border extends for some distance out from the developing spherulite. The general lamellar texture in between spherulites, is very similar to figure 7.7(b), which shows the same blend, but crystallised for zero time (ie: quenched). The band period of the spherulites (~0.5 μm) shown in figure 7.7(b), concurs with that of the halos in figure 7.7(a). This confirms that the halos around the developing spherulites are formed during quenching from residual LPE rich material, which has not yet isothermally crystallised. The spherulites, where they have formed, contain much larger lamellae, which have crystallised isothermally.

Figure 7.7(c) shows a very different space filling morphology obtained when the full 5 minutes of crystallisation was allowed prior to quenching. In this system all of the space available is clearly populated with larger isothermally crystallised lamellae and no interspherulitic space is apparent. No significant changes in morphology could be found even after 100 hours annealing (figure 7.7(d)) which concurs with (5). Visual examination did not indicate evidence of oxidation (ie: a yellowing of the polymer film), which might have influenced the electrical strength, despite being annealed in air.

7.2.3 Electrical test data

Temperature window. Figure 7.8(a) shows the electrical test data from the BPA blend crystallised at various temperatures to completion. Tests were performed on 70 micron thick samples at 50 volts/sec ramp rate with a 50 Hz A.C sinusoidal voltage, see chapter 2

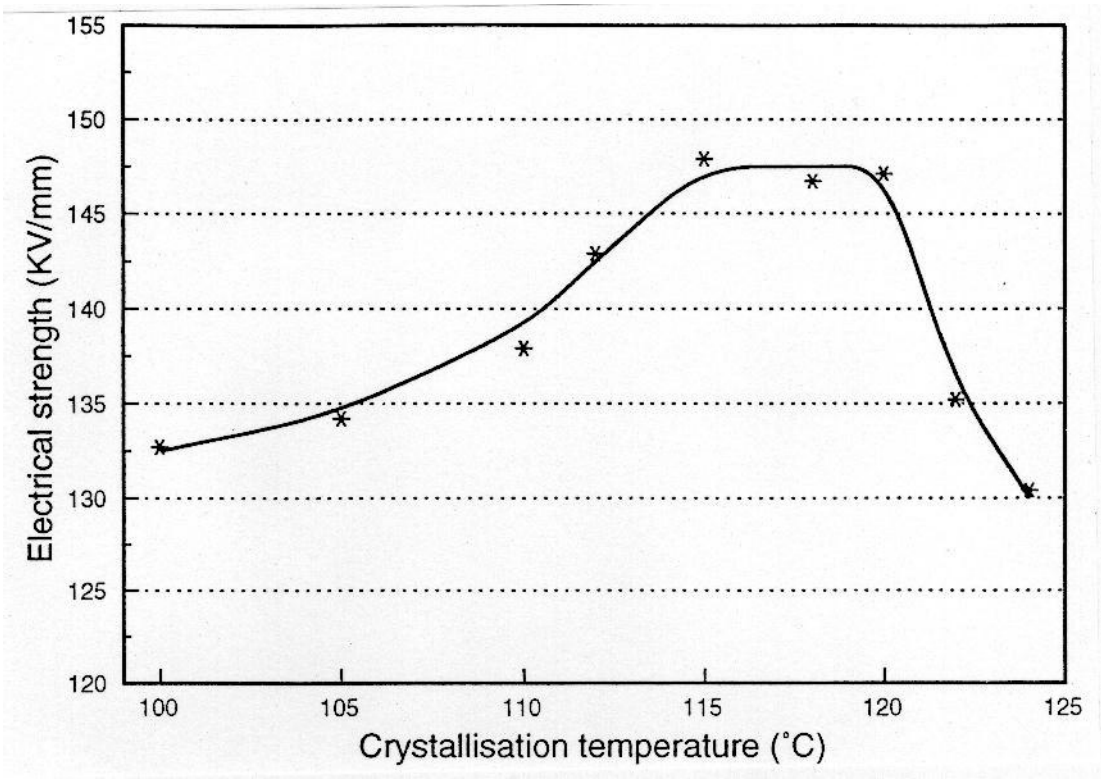

Figure 7.8(a): Dependence of electrical strength on crystallisation temperature.

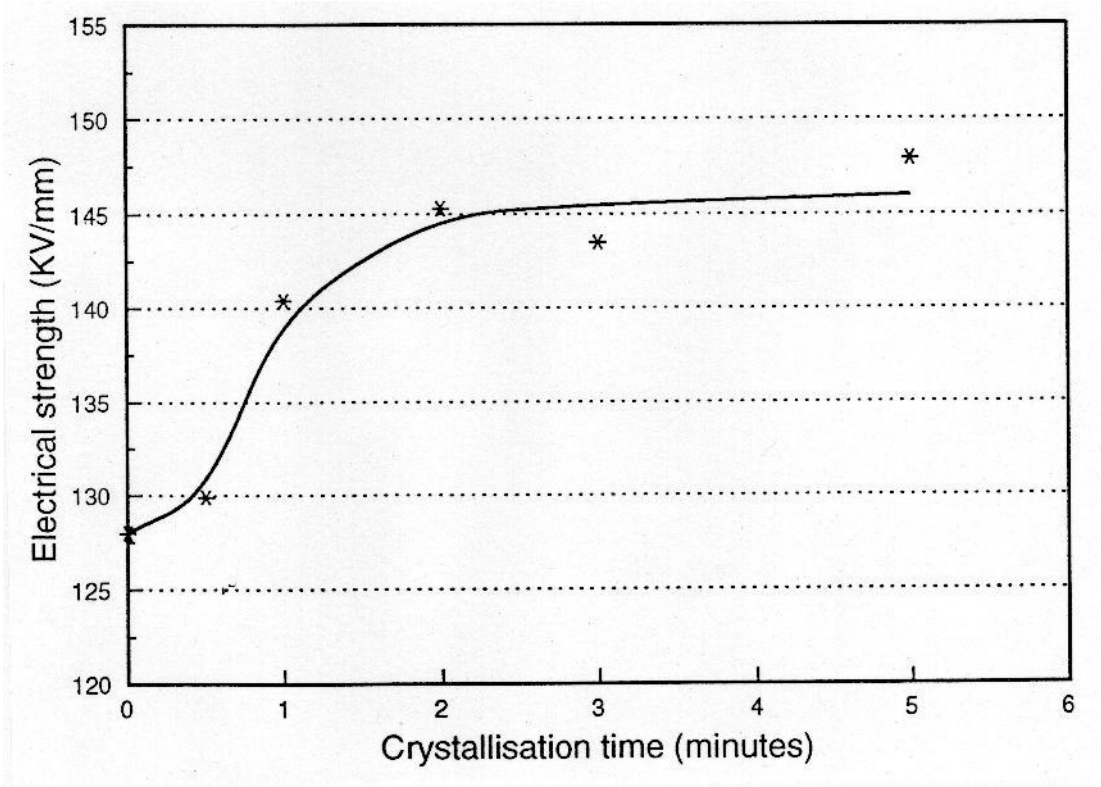

FiFi

gure 7.8(b): Dependence of electrical strength on crystallisation time, BPA 115/20 M.

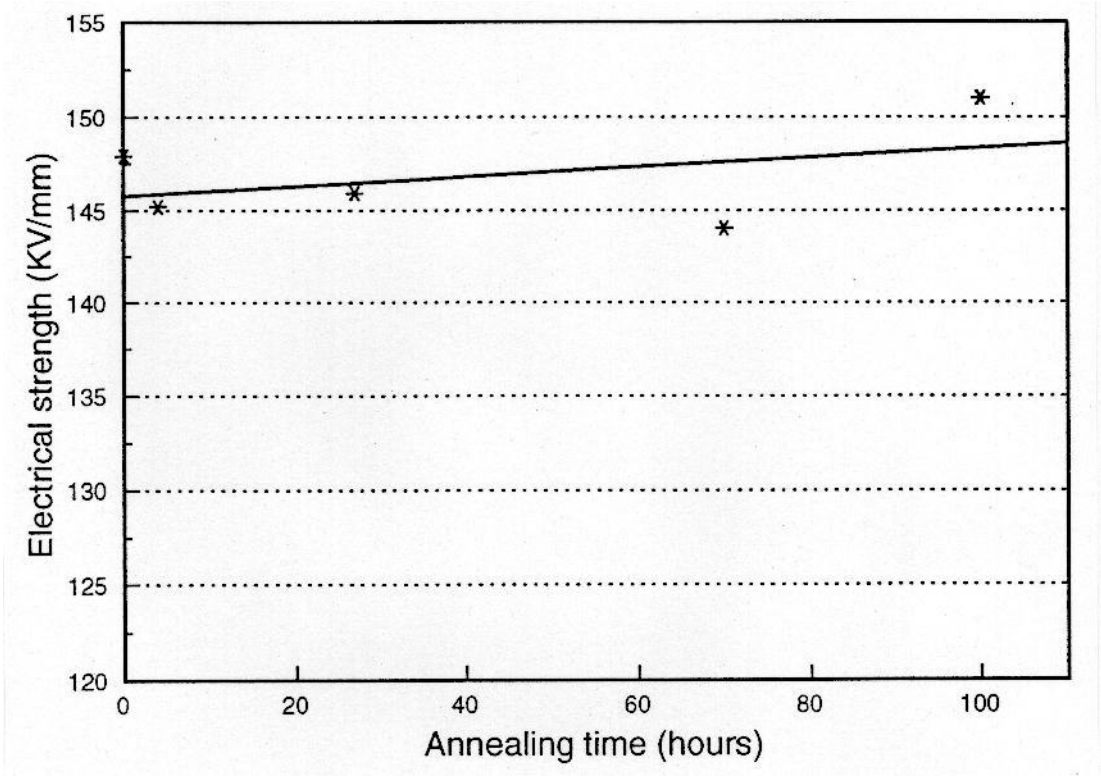

Figure 7.8(c): Dependence of electrical strength on annealing, BPA 115/20 M.

for testing procedure. The morphology of all samples was verified prior to electrical testing. Clearly the maximum electrical strength is obtained when isothermal crystallisation occurs between 112 and 120°C. This temperature range represents a range strength on the crystallisation time of BPA 115/20 M. It would appear that the bulk of the electrical strength improvement is obtained by allowing the sample 1 minute or more to crystallise, this concurs with the TEM data which shows that 1 minute is sufficient to achieve a space filling structure. By allowing the sample less time to crystallise the electrical strength tends towards that for quenched samples (128 KV/mm-see chapter 3), which would be expected. As speculated in chapter 3 a space filling morphology is key at ensuring a high dielectric breakdown strength.

Annealing. Figure 7.8(c) shows the behaviour of electrical strength with annealing time at an annealing temperature of 105°C. Even 100 hours annealing at 105°C did not significantly decrease the electrical strength, which concurs with the TEM data, which showed no significant changes in morphology due to annealing. The data, bearing in mind the 95% confidence intervals of ±5 KV/mm on the electrical strength data, shows a slight increase in electrical strength due to annealing. This is in general agreement with data reported by Ishida et. al. (4) and Phillips (3). However it is clear that annealing in air at extended temperatures for the time scales considered here, is not having a detrimental effect on the electrical strength of the material considered, a result which concurs with Blacker et. al. (5).

7.3 Discussion

Processing window. The BPA 20% blend showed enhanced electrical strength over a wide range of temperature from 112-120°C, this corresponded to a range of morphologies all of which exhibited a space filling texture. At higher temperatures distinctive borders are apparent around spherulites, such borders constitute electrically weak material (8), as a result the electrical strength dropped off abruptly in this regime. In the low temperature region the morphology and electrical strength tended towards those of quenched material. At lower temperatures, particularly below the melting point of the BPE used (~113°C), more and more of the material is being quenched, rather than being isothermally crystallised.

Crystallisation times. Only the first minute of isothermal crystallisation is needed to give the bulk of the required electrical strength, this corresponded to the establishment of a space filling structure. For times of less than this minimum time, spherulites have not had sufficient time to form to completion and the inter-spherulitic regions do not consist of space filling LPE rich lamellae, as a result the electrical strength is much less.

However crystallising for longer than is needed yields no further benefit, and in a commercial application would want to be avoided if maximum production is required. In an academic study, crystallising polymer blends for more than the minimum time required as determined by DSC, as done in previous chapters, does not invalidate the electrical data.

Annealing. We have tried to simulate the worst case conditions near the conductor in a practical cable application, by annealing at 105°C in air for extended periods. Up to 100 hours annealing, no detrimental effects on the morphology or electrical strength of this insulation material were found, these general results concurred with the literature (3-5).

7.4 Conclusions

1) A polyethylene blend containing 20% 140/60 LPE in 4901 BPE was studied because of it's enhanced properties when isothermally crystallised at 115°C. These properties could also be attained by crystallising between 112 and 120°C, a regime where space filling morphologies occurred. This material is therefore suitable for possible industrial manufacture.

2) The crystallisation time required to achieve maximum electrical strength was less than that conventionally assigned for complete crystallisation on the basis of DSC exotherms. At 115°C the crystallisation time required was only 1 minute instead of the previously determined 4 minutes, however crystallising for longer periods is not detrimental to the polymer. This minimum time, on the basis of morphological evidence, corresponded with the formation of a space filling texture.

3) Even after annealing for long periods at 105°C, no evidence for oxidation or significant morphological change was found and the enhanced electrical properties were retained. Annealing was exhibited in DSC traces, however no observable morphological changes were found.

4) These results complement those of previous chapters, and show that manufacture of cables with enhanced properties using binary polyethylene blends, prepared by melt mixing, is feasible.

7.5 References

1) J. P. Crine, S. Pelissou and J. Parpal, IEEE Trans. Electr. Insul. 1991, **26**, 140.

2) A. Vatansever and P.J Phillips, IEEE Trans. Electr. Insul. 1989, **6**, 1121.

3) P.J Phillips, "Morphology of extruded dielectric cable insulation", 1988 Electric Power Institute report EL-5921.

4) M. Ishida and T. Okamoto, Electrical Engineering in Japan, 1993, **113**, 1.

5) R.S Blacker, A.S Vaughan, D.C Bassett, S.M Moody and R.N Hampton, Proc. 1995 IEEE International Conference on Conduction and breakdown in solid dielectrics, 214.

6) Y.S Yadav and P.C Jain, Polym. Comm. 1989, **30**, 229.

7) J.D Hoffman and J.J Weeks, J. Chem. Phys. 1962, **37**, 1723.

8) S.N Kolesov, Polym. Sci. USSR 1980, **21**, 1993.

CHAPTER 8 - A SIMPLE COMPUTER SIMULATION OF DIELECTRIC BREAKDOWN BY ELECTRICAL TREEING

8.1 Introduction

In chapter 3 the difficulties of examining an electrical tree in a thin film sample were discussed, problems were formidable and prevented their direct examination under the testing conditions used in the investigation. After sample failure all traces of treeing were destroyed, so in order to see a tree, a test must be stopped just before failure occurred, however, scatter in the experimental data prevented the accurate determination of this point. Other problems were associated with finding and imaging a tree structure of undefined dimensions in an opaque sample, a structure which could have started anywhere within an area of a few square mm. An alternative solution was to grow trees in thicker samples under constant electrical stress between needle electrodes, which simplified matters. Times to sample failure were extended considerably, and a needle electrode gave a well defined tree starting point which aided location. Even under these conditions laborious sectioning procedures were required before the tree could be imaged successfully.

Despite these complications an examination of such a tree was not altogether in vain. It was demonstrated that the tree pathways *were* influenced by macroscopic spherulitic structures and therefore, as the breakdown data suggested, morphology has an influence on tree propagation and therefore on electrical strength. However trees grown under these test conditions may be unrepresentative of tree structures formed under the same conditions used to obtain the breakdown data.

In chapter 4 the effects of molecular variation were examined in a series of binary polyethylene blends, it was concluded that morphological rather than molecular factors were key at influencing breakdown data. However, on changing the BPE used in the blend to one exhibiting a lower electrical strength, the result was a similar change in the electrical strength of the blend. It was clear from this data, that both morphology, and the nature of the BPE matrix material, played a dominant role in breakdown behaviour.

In chapter 5 it was shown that measured electrical strength was also dependent on the

testing conditions and sample geometries employed. An attempt was made to understand the reasons behind these variations by the use of a modified Weibull function, however the results of this analysis were inconclusive.

Clearly a direct examination of tree structures, formed under the short term ramp testing conditions used in these investigations, would be useful in explaining some of these observations. However such work would be very difficult, without major refinements to the electrical testing procedure, which would then alter the data obtained. An alternative method is to simulate the growth of electrical trees on a computer. Many sophisticated models of electrical treeing have been developed (1-3) in 2 and 3 dimensions, and the success of these models cannot be under rated. Here we present a very simple 2 dimensional simulation of the growth of an electrical tree between parallel plate electrodes, with the intention of performing a preliminary investigation into the effects of test conditions and morphology on simulated dielectric breakdown data.

8.2 The model

8.2.1 Basis of model

The model presented here is based upon the general considerations of the Wiesmann and Zeller (W-Z) model (2), which gives consistent and reliable representation of real tree growth in solid dielectrics. In the W-Z model the tree is modelled as a conducting entity which can propagate as a series of steps of defined length. A lattice is then defined which holds values of the electrical potential at points in the simulated sample. The tree can propagate and lengthen by a stepwise addition of new lattice points into the structure. The probability of growth, to any particular point adjacent to the existing tree structure, is random but weighted according to the local field at that point, with a minimum value of field being required for propagation. Stepwise propagation of the tree then leads to simulated dielectric failure after which the time to failure can be estimated. The simulation presented here is based upon this model but incorporating the following assumptions;

1) The internal resistance of the tree structure is assumed to be negligible compared to the polymer.

2) Effects of space charge will be ignored.
3) A minimum local field E_c for growth is defined in line with the W-Z model, such that below this field no damage generating processes can occur and above this field the tree can propagate.
4) An AC electric field was used in the experiments, however the effects of the AC waveform on the electric field within the dielectric are not modelled explicitly, instead the model considers only the rms AC value in calculating electric fields.
5) Trees propagate by a series of localised partial discharges (4, 5). Electrons within tree channels are accelerated by the local electric field, this energy is then transferred to the polymer, causing vaporisation and extension of the tree channel.
6) The tree is assumed to be well vented such that gas generation is of no consequence to the partial discharge process.
7) One damage generating discharge occurs per half cycle of the applied AC voltage (ie: when the applied electric field is at it's maximum value).
8) The initiation phase is not explicitly modelled.

8.2.2 Definition of lattice

The simulation is based on a square lattice with spacing A between adjacent points. In order for the sample thickness to be changed in the simulation, the height of the lattice is scaled according to the required sample thickness in terms of A. Deciding on a width for the lattice was more difficult and was a matter for experimentation. If the width is not large compared to the size of the tree, errors will occur in calculating the electrical fields in the lattice, particularly when tree segments approach the edges. The lattice width was chosen so that trees stay well away from these edges.

8.2.3 Calculation of electrical potentials

Since the electrical tree is conducting, an additional length of tree will change the electrical potentials in its neighbourhood, therefore each time the tree grows the potentials in the lattice need to be recalculated. The potential is calculated within the lattice by using

Laplace's equation, the boundary conditions being set by the developing tree and the geometry. The bottom electrode and the tree are held at zero potential, whilst the top electrode has potential Rt, where R is the voltage ramp rate and t is the time. In the absence of space charges, the discrete form of Laplace's equation (equation 1) is used, as employed in the W-Z model, to recalculate the potentials using an iterative procedure.

$$V(x, y) = 0.25 * (V(x + 1, y) + V(x - 1, y) + V(x, y + 1) + v(x, y - 1))$$

During successive iterations across the whole dielectric, the potentials converge to stable values and a check on this convergence is therefore required. Sufficient iterations are performed, such that values of potential from successive iterations at any given point, do not change more than a certain amount, this amount is defined as a percentage. The lower this percentage the more accurate the determination of the internal electric field, however, more iterations then need to be performed which uses up more computer time.

8.2.4 Selection of new tree growth points

Before a new tree segment is added to the lattice all possible growth sites are found. Here, as in the W-Z model, this is all lattice points adjacent to the existing tree structure which exceed the minimum field E_c, allowing diagonal, horizontal and vertical growth. After a list of these points has been made, a new point for growth (x1, y1) is picked randomly but has a probability of being picked, P, proportional to the field at that point (2). Since the tree has negligible resistance;

$$p(x1, y1) = \frac{V(x1, y1)}{\sum_{i=1}^{n} V(x1_i, y1_i)}$$

8.2.5 Tree initiation

Tree initiation time stems from the proposal that a minimum local electric field is needed

at the point of initiation to cause damage generating processes in the material (ie: chain scission, thermal heating etc). If we consider the simple case of a minimum field for growth E_c then this field must be exceeded initially for growth to occur. In this case the mathematics is very simple;

$$t_i = \frac{E_c a}{R V(x1, y1)}$$

The initiation process here is assumed to start at a small void at the surface, which has a depth of 1 micron. This depth was determined by examining actual samples which had surface roughnesses of around 1 micron, this was thought to be due to the aluminium foils employed during film making. Tree initiation could also occur at dust particles, defects in the electrodes etc. but the exact initiation source does not affect the mathematics above.

8.2.6 Estimation of tree growth time

Although the following simplistic analysis is expressed in terms of an electrical tree, the same general argument will apply to any damage formation process which propagates through the material.

Consider the tree segment in figure 8.1. Each AC half cycle the local field may exceed the critical field E_c and some of the gas in the column will be ionised. Electrons are the most mobile carriers and are free to be accelerated by the local field E_l. Although the process of multiple ionisation is complex (10), for this simple simulation we will consider that each molecule of gas contributes 1 electron. Furthermore, we consider the ions as immobile and essentially fixed in position, the effects of localised space charges due to these ions will also be ignored. Defining the mean free path between collisions as ß, and considering N_v molecules per unit volume, each electron gains an average energy of

$$eE_l \beta$$

The total number of carriers in the column is simply defined by the geometry as

$$N_v \pi w_o^2 l_o$$

Then the average total energy E is given by

$$E = e\beta E_l N_v \pi w_o^2 l_o$$

If H kJ/kg of energy are required to vaporise a length of polymer δl, of density σ then ignoring other thermal losses;

$$E = H\sigma\pi w_o^2 \delta l$$

Equating the previous two lines and rearranging gives

$$\delta l = \frac{e E_l \beta N_v l_o}{H\sigma} = K_g E_l l_o$$

with K_g being the growth constant for the process. E_l is defined according to figure 8.1 and assuming δl is less than the total gap l to be bridged, then;

$$E_l = \frac{V(x1, y1)}{l(x, y) + l - l_o}$$

with l being the relevant lattice dimension (A for horizontal or vertical segments or $2^{1/2}$A for a diagonal segment).

The final equation above, relates the amount of material removed δl, with the local field at the tree tip selected for growth. For a tree segment to be completed in the simulation, length l of tree must form, and more importantly the time to do this must be estimated. Assuming 1 discharge per half cycle of AC at frequency f, a time of 1/2f is required to add a length of tree δl. This small length is then added to the growing tip and eventually sufficient half cycles will elapse so that the link is completed. Finally the total number of half cycles gives an estimation of the time to complete the link.

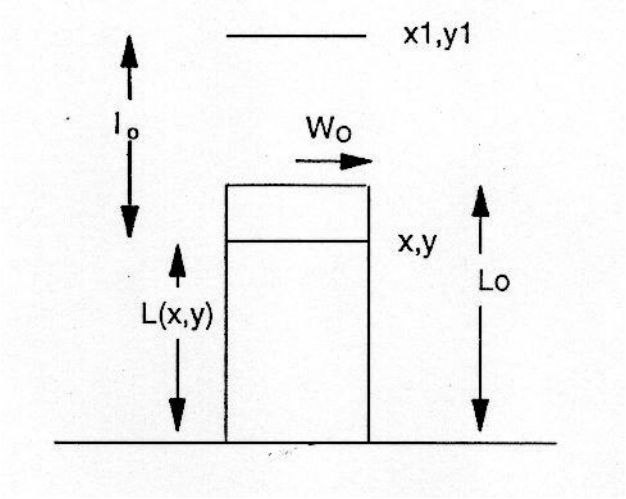

Figure 8.1: Definition of geometry at a tree growth tip, the width of the tree has been exaggerated for clarity.

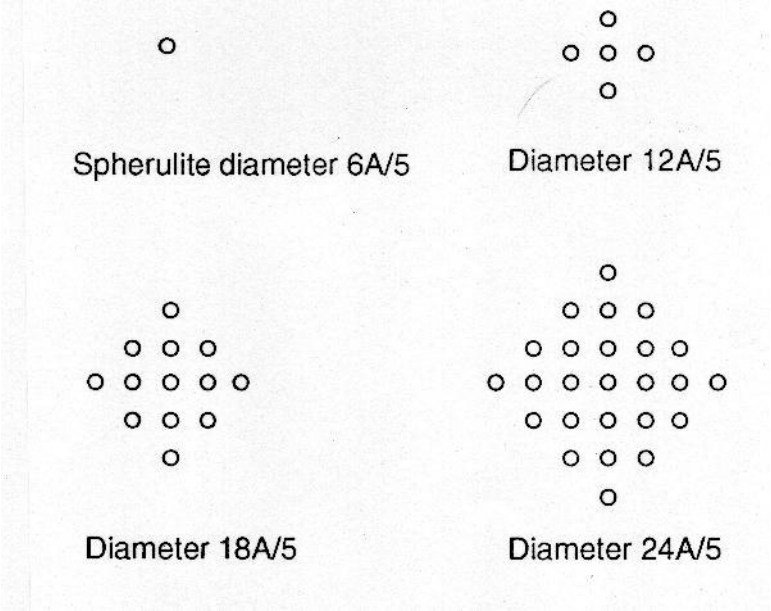

Figure 8.2: The definition of spherulites on a square grid is as patterns on the lattice approximating circles.

The equation above is only valid in estimating a time for length l of tree to form provided $l>\delta l$. Assuming a frequency of 50 Hz, each tree step must take longer than 0.01seconds to complete. As shown later, this criterion is met for all of the simulated trees. Also the effect of the growing tree on the potential at the point (x1, y1) is ignored until the complete link is formed.

8.2.7 Addition of spherulites

The concept of adding a spherulite is simple in essence, we just define lattice points and ensure trees avoid growing in these areas. Such ideas are consistent with the general patterns of tree growth discussed in chapter 3, however, being this simplistic in the model causes problems, particularly where the morphology is space filling, where a tree could not grow. We know from experiment that trees do grow in such systems, so they must be allowed to penetrate spherulites in the simulation. Two growth constants are therefore required appropriate to the matrix and to spherulites. This idea is consistent with observations that the electrical strength in such regions is higher than the surrounding matrix (6).

A number of spherulites are defined as approximations to a circle on the lattice (fig. 8.2). This has drawbacks with large lattice spacing A, in particular, only set sizes of spherulites can be defined. This may, or may not, be a problem, depending on A, obviously a smaller value of A results in more choice in available spherulitic sizes, but with an increase in the time it takes to run the simulation.

8.2.8 Calculation of constants

For a list of the constants used in the simulation and their sources the reader is referred to appendix 1. The minimum field for initiation and growth was estimated to be 105 KV/mm on the basis of 7 eV electrons being required to cause chain scission in the material, which is a value not inconsistent with the literature (7,8). To calculate this minimum field the mean free path of electrons in air (ie: in the tree channels) is assumed to be 6.63×10^{-8}m (9).

The growth constants for spherulites and the matrix were estimated to be 3.22×10^{-5} and 3.84×10^{-5} μm/V using the parameters listed in the appendix.

8.3 The program

The program was written in Microsoft Quick Basic as this programming language has the advantage of easily defined variables, arrays, useful graphics routines and the ability to have the code compiled to decrease execution time. The program was compiled under Borland Turbo Basic, this had the advantage of co-processor support and the ability to generate very fast optimised machine codes. The compiled code was run on an Research Machines PC-466 personal computer.

The physics of the simulation has already been discussed above so we will not dwell on it here, but instead give a quick summary of the main blocks of the coding without too much detail. Some form of documentation is essential so that future users can understand, and more importantly, improve the simulation. The program is quite long so is contained in appendix 2.

1) Initialise. This section sets the screen mode to output graphics and text in colour and clears the memory of unwanted data since the program requires a great deal of memory.

2) Sort out constants. Here the constants of the model are defined. Three constants for initiation and growth are employed. E_c is the minimum field for growth, K_{gm} is the tree growth constant in the matrix and K_{gs} is the growth constant for spherulitic regions. The two other constants are sr the roughness of the sample, and A the lattice spacing.

3) Display menu. All user defined parameters are entered here, sample thickness, ramp rate and test frequency. A choice of available spherulitic sizes is offered, as well as various routines to cope with possible mistakes in inputting the data.

4) Sort out geometry. The lattice of potentials is defined as an array in memory of dimensions nx by ny, nx is set by the lattice spacing A and by the sample thickness, and ny is set high enough so that the tree does not go near the side boundaries. Radius and rad are used in setting up the spherulites, and dt is the time between each partial discharge. The number of spherulites is calculated according to the lattice size and the input data (number of spherulites per unit area).

5) Define storage arrays. A number of parameters need to be stored. The two dimensional array tree(x, y) holds a numeric value as follows; 0=dielectric 1=spherulite, 9=tree or electrode. This tells the program where everything is. V(x, y) holds the potentials as solved by Laplace's equation. The remaining 1 dimensional arrays are used to store temporarily the various possible growth sites, allowing one to be selected as the tree grows.

6) Set up spherulites. First the tree(x,y) array is set to zero, this removes extraneous values which may be initially present in these locations. Next a site (x, y), within the sample, is chosen where a spherulite will be placed. After checking that the spherulite is not placed upon another (allowing impingement but not multiple `nucleation' on the same site), the spherulite is defined in the array, and is then drawn on the screen having the appropriate radius. This continues until all the spherulites are drawn. Finally, scraps of spherulites outside the borders are deleted which makes the screen look more tidy.

7) Draw the sample borders. Two electrodes are drawn on the screen and the parameters are listed. In this model, thicknesses up to 140 microns are drawn on the screen so samples that are thicker appear thicker.

8) Set up initial lattice. In the absence of a tree, the initial potential lattice is defined using the boundary conditions of the electrodes.

9) Initiate the tree. The initiation time and voltage are calculated.

10) Initial growth routine. A length of tree (length A) is formed starting at the initiation site and is grown by incrementing the time and voltage by appropriate amounts. The appropriate growth constant is selected depending on whether the tree is in spherulitic material or not. The arrays and potentials are then updated and the segment drawn on the screen.

11) Calculate new field potentials. The potentials in the lattice are recalculated including the boundary conditions and the effects of any new tree growth. Iterations continue until changes become small (here a difference in potentials between successive iterations of at most 0.1%).

12) Find new growth sites. The computer then looks at lattice points, adjacent to those which are already part of the tree, and checks whether the local field is above the required minimum value E_c. If this condition is met, the site is stored in a temporary array, so that later one of these sites can be selected for growth. n is a dummy variable which

incrementally increases as new sites are found.

13) Sum all growth sites. All the local fields over all the possible growth sites are summed to give normalisation in the next routine.

14) Choose a growth site. Out of all the possible growth sites available, one site is randomly chosen for growth on the basis of it's local field. The time taken to grow that length of channel is estimated and added to the growth time. Finally the arrays are updated to take account of the new tree segment, which is then drawn on the screen.

15) Check for breakdown event. The top of the lattice is checked to see if a tree segment has touched the top electrode, if it has, the dielectric strength of the sample is calculated, the initiation and growth times are displayed, and the program ends. If no breakdown occurs steps 11 - 15 are repeated.

8.4 RESULTS

8.4.1 Effect of model parameters on simulation data

Before any meaningful results can be obtained from the simulation, checks must be carried out that the data obtained is not grossly influenced by excessively high lattice spacings, or insufficient iteration accuracy. For this set of runs, 4901 BPE was simulated, by adding 12μm diameter spherulites with a number density of 3/1000μm^2. A set of 7 typical test conditions were chosen for this investigation. D is the sample thickness in microns, R is the ramp rate in V/s and f is the frequency in Hz.

Effect of lattice spacing A. This is perhaps the most important variable in terms of accuracy of the simulation, a low value for A is favoured for accuracy, but in practise a compromise must be made between speed of program execution and accuracy. Values of 3, 5, 8 and 10 were chosen for A, and an average was taken of 3-4 runs of the program, with an iteration parameter of 0.1%.

The resulting simulation data is summarised in table 1. The top line in each box contains the initiation and growth time, and the figure in bold is the simulated electrical strength. For values of A less than 8, all values are stable with further decrease in lattice spacing, the main problem at small A being exhibited in thin samples. Figure 8.3(a) shows a tree grown with

	D=30 R=50 f=50	D=75 R=50 f=50	D=140 R=50 f=50	D=75 R=20 f=50	D=75 R=70 f=50	D=75 R=50 f=40	D=75 R=50 f=80
A=3	73,4.6 **130**	166,6.8 **115**	303,12.4 **113**	419,7.0 **113**	122,6.6 **120**	168,9.5 **118**	167,4.6 **114**
A=5	73,4.2 **130**	168,6.5 **116**	304,11.2 **113**	420,5.9 **113**	121,6.5 **119**	168,8.4 **118**	168,3.6 **114**
A=8	84,4.5 **147**	168,5.4 **116**	319,9.8 **117**	420,6.2 **114**	120,8.1 **119**	168,7.7 **117**	168,4.4 **115**
A=10	84,5.3 **150**	189,7.6 **131**	315,10.4 **117**	472,6.4 **128**	135,6.0 **132**	189,7.0 **131**	189,4.2 **129**

Table 1: The effects of lattice spacing A on simulated breakdown data.

Allowable error	d=30 r=50 f=50	d=75 r=50 f=50	d=140 r=50 f=50	d=75 r=20 f=50	d=75 r=70 f=50	d=75 r=50 f=40	d=75 r=50 f=80
0.01%	73,4.2 **130**	168,6.0 **116**	305,13 **113**	421,5.8 **114**	121,6.3 **119**	168,8.9 **118**	168,3.1 **114**
0.1%	73,4.2 **130**	168,6.5 **116**	304,11 **112**	421,5.9 **114**	121,6.5 **119**	168,8.4 **118**	168,3.6 **114**
1%	73,4.3 **130**	168,7.0 **117**	305,14 **113**	421,5.9 **114**	121,6.5 **119**	168,9.2 **118**	168,3.5 **114**
10%	73, 8.5 **136**	168,13 **122**	304,24 **117**	422,14 **116**	120,12 **123**	168,13 **121**	168,8.6 **118**

Table 2: The effect of iteration accuracy on simulated breakdown data.

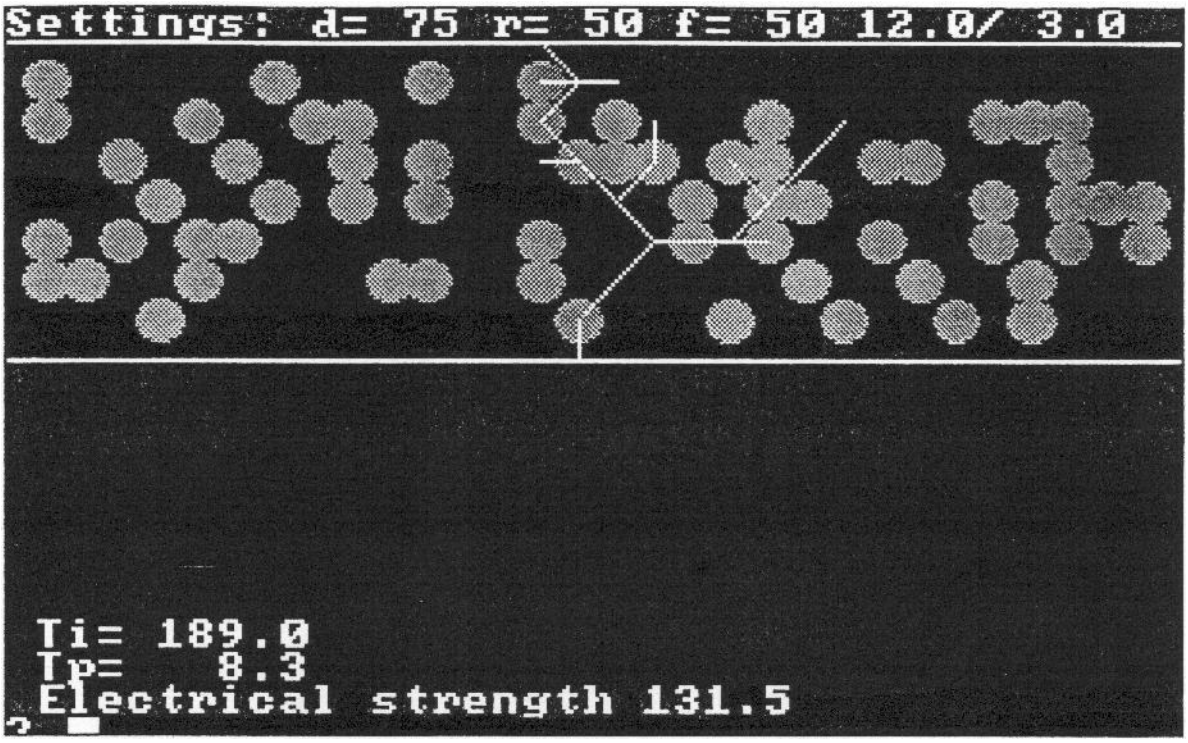

Figure 8.3(a): Tree grown with lattice spacing A=10, the tree looks reasonable but the spherulitic distribution looks unrealistic.

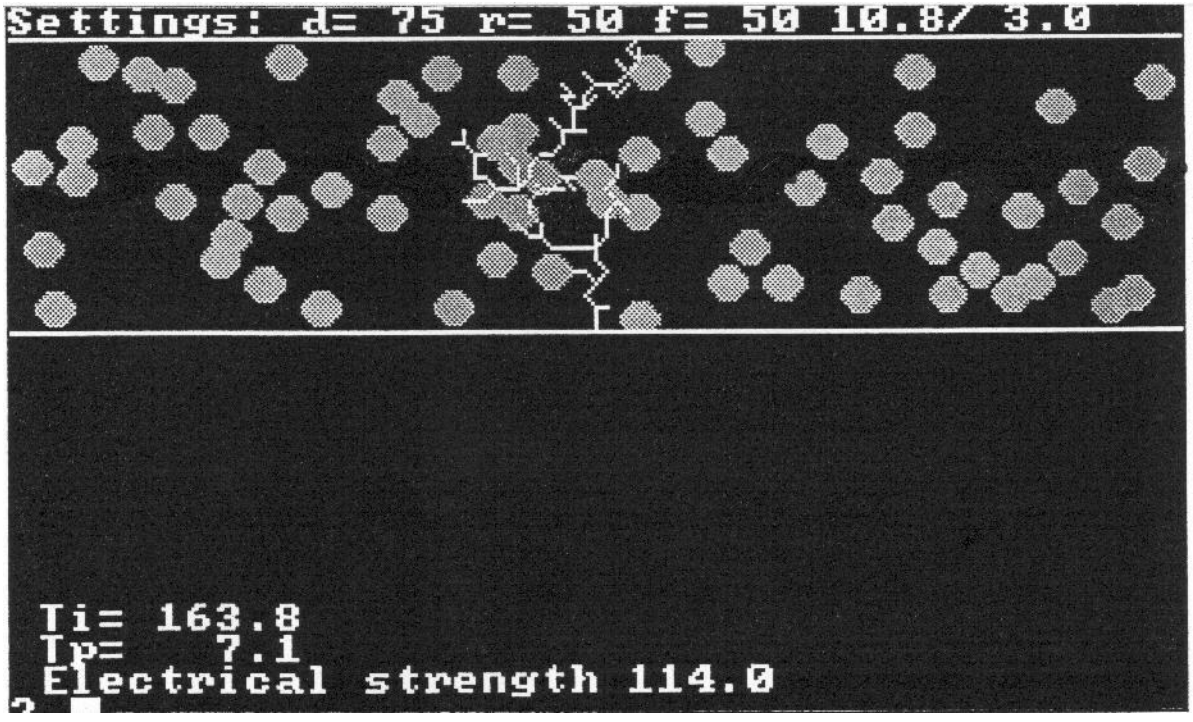

Figure 8.3(b): Tree grown with a lattice spacing, A=3.

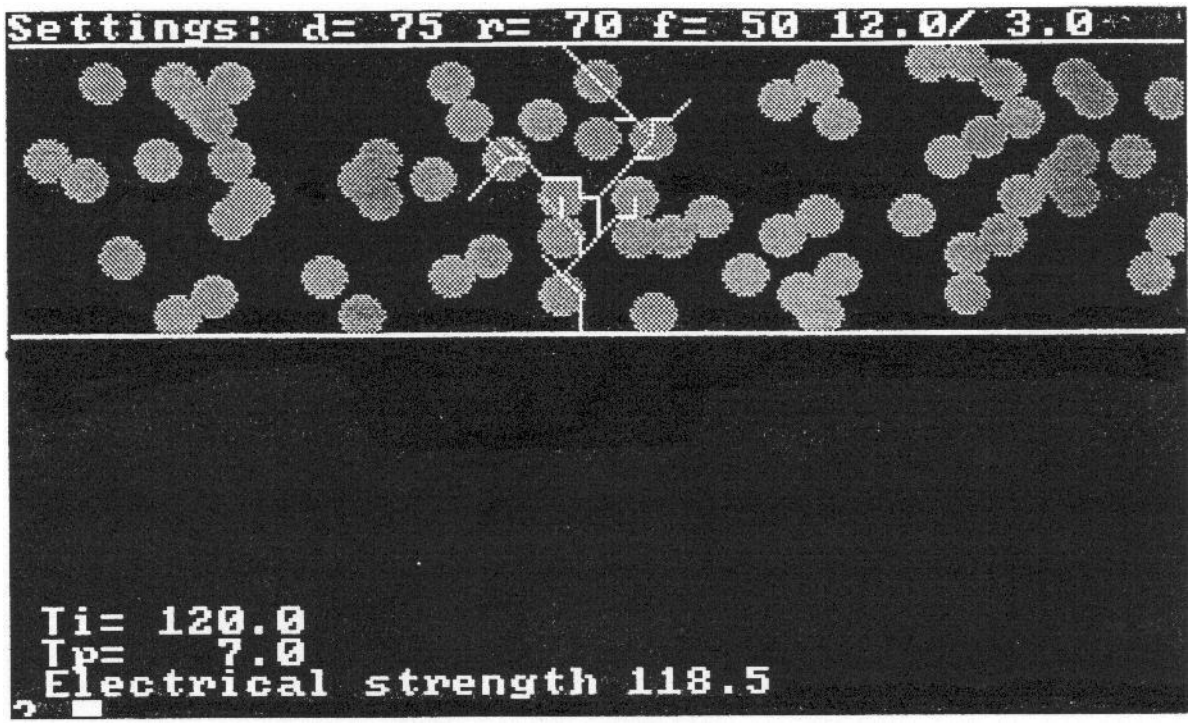

Figure 8.4(a): Tree grown with iteration parameter set to 0.01%.

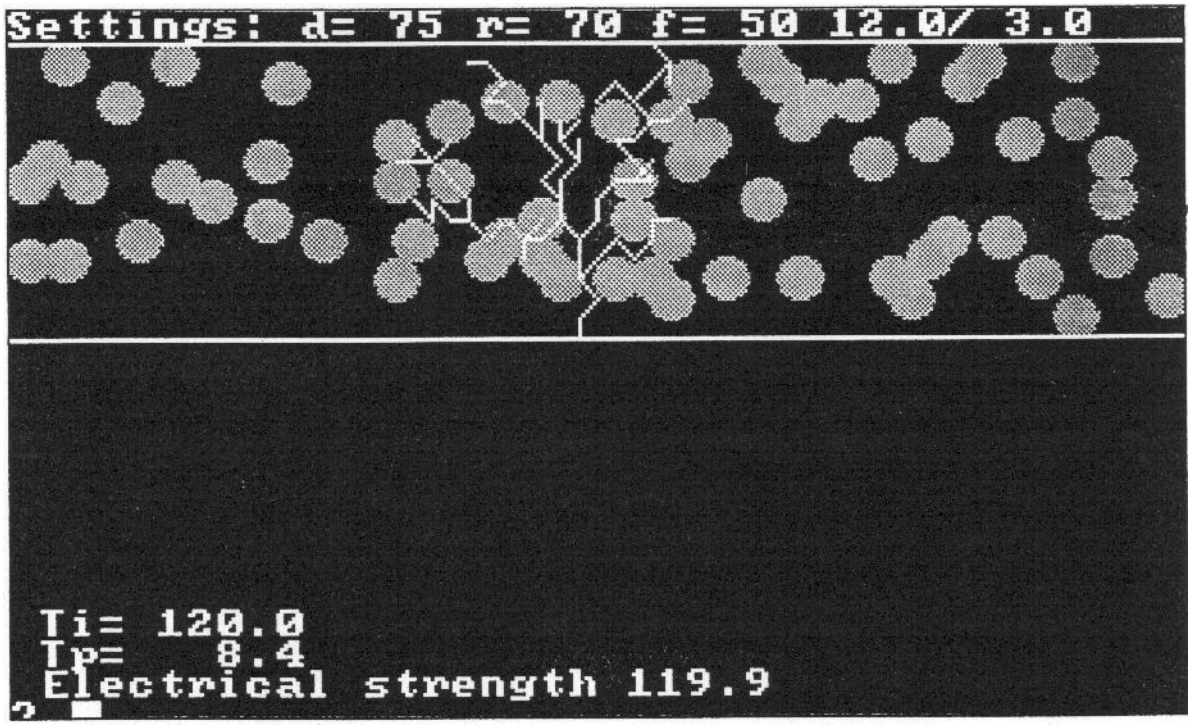

Figure 8.4(b): Tree grown with iteration parameter set to 25%

lattice spacing A = 10, notice particular problems with spherulitic arrangement - the distribution of spherulites looks very artificial. With a = 3 (figure 8.3(b)) the general structure of the simulated tree far better approximates those in the literature (2,3), and the spherulitic distribution far better approximates real systems. A spacing A = 5 corresponds to 5 μm in real space, a lattice spacing which is not inconsistent with that used in the W-Z model (2) and it's modifications (3).

Effect of iteration accuracy, in the iteration routine to calculate the potentials the constant in the self check was changed so that the iterations became more or less accurate. We checked primarily that our results were not being adversely affected, if for example, the iteration accuracy was insufficient to determine the potentials in the lattice. With less accuracy, less iterations need to be performed, a saving on computer time. Table 2 shows the dependence of simulation data on iteration accuracy for a lattice spacing of 5. Even at 1% allowable difference in potential between successive iterations, the values obtained are similar to those at higher accuracies, however at 10% allowable difference the values differ considerably.

The main work of the iteration routine is to decrease the potentials around new tree growth points and if insufficient iterations are performed the potentials in the locality of the tree are too high. This results in more choice of possible growth points and a more bushy tree, which leads to the observed increase in electrical strength if insufficient iterations are performed. This sort of behaviour can be seen in the tree growth patterns, and figure 8.4 shows two extreme examples. Figure 8.4(a) shows a tree grown with the parameter set to 0.01% and figure 8.4(b) shows a somewhat more bushy tree grown with the parameter set to 25%. A value of 0.1% is a good compromise between accuracy and speed.

8.4.2 Simulation and connections to real data

Here the model is taken a little further by attempting to reproduce some of the effects seen in the experiments. In chapter 5 the effects of ramp rate, sample thickness and frequency on electrical data was investigated. Electrical strength was reduced with increasing sample thickness, decreased ramp rate or increased A.C frequency. Simulated 4901 was used in the model over a series of 20 conditions to investigate the effects of ramp rate and sample

	D=30μm	D=50μm	D=75μm	D=100μm	D=140μm
R=20	184, 4.8 **125** (141±4)	288, 5.4 **117** (129±4)	420, 5.9 **113** (118±3)	550, 6.5 **111** (106±3)	756, 8.3 **109** (93±3)
R=30	123, 4.5 **127** (150±6)	192, 5.9 **119** (142±4)	280, 6.8 **115** (122±4)	367, 7.8 **113** (115±4)	507, 9.5 **111** (99±3)
R=50	73, 4.2 **130** (157±5)	115, 5.4 **121** (148±4)	168, 6.5 **116** (130±5)	220, 8.7 **115** (120±5)	304, 11.2 **113**(104±2)
R=70	53, 4.6 **133** (164±8)	83, 4.2 **122** (152±8)	121, 6.5 **119** (136±5)	157, 8.3 **116** (126±7)	217, 10.8 **114** (108±5)

Table 3: Effect of ramp rate and sample thickness on simulation data.

	Model prediction	Experimental
f=40 Hz	168,8.4 **118**	(131±5)
f=50 Hz	168,6.5 **116**	(128±4)
f=80 Hz	168,5.0 **115**	(114±4)

Table 4: Effect of AC frequency on simulated data.

Spherulites	Simulation	Closest experimental value
1.6 per 1000μm^2, 6μm dia.	168, 3.0 **114**	BPA 124/1-(110±6)
3 per 1000μm, 12μm dia.	168, 6.5 **116**	BPA Q/0-(128±4)
3 per 1000μm, 24μm dia.	168, 14 **121**	BPA 115/20-(147±4)

Table 5: Effect of spherulites on simulation data.

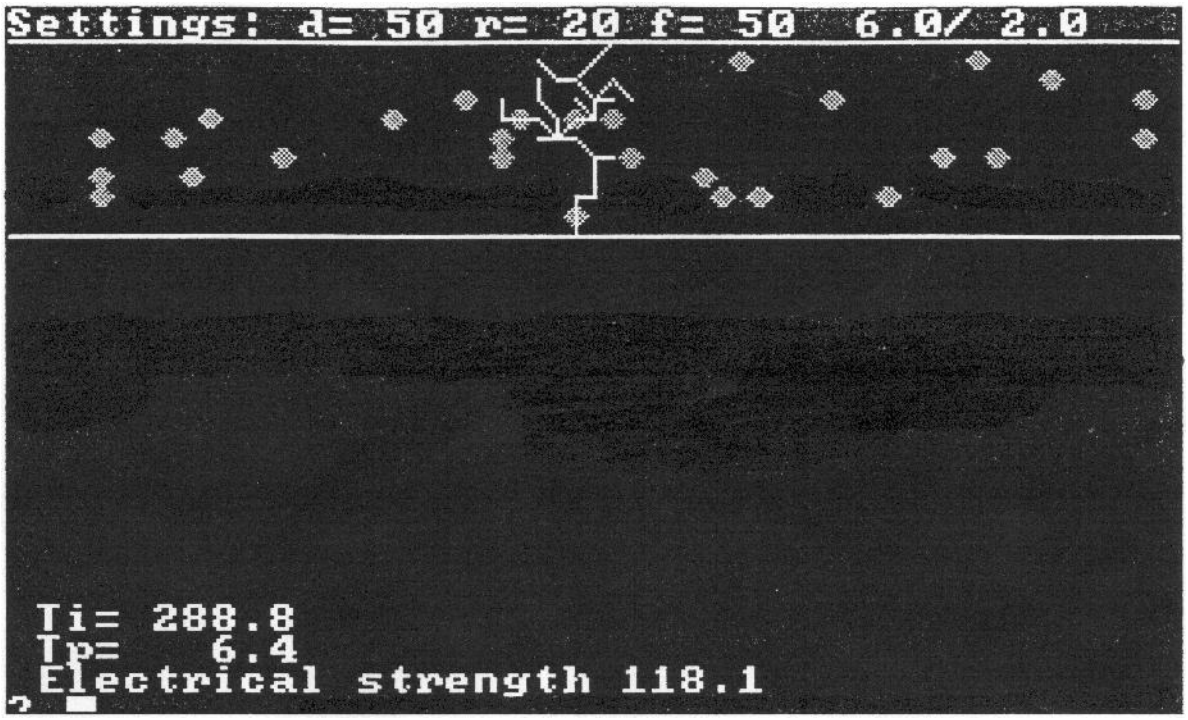

Figure 8.5(a): Simulated tree in BPA 124/1 equivalent.

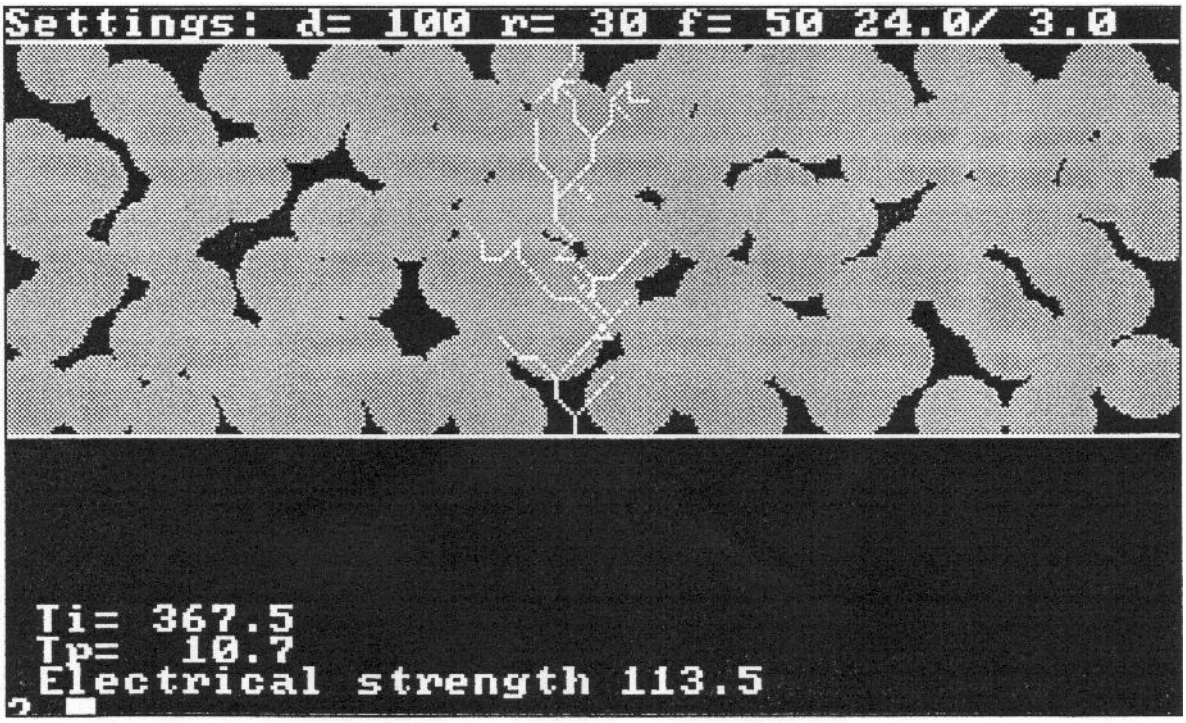

Figure 8.5(b): Simulated tree in BPA 115/20 equivalent.

thickness on simulated data. Table 3 shows these results and is arranged in the same format as tables 1 and 2, with experimental values given in brackets. Agreement with experimental values would not be expected with such a simple simulation, however as the two testing conditions were changed the model shows the same *trends* as the experimental data. The same general agreement between the model and the experimental data is seen when the frequency is changed (table 4).

Furthermore in chapter 3 the effects of morphology on electrical strength were examined and a correlation between spherulitic development and electrical strength was found.

The numbers and sizes of spherulites were next changed in a set of 3 runs to see if these experimental trends could be duplicated and the data is shown in table 5. Since only a set of sizes of spherulites are available in the simulation the nearest experimental equivalent material is shown for comparison with the simulation data. A general increase in the simulated breakdown values with spherulitic content in line with experimental data, is clearly seen here, a surprising result from such a crude model. Simulated trees grown in the first and latter samples are shown in figure 8.5, although the tree growth patterns are generally similar in the two cases, the tree growth times are increased in the latter case (table 5). Clearly a more explicit definition of spherulites is required in this simulation, to better model the interaction of the tree with the spherulitic architecture.

8.4.3 Tree growth behaviour

The last set of data is very encouraging from such a simplistic model of electrical tree behaviour, so a brief analysis of the time dependence of tree growth was performed to determine how accurately the model predicted tree behaviour. Figure 8.6 shows a plot of tree growth length in lattice spacings as a function of the time since initiation occurred. Despite clear scatter in the data points, clear trends of tree growth are evident. A long initiation time (up to t=0 here) is followed by initially slow tree growth. The field enhancement due to the tree itself promotes a period of rapid growth after which failure occurs quickly. This general pattern of behaviour is not unexpected (10,11).

From these results we can ask how probable is it to find a tree in actual samples assuming the simulation is reasonable? For conditions of a 75μm sample with a ramp rate of 50

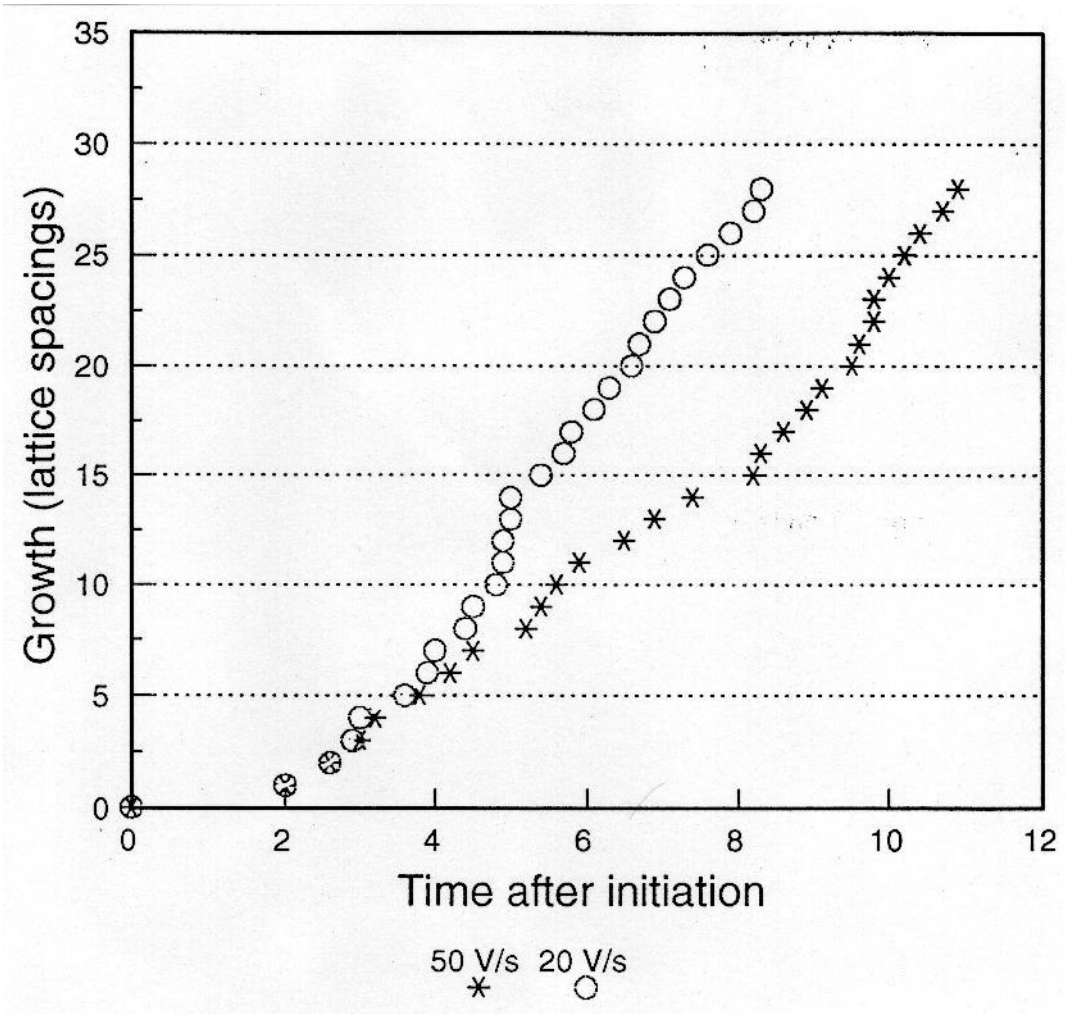

Figure 8.6: Tree growth behaviour in the same simulation but set for different ramp rates.

volts per second at 50 Hz, the results from the simulation show a growth time of around 6 seconds, that 6 seconds represents a rise of voltage of 300 Volts after maybe applying 8.4 KV just to initiate the tree. To stop a test in this time requires an accurate determination of when the tree starts growing to a reasonable size, unfortunately this is not probable owing to the scatter in the experimental breakdown data of typically (expressed in volts) 1.2 KV. From statistical tables (12) and assuming a normal distribution of breakdown values, the probability of doing this successfully and seeing any trace of a tree is around 10%. Assuming the model is at least a reasonable approximation, this is a result which certainly agrees in general with the inability to see any traces of treeing prior to breakdown.

8.5 Discussion

The model presented here is a preliminary study of electrical tree growth in one of the polyethylene blends considered in this thesis. Despite gross simplifications, both in calculating the constants and in the physics of the model, experimental trends are duplicated in the model with simulated electrical strength values not being grossly out of line with experimental data, a surprising result.

Tree growth is restricted to 2 dimensions in this simulation but in reality electrical trees grow in three dimensions. This is a very simplistic model and the fact that we obtained reasonable any reasonable data suggests that the basic notions employed cannot be too unreasonable.

Obviously there is huge scope for modifying and improving this simulation program and one of the simplest ways to improve the simulation is to allow growth in three dimensions, however tree growth is a complex subject (10) and some possible improvements are listed below.

In the simulation effects of pressure increases due to gas evolution during tree formation were ignored, such effects could be included, by modifying the value of the mean free path ß in the simulation. A pressure increase immediately following a partial discharge would then have a negative effect on tree growth, increasing growth times.

During tree initiation significant amounts of space charge is injected into the dielectric (13-

15) this could be catered for by modifying Laplace's equation to include the effects of this stored charge.

A further charge storage process occurs during growth, ions are obviously left in growth tips, which for the purposes of this model are considered immobile and ignored. These ions may settle on the tree walls (11), altering the electric field at the tree tips to non-zero values.

Tree resistance is also ignored in the simulation but it's effects may be included by giving new tree growth points a non-zero value of potential (3) which would then serve to reduce the local field at tree tips, so increasing tree growth times.

Analysis of real trees is required to fully understand the interactions between spherulitic structures and electrical trees, which would enable more explicit definition of spherulitic structures in the simulation. Clearly an analysis of real trees in conjunction with the simulation would be useful in pointing at deficiencies in the model.

8.6 Conclusions

1) A very simple 2 dimensional simulation of electrical tree growth is presented, based on a cumulative damage model with two growth constants corresponding to spherulitic and non-spherulitic material respectively. Despite considerable simplifications the simulation duplicated experimental trends.

2) Simulated electrical strength values depended on sample thickness, ramp rate and test frequency as well as spherulitic make up and showed similar trends to experimental data.

3) The tree growth behaviour was investigated as a function of time. The simulated growth patterns were not grossly out of line with expectations.

4) Tree initiation times were long and growth times short, this concurs with the general difficulty in locating and imaging tree structures as found experimentally.

5) These results are very encouraging from such a simplistic simulation and there is plenty of scope for refining the existing model.

8.7 References

1) L. Niemeyer, L. Pietronero and H.J Wiesmann, Phys. Rev. Letts, **52**, 12, March 1984,

p1033.

2) H.J Wiesmann and H.R Zeller, J. Appl. Phys., **60**, 5, Sept 1986, p1770.

3) A.L Barclay, P.J Sweeney, L.A Dissado and G.C Stevens, J. Phys. D, **23**, 1990, p1536.

4) E.O Forster, J. Phys. D: Appl. Phys. 1990, **23**, 1506.

5) M. Leda, IEEE Trans. Electr. Insul. 1980, **15**, 206.

6) S.N Kolesov, Polym. Sci. USSR 1993, **21**, 1993.

7) T.J Lewis, J. Phys. D: Appl. Phys. 1990, **23**, 1469.

8) R. Patsche, IEEE Trans. Electr. Insul. 1992, **27**, 532.

9) The Open University science data book, Ed: R.M Tennent, Oliver and Boyd, Edinburgh, 1989.

10) L.A Dissado and J.C Fothergill, `Electrical degradation and breakdown in polymers', ed. G.C Stevens, Peter Peregrinus, London, 1992.

11) L.A. Dissado, personal communication.

12) J.R Taylor, `Introduction to error analysis', University Science Books, Oxford University Press, CA, 1982.

13) J. Fraile, A. Toaes, J. Jimenez, J. Mat. Sci. 1989, **24**, 1323.

14) R. Patsche, J. Phys. D: Appl. Phys. 1990, **23**, 1497.

15) G. Krause, D. Meurer and D. Klee, IEEE Trans. Electr. Insul. 1989, **24**, 419.

CHAPTER 9 - SUMMARY AND CONCLUSIONS.

9.1 Summary of thesis

The aim of this thesis, as described in chapter 2, was to determine structure-property relationships in polyethylene blends and particularly to relate the electrical strength of a material to its microstructure, this aim has been achieved. Through the use of binary polyethylene blends of linear (LPE) and branched (BPE) materials, the role of morphology and molecular variations on electrical strength could be studied independently. Furthermore an enhanced material for cable manufacture has also been formulated based upon a polyethylene blend. This material has a breakdown strength 16% higher than conventional BPE as determined by short term ramp tests.

Polyethylene blends, which had been quenched and crystallised isothermally, have been examined. In the case of quenched samples (chap. 3), which represent systems with a constant morphology but variable composition, the electrical strength was found to be invariant. A similar conclusion was found when the linear and branched polyethylenes used were substituted for materials covering a wide range of molecular weights and architectures (chap. 4). For the most part the morphology did not change, and consequently the electrical strength remained unchanged.

Isothermal crystallisation at 115°C and 124°C, led to banded spherulites and compact lamellar aggregates respectively, in a branched polyethylene (BPE) rich matrix of constant composition (chap. 3). Spherulitic size was primarily determined by LPE content. Albeit low amounts of LPE led to small spherulites, which caused a drop in electrical strength, higher amounts of LPE led to larger spherulites which led to a significant increase in electrical strength. In cases where material substitutions caused a change in morphology (chap. 4) this always led to a change in electrical strength.

From these investigations it was clear that morphological, rather than molecular factors are key at influencing breakdown data. Therefore by controlling the morphology the electrical strength can be changed and improved.

A blend based upon 20% LPE in BPE could be crystallised isothermally over a wide range of temperatures (112-120°C) yielding morphologies composed of space filling banded

spherulites. Materials containing such morphologies were found to exhibit enhanced electrical strength (chap. 7), and as such, are candidates for improved cable insulation. Analysis of electrical strength as a function of crystallisation time in the same chapter, confirmed that a space filling morphology was essential for high electrical strength. Impurities have been shown to cause detrimental effects to electrical strength in chapter 3, where the effects of various inorganic filler particles were investigated. Melt mixing (chap. 5) was found to be a viable procedure for blending materials on an industrial scale, as no similar detrimental effects, possibly due to impurities added during mixing were found. Crosslinking such materials for cable manufacture was discussed in chapter 4, and no detrimental effects of crosslinking on electrical strength were found. Based on these results production of an enhanced crosslinked cable material based on polyethylene blends is feasible. Although mechanical deformation did reduce the electrical strength of such materials (chap. 6), it was found, as far as practical usage is concerned, that any such loss of performance would be quickly annealed out under typical cable operating temperatures.

The electrical strength was found to be dependent on the testing conditions and sample geometry employed (chap. 5), which makes an estimation of the possible improvement in cable lifetime difficult. In any academic investigation the same testing procedure and sample geometries need to be employed for comparative tests, however even for thicker insulation, an enhanced insulator is still possible.

An electrical tree was examined (chap 3), which revealed a tortuous path, primarily avoiding spherulitic regions, thus it was found that morphology *does* influence electrical tree growth as shown in chapters 3 and 4. A computer simulation of tree growth was discussed in chapter 8), which, despite its simplicity, was highly successful, sensibly predicting electrical strength variations due to test parameters and morphological structure, in line with experimental data. Long tree initiation times and short growth times predicted by the model, concurred with the experimental difficulties in finding pre-breakdown features discussed in chapter 3. The model has demonstrated that failure of thin film samples due to electrical treeing, or some related damage phenomena which primarily avoids regions of high crystallinity, is not unreasonable.

9.2 Suggestions for further work

This thesis contains a great deal of data linking the electrical properties to morphology and other processing factors. Although the main factors influencing electrical strength have been established in this thesis, further work, particularly to verify that these trends also apply to other materials is needed. In this investigation we have employed polyethylene blends due to the systematic control of morphology achievable in these systems. However the general trends, particularly relating high electrical strength to a space filling morphology and its invariance with molecular parameters, could have wide ranging implications applicable to other polymeric systems. It is clear that breakdown data is influenced by testing conditions, however no long term tests were performed, and the results presented are based upon short term tests which are very different to actual cable service conditions. Longer term tests, particularly at constant voltage stress better approximating conditions found in service, are required before the reported enhancement in electrical strength can be linked to real parameters such as cable lifetime. A useful increase in cable lifetime could then be established by the use of a polyethylene blend. Chapter 7 showed that processing such a material into a commercial cable is not a formidable task once the improvement in properties could be better ascertained.

From the data presented in chapter 6, the response of a polymeric system to mechanical deformation is a rich and potentially exciting field to explore. Low LPE content blends, with their simple morphological structure, could considerably aid in the understanding of deformation mechanisms on both individual lamellae and in spherulites as a whole. This is an important area, which is often complicated by morphologies which are difficult to interpret. The model presented in chapter 8 has a wide potential for improvement and certainly warrants additional modifications, particularly to extend to 3 dimensions and include the effects of space charge. The model as it stands is a good framework from which to begin a systematic study of treeing phenomena in general, particularly through the controlled morphologies achievable in polyethylene blends. If the problems associated with imaging and growing real trees could be overcome, then a systematic comparison of the model with real trees could be performed, which as well as highlighting deficiencies and improvements to the model, could advance the understanding of electrical treeing.

Appendix 1: Data used in the computer simulation in chapter 8.

Description	Symbol	Value	Source
Constants;			
Vaporisation temperature of PE	T_v	470±30 °C	TGA data
Single C-C bond energy of PE	-	348 kJ/mol	ref 1
Double C=C bond energy of PE	-	612 kJ/mol	ref 1
Density of 4901 BPE	σ_{4901}	910 kg/m^3	Borealis chem.
Density of 140/60 LPE	$\sigma_{140/60}$	985 kg/m^3	B.P. chemicals.
Heat capacity of PE	C_p	2.3±0.2 kJ/kg	DSC data
Latent heat of fusion (4901)	F_{4901}	86±6 kJ/kg	DSC data
Latent heat of fusion (140/60)	$F_{140/60}$	256±12 kJ/kg	DSC data
Mean free path in air	ß	6.63x10^{-8} m	ref 2
Electronic charge	e	1.6x10^{-19} C	ref 2
Number of charge carriers	N_v	1.27x10^{25} m^{-3}	ref 2
Molar mass of ethylene (C_2H_4)	A_e	28.05	ref 2
Derived values			
Heat of vaporisation of PE	L_v	84 kJ/mol	note 1
Ionisation energy PE	I	7 eV	note 2
Heat of vaporisation of 4901 BPE	V_{4901}	2730 kJ/kg	note 3
Heat of vaporisation of 140/60	$V_{140/60}$	2955 kJ/kg	note 3
Degradation energy of 4901 BPE	H_{4901}	3851 kJ/kg	note 4
Degradation energy of 140/60	$H_{140/60}$	4246 kJ/kg	note 4

Notes

1) Calculated from the energy required to break two single bonds minus the energy gain on creating one double bond.

2) Minimum energy to create 1 ethylene molecule and therefore vaporise the polymer, two single bonds are broken.

3) Heat of vaporisation $V = L_v\sigma/A_e$ (kJ/kg) choosing the appropriate constants for the material considered.

4) Defined as the total energy required to heat, melt and vaporise the polymer.

$H = C_p(T_v\text{-}20) + F + V$, with V and F being appropriate to the material.

The minimum field for tree growth was calculated from the relation $E_c = I/ß$.

References

1) J.G Stark and H.G Wallace, `Chemistry data book', John Murray, London, 1976.

2) R.M Tennant, `Science data book', Oliver and Boyd, Edinburgh, 1989.

Appendix 2: Computer program for electrical tree simulations.

```
REM Electrical tree growth simulation
REM Based on Wiesmann-Zeller model and solving laplace
REM equation for potentials, written by I. Hosier.
REM ************************INITIALISE****************************
CLEAR
SCREEN 1, 0
CLS
RANDOMIZE TIMER
REM ****************SORT OUT MODEL CONSTANTS***************
REM general-latt. spacing, surf. roughness
a = 5: sr = 1: ec = 105
REM growth constants for matrix and spherulites
kgm = .0000384: kgs = .0000322
REM ******DISPLAY MENU FOR EXPERIMENTAL PARAMETERS******
REM set variables-thickness, ramp rate, frequency, spherulites
PRINT "Dielectric failure by electrical treeing"
PRINT "----------------------------------------"
INPUT "Enter sample thickness"; d
INPUT "Enter ramp rate"; r
INPUT "Enter test frequency"; f
PRINT "SELECT SPHERULITE SIZE"
i = 6 * (a / 5)
b = CINT(i)
c = CINT(2 * i)
e = CINT(3 * i)
g = CINT(4 * i)
h = CINT(5 * i)
PRINT "0-none       , 1-diam."; b; "um"
PRINT "2-diam."; c; "um, 3-diam."; e; "um"
PRINT "4-diam."; g; "um, 5-diam."; h; "um"
INPUT sphsize
IF sphsize < 0 OR sphsize > 5 THEN sphsize = 0
IF sphsize = 0 THEN GOTO jump
INPUT "Enter a spherulitic number density"; num
IF num <= 0 THEN sphsize = 0
jump:
REM ******************SORT OUT GEOMETRY**********************
nx = CINT(325 / a)
ny = CINT(2 + (d / a))
n = CINT((a * a * (ny - 3) * (nx - 2) * num) / 1000)
radius = (a / 5) * 3 * sphsize
rad = sphsize - 1
dt = 1 / (2 * f)
REM ****************DEFINE STORAGE ARRAYS******************
```

```
DIM tree(nx, ny)
DIM v(nx, ny)
DIM lt(nx, ny)
DIM xs(nx * ny)
DIM ys(nx * ny)
DIM xe(nx * ny)
DIM ye(nx * ny)
DIM el(nx * ny)
DIM ls(nx * ny)
REM **************SET UP SPHERULITES********************
redist:
CLS
IF sphsize = 0 THEN GOTO setupborders
LOCATE 22, 2: PRINT "Setting up spherulites"
FOR x = 1 TO nx
FOR y = 1 TO ny
tree(x, y) = 0
NEXT y
NEXT x
REM choose a point at random but not within another spherulite
FOR m = 1 TO n
musttryagain:
x = CINT(2 + ((nx - 3) * RND))
y = CINT(3 + ((ny - 4) * RND))
IF tree(x, y) = 1 THEN GOTO musttryagain
REM now define spherulite on the tree grid
FOR x1 = (x - rad) TO (x + rad)
factor = rad - ABS(x1 - x)
FOR y1 = (y - factor) TO (y + factor)
IF x1 < 1 OR x1 > nx OR y1 < 1 OR y1 > ny THEN GOTO nomatrix
tree(x1, y1) = 1
nomatrix:
NEXT y1
NEXT x1
REM and draw the spherulite on the screen
xc = (x - 1) * a
yc = 8 + ((y - 2) * a)
CIRCLE (xc, yc), radius, 2
PAINT (xc, yc), 2, 2
NEXT m
REM finally get rid of excessive spherulitic bits outside borders
xp = (nx - 1) * a
yp = 8 + ((ny - 2) * a)
FOR j = 1 TO 10
DRAW "b m0," + STR$(yp + j) + " c0"
DRAW "m" + STR$(xp) + "," + STR$(yp + j) + " c0"
NEXT j
```

```
REM **************DRAW THE SAMPLE BORDERS*******************
setupborders:
xp = (nx - 1) * a
yp = 8 + ((ny - 2) * a)
DRAW "b m0,8 c7"
DRAW "m" + STR$(xp) + ",8 c7"
DRAW "b m0," + STR$(yp) + " c7"
DRAW "m" + STR$(xp) + "," + STR$(yp) + " c7"
LOCATE 1, 1: PRINT "                                    "
LOCATE 1, 1: PRINT "Settings: d="; d; "r="; r; "f="; f;
PRINT USING "##.#"; (i * sphsize);
PRINT "/"; USING "##.#"; num
IF sphsize = 0 GOTO setuplatt
LOCATE 22, 2: INPUT "Is this distribution OK (y/n)"; a$
IF UCASE$(a$) = "N" THEN GOTO redist
REM ***************SET UP INITIAL LATTICE****************
setuplatt:
REM v: potential always between 0 and 1, tree at zero potential,
REM use infinite boundry field conditions to start off with
FOR y = 1 TO ny
FOR x = 1 TO nx
lt(x, y) = 0
v(x, y) = (ny - y) / (ny - 1)
NEXT x
NEXT y
REM **************TREE INITIATION ROUTINE*******************
REM Initiate the tree.  Probability of failure is zero below
REM critical field so calculate time to reach critical field
LOCATE 22, 2: PRINT "Initiating tree.....           "
x1 = CINT(nx / 2)
y1 = ny - 1
x = x1
y = ny
ti = (ec * a) / (v(x1, y1) * r)
LOCATE 20, 2: PRINT "Ti= ";
LOCATE 20, 6: PRINT USING "###.#"; ti
REM **************INITIAL GROWTH ROUTINE*******************
REM discharges at frequency 2f erode a channel into the dielectric
REM here find time to go in one lattice spacing by solving growth equation
REM for each half cycle of ac cycle since applied voltage increases
IF tree(x1, y1) = 0 THEN k = kgm
IF tree(x1, y1) = 1 THEN k = kgs
t = ti
lo = sr
tryagain:
t = t + dt
l = lo + ((k * lo * v(x1, y1) * r * t) / (a - lo))
```

```
lo = l
IF l < a THEN GOTO tryagain:
LOCATE 21, 2: PRINT "Tp= ";
LOCATE 21, 6: PRINT USING "###.#"; (t - ti)
REM update the tree structure and potentials
tree(x1, y1) = 9
lt(x1, y1) = a
v(x1, y1) = 0
REM draw the new segment on the screen
xp = ((x - 1) * a): yp = 8 + ((y - 2) * a)
xp1 = ((x1 - 1) * a): yp1 = 8 + ((y1 - 2) * a)
DRAW "b m" + STR$(xp) + "," + STR$(yp) + "c7"
DRAW "m" + STR$(xp1) + "," + STR$(yp1) + "c7"
nxt:
REM ***********CALCULATE NEW FIELD POTENTIALS***************
REM find the potential in the dielectric by iterating laplace equation in 2D
REM Self check for accuracy so no more iterations than neccesary are done
i = 0
start:
fl = 0
i = i + 1
LOCATE 22, 2: PRINT "finding new field potentials       "
LOCATE 22, 30: PRINT i
FOR y = ny - 1 TO 2 STEP -1
FOR x = 2 TO nx - 1
IF tree(x, y) = 9 THEN GOTO skip
newv = .25 * (v(x, y + 1) + v(x, y - 1) + v(x + 1, y) + v(x - 1, y))
change = ABS(v(x, y) - newv)
IF change > .001 THEN fl = 1
v(x, y) = newv
skip:
NEXT x
NEXT y
IF fl = 1 THEN GOTO start
REM ***************FIND NEW GROWTH SITES****************
REM find a point of tree then scan round to calculate potential
REM gradient and possible points unoccupied by tree for growth
LOCATE 22, 2: PRINT "Finding new growth sites          "
LOCATE 22, 30: PRINT mf
n = 0
FOR y = 2 TO ny - 1
FOR x = 2 TO nx - 1
IF tree(x, y) <> 9 THEN GOTO again
FOR x1 = x - 1 TO x + 1
FOR y1 = y - 1 TO y + 1
IF tree(x1, y1) > 1 THEN GOTO trynextpos
lseg = a * SQR(((x1 - x) ^ 2) + ((y1 - y) ^ 2))
```

```
elocal = (v(x1, y1) / lseg)
IF (elocal * r * t) < ec THEN GOTO trynextpos
n = n + 1: el(n) = elocal: ls(n) = lseg
xs(n) = x: ys(n) = y: xe(n) = x1: ye(n) = y1
trynextpos:
NEXT y1
NEXT x1
again:
NEXT x
NEXT y
REM handle an unlikely error situation
IF n = 0 THEN LOCATE 22, 2: PRINT "Growth ceased": GOTO ask
REM *****SUM ALL GROWTH PROBABILITIES FOR NORMALISATION*****
sum = 0
FOR m = 1 TO n
sum = sum + el(m)
NEXT m
REM ********NOW CHOOSE A GROWTH SITE AND DIRECTION**********
REM biased to select on basis of local field in that direction
LOCATE 22, 2: PRINT "Choosing a growth site              "
ag:
m = 1 + INT(n * RND)
IF m > n THEN GOTO ag
chance = RND
IF chance > (el(m) / sum) THEN GOTO ag
REM now growth points are found extract data from matrix
x = xs(m)
y = ys(m)
x1 = xe(m)
y1 = ye(m)
lseg = ls(m)
elocal = el(m)
REM ************FIND THE CHANNEL GROWTH TIME*****************
LOCATE 22, 2: PRINT "Finding growth time              "
REM find the time taken to produce the link by partial discharges
REM checking to see what type of material it is growing through
IF tree(x1, y1) = 0 THEN k = kgm
IF tree(x1, y1) = 1 THEN k = kgs
lo = lt(x, y)
dogain:
t = t + dt
l = lo + ((k * lo * v(x1, y1) * r * t) / (lseg + lt(x, y) - lo))
lo = l
IF (l - lt(x, y)) < lseg GOTO dogain:
LOCATE 21, 6: PRINT USING "###.#"; (t - ti)
REM ********DRAW THE TREE SEGMENT ON SCREEN*******************
xp = ((x - 1) * a): yp = 8 + ((y - 2) * a)
```

```
xp1 = ((x1 - 1) * a): yp1 = 8 + ((y1 - 2) * a)
DRAW "b m" + STR$(xp) + "," + STR$(yp) + " c7"
DRAW "m" + STR$(xp1) + "," + STR$(yp1) + " c7"
REM ********UPDATE THE TREE STRUCTURE AND POTENTIALS**********
LOCATE 22, 2: PRINT "Updating tree structure        "
lt(x1, y1) = lt(x, y) + lseg
tree(x1, y1) = 9
v(x1, y1) = 0
REM ***************CHECK FOR BREAKDOWN EVENT**************
bdf = 0
FOR x = 2 TO nx - 1
IF tree(x, 2) = 9 THEN bdf = 1
NEXT x
IF bdf = 0 THEN GOTO nxt
strg = (r * t) / d
LOCATE 22, 2: PRINT "Electrical strength "; USING "###.#"; strg
ask:
INPUT a
END
```